




Universitat Autònoma de Barcelona

**ADVERTIMENT.** L'accés als continguts d'aquesta tesi doctoral i la seva utilització ha de respectar els drets de la persona autora. Pot ser utilitzada per a consulta o estudi personal, així com en activitats o materials d'investigació i docència en els termes establerts a l'art. 32 del Text Refós de la Llei de Propietat Intel·lectual (RDL 1/1996). Per altres utilitzacions es requereix l'autorització prèvia i expressa de la persona autora. En qualsevol cas, en la utilització dels seus continguts caldrà indicar de forma clara el nom i cognoms de la persona autora i el títol de la tesi doctoral. No s'autoritza la seva reproducció o altres formes d'explotació efectuades amb finalitats de lucre ni la seva comunicació pública des d'un lloc aliè al servei TDX. Tampoc s'autoritza la presentació del seu contingut en una finestra o marc aliè a TDX (framing). Aquesta reserva de drets afecta tant als continguts de la tesi com als seus resums i índexs.

**ADVERTENCIA.** El acceso a los contenidos de esta tesis doctoral y su utilización debe respetar los derechos de la persona autora. Puede ser utilizada para consulta o estudio personal, así como en actividades o materiales de investigación y docencia en los términos establecidos en el art. 32 del Texto Refundido de la Ley de Propiedad Intelectual (RDL 1/1996). Para otros usos se requiere la autorización previa y expresa de la persona autora. En cualquier caso, en la utilización de sus contenidos se deberá indicar de forma clara el nombre y apellidos de la persona autora y el título de la tesis doctoral. No se autoriza su reproducción u otras formas de explotación efectuadas con fines lucrativos ni su comunicación pública desde un sitio ajeno al servicio TDR. Tampoco se autoriza la presentación de su contenido en una ventana o marco ajeno a TDR (framing). Esta reserva de derechos afecta tanto al contenido de la tesis como a sus resúmenes e índices.

**WARNING.** The access to the contents of this doctoral thesis and its use must respect the rights of the author. It can be used for reference or private study, as well as research and learning activities or materials in the terms established by the 32nd article of the Spanish Consolidated Copyright Act (RDL 1/1996). Express and previous authorization of the author is required for any other uses. In any case, when using its content, full name of the author and title of the thesis must be clearly indicated. Reproduction or other forms of for profit use or public communication from outside TDX service is not allowed. Presentation of its content in a window or frame external to TDX (framing) is not authorized either. These rights affect both the content of the thesis and its abstracts and indexes.

The background of the cover is a collage of fluorescence microscopy images of cardiomyocytes. The images show various cellular structures, including nuclei, mitochondria, and sarcomeres, rendered in a variety of colors such as blue, yellow, red, green, and purple. The text is overlaid on this background.

# **Defective $F_0F_1$ -ATP Synthase in Cardiomyocyte Aging: Role of Dicarbonyl Stress**

**Diana Bou Teen**

**Doctoral Thesis  
2021**





**AUTONOMOUS UNIVERSITY OF BARCELONA  
DEPARTMENT OF MEDICINE**

**DOCTORAL THESIS**

# **Defective $F_0F_1$ -ATP Synthase in Cardiomyocyte Aging: Role of Dicarbonyl Stress**

**DIANA BOU TEEN**

DOCTORAL THESIS PRESENTED BY DIANA BOU TEEN TO OPT FOR THE GRADUATE DEGREE OF  
DOCTOR FROM THE AUTONOMOUS UNIVERSITY OF BARCELONA

**Directors:** Dra. Marisol Ruiz-Meana  
Dr. David García-Dorado (2017-2019) +  
Dr. Artúr Evangelista Masip (2019-2021)

**Tutor:** Dr. David García-Dorado (2017-2019) +  
Dr. Ignacio Ferreira González (2019-2021)

Doctorate in Medicine Program  
Department of Medicine

**Barcelona, 2021**



# *Acknowledgements*

---



My PhD has been a very long journey with all its ups and downs, but I know for sure that every step has been essential for my professional growth as I have acquired so much knowledge along the way. This doctoral thesis wouldn't have concluded successfully hadn't it been for the presence of very important people who have provided their support, advice and experience when needed, and without hesitation.

My first and biggest thank you goes to Dr. Marisol Ruiz-Meana who has not only set an example of what a good boss should be like research-wise, but also humane-wise. Learning from you has been so enriching because you generously transfer your knowledge, teach how to observe things from a different perspective and with creativity, and very importantly you care about the wellbeing of your employees with an openness to listen, advice and help. You embody so many qualities that make learning from you an enjoyable process. Thank you for your guidance and for all that you have taught me. Thank you for not giving up on me even when I gave up on myself.

To Eli, the saviour, I don't think my thesis would have come this far without your essential technical interventions, to that I'm more than grateful. To Kelly, whose stubbornness was the solution for the Seahorse experiment; to Angeles, for helping me over and over again with the cardiomyocyte isolations; to Laia, David, Marta, and Sara, thank you for just being there and relating to all the ups and downs of a PhD.

With no doubt, a very big thank you goes out to my parents and sisters who have been nothing but supportive from day one. A special thank you goes to my dad, who, like any proud father who wants to see his child succeed, is still hoping that one day I will be awarded the Nobel Prize. To my sister Jinan who celebrates my little triumphs with more joy than I did. I believe that if I have come so far, it's because for you, my success was already a reality, and you helped me visualize it as I took tiny steps forward.

Last, but most importantly, I would like to give a whole-heartedly thank you to Dr. David García-Dorado, may your soul rest in peace. You were the type of person who leaves a huge impact even after a very brief introduction. Your passing has been a loss to each and every element that makes up your lab and to the entire scientific and medical community. It was admirable to see your passion, strength of will and energy despite it all. I'm thankful I had the chance to know you and it's a huge pleasure for me to dedicate this thesis to you.







**Dr. David García-Dorado**

1953-2019



# *Abbreviations*

---



- 3-DG: 3-deoxyglucosone
- 6.8PL: 6.8 proteolipid
- ADP: adenine diphosphate
- AGEs: advanced glycation end products
- ANT: adenosine nucleotide transferase
- ATP: adenine triphosphate
- CICC: calcium-induced calcium release
- CML: carboxymethyl lysine
- CsA: cyclosporine A
- CVDs: cardiovascular diseases
- CyP-D: cyclophilin D
- DAPIT: diabetes-associated protein in insulin sensitive tissue
- ETC: electron transport chain
- GLO: glyoxalase
- GSH: glutathione
- HC: hypercontracture
- HF: heart failure
- I/R: ischemia/reperfusion
- IF1: inhibitory factor 1
- IFM: interfibrillar mitochondria
- IMM: inner mitochondrial membrane
- MAGEs: methylglyoxal-derived modifications
- MDA: malondialdehyde
- MG-H1: methylglyoxal-derived hydrimidazolone
- MGO: methylglyoxal
- MICOS: mitochondrial contact site and cristae organization system
- mPTP: mitochondrial permeability transition pore
- mtDNA: mitochondrial DNA
- NCX: sodium calcium exchanger
- NHE: sodium hydrogen exchanger
- OMM: outer mitochondrial membrane
- OPA1: optic atrophy 1
- OSCP: oligomycin-sensitivity conferring protein
- OXPHOS: oxidative phosphorylation

- PiC: phosphate carrier
- PNM: perinuclear mitochondria
- PTMs: post translational modifications
- RAGE: receptor for advanced glycation end products
- RIRR: ROS-induced ROS release
- ROS: reactive oxygen species
- RyR: ryanodine receptor
- SERCA: Sarcoplasmic-Endoplasmic Reticulum ATPase
- SR: sarcoplasmic reticulum
- SSM: subsarcolemmal mitochondria
- VDAC: voltage dependent anion channel
- $\Delta\psi_m$ : mitochondrial membrane potential

## Table of contents:

<i>Summary</i> .....	1
<i>Resumen</i> .....	5
<b>1. Introduction</b> .....	7
1.1 The Aging Heart and the Link between Dysfunctional Mitochondria and Cardiovascular Disease.....	11
<b>1.1.1. Characteristic of the aged heart</b> .....	12
<b>1.1.2. Molecular properties of the aged cardiomyocyte</b> .....	13
<b>1.1.3. Mitochondrial dysfunction in the aged cardiomyocytes</b> .....	14
<b>1.1.4. Mitochondria in I/R injury: Sentenced to death by mitochondria</b> .....	16
<b>1.1.5. Contribution of aging to mitochondria-induced cell death</b> .....	18
1.2. Mitochondrial Structure .....	20
<b>1.2.1. Mitochondrial location determines its vulnerability to damage</b> .....	21
<b>1.2.2. The ugly side of mitochondria: Pathological cristae morphology</b> .....	22
1.3. Mitochondrial $F_0F_1$ -ATP Synthase.....	25
<b>1.3.1. The intricate structure of the <math>F_0F_1</math>-ATP synthase</b> .....	25
<b>1.3.2. The role of <math>F_0F_1</math>-ATP synthase in producing the bio-energetic currency of life, ATP</b> .....	27
<b>1.3.3. <math>F_0F_1</math>-ATP synthase in ATP hydrolysis: What doesn't kill you doesn't necessarily make you stronger</b> .....	29
<b>1.3.4. The <math>F_0F_1</math>-ATP synthase dimers bestow the IMM its structure</b> .....	30
1.4. The Unresolved Puzzle of the mPTP Identity; $F_0F_1$ -ATP Synthase as a Primary Suspect.....	33
<b>1.4.1. The pathophysiology of the mPTP death hole</b> .....	33
<b>1.4.2. Mitochondrial ATP synthase plays God: "I give you life and I take it away from you" ...</b>	34
<b>1.4.2.1. Dimers of <math>F_0F_1</math>-ATP synthase form the mPTP</b> .....	34
<b>1.4.2.2. The C-ring models of mPTP</b> .....	35
<b>1.4.2.3. mPTP models involving other mitochondrial proteins</b> .....	36
1.5. Entropy and Terminal Protein Damage .....	38
<b>1.5.1. Entropy reigns in aging</b> .....	38
<b>1.5.2. Dicarbonyl stress as a prominent mechanism of age-related molecular damage</b> .....	39
<b>1.5.2.1. Dicarbonyls and terminal protein damage</b> .....	39
<b>1.5.2.2. What makes dicarbonyls and the modification they produce pathogenic?</b> .....	40
<b>1.5.3. Aging transforms mitochondria into a hub of molecular damage</b> .....	43
<b>2. Hypothesis</b> .....	45



3. Objectives.....	43
4. Materials and Methods.....	47
4.1. Biological Models.....	55
4.2. Biochemical Determinations.....	59
4.3. Microscopy studies.....	64
4.4. Functional Assays.....	68
4.5. Statistical Analysis.....	75
5. Results.....	79
5.1. Aging increases the accumulation of dicarbonyl-derived protein modifications in the aged mouse myocardium and F <sub>0</sub> F <sub>1</sub> -ATP synthase is a prominent modification target.....	81
<b>5.1.1. The myocardium predominantly accumulates dicarbonyl-induced modifications</b> .....	81
<b>5.1.2. Myocardial dicarbonyl adducts almost exclusively affect lysine and arginine</b> .....	82
<b>5.1.3. Dicarbonyl-induced modifications majorly accumulate on mitochondrial proteins</b> .....	82
<b>5.1.4. The F<sub>0</sub>F<sub>1</sub>-ATP synthase is a prominent target of dicarbonyl-modification in aged myocardium</b> .....	85
5.2. F <sub>0</sub> F <sub>1</sub> -ATP synthase dimerization is impaired in hearts from aged mice.....	90
<b>5.2.1. Aging decreases the proportion of oligomerized mitochondrial F<sub>0</sub>F<sub>1</sub>-ATP synthase and increases its monomeric form</b> .....	90
<b>5.2.2. Aging decreases F<sub>0</sub>F<sub>1</sub>-ATP synthase dimerization in mouse cardiomyocytes</b> .....	91
5.3. F <sub>0</sub> F <sub>1</sub> -ATP synthase expression is preserved in the aged heart.....	93
<b>5.3.1. The expression of F<sub>0</sub>F<sub>1</sub>-ATP synthase is not modified in aging</b> .....	93
<b>5.3.2. Aging does not alter the expression of other cristae-shaping proteins</b> .....	95
5.4. Impact of Aging on F <sub>0</sub> F <sub>1</sub> -ATP Synthase activity.....	97
<b>5.4.1. Dicarbonyl modification of F<sub>0</sub>F<sub>1</sub>-ATP synthase is associated with decreased mitochondrial state 3 respiration</b> .....	97
<b>5.4.2. Aging does not modify F<sub>0</sub>F<sub>1</sub>-ATP synthase hydrolytic activity</b> .....	98
5.5. Mitochondrial Ultra-Structural Alterations in Aging.....	100
<b>5.5.1. Aging disturbs mitochondrial organization and ultrastructure in mouse hearts</b> .....	100
5.6. F <sub>0</sub> F <sub>1</sub> -ATP Synthase dicarbonyl-induced modification favours mitochondrial energy collapse.....	103
<b>5.6.1. F<sub>0</sub>F<sub>1</sub>-ATP synthase dicarbonyl modification increases the susceptibility to mPTP</b> .....	103
5.7. Induction of dicarbonyl modification of F <sub>0</sub> F <sub>1</sub> -ATP synthase in H9c2 cells recapitulates the age-dependent alteration in OXPHOS deficiency and increases mPTP susceptibility.....	105
<b>5.7.1. Dicarbonyl stress does not alter GLO-I expression but induces MAGE accumulation</b> ..	105
<b>5.7.2. Dicarbonyl stress induces F<sub>0</sub>F<sub>1</sub>-ATP synthase modification</b> .....	108

5.7.3. Dicarbonyl stress reduces F <sub>0</sub> F <sub>1</sub> -ATP synthase dimerization .....	109
5.7.4. Increased MAGE accumulation does not affect F <sub>0</sub> F <sub>1</sub> -ATP synthase expression levels ..	110
5.7.5. Reduced F <sub>0</sub> F <sub>1</sub> -ATP synthase dimerization decreases the mitochondrial OXPHOS capacity .....	111
5.7.6. F <sub>0</sub> F <sub>1</sub> -ATP synthase dicarbonyl-induced modification does not alter its <i>in vitro</i> activity	112
5.7.7. Altered F <sub>0</sub> F <sub>1</sub> -ATP synthase dimerization increases the susceptibility to mPTP .....	113
5.7.8. Altered F <sub>0</sub> F <sub>1</sub> -ATP synthase dimerization reduces cell survival .....	114
5.7.8.1. Altered F <sub>0</sub> F <sub>1</sub> -ATP synthase dimerization increases spontaneous mPTP .....	114
5.7.8.2. Reduced F <sub>0</sub> F <sub>1</sub> -ATP synthase dimerization decreases cell viability .....	115
Summary of results: .....	1117
6. <i>Discussion</i> .....	1119
6.4. Dicarbonyl stress and protein damage in the aged myocardium .....	122
6.5. Aging increases dicarbonyl modification of mitochondrial F <sub>0</sub> F <sub>1</sub> -ATP synthase in the heart .....	124
6.6. Modification of F <sub>0</sub> F <sub>1</sub> -ATP synthase is associated with remodelled mitochondrial cristae secondary to its reduced dimerization .....	125
6.7. Defective F <sub>0</sub> F <sub>1</sub> -ATP synthase reduces mitochondrial energy efficiency .....	127
6.8. Glycation of F <sub>0</sub> F <sub>1</sub> -ATP synthase increases mPTP susceptibility .....	129
6.9. Induction of dicarbonyl stress in H9c2 cells simulates age-dependent changes in F <sub>0</sub> F <sub>1</sub> -ATP synthase .....	131
7. <i>Conclusion</i> .....	135
8. <i>Future Studies</i> .....	139
9. <i>Bibliographic References</i> .....	143



# *Summary*

---



Being the organ with the highest energetic demand of the entire biological system, the heart becomes especially vulnerable to diseases related to energetic deficiencies where mitochondria play a prominent role. During aging, the heart develops an energy supply/demand mismatch that underlies its reduced tolerance to exercise and stress, and the increased vulnerability to injury following ischemia/reperfusion, and to the onset of heart failure. The mitochondrial  $F_0F_1$ -ATP synthase plays a fundamental role in energy production in the heart (>90% of ATP) through oxidative phosphorylation and mitochondrial cristae morphogenesis. The spontaneous assembly of  $F_0F_1$ -ATP synthase monomers into dimers bend the inner membrane and build the cristae morphology; a mechanism that optimizes the energy efficiency and is essential for matching energy supply to demand. Recent evidences suggest that it may be the true molecular entity of the pathological mitochondrial permeability transition pore (mPTP), and proposed a model in which an alteration in its dimerization state induces pore opening. During aging, and due to its highly metabolic environment, the mitochondria become particularly susceptible to attack by dicarbonyl compounds that interact with positively charged amino acids causing irreversible structural and functional consequences in the target proteins.

Since  $F_0F_1$ -ATP synthase is rich in arginine residues that are highly susceptible to dicarbonyl attack, and since mitochondrial dysfunction is a hallmark of aging, this thesis hypothesized that the dicarbonyl-induced modification of  $F_0F_1$ -ATP synthase in aging can be the underlying cause for the age-associated energetic deficiency and the decreased tolerance to stress in cardiomyocytes. An age-dependent increase in dicarbonyl-modified proteins was found to particularly affect mitochondrial proteins as disclosed by a high throughput proteomics analysis of young (4-6 months) and old mice ( $\geq 20$  months) myocardium and by Western Blot analysis in isolated mitochondria. Importantly,  $F_0F_1$ -ATP synthase was identified as a prominent target of dicarbonyl attack during aging in several of its subunits as detected by proteomics in mouse myocardium, and corroborated by immunofluorescence co-localization and proximity ligation assay (PLA) in isolated mouse cardiomyocytes.

Because dicarbonyl-induced modifications can alter the structure and function of the target proteins, we evaluated the effect of  $F_0F_1$ -ATP synthase modification on its dimerization and on its enzymatic function. First, a significant reduction in  $F_0F_1$ -ATP synthase dimers and oligomers during aging was identified by BN-electrophoresis in solubilized IFM mitochondria and by PLA in permeabilized cardiomyocytes. A preserved expression of several  $F_0F_1$ -ATP synthase subunits detected by proteomics (myocardium), Western Blot (isolated mitochondria) and immunofluorescence (permeabilized cardiomyocytes) discarded changes in its abundance as the cause

## Summary

behind its decreased dimerization in aging. The decreased  $F_0F_1$ -ATP synthase dimerization was associated with a significant decline in the ADP-dependent mitochondrial respiration (state 3) in IFM of aged mouse hearts, a role which is directly coupled to  $F_0F_1$ -ATP synthase function and depends on the electron transport chain. The ATPase activity on the other hand, was found to be preserved during aging as demonstrated from in vitro analysis and from ATPase in gel activity in solubilized mitochondria. Since  $F_0F_1$ -ATP synthase was proposed to form the mPTP, we evaluated whether its increased modification in aging would increase the susceptibility to mPTP. Aging was associated with increased susceptibility to mPTP as a response to a ROS overload in isolated mouse cardiomyocytes.

Because  $F_0F_1$ -ATP synthase dimers play a role in cristae morphogenesis, which are intimately related to the mitochondrial bio-energetic function, we evaluated whether the age-dependent decrease in dimerization manifests in modification of mitochondrial ultrastructure. TEM images obtained from myocardium of young and old mice, revealed altered cristae morphology (less densely-packed with concentric onion-like organization) in addition to a significant decrease of cristae tip curvature affecting the mitochondria of the old mouse hearts.

The cause-effect relationship between  $F_0F_1$ -ATP synthase dicarbonyl-induced modification and the observed functional consequences were corroborated in H9c2 myoblasts in which an induction of dicarbonyl stress induced intracellular accumulation of dicarbonyl-modified proteins, and produced a modification of  $F_0F_1$ -ATP synthase, reduced its dimerization, and decreased its OXPHOS capacity. Similarly to what was observed in old mouse hearts,  $F_0F_1$ -ATP synthase dicarbonyl-induced modification was also associated with an increased susceptibility to mPTP and to cell death.

As a conclusion, this thesis provides a novel mechanism by which an altered dimerization of  $F_0F_1$ -ATP synthase secondary to its dicarbonyl-induced modification in aging produces pathophysiological consequences at the level of cristae morphogenesis, energy production and mPTP in the aged hearts.

# *Resumen*

---





Siendo el órgano con la mayor demanda energética de todo el sistema biológico, el corazón se vuelve especialmente vulnerable a enfermedades relacionadas con deficiencias energéticas donde las mitocondrias juegan un papel destacado. Durante el envejecimiento, el corazón desarrolla un desajuste entre la oferta y la demanda energética que subyace a su reducida tolerancia al ejercicio y al estrés, y a la mayor vulnerabilidad al daño provocado por la isquemia/reperfusión y al desarrollo de insuficiencia cardíaca. La  $F_0F_1$ -ATP sintasa mitocondrial juega un papel fundamental en la producción de energía en el corazón (> 90% de ATP) a través de la fosforilación oxidativa y la morfogénesis de las crestas mitocondriales. El ensamblaje espontáneo de los monómeros de la  $F_0F_1$ -ATP sintasa en dímeros dobla la membrana interna y construye la morfología de las crestas; un mecanismo que optimiza la eficiencia energética y es fundamental para ajustar la oferta energética a la demanda. Evidencias recientes sugieren que la  $F_0F_1$ -ATP sintasa puede ser la verdadera entidad molecular del patológico poro de transición de permeabilidad mitocondrial (mPTP), y se propuso un modelo en el que una alteración en su estado de dimerización induce la apertura del poro. Durante el envejecimiento, y debido a sus altas tasas metabólicas, las mitocondrias se vuelven particularmente susceptibles al ataque de compuestos dicarbonílicos que interactúan con aminoácidos cargados positivamente causando consecuencias estructurales y funcionales irreversibles en las proteínas diana.

Dado que la  $F_0F_1$ -ATP sintasa es rica en residuos de arginina que son altamente susceptibles al ataque dicarbonílico, y dado que la disfunción mitocondrial es un sello distintivo del envejecimiento, esta tesis planteó la hipótesis de que la modificación de la  $F_0F_1$ -ATP sintasa inducida por dicarbonilos en el envejecimiento, puede ser la causa subyacente a la deficiencia energética asociada a la edad y a la disminución de la tolerancia al estrés en los cardiomiocitos. Se ha visto un aumento dependiente de la edad en las proteínas modificadas por dicarbonilos que afectan particularmente a las proteínas mitocondriales, mediante un análisis proteómico de alto rendimiento en miocardio de ratones jóvenes (4-6 meses) y viejos ( $\geq 20$  meses) y mediante análisis de Western Blot en mitocondrias aisladas. La  $F_0F_1$ -ATP sintasa se identificó como un objetivo prominente del ataque por dicarbonilos durante el envejecimiento en varias de sus subunidades, según detectado por proteómica en el miocardio de ratón, y corroborado por colocalización por inmunofluorescencia y ensayo de ligadura de proximidad (PLA) en cardiomiocitos aislados de ratón.

Debido a que las modificaciones inducidas por dicarbonilos pueden alterar la estructura y la función de las proteínas diana, hemos evaluado el efecto de la modificación de la  $F_0F_1$ -ATP sintasa en su dimerización y en su función enzimática. En primer lugar, se identificó una reducción significativa en los dímeros y oligómeros de la  $F_0F_1$ -ATP sintasa durante el envejecimiento mediante

## Resumen

electroforesis BN en mitocondrias IFM solubilizadas y por PLA en cardiomiocitos permeabilizados. Una expresión preservada de varias subunidades de  $F_0F_1$ -ATP sintasa detectadas por proteómica (miocardio), Western Blot (mitocondrias aisladas) e inmunofluorescencia (cardiomiocitos permeabilizados) descartó que la causa de la disminución de la dimerización en el envejecimiento fuera debidos a cambios en su abundancia. La disminución de la dimerización de la  $F_0F_1$ -ATP sintasa se asoció con una disminución significativa en la respiración mitocondrial dependiente de ADP (estado 3) en IFM de corazones de ratón envejecidos; una función directamente acoplada a la función de  $F_0F_1$ -ATP sintasa y dependiente de la cadena de transporte de electrones. Por otro lado, se descubrió que la actividad de la ATPasa se mantiene preservada durante el envejecimiento, como se demostró a partir del análisis *in vitro* y en gel de la actividad de la ATPasa en mitocondrias solubilizadas. Dado que la  $F_0F_1$ -ATP sintasa se ha propuesto como la identidad que forma el mPTP, hemos evaluado si su modificación en el envejecimiento aumenta la susceptibilidad a mPTP. El envejecimiento se asoció a una mayor susceptibilidad a sufrir mPTP como respuesta a una sobrecarga de ROS en cardiomiocitos de ratón aislados.

Debido a que los dímeros de  $F_0F_1$ -ATP sintasa juegan un papel en la morfogénesis de las crestas, una estructura íntimamente relacionada con la función bioenergética mitocondrial, hemos evaluado si la disminución en la dimerización de la  $F_0F_1$ -ATP sintasa en la edad avanzada se manifiesta en la modificación de la ultra-estructura mitocondrial. Las imágenes TEM obtenidas a partir de miocardio de ratones jóvenes y viejos revelaron una morfología alterada de las crestas (empaquetadas con menos densidad y con una organización concéntrica similar a una cebolla) además de una disminución significativa de la curvatura de la punta de las crestas que afecta a las mitocondrias de los corazones de los ratones viejos.

La relación causa-efecto entre la modificación de la  $F_0F_1$ -ATP sintasa inducida por dicarbonilos y las consecuencias funcionales observadas, se corroboraron en mioblastos H9c2 en los que una inducción de estrés dicarbonílico indujo la acumulación intracelular de proteínas modificadas y produjo una modificación de la  $F_0F_1$ -ATP sintasa, redujo su dimerización y disminuyó su capacidad OXPHOS. De manera similar a lo que se observó en corazones de ratones viejos, la modificación de la  $F_0F_1$ -ATP sintasa inducida por dicarbonilo también se asoció con una mayor susceptibilidad a mPTP y a la muerte celular.

Como conclusión, esta tesis proporciona un mecanismo novedoso por el cual una dimerización alterada de la  $F_0F_1$ -ATP sintasa, como consecuencia de su modificación por dicarbonilos, produce efectos fisiopatológicos a nivel de morfogénesis de crestas, producción de energía y mPTP en corazones envejecidos.

# 1. *Introduction*

---



## 1.1 The Aging Heart and the Link between Dysfunctional Mitochondria and Cardiovascular Disease

Due to healthcare advancements in the last few decades, the average life expectancy has been on the rise and is expected to continue increasing rapidly within the coming years to result in a huge growth in the elderly population. In fact, and according to a UN study from 2017, by the year 2080, it is expected that the aging population (>65 years) exceeds that of the young population aged less than 15 years (Fig. 1). The current Covid-19 pandemic, however, seems to have influenced negatively on this trend of increased life expectancy<sup>1</sup> as it has led to premature death and lowered the life span by as much as 2.2 years for men in USA and to a lesser extent in women.

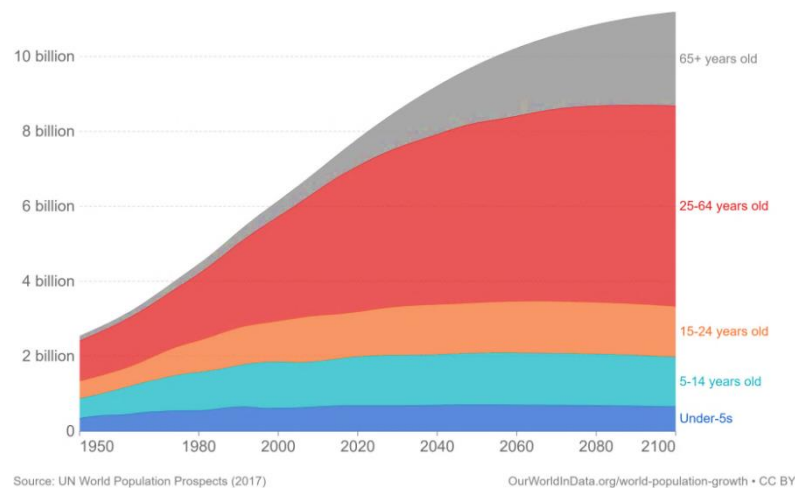


**Figure 1:** Total population by broad age group, with historical estimates from 1950 to 2015 and projections to 2100 based on the UN's medium population scenario from the *UN World Population Prospects 2017*.

Biologically, aging is defined as the time-dependent decline in physiological functions which increases the vulnerability of the organism to disease and the likelihood of death. Aging has long been known as an independent risk factor for the development of cardiovascular diseases (CVDs) and is the most important determinant of cardiovascular health. The growing elderly population therefore poses a continually increasing risk of CVDs<sup>2</sup> that have been (Fig. 2) and will continue to be the leading cause of death globally. However, many biological processes that occur in the heart during aging are still unknown, and hence it remains vital to understand why advanced age is such a critical component of the aetiology of CVDs. With the increased demographic shift towards an aging population worldwide, this matter has become of pressing urgency and even more now with the current Covid-19 infections that have been associated with increased cardiovascular complications<sup>3,4</sup>.

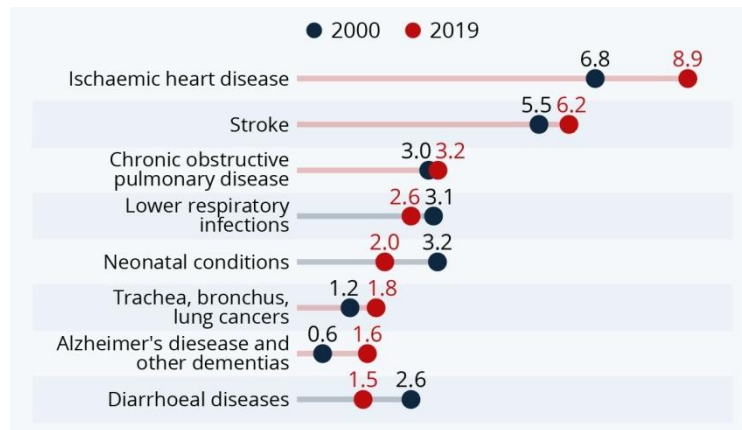


**Figure 2:** The world's leading causes of death comparison 2009 and 2019. Adapted from *World Health Organization 2020*

### 1.1.1. Characteristic of the aged heart

“The Heart”, the organ that is not allowed to go on vacation or to even take a brief pause, is essential for keeping us alive and is unique in many ways, especially that, in contrast to many other organs, it cannot be repaired or regenerated, and therefore, its long-term maintenance throughout our entire existence is crucial or otherwise its functional cessation produces death. Nevertheless, the cardiac tissue, like any other in a biological system, ages, and the aging heart accumulates many structural and functional changes that cause a general decline in its function, reduce its capacity to respond to increased work demand and stress, and decrease its threshold to develop CVDs all the while augmenting their severity.

The phenotypical changes of the aged heart are extremely diverse and complex, and affect different cardiac cellular types<sup>5</sup>, but are out of the scope of the current thesis which focuses on the aged cardiomyocyte in particular. Briefly, at the whole organ level, some of those alterations are seen as an increase in fibrosis and extracellular matrix remodelling, a decrease in the number of cardiomyocytes and an increase in their volume, contractile impairment, abnormalities in sympathetic modulation and electric conduction, endothelial dysfunction, vascular thickening and increased stiffness<sup>2,6,7</sup>. At the clinical level, all of these changes can be translated into an increased risk to develop arrhythmias, atherosclerosis, myocardial ischemia, increased systolic pressure, and are frequently associated with left ventricular afterload, reduced cardiac output and decreased heart rate<sup>5,8,9</sup>. The severity of those pathological factors can determine the occurrence of overt hypertension, thrombosis, stroke, coronary heart disease (myocardial infarction), peripheral vascular disease, and heart failure (HF), all of which are diseases with the highest occurrence in the elderly population<sup>5,8,9</sup>.

### 1.1.2. Molecular properties of the aged cardiomyocyte

At the cellular level, aging is characterized by nine different molecular hallmarks<sup>10</sup> whose mutual interrelation is object of intense research. These hallmarks are: (1) genomic instability, (2) telomere attrition, (3) epigenetic alterations, (4) loss of proteostasis, (5) deregulated nutrient-sensing, (6) mitochondrial dysfunction, (7) cellular senescence, (8) stem cell exhaustion, and (9) altered intracellular communication (Fig. 3). The contribution of each of these hallmarks to the overall aging phenotype largely depends on the cell type. The heart contains several types of cells, but up to 70% of its volume is occupied by the highly specialized contracting cardiomyocytes. The terminally differentiated cardiomyocytes are almost entirely dependent on mitochondria for their energetic needs, and undergo extremely limited to no proliferation<sup>11</sup> and therefore cannot be replenished neither can they segregate accumulated damage to daughter cells<sup>12</sup>. Therefore, in such a scenario, mitochondrial dysfunction (discussed in 1.3.) and loss of proteostasis are expected to have the most significant pathophysiological contribution to cardiomyocyte dysfunction during aging.

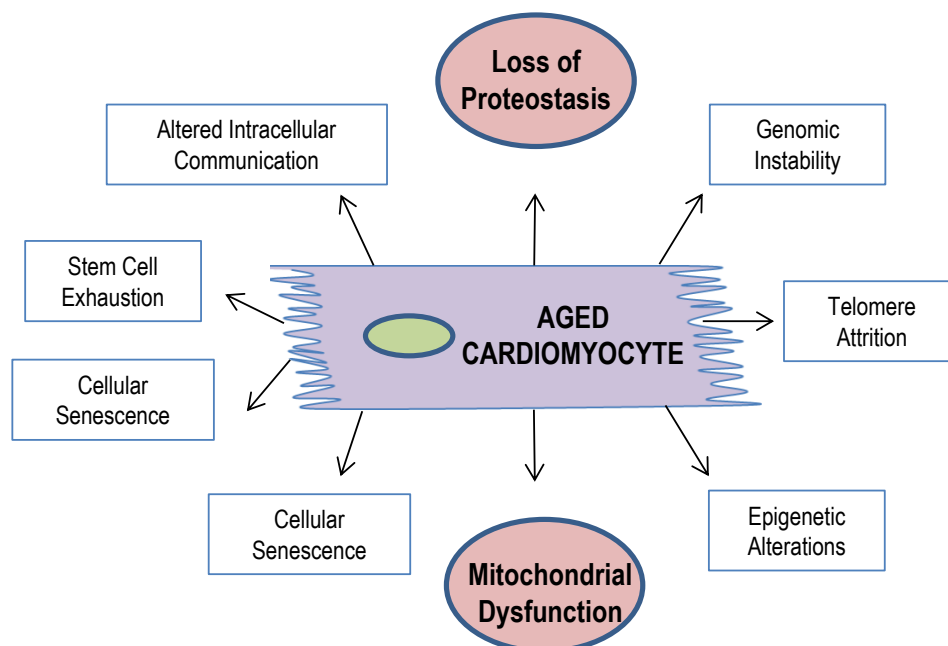


**Figure 3:** A schematic representation of the 9 hallmarks of aging with emphasis on the most relevant ones in cardiomyocyte aging.

Proteostasis (or protein homeostasis) refers to the whole set of cellular mechanisms implicated in the synthesis, folding, conformational stability, trafficking, assembly and turnover of proteins<sup>13</sup> and is therefore responsible for the maintenance of a healthy and functional proteome. Several mechanisms involved in proteostasis become defective in the aged cardiomyocytes, therefore contributing to the accumulation of dysfunctional proteins that pave the way towards a pathological setting<sup>14</sup>. First, the efficiency of the two main proteolytic systems (ubiquitin-



## Introduction

proteasome and lysosome-mediated pathway) declines during aging<sup>14,15</sup>. Apart from reduced proteolysis, other factors contribute to the aggravation of the overall quality of the proteome in aging including the age-dependent increase in dicarbonyl stress<sup>16</sup> and oxidative stress<sup>17</sup>. Dicarbonyl stress constitutes one of the most prominent causes of terminal protein damage and can along with oxidative stress increase the load of defective proteins and further overwhelm the proteostasis system<sup>24</sup>. This accumulation of post-translationally modified proteins is concomitant with reduced anti-oxidant mechanisms<sup>19</sup> in addition to a loss of efficiency of the glyoxalase system which detoxifies more than 90% of the most reactive dicarbonyl compounds<sup>20</sup> in the aged heart. These mechanisms facilitate the deposition of lipofuscin, granules formed of cross-linked and oxidized proteins, lipids and transition metals which are considered as a marker of cellular aging and disrupt cellular function<sup>21</sup>. The accumulation of defective proteins can consequently affect the homeostasis of the entire organ and may lead to a deteriorated cardiac performance.

### 1.1.3. Mitochondrial dysfunction in the aged cardiomyocytes

Due to the huge and uninterrupted energy demand of contracting cardiomyocytes and their almost exclusive dependence on mitochondrial energy production, these cells are particularly vulnerable to mitochondrial dysfunction and the latter plays a major role in many age-related cardiac diseases. Although the most recognized role of mitochondria is adenine triphosphate (ATP) production through oxidative phosphorylation (OXPHOS)<sup>22</sup>, they exert a plethora of other essential physiological roles including intracellular Ca<sup>2+</sup> buffering and homeostasis<sup>23</sup>, reactive oxygen species (ROS) production and signalling<sup>24</sup>, inter-organelle communication<sup>25</sup>, thermogenesis<sup>26</sup>, participation in several catabolic and anabolic pathways, and regulation of cell death and survival through several mechanisms<sup>27,28</sup>, including the opening of mitochondrial permeability transition pore (mPTP) which is of great relevance in ischemia/reperfusion (I/R) injury<sup>29</sup>.

In the healthy heart, one of the most essential components for normal mitochondrial function is mitochondrial Ca<sup>2+</sup> homeostasis. Mitochondrial Ca<sup>2+</sup> uptake after its release from the sarcoplasmic reticulum (SR) promotes energy production by activating Krebs' cycle dehydrogenases and electron transport chain (ETC) complexes activity<sup>30</sup>, and also regulates the regeneration of NAD(P)H which plays an antioxidant role<sup>31</sup>. In aging, mitochondria present abnormalities in the respiratory chain and OXPHOS<sup>25</sup>, in addition to Ca<sup>2+</sup> deregulation<sup>32,33</sup> both of which result in an increased mismatch between energy supply and demand<sup>34</sup>. Results from our lab have provided several mechanisms that may underlie this age-dependent mitochondrial functional decline. On the one hand, we have identified an altered SR-mitochondrial communication (decreased spatial proximity) in aged cardiomyocytes which was associated with defective inter-organelle Ca<sup>2+</sup>

transmission (Fig. 4), decreased NAD(P)H regeneration, and increased mitochondrial ROS production<sup>25</sup>. In an independent study, we identified a dicarbonyl modification of the ryanodine receptor (RyR) secondary to an age-dependent increase in dicarbonyl stress as the mechanism responsible for this altered  $\text{Ca}^{2+}$  handling; this promoted a chronic SR  $\text{Ca}^{2+}$  leak and led to intra-mitochondrial  $\text{Ca}^{2+}$  deposition that ultimately drives mitochondrial dysfunction<sup>20</sup>. We have also identified aging of the heart in humans to be associated with a decrease in the total mitochondrial pool and a decrease in mitochondrial respiration which can both decrease the energetic efficiency of the organelle<sup>20</sup>. Defective mitochondria in aging may also be demonstrated by the decreased threshold to develop mPTP following I/R in aged perfused hearts and isolated cardiomyocytes<sup>35</sup>.

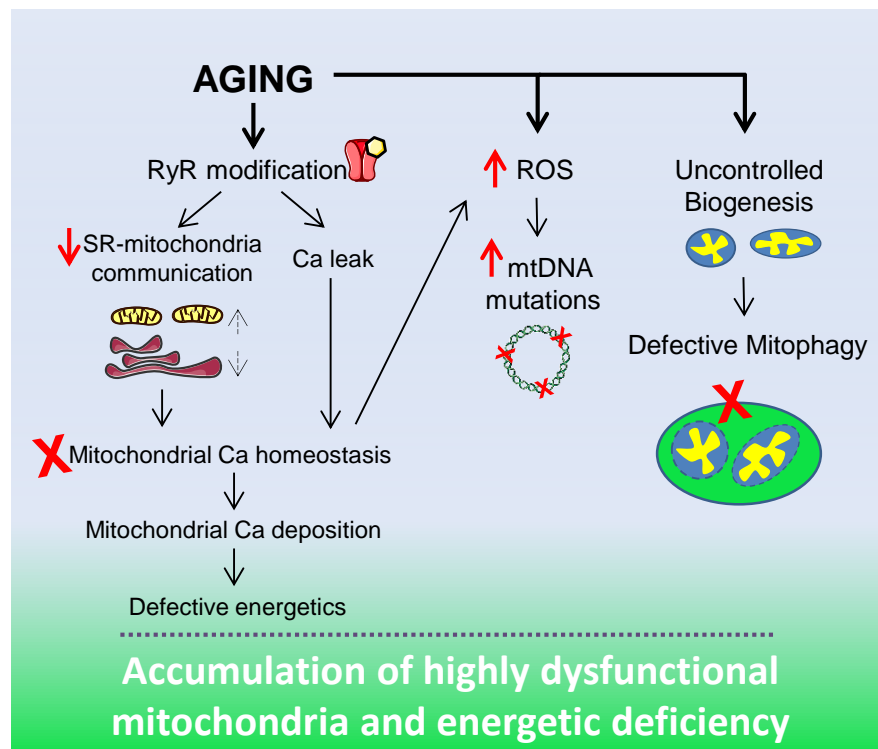


**Figure 4:** A schematic representation of some of the age-dependent mitochondrial alterations. Each of the disrupted SR-mitochondria communication, loss of  $\text{Ca}^{2+}$  homeostasis, increased ROS production and uncontrolled biogenesis may play an important role in the accumulation of dysfunctional mitochondria in aging.

Other age-associated mitochondrial alterations are uncontrolled mitochondrial biogenesis (fission and fusion)<sup>36</sup> and deregulation of the mitophagy pathway<sup>37</sup>, accumulation of mtDNA mutations<sup>38</sup>, and loss of structural integrity<sup>39</sup> which may destabilize the macromolecular organization of mitochondrial membranes. All of these simultaneous occurrences can lead to the persistence of dysfunctional mitochondria in the old heart, and can promote a vicious cycle that exacerbates organelle damage and dysfunction in aging and may exhibit complex and severe clinical manifestations in tissues that are highly dependent on their energy supply such as the heart.

#### 1.1.4. Mitochondria in I/R injury: Sentenced to death by mitochondria

When a coronary artery is obstructed with a thrombus, the myocardium becomes oxygen-deprived and this situation leads to rapid ATP deficiency and loss of ionic homeostasis<sup>40</sup>. While the reperfusion of the ischemic heart is the only therapeutic option to restore the oxygen to the ischemic area and to salvage the affected myocardium, abrupt normalization of blood flow may paradoxically precipitate cardiomyocyte damage and death (Fig. 5) by several mechanisms that have been extensively characterized in preclinical studies<sup>41</sup>. Mitochondria take center stage and play the protagonist role as the “decision-makers” that determine the destiny of cardiomyocytes in both ischemia and reperfusion.

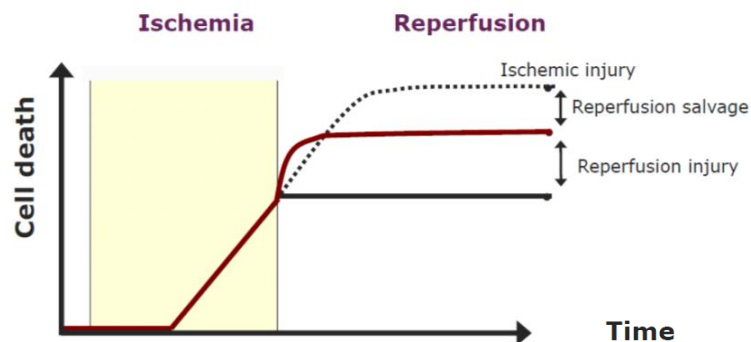


**Figure 5:** Illustration of cell death as a result of I/R injury. Cell death is produced during ischaemia proportionally to the time elapsed. Upon reperfusion, there is increased cell death that surpasses that theoretically obtained with ischemia during the same time period. Adapted from *García-Dorado et al.* 2005.

During ischemia, mitochondria cease to respire and from then on all the cellular mechanisms that can produce cell death become activated. First, the inhibition of mitochondrial respiration suppresses ATP production and causes energy exhaustion (Fig. 6), which is further aggravated by ATP hydrolysis due to the reversion of  $F_0F_1$ -ATP synthase into an ATPase<sup>42</sup>, a compensatory mechanism of mitochondria intended to re-establish the  $H^+$  gradient. This interruption of mitochondrial respiration is the mechanism that triggers the massive loss of ionic homeostasis that eventually determines the fate of the cells. In the first place, ATP exhaustion inhibits both the  $Na^+/K^+$  pump and the sarcoplasmic/endoplasmic reticulum ATPase (SERCA) therefore favouring the intracellular accumulation of  $Ca^{2+}$  according to the following sequence of events. First, the switch to anaerobic glycolysis upon oxygen deprivation leads to lactic acid production and acidifies the pH of the cell ( $pH < 7$ )<sup>43</sup>. To normalize the pH, the energy-independent sodium/hydrogen exchanger (NHE) becomes activated, but this consequently produces a cytosolic  $Na^+$  overload upon the import of  $Na^+$  in exchange with  $H^+$ . As a consequence, the  $Na^+/Ca^{2+}$  exchanger (NCX) reverses its mode of operation, extruding  $Na^+$  at the expense of cytosolic  $Ca^{2+}$  increase. This is when the control over one of the most

important cations in the heart,  $\text{Ca}^{2+}$ , which in physiological conditions is strictly regulated, becomes lost.

Once the blood flow to the coronary artery is re-established, the abrupt re-oxygenation of the heart and the rapid pH normalization set in motion a series of deleterious events, again orchestrated by the mitochondria, which eventually cause the so-called lethal reperfusion injury<sup>44</sup> (Fig. 6). The correction of the intracellular acidic pH worsens the cytosolic  $\text{Na}^+$  overload, and consequently produces an even greater increase in  $\text{Ca}^{2+}$  influx<sup>45</sup> which in turn triggers most of the mechanisms that drive cell death during the first minutes of reperfusion<sup>46</sup>. If OXPHOS resumes rapidly, the availability of ATP in the presence of this  $\text{Ca}^{2+}$  overload re-activates the SERCA leading to rapid SR  $\text{Ca}^{2+}$  oscillations which can impose an excessive mechanical force and precipitate cardiomyocyte hypercontraction (HC) and sarcolemmal disruption<sup>47</sup>. Moreover, the normalization of pH in the presence of excessive cytosolic  $\text{Ca}^{2+}$  can activate proteases such as calpains that degrade cellular components, including the cytoskeletal components that stabilize  $\text{Na}/\text{K}^+$  pump<sup>48</sup>. If OXPHOS recovers partially, the defective mitochondrial respiration can lead to a great increase in ROS production<sup>49</sup> which may lead to cell death by oxidative damage. Finally, both the  $\text{Ca}^{2+}$  deregulation (intra-mitochondrial  $\text{Ca}^{2+}$  overload) and the ROS accumulation can lead to mPTP<sup>46</sup> in which the mitochondria cannot recover at all, and the cell dies from extreme energetic collapse. Therefore, the degree and time-course of mitochondrial energy resumption during reperfusion is the main determinant of the survival or death of cardiomyocytes.

Opening of mPTP, a non-specific pore that allows the passage of molecules of up to 1.5 kDa at the normally highly selective and impermeable inner mitochondrial membrane (IMM), is a pathological response of mitochondria to a variety of triggers, the most important of which being increased  $\text{Ca}^{2+}$  and ROS levels<sup>50</sup>. It induces mitochondrial depolarization and OXPHOS uncoupling, therefore disrupting the mitochondria's capability to produce ATP<sup>29</sup>. In addition, upon pore opening the mitochondria releases its  $\text{Ca}^{2+}$  into the cytosol. This triggers  $\text{Ca}^{2+}$ -induced  $\text{Ca}^{2+}$  release (CICR) from adjacent mitochondria and aggravates the SR- $\text{Ca}^{2+}$  oscillations<sup>46</sup> which can produce lethal cardiomyocyte HC. mPTP is also associated with the release of mitochondrial ROS that can similarly induce ROS-induced ROS release (RIRR)<sup>51</sup> and provoke great molecular damage. Finally, the free entrance of solutes into the matrix also causes mitochondrial swelling where the matrix expands to a point that causes the rupture of the outer mitochondrial membrane (OMM) and hence irreparable mitochondrial damage and energy collapse occur.

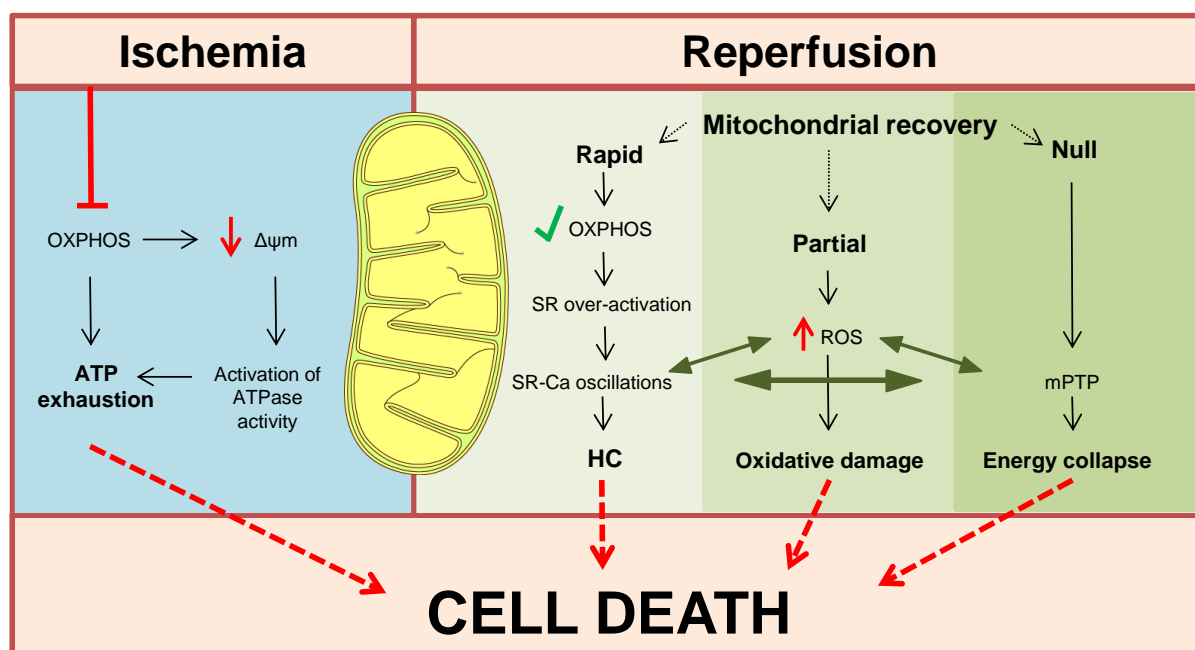


**Figure 6:** Graphical representation of the different mechanisms orchestrated by the mitochondria that lead to cell death during I/R injury.

### 1.1.5. Contribution of aging to mitochondria-induced cell death

Importantly, in experimental studies, there is a significant body of evidence demonstrating that aged hearts have a greater susceptibility to mPTP<sup>35,52,53</sup>. This might be one of the factors that lead to an increased infarct size in elderly patients that suffer from myocardial infarction. Not only does the incidence of myocardial infarction increase with age, but also hearts from old subjects suffer a greater extension of the necrotic area following I/R injury<sup>35,54</sup> which worsens their prognosis and quality of life, and decreases their survival on the long term. In addition, cardio-protective strategies such as pre- and post-conditioning that reduce cell death following I/R injury by activating a range of protective proteins and cell survival pathways, seem to offer little to no protection in old hearts when compared to young ones<sup>55</sup>. It is however, quite difficult to attribute the size of an infarct in elderly patients solely to their age, as the extension of the necrotic zone may be affected by the presence of other comorbidities and risk factors. For instance, in those patients that suffer from angina, this pathology seems to result in a smaller infarct size as it is thought to play a pre-conditioning role prior to the occurrence of a myocardial infarction<sup>56,57</sup>. Hyperglycemia and metabolic syndrome on the other hand are two co-morbidities that are associated with an increase in the infarct size<sup>58,59</sup>. Nevertheless, experiments in isolated organs (Langendorff-perfused hearts) in the absence of comorbidities and other extra-cardiac factors, demonstrate that the age of the animal is an independent determinant of infarct size and that advanced age increases cell death following I/R. In addition, I/R experiments performed in isolated cardiomyocytes where there is no

participation of extracellular matrix, vascular factors or other cell types also indicated that the cells from old animals had a lower intrinsic tolerance to I/R injury and developed higher rates of HC<sup>35</sup>.

Of note, increased infarct size can lead to higher risk of adverse myocardial remodelling on the long-term, which eventually favours the development of HF. Although HF, which has a particularly higher prevalence in elderly individuals, is a complex syndrome with multiple aetiologies, a decrement in bioenergetics seems to be central for the development and progression of this disease and this can be due to several co-existing factors that converge again at the mitochondria. To name a few, HF is associated with a variety of defects in several components of the phosphorylation apparatus<sup>60</sup>, decreased membrane potential<sup>61</sup>, a decrease in cellular phosphocreatine levels<sup>62</sup>, increased ROS formation<sup>63</sup> and a down-regulation of mitochondrial biogenesis<sup>64</sup>. Finally, HF is also characterized by a shifted metabolic substrate utilization where the heart relies more on glycolytic instead of fatty acid metabolism<sup>65,66</sup>, a metabolic pathway that is less efficient in ATP production. As a result, cardiac ATP is progressively depleted and the energetic deficiency in the aging heart persists, transforming the heart in an energy-compromised organ. Therefore, mitochondrial failure is a fundamental player in HF pathophysiology.

To conclude, with all that being said about the relationship between aging, mitochondrial dysfunction and the increased susceptibility to IR injury and HF, the question remains what are the factors that govern mitochondrial function and how does aging alter them? Is there any structural and/or chemical mitochondrial alteration specifically prevalent in aging that might be involved in their deteriorated performance and in their increased susceptibility in inducing cell death mechanisms (through mPTP) in the senescent heart? Let's take a look at mitochondrial structure and how the structure is essential to meet its function in chapter 2.

## 1.2. Mitochondrial Structure

The origin of mitochondria might be one of the most intriguing in biology, as the now established intracellular organelles present in almost each and every cell type of plants, animals and simpler organisms were originally bacteria that infected a cell and established a permanent symbiotic relationship with it<sup>67</sup>. The double membrane structure of the mitochondria indicates their endosymbiotic origin. They possess an OMM and the IMM separated by the inter-membrane space, while that restricted at the center within the IMM is known as the mitochondrial matrix (Fig. 7). The IMM harbours highly organized invaginations with a negative curvature that protrude into the mitochondrial matrix, the cristae. The sections of the IMM that run parallel to the OMM are known as the inner boundary membranes and the points of connection between the IBM and the cristae are known as the cristae junctions<sup>68,69</sup>.

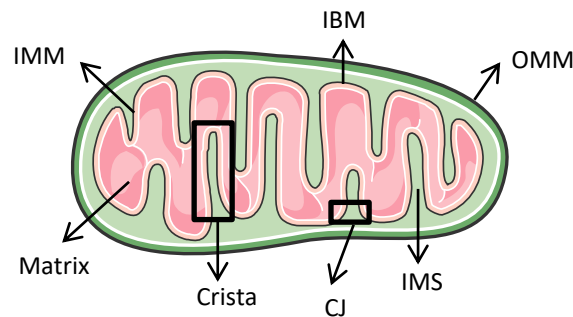


**Figure 7:** Schematic representation of mitochondrial architecture. The outer mitochondrial membrane (OMM), the inner mitochondrial membrane (IMM), the inter-membrane space (IMS), the crista, the cristae junctions (CJs), and the inner boundary membrane (IBM) are depicted.

The folding of the IMM massively increases the surface area onto which molecules with an energetic role can be incorporated and also create  $H^+$  traps at the most tightly folded areas (cristae tips) to facilitate energy production<sup>68</sup>. This hugely increases the energetic efficiency of the organelle and is what made complex multicellular life possible. This organelle has had and continues to have an immense impact on our evolution and has become one of the most essential for our survival. Mitochondria are exceptional organelles with very particular physical and functional characteristics that need to be highly regulated so they can meet their biological roles. These extremely complicated yet fascinating organelles constitute 30-40% of the total cardiomyocyte volume and are indispensable considering that a failure in their function is unequivocally translated into our demise. In fact, cardiomyocytes are the cells that contain the biggest number of mitochondria in the entire organism, and cardiac mitochondria particularly have the most highly folded and densely packed cristae of all cells.

### 1.2.1. Mitochondrial location determines its vulnerability to damage

The cytosol of cardiomyocytes is so dense with myofibrils that they create a cyto-structure that limits the mobility of mitochondria and separates them into distinct specialized subpopulations with specific functional and structural traits and different vulnerability to damage. The mitochondria located along the myofibrils are denominated the interfibrillar mitochondria (IFM), those that are in close contact with the cell membrane are the subsarcolemmal mitochondria (SSM) and the ones that lie around the nucleus are the perinuclear mitochondria (PNM)<sup>70</sup> (Fig. 8). The IFM are the most abundant type while SSM and PNM are less abundant.

The IFM are the most efficient in ATP production. They produce the energy required for myofibrillar contraction and have a prominent role in  $\text{Ca}^{2+}$  signalling, as they are in intimate contact with the SR. In fact, these two organelles lie 15 and 20nm<sup>71,72</sup> apart and are physically tethered at the level of the mitochondrial voltage-dependent anion channel (VDAC) and the sarcoplasmic RyR proteins<sup>25,73</sup>. This intimate connection facilitates inter-organelle cross-talk and creates a concentrated local  $\text{Ca}^{2+}$  micro-domain which allows the transfer of this cation from the SR to the mitochondria. This placement of the IFM in a highly energy demanding environment with constant exposure to  $\text{Ca}^{2+}$  from the SR makes the IFM more sensitive to the age-associated functional deteriorations. Indeed, several studies from different groups consistently demonstrated that IFM are the mitochondria that experience more pronounced changes in bioenergetics efficiency seen as a decreased mitochondrial respiration and oxidative capacity<sup>74,75</sup>. Importantly, chronic exposure to SR  $\text{Ca}^{2+}$  has also been demonstrated to induce matrix  $\text{Ca}^{2+}$  precipitation in the IFM during aging, both in mice and humans<sup>20</sup> a mechanism that has also been involved in the pathophysiology of HF<sup>76</sup>. Excessive matrix  $\text{Ca}^{2+}$  could be one of the mechanisms involved in mitochondrial damage and the reduced number of respiring mitochondria observed in the cardiac tissue of elderly patients<sup>20</sup>.

SSM function on the other hand, is probably related to energy production for ion channel function and since they aren't chronically exposed to  $\text{Ca}^{2+}$  as are the IFM, they are more sensitive to  $\text{Ca}^{2+}$  overload which lowers their threshold to I/R injury<sup>77</sup>. Also during aging, the SSM seem to have a greater contribution in the overall ROS production<sup>78</sup>. Finally, the PNM are the least studied and are thought to provide the energy required for gene transcription<sup>79</sup>. Nevertheless, the underlying cause between the differences in the specialized function of the different cardiac mitochondria is still unknown, neither is its relevance in the context of cardiac aging.



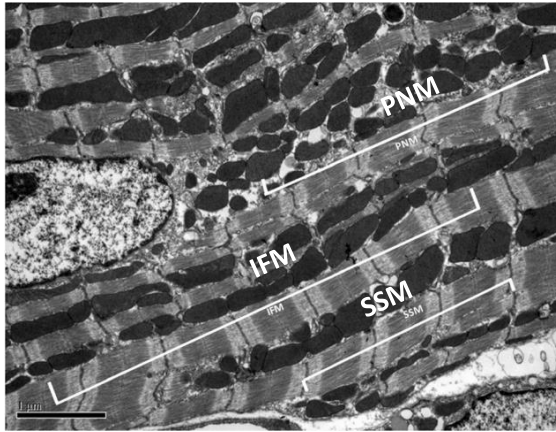


**Figure 8:** Electron transmission microscopy image depicting the different mitochondrial subpopulations in an adult cardiomyocyte. PNM: perinuclear, IFM: interfibrillar, SSM: subsarcolemmal. Adapted from Sang-Bing et al. 2017

### 1.2.2. The ugly side of mitochondria: Pathological cristae morphology

Mitochondrial function is intimately related to its structure; therefore, a pathological structural modification to any component of the outer or inner membranes may have deleterious and lethal consequences. In general, mitochondria have a lot of structural plasticity that allow them to adapt to the cell's energy status, the most important of which probably occur at the level of the cristae. Not only the shape, but also the size and number of cristae are constantly changing based on varying energy demands or other physiological signals. These adaptations include cristae narrowing and lengthening in starvation<sup>80,81</sup>, cristae widening in cell death<sup>82</sup>, and reversible changes from the *orthodox* state (low ADP levels) where cristae have a less dense matrix to the *condensed* state (high ADP levels) where cristae are enlarged and have a condensed matrix in response to an energetic demand<sup>83</sup>.

However, not all structural adaptations are physiological; rather some may be indicating the presence of a pathological state. Interestingly, in mice and humans with systolic HF<sup>84</sup>, mitochondria presented features indicative of mitochondrial damage, and these alterations were categorized from mild to severe. The earliest finding was the presence of onion-like mitochondria with concentric layers of IMM, and the damaged phenotype progressed to the dissolution of cristae in one or various zones (observed as areas where the cristae have lost their definition or as whitish cristae-free areas), until total cristae degeneration was observed. This degeneration finally culminated in mitochondrial swelling and the permeabilization of the IMM followed by OMM rupture. In another study, mitochondria with concentric onion-like cristae were also observed in aged rat hearts indicating a dysfunctional age-related structural alteration<sup>85</sup> (Fig. 9). A different pathological aspect of cristae morphology is the vesiculation of the IMM observed in several disease conditions<sup>86</sup> and in an aged model of yeast<sup>87</sup>.

Another example of altered cristae structure in disease conditions is seen in Leigh syndrome in which patients have profound disturbances of mitochondrial cristae ultrastructure and present

blunted instead of highly curved cristae tips<sup>88</sup>. While acutely curved cristae are suggested to concentrate protons, thereby maximizing the proton gradient that powers ATP synthesis, blunted cristae tips may not be as efficient in concentrating protons resulting in a decreased proton motive force, which may yield a lower respiratory capacity.

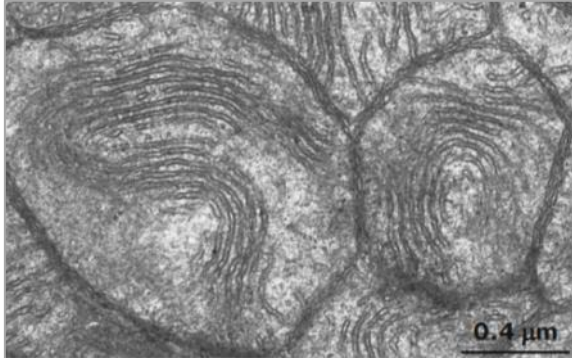


**Figure 9:** Electron microscopy image of mitochondria with concentric onion-like cristae arrangement from old rat heart, adapted from *El'darov et al.* 2015.

In conclusion, the proper organization and folding of the IMM determines the organelle's function while its deregulation is related to pathological conditions including cardiomyopathies, neurodegenerative disorders, metabolic diseases, and cancers<sup>84,89</sup>. These observations suggest a strict relationship between the modulation of cristae structure and the capability of the mitochondria to fulfil their function and therefore imply that mitochondrial function is governed by specific and determined IMM structures.

Importantly, one of the most important cristae modulators is the  $F_0F_1$ -ATP synthase predominantly enriched at the mitochondrial cristae apex. Spontaneous dimerization of  $F_0F_1$ -ATP synthase monomers into long row of dimers/oligomers is thought to be essential for bending the IMM into cristae invaginations<sup>69</sup> (discussed in detail in chapter 3). Other mitochondrial proteins participate in cristae shaping and maintenance, like the mitochondrial contact site and cristae organizing system (MICOS) and optic atrophy 1 (OPA1) which are primarily present at the CJs. MICOS, a large hetero-oligomeric protein, and OPA1, that has several pleiotropic functions, control CJ diameter and tightness and are essential to maintain the negative curvature at the cristae junctions<sup>81,82</sup> thereby sustaining a narrow cristae width<sup>90</sup> and stabilizing the respiratory complexes<sup>91</sup>. Importantly, the physical interaction between these three proteins has been demonstrated but the functional interplay remains elusive<sup>92,93</sup>. Finally, the strictly mitochondrial inhibitory factor 1 (IF1) is suggested to play an indirect role in cristae stabilization by sustaining the  $F_0F_1$ -ATP synthase in a dimerized form<sup>94,95</sup>.

## Introduction

To wrap up, very little to no evidence has been provided on the direct effect of aging on mitochondrial ultra-structural modifications in mammals and the consequences this may have on mitochondrial energy efficiency and vulnerability to damage in cardiac myocytes. Due to its fundamental role in mitochondrial cristae shaping and energy production, the  $F_0F_1$ -ATP synthase is postulated as an important player in cardiomyocyte aging. Therefore, let's take a look at the structure and function of  $F_0F_1$ -ATP synthase in chapters 3.

## 1.3. Mitochondrial F<sub>0</sub>F<sub>1</sub>-ATP Synthase

The F<sub>0</sub>F<sub>1</sub>-ATP synthase, also known as the mitochondrial ATP synthase or respiratory complex V is the universal bio-energetic molecular engine of aerobic life. This highly conserved molecule located at the IMM produces up to 95% of the total cellular energy in eukaryotic cells. It transforms the electrical power generated by the respiratory complexes (H<sup>+</sup> gradient) into energy-containing chemical power (ATP), following the chemiosmotic principle that governs the life of all eukaryotic organisms; a principle described by the Nobel prize award winner, the British biochemist Peter Mitchell in 1961. This nano-machine is an extremely efficient engine that can generate up to 10<sup>21</sup> molecules of ATP per second and is one of the most ubiquitous and abundant proteins on Earth. In fact, only a 30% residual activity of ATP synthase is required for normal physiological functions, and it is only when ATP synthase activity goes beneath this threshold that disease manifestations appear and metabolic remodelling occurs<sup>96</sup>.

Deficiency in F<sub>0</sub>F<sub>1</sub>-ATP synthase or other genes that affect complex V biogenesis or function usually manifest in very severe disease phenotypes such as NARP (Neuropathy, Ataxia, and Retinitis Pigmentosa), MILS (Maternally Inherited Leigh Syndrome) or FBSN (Familial Bilateral Striatal Necrosis) that arise from a functional or structural injury to F<sub>0</sub>F<sub>1</sub>-ATP synthase, usually present very early in life and often have fatal clinical outcomes<sup>97</sup>. The lethality associated with these mutations reinforces the importance of this molecule for our survival since an abnormal structure, expression or activity is ultimately incompatible with life. That said, the F<sub>0</sub>F<sub>1</sub>-ATP synthase may be considered one of the most essential proteins in an organ like the heart that has the highest energy demand of the entire organism and derives the absolute majority of its energy from mitochondrial OXPHOS on beat-to-beat basis.

### 1.3.1. The intricate structure of the F<sub>0</sub>F<sub>1</sub>-ATP synthase

The structure of the F<sub>0</sub>F<sub>1</sub>-ATP synthase may be one of the most complex in biology, as all its pieces have to fit perfectly together like a puzzle so it can successfully perform its function. This molecule consists of 17 different types of subunits, with different copy numbers per each, adding up to 28 total subunits (620 kDa per molecule). The structural identification of the F<sub>0</sub>F<sub>1</sub>-ATP synthase was made possible due to X-ray crystallography and cryo-electron microscopy studies and the first scientist to resolve its full structure in yeast was the British Chemist Sir John E. Walker who shared the Noble Prize with Paul D. Walker in 1997 for their work on mitochondrial ATP synthase: "the enzymatic mechanism underlying the synthesis of adenosine triphosphate (ATP)."

## Introduction

The  $F_0F_1$ -ATP synthase consists of a lipophilic  $F_0$  domain embedded in the IMM and an extra-membranous hydrophilic  $F_1$  domain that projects towards the mitochondrial matrix (Fig. 10.a.). The  $F_0$  domain is made up of a rotary proton turbine called the c-ring and a stator peripheral stalk, while the  $F_1$  domain is made up of a rotary central stalk and a stator catalytic headpiece, such that both  $F_0$  and  $F_1$  accommodate a dynamic and a fixed portion. The central and peripheral stalks are what connect the c-ring and the catalytic unit together<sup>98</sup>.

In humans, the c-ring has 8 copies of subunit c, although this number varies between 8 and 15 according to the species<sup>99</sup> (Fig. 10.b.). The  $F_0$  also contains a single copy of each of subunits a, b, d,  $F_6$ , oligomycin-sensitivity conferring protein (OSCP), e, f, g, A6L, diabetes-associated protein in insulin-sensitive tissue (DAPIT) and mammalian 6.8-kDa proteolipid (6.8PL). Subunits b, d,  $F_6$  and OSCP form the stator peripheral stalk of the  $F_0$  which lies to one side of the c-ring and extends from the IMM to the top of the catalytic headpiece of the  $F_1$  domain<sup>97</sup>. Subunits a, A6L and DAPIT also constitute part of the peripheral stalk, and lie next to the c-ring. Finally, subunits e and g which also lie to the side of the c-ring are indispensable for dimer  $F_0F_1$ -ATP synthase formation<sup>97,100</sup>.

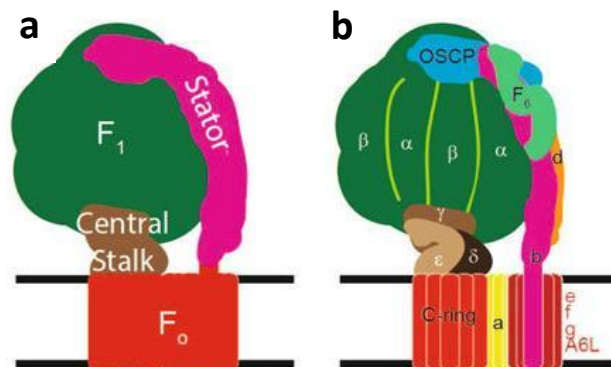


**Figure 10:** a) Schematic representation of the domains of an ATP synthase monomer being the  $F_0$  in orange, the  $F_1$  in green, the central stalk in brown and the peripheral stalk in pink. b) Schematic representation of the different subunits that make up the different domains of the mammalian ATP synthase. Adapted from *Beutner et al.* 2017.

The catalytic headpiece is a hexamer formed from 3 alpha ( $\alpha$ ) and 3 beta ( $\beta$ ) subunits that are organized in an alternating fashion, such that ATP synthesis occurs at the interface of  $\alpha$  and  $\beta$ . Finally, the central stalk consists of one copy of each of  $\gamma$ ,  $\delta$  and  $\epsilon$  subunits where the upper extremity of  $\gamma$  is found embedded in the core of the catalytic unit, while the lower extremity is in contact with the c-ring<sup>97</sup>.

### 1.3.2. The role of $F_0F_1$ -ATP synthase in producing the bio-energetic currency of life, ATP

The  $F_0F_1$ -ATP synthase is a dynamic enzyme that uses the electrical energy accumulated in the form of  $H^+$  gradient (at the inter-membrane space) to synthesize ATP from ADP (Fig. 11). Simply put, the energy dissipated when  $H^+$  ions return to the mitochondrial matrix is converted into a rotary energy by the  $F_0F_1$ -ATP synthase, and this rotary energy becomes coupled to conformational changes in the  $F_1$  domain allowing the synthesis of ATP to be successfully carried out<sup>101</sup>. Only in the healthy heart, the  $F_0F_1$ -ATP synthase generates up to 6kg/day of ATP. ATP synthesis is strictly dependent on the  $H^+$  gradient produced by complexes I, II, III and IV of the ETC and if this gradient becomes dissipated, ATP synthesis becomes inhibited.

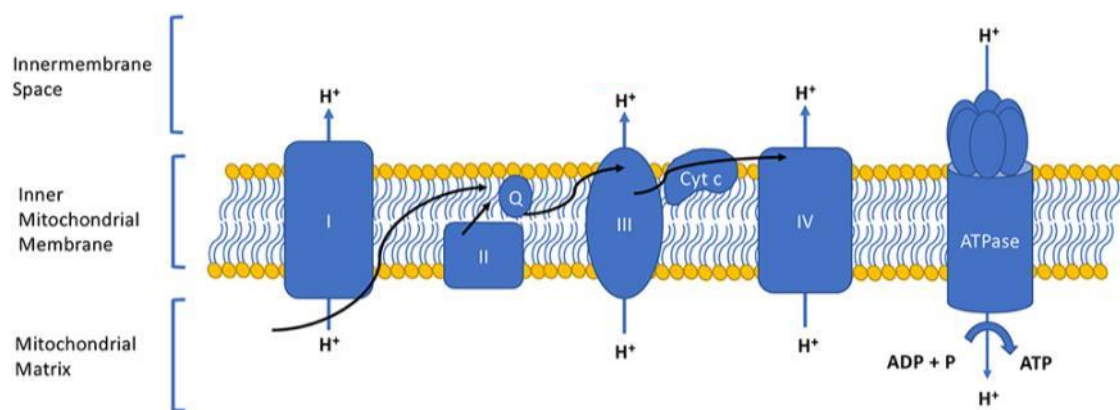


**Figure 11:** Schematic representation of the ETC complexes I, II, III and IV in addition to complex V ( $F_0F_1$ -ATP synthase). The electron chain complexes build the  $H^+$  gradient on the mitochondrial inter-membrane side while complex V dissipates it towards the matrix side while coupling it to ATP production. Adapted from *Elmore et al.* 2019.

To understand how ATP synthesis occurs, a closer look should be taken at the structure and the dynamics of the different subunits of the  $F_0F_1$ -ATP synthase. The highly conserved subunit a of the  $F_0$  domain has a U-like structure that wraps around the c-ring. It possesses two proton translocation offset half-channels, one open at the inter-membrane space side and the other at the matrix side. When a normal membrane potential is established (i.e. more protons on the inter-membrane space side),  $H^+$  enter complex V through the inter-membrane space side half-channel and are subsequently transferred to the c-ring to be finally released into the matrix by the matrix side half-channel, thereby dissipating against their electrochemical gradient<sup>99,102,103</sup>.

The collision and binding of a proton to a c-subunit causes the rotation of the c-ring as a result of Brownian motion, therefore transforming  $H^+$  flux into  $F_0$  rotation<sup>101,104</sup>. The rotation of the c-ring generates torque, which is a twisting force applied to the  $\gamma$ -subunit of the central stalk. Given that this structurally asymmetric  $\gamma$ -subunit is embedded at the core of the catalytic headpiece, its

## Introduction

rotation induces conformational changes in the catalytic unit that are essential for ATP synthesis<sup>99,105</sup>.

During  $\gamma$ -subunit rotation, each of the catalytic sites located in three  $\beta$ -subunits, adopts one of three conformational states that determine their binding capacity and occupancy, such that they either favour ADP and inorganic phosphate (Pi) binding, ATP formation or ATP release. This concept was first proposed by Paul D. Boyer in 1975 as a “binding change” mechanism and these conformations were denominated the “Boyer states” after him<sup>99,106</sup> (Fig. 12). Whenever the  $\gamma$ -subunit rotates  $120^\circ$ , one of the conformational states is produced<sup>105</sup>. Therefore, for every 8 protons translocated, i.e. for every complete c-ring rotation ( $360^\circ$ ), 3 ATP molecules are manufactured.

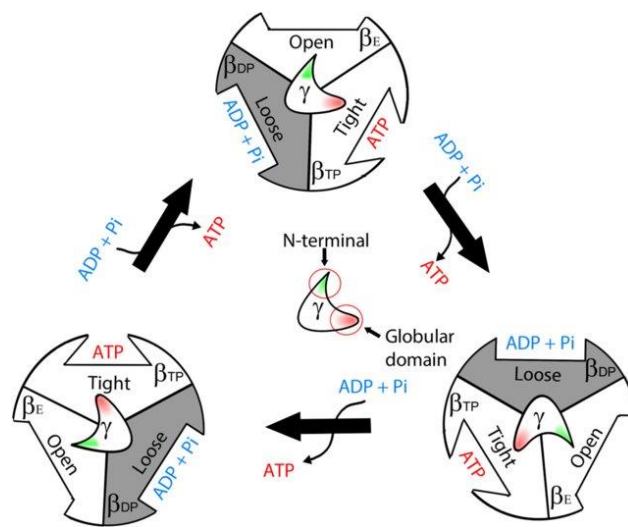


**Figure 12:** Model of the “binding change mechanism”. The conformational states adopted by the  $\beta$ -subunit upon  $\gamma$ -subunit rotation are depicted by the open, loose and tight conformations which are either empty, bind ADP and Pi, or ATP, respectively. Adapted from *Mendoza-Hoffmann et al.* 2018.

However, and importantly, for these conformational changes to occur, the rotation of the catalytic headpiece along with central stalk should be inhibited. This is achieved by the binding of the OSCP subunit of the peripheral stalk to the top of the catalytic headpiece, thereby anchoring it in place and counteracting its tendency to rotate along with the central stalk<sup>105</sup>. The correct positioning of the OSCP at the crown of the catalytic headpiece is what also allows ATP synthase to be sensitive to the bidirectional enzyme inhibitor oligomycin<sup>97,107</sup> because otherwise, c-ring rotation would be uncoupled from proton movement and ATP production in the first place. The other subunits of ATP synthase are required for structural support, stability, assembly and biogenesis.

This absolutely delicate interconnectivity among the different subunits and the intricate relationship between the ATP synthase architecture and function depicts how crucial the structural integrity of this nano-machine is for its capacity to meet the functional demands relayed upon it. Any

minor disruptions to the structure or conformation of  $F_0F_1$ -ATP synthase can result in a complete functional inhibition. Importantly, the decreased energetic capacity of mitochondria in aging and age-related CVDs may be attributed to an inefficient ATP synthase function, however, and due to the complete dependence of the enzyme on the  $H^+$  gradient constructed by the respiratory enzymes for ATP synthesis, it may be difficult to dissect the functional inefficiency of ATP synthase from an inefficiency in the ETC.

### **1.3.3. $F_0F_1$ -ATP synthase in ATP hydrolysis: What doesn't kill you doesn't necessarily make you stronger**

The mitochondrial  $F_0F_1$ -ATP synthase is a bidirectional enzyme that not only can produce ATP, but can also hydrolyse it under certain conditions. The normal mitochondrial membrane potential ( $\Delta\psi_m$ ) produced by oxidative reactions of the ETC enzymes is estimated at a negative 150-180mV with respect to the cytosol, and the maintenance of this  $\Delta\psi_m$  is vital for essentially all mitochondrial functions. Therefore, when  $\Delta\psi_m$  becomes dissipated and the ETC fails to rebuild it, the mitochondria must find another route to re-establish it. The  $F_0F_1$ -ATP synthase become activated in its reverse mode where it will consume ATP at the expense of re-establishing the  $\Delta\psi_m$ <sup>108</sup>.

Myocardial ischaemia and mutations that target the mitochondrial respiratory enzymes can both compromise the electrochemical gradient across the IMM and provoke the switch of enzyme function from ATP synthesis to hydrolysis<sup>97</sup>. When the enzyme function is reverted, the energy obtained from the hydrolysis of ATP into ADP and Pi at the catalytic  $\beta$ -subunit will be coupled to the pumping and the translocation of protons from the mitochondrial matrix to the mitochondrial inter-membrane space rather than from inter-membrane space towards the matrix which normally occurs during ATP synthesis, which consequently restores the electrochemical gradient<sup>108</sup> (Fig. 13).

Therefore, the direction of the c-ring rotation depends on the  $\Delta\psi_m$ , such that when the IMS is more positive as in normal physiological conditions, there is a higher probability of protons entering from the inter-membrane space half-channel and therefore ATP catalysis occurs, while when the matrix is more positive, i.e when the  $\Delta\psi_m$  is dissipated, there is higher probability of protons entering from the matrix half channel and therefore ATP hydrolysis occurs<sup>103</sup>.



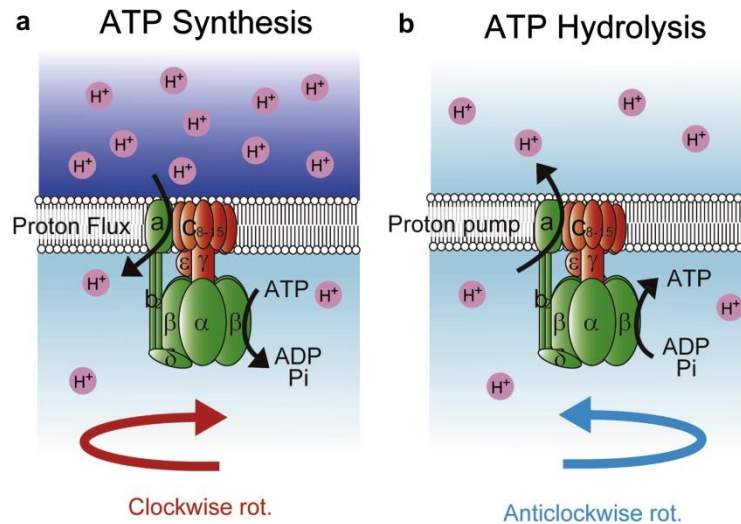


**Figure 13:** Illustration demonstrating the direction of rotation and of  $H^+$  translocation in ATP a) synthesis and b) hydrolysis. Adapted from *Watanabe et al.* 2013.

While hydrolysing ATP can salvage and reconstitute a dissipated  $H^+$  gradient in mitochondria, it accelerates energy exhaustion in cells that are already jeopardized by the lack of oxygen during anoxia or ischemia, further aggravating energetic deficiency. This paradoxical role of ATP synthase may represent a vestige of the endosymbiotic origin of mitochondria that try to reconstitute their  $H^+$  gradient at the expense of cell survival. Interestingly, a previous study from our lab has demonstrated that in the aged heart, there is a significant delay in the switching of  $F_0F_1$ -ATP synthase from ATP synthesis to hydrolysis which accelerates mitochondrial membrane depolarization during ischemia and results in a less efficient mitochondrial energy recovery upon reperfusion<sup>35</sup>. Therefore, ATP hydrolysis may play a harmful role although it is essential for re-establishing the  $H^+$  gradient.

The IF1 was initially described to play an inhibitory role on ATP hydrolysis by complex V at acidic conditions present during ischemia<sup>109</sup>. However, later it was discovered that IF1 can inhibit complex V in both its synthase and hydrolase forms<sup>110,111</sup>. It seems that under physiological conditions, a percentage of  $F_0F_1$ -ATP synthase remains blocked by IF1 and functions as a reservoir that becomes unblocked when there is increased energetic demand<sup>110</sup>. Interestingly, these tissues with high-energy demand, like the heart, have the highest content of IF1.

#### 1.3.4. The $F_0F_1$ -ATP synthase dimers bestow the IMM its structure

Recent evidences indicate that the self-association of  $F_0F_1$ -ATP synthase monomers into long rows of dimers shape the IMM of eukaryotic cells. The  $F_0F_1$ -ATP synthase can associate into dimers thanks to specific subunit-subunit interactions that produce the curvature of the IMM which is

responsible for the formation of the hallmark signature of mitochondrial morphology, the cristae (Fig. 14). For dimer formation subunits e and g are essential<sup>69,100,112</sup>; the disulphide bonds between e and g form an unusually shaped domain that bends the IMM, and bring together two adjacent monomers that ultimately establish direct contacts to form the V-shaped dimer. In mammals, the two e/g domains at the monomer/monomer interface bend the membrane at a 90° angle<sup>113</sup>. This V-shape created by the dimer allows the spontaneous back-to-back assembly of highly organized dimer rows or ribbons that extend for hundreds of nanometers along the rims of the invaginations of the IMM<sup>114,115</sup>. The dimers can further associate into tetramers and oligomers in which subunits e, g and DAPIT have a role in their formation<sup>95</sup>. Therefore, ATP synthase dimers are a cornerstone in cristae morphogenesis, and are essential to create the highly conserved IMM morphology. Allen was the first to propose this relationship between IMM invagination and F<sub>0</sub>F<sub>1</sub>-ATP synthase<sup>116</sup>.

Many studies have demonstrated that subunits e and g are indispensable for dimer formation, and that their depletion yields ultra-structural IMM modifications. While subunit e down-regulation reduces cristae number and leads to the formation of septate (interconnected) cristae with lesser tips<sup>117</sup>, the complete depletion of any of subunits e or g greatly alters IMM morphology and produces onion-link cristae with concentric layers of IMM<sup>69,100,112,118–121</sup>. Interestingly, in an aged yeast model, an age-dependent decline in F<sub>0</sub>F<sub>1</sub>-ATP synthase dimers and the concomitant increase in monomers were associated with the remodelling of the IMM ultrastructure and the appearance of vesiculated cristae<sup>87</sup>. The latter study demonstrated for the first time a relationship between an age-dependent decrease in F<sub>0</sub>F<sub>1</sub>-ATP synthase dimers and altered cristae morphology, although similar results in mammals still lack. Evidence on the relationship between cristae structure and function comes from experiments in which subunits e or g knockout significantly decreased mitochondrial respiration and membrane potential<sup>69,117,120–122</sup>. These results indicate a morpho-functional role of ATP synthase dimerization.

Importantly, the F<sub>0</sub>F<sub>1</sub>-ATP synthase monomer is a completely functional unit capable of ATP synthesis, however, the physiological association of the enzyme into dimers and oligomers plays both a structural and a functional role that contributes to a higher catalytic efficiency. First, the two monomers interact at an angle, which is thought to drive the membrane bending responsible for cristae formation and stability. This membrane conformation increases the surface area, allowing more layers of IMM to be stacked inside the mitochondria, and therefore permits the accommodation of more respiratory chain complexes and F<sub>0</sub>F<sub>1</sub>-ATP synthase molecules which consequently increase the OXPHOS capacity and renders the mitochondria more bio-energetically efficient. Second, the clusters of ATP synthase at the apex of the cristae form a proton trap, as seen



## 1.4. The Unresolved Puzzle of the mPTP Identity; F<sub>0</sub>F<sub>1</sub>-ATP Synthase as a Primary Suspect

The mPTP is a pore of the IMM which abruptly opens in response to mitochondrial Ca<sup>2+</sup> or ROS overload and that can precipitate cell death. Although it was first described by Haworth and Hunter in the 1950s, and despite its pathophysiological consequences being widely known and characterized, the identity of the molecular entity that forms the mPTP, initially known as the mitochondrial mega-channel (MMC), is still a matter of debate. Due to its harmful consequences on cell survival in several contexts, including myocardial I/R and neurological disorders, in the last years, much effort has been invested in trying to uncover the identity of this pore. Several studies have suggested that the F<sub>0</sub>F<sub>1</sub>-ATP synthase is the molecule that forms this energy-dissipating death hole although other models of mPTP involving other proteins also exist.

### 1.4.1. The pathophysiology of the mPTP death hole

Although the mPTP has been a hot topic of research for decades, it remains very ambiguous as neither its true molecular identity nor how its triggers and inhibitors interact and exert their effect are well understood. In the first place, two forms of mPTP are thought to exist. A physiological mPTP which opens only transiently and is thought to play an important role in relieving the mitochondrial Ca<sup>2+</sup> overload and mediate mitochondrial ROS signalling<sup>124</sup>, and a pathological mPTP which opens for an extended period of time and leads to grave lethal consequences. This second form is the one that has been extensively described in the context of reperfusion injury.

As previously discussed in detail in (chapter 1, section 1.4), the massive Ca<sup>2+</sup> and ROS overload produced in the first minutes of reperfusion are the most important triggers of mPTP. Briefly, the activation of mPTP opening can result in a sudden disruption of trans-membrane H<sup>+</sup> gradient, the interruption of OXPHOS, water diffusion, matrix swelling, and OMM rupture. These events can lead to cell death either upon the extreme energetic collapse produced or as a result of the intra-mitochondrial Ca<sup>2+</sup> release into the cytosol that exacerbates the cytosolic Ca<sup>2+</sup> oscillations and produces cardiomyocyte HC. Although mPTP and HC are interrelated, HC seems to produce more cell death after brief ischemic episodes while mPTP appears to be the main driver of cell death following a prolonged ischemic episode<sup>125</sup>. In fact, although mPTP is not the only mechanism responsible for cell death in reperfusion injury, it is thought to be one of the most important<sup>126,127</sup>; and importantly, aging seems to be an independent risk factor that increases the propensity of cardiomyocytes to develop mPTP<sup>35</sup>.

The pre- and post-conditioning strategies aimed to decrease myocardial infarct size are thought to work partially by inhibiting mPTP opening and therefore reducing the extension of cell death<sup>128-130</sup>. Apart from pre- and post-conditioning strategies, other interventions have been aimed to inhibit mPTP. One of the most commonly used pharmaceutical approaches is the cyclosporine A (CsA) which inhibits mPTP by interacting with cyclophilin D (CyP D), an mPTP channel modulator. Although many experimental studies provided evidence on the protective role of CsA<sup>131</sup>, the CIRCUS clinical trial in which CsA was tested in patients suffering a myocardial infarction, failed to demonstrate a clear reduction in infarct size<sup>132</sup>. In addition, the chronic use of this drug is not possible due to its adverse effects which include nephrotoxicity, hypertension, hyperlipidaemia, neurotoxicity, hepatotoxicity, among others<sup>131</sup>, although more recently a CsA specifically targeted to the mitochondria has been developed to avoid these toxic effects<sup>133</sup>. Another employed therapeutic strategy has been the acidic reperfusion of the heart to prolong the intracellular acidosis which blocks mPTP during the first few minutes of reperfusion<sup>134</sup>. To conclude, it is important to note that while the knowledge about the components of the mPTP is incomplete, it may be difficult to find an effective therapy that is effective enough in inhibiting mPTP regardless of the model (cells, animals, humans) being used. The last years have provided evidence on the role of mitochondrial  $F_0F_1$ -ATP synthase as the true molecular entity of the mPTP.

### **1.4.2. Mitochondrial ATP synthase plays God: “I give you life and I take it away from you”**

While the mitochondrial  $F_0F_1$ -ATP synthase produces the energy currency of life, there are many arguments and proofs that suggest a dual role for this molecule in cell death through the formation of the mPTP. Several models for the mPTP that involve different domains and/or subunits of  $F_0F_1$ -ATP synthase have been proposed, and the most interesting of all may be that describing an involvement of ATP synthase dimers in pore formation.

#### **1.4.2.1. Dimers of $F_0F_1$ -ATP synthase form the mPTP**

Bernardi's group has presented evidence on the implication of  $F_0F_1$ -ATP synthase dimers in the formation of the pore where purified dimers demonstrated channel activity with ionic currents and molecule permeability indistinguishable from that of mPTP while monomers didn't<sup>135,136</sup>. According to their proposed model (Fig. 15),  $Ca^{2+}$  binding at the  $\beta$ -subunit of the catalytic headpiece, induces structural changes that are translocated from the headpiece, through the lateral stalk (OSCP subunit), to the dimerization subunits e and g where the pore finally forms<sup>137</sup>. Further evidence on the role of ATP synthase dimers in the formation of the pore come from studies in which yeast knockouts for e and g subunits, significantly decreased  $Ca^{2+}$  sensitivity<sup>138</sup> and reduced the conductance of the formed channels<sup>121</sup>.

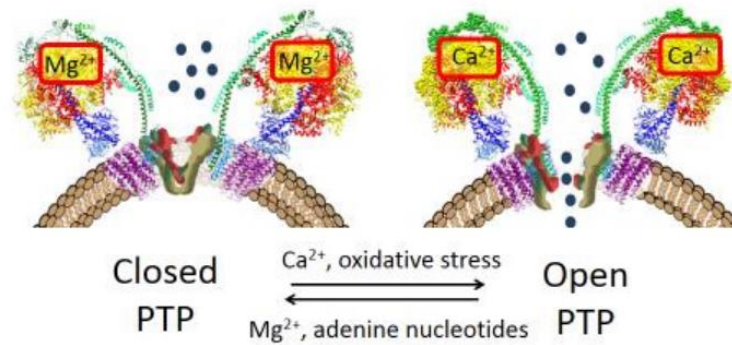


**Figure 15:** Model of mPTP involving ATP synthase dimers. In the presence of inhibitors ( $\text{Mg}^{2+}$  and adenine nucleotides), the PTP remains closed while in the presence of triggers ( $\text{Ca}^{2+}$  and oxidative stress), the PTP forms at the interface between two monomers that form the ATP synthase dimer. Adapted from *Giorgio et al.* 2017.

Work from Bonora et al. suggested that the dissociation of these dimers is what forms the pore, however his model implied an involvement of the c-ring<sup>139</sup>. This study demonstrated that exposure of mitochondria to  $\text{Ca}^{2+}$  increased the proportion of monomers to dimers, while dimer stabilization inhibited pore opening suggesting that the disassembly of these dimers is what triggers pore formation. These models are challenged by the study in which monomeric  $\text{F}_0\text{F}_1$ -ATP synthase presented channel activity<sup>140</sup>.

#### 1.4.2.2. The C-ring models of mPTP

Other authors<sup>141–143</sup> proposed a model in which the dissociation of the c-ring per se created the pore. According to this model, the exposure to triggers dislodges the c-ring from the  $\text{F}_1$  domain of the  $\text{F}_0\text{F}_1$ -ATP synthase, followed by the expansion and the dissociation of the c-ring where the pore forms (Fig. 16). In a model denominated the “death finger”, it is thought that the conformational changes in the  $\text{F}_0\text{F}_1$ -ATP synthase upon exposure to triggers modify the interaction between subunits e and 6.8PL creating a force that pulls at this lipid plug that occupies the core of the c-ring, therefore opening the pore at the center of the ring<sup>98</sup>.

However, the formation of the mPTP at the c-ring received many critics especially since early mPTP is a reversible mechanism, therefore, it is hard to think about the disassembly of the c-ring as a quick reversible process especially that, *in vitro*, very harsh conditions are required to dislodge and expulse the c-ring<sup>144</sup>. Also, opening of only a few c-rings may be sufficient to depolarize the entire mitochondria, as the conductance of this pore is larger than that normally documented for the mPTP. In addition, a knockout model of c-ring in cells was associated with the persistence of mPTP<sup>145</sup>.

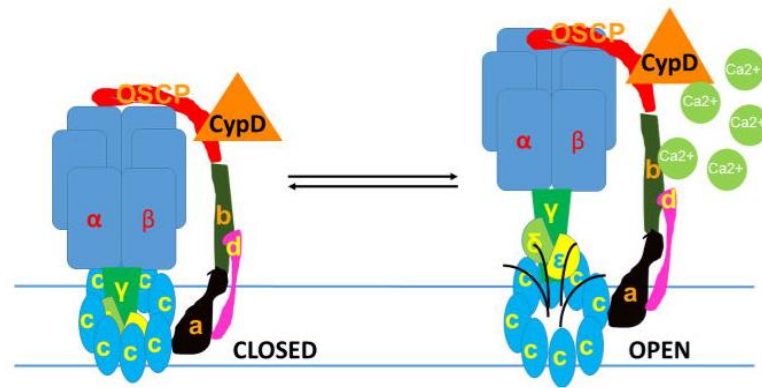


**Figure 16:** Model of mPTP involving ATP synthase c-ring. In the absence of triggers such as  $\text{Ca}^{2+}$  the c-ring remains tight and closed while in the presence of triggers such as  $\text{Ca}^{2+}$  the c-ring dissociates from the  $\text{F}_1$  producing the mPTP. Adapted from *Jonas et al.* 2015.

It is to mention that the genetic knockout of several  $\text{F}_0\text{F}_1$ -ATP synthase did not inhibit pore formation<sup>145–148</sup>. However, it should be noted that knockouts may modify the final structure and assembly of the ATP synthase which may be an important factor that influences the persistence of the pore even in the absence of the subunits suspected to form it. Yet, it is still very difficult to debunk the mitochondrial  $\text{F}_0\text{F}_1$ -ATP synthase as a primary candidate of the mPTP especially that many triggers and inhibitors of the latter directly bind to the  $\text{F}_0\text{F}_1$ -ATP synthase to induce their function. For instance,  $\text{Ca}^{2+}$ , one of the most important triggers of the mPTP binds to the  $\beta$ -subunit of the  $\text{F}_0\text{F}_1$ -ATP synthase<sup>149</sup>, and  $\text{H}^+$ , one of the most potent inhibitors of mPTP (acidic pH), binds and protonates a histidine on the OSCP-subunit to exert its inhibitory effect<sup>150</sup>. Also, the nucleotides ADP and AMP that inhibit channel opening both bind to the catalytic headpiece of  $\text{F}_0\text{F}_1$ -ATP synthase and constitute substrates for this enzyme<sup>135</sup>, while the pharmacological inducer Bz423 binds subunit OSCP<sup>151</sup>. Finally, the  $\text{F}_0\text{F}_1$ -ATP synthase interacts with other proteins (ANT, PiC) that were initially thought to form the pore before they were concluded to have a regulatory role.

#### 1.4.2.3. mPTP models involving other mitochondrial proteins

Halestrap suggested that the core components of the mitochondrial pore were constituted of the adenosine nucleotide translocase (ANT) and the phosphate carrier (PiC), and is triggered by cyclophilin D (Cyp-D) binding<sup>152</sup>. Another model suggested the involvement of the VDAC. However, while Cyp-D knockout mice were highly resistant to  $\text{Ca}^{2+}$ -induced mPTP<sup>153</sup> animal models lacking ANT<sup>154</sup>, VDAC<sup>155</sup>, or PiC<sup>156</sup> still developed a CsA-sensitive mPTP, therefore suggesting a regulatory role rather than an essential structural component of these proteins in pore formation. In another model, He and Lemasters proposed that misfolded and aggregated proteins of the mitochondrial membrane formed the pore<sup>157</sup>. However, this model does not explain the role of  $\text{Ca}^{2+}$  in inducing the pore, or its regulation by  $\Delta\psi_m$ , matrix pH and adenine nucleotides.

In conclusion, the only consensus in relation to the identity of the mPTP is that it is far from being discovered. The accumulated evidence may be pointing to the existence of several pores that may open simultaneously by the different triggers, which if true, complicates the pharmacological inhibition of this pore as different molecules instead of a single one must be targeted. What we know with certainty is that mPTP occurs with more frequency and relevance in the aged heart and it would be interesting to understand the mechanism behind this higher propensity to pore opening in advanced age. Could a post-translational modification be the responsible for this age-associated increase in the lethal mPTP? Let's take a look at the pathological consequences of dicarbonyl stress in aging in chapter 5.



## 1.5. Entropy and Terminal Protein Damage

Although our body is equipped with the necessary mechanisms to correct almost any possible biological error, the time-dependent loss of the efficiency of the repairing mechanisms underlies the progressive occurrence of molecular damage that eventually determines the aging phenotype. Repairing mechanisms are genetically-determined and have been evolutionarily selected to increase our fitness. It has been described that after the age of reproductive maturity, these mechanisms start to lose their strength and efficiency in all biological systems. By contrast, loss of molecular fidelity follows a random pattern and represents the direct consequence of the reduced activity of the repairing systems and the decreased turnover capacity. This trade-off between repairing systems and molecular damage is what ultimately determines our longevity as individuals and species. Since bio-energetic deficiency seems to be a hallmark of aging, and since energy is also a currency that needs to be paid so our systems maintain a functional status, mitochondria again seem to play an important role in favouring the failure of our systems in advanced age.

### 1.5.1. Entropy reigns in aging

For any given situation, the probability of disorder is always higher than that of order, of randomness higher than organization, of failure higher than success... This concept delineates the Second Law of Thermodynamics that governs the physical world and biological systems and describes the notion of entropy, where entropy is a measure of disorder. This tendency to fall into disorder increases with time, and entropy can only be reversed or halted by investing energy and effort into putting things back in their place.

How does this apply to a biological system? Live organisms represent a temporary challenge to the second law of thermodynamics and organize into highly structured and regulated systems at the expense of high energy consumption. Our bodies are equipped with boundless repair and maintenance mechanisms that expend a massive amount of energy into amending and reversing the effects of entropy on our system. However, since the efficiency of the repairing mechanisms declines with the passing of time<sup>158</sup> (Fig. 17), and since survival pathways and stress resistance pathways slow down significantly, our cells start to accumulate irreversible damage at the level of proteins, DNA, RNA which are the principle targets of molecular damage. Therefore, the net molecular entropy gradually but steadily increases with time and presents a mechanism that increases the likelihood of diseases and death and molecular damage becomes a natural and inevitable constituent of physiological aging. Moreover, since entropy is counteracted by energy, this again takes us back to

the mitochondria and in particular to the  $F_0F_1$ -ATP synthase, and points to the prominent role that energy deficiency may have in driving the aging process.

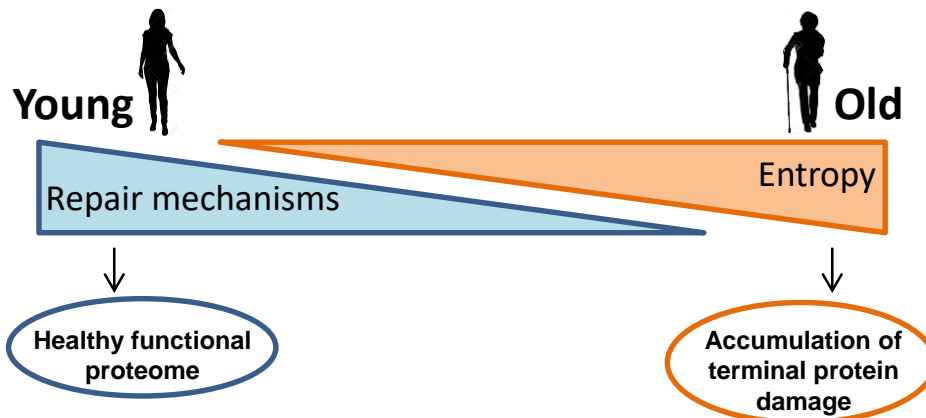


**Figure 17:** Illustration depicting the time-dependent decline from efficient repair mechanism and the shift towards entropy and loss of molecular fidelity.

### 1.5.2. Dicarbonyl stress as a prominent mechanism of age-related molecular damage

For the absolute majority of the modifications that can occur at the level of proteins, even when damaging, there usually exists an endogenous system that can reverse or remove them. The problem in aging lies in that the mechanisms that can impede the progression towards an irreparably damaged phenotype decline significantly, while damaging pathways become more active. One of the most prominent mechanisms that induce age-related molecular damage is dicarbonyl stress, in which cytotoxic by-products accumulate and react with proteins to render them irreversibly dysfunction, therefore facilitating the transition to a phenotype where molecular “chaos” predominates.

#### 1.5.2.1. Dicarbonyls and terminal protein damage

Dicarbonyl compounds are highly reactive and toxic by-products that arise from several endogenous metabolic pathways including glycolysis<sup>159,160</sup>, the catabolism of ketone bodies<sup>159,160</sup>, the pentose phosphate pathway, the polyol pathway<sup>161</sup>, lipid peroxidation, the degradation of Schiff bases, and the enolization of the Amadori products from the Maillard reaction<sup>162</sup>. The most important dicarbonyl products are methylglyoxal (MGO), glyoxal (GO) and 3-deoxyglucosone (3-DG) of which MGO is the most reactive and the most infamous for its cytotoxic and damaging effects<sup>160</sup>. If not properly eliminated, these compounds can accumulate and produce dicarbonyl stress which leads to grave pathological consequences upon initiating non-enzymatic chemical transformation of target proteins and other macromolecules that eventually lead to a complex and heterogeneous set of modified compounds collectively named as advanced glycation end products (AGEs). Unlike

oxidations<sup>163</sup>, phosphorylations<sup>164</sup>, acetylations<sup>165</sup> and other post-translational modifications (PTMs), these chemical reactions occur spontaneously, are irreversible and do not participate in the regulation of protein function. Dicarbonyl stress has been directly implicated in aging and disease<sup>16,166,167</sup>, while efficient dicarbonyl removal was associated with healthy aging<sup>168</sup>.

### 1.5.2.2. What makes dicarbonyls and the modification they produce pathogenic?

The cytotoxicity of dicarbonyl compounds is due to several factors including their extremely high reactivity and to the functional and structural consequences they produce upon modifying molecular targets among others. These compounds can react with positively charged amino acids (arginine and lysine in particular<sup>169-171</sup>) to produce terminally modified chemical compounds in a time frame as short as 24 hours<sup>172</sup>, and the immense reactivity of MGO is illustrated by up how to 99% of free MGO is bound to biological macromolecules<sup>161,173</sup>. The reaction usually involves condensation between a carbonyl group of a protein with the aldehyde group of MGO<sup>162</sup>. Dicarbonyls modify proteins by forming adducts or covalent cross-links that can yield irreversibly dysfunctional proteins as a consequence of the produced structural deformity in the native conformation and/or alteration in the functional unit of a protein (Fig. 18). Importantly, these modifications can fall in protein-protein, enzyme-substrate, receptor-antigen, or protein-DNA interaction sites<sup>174</sup> and ultimately cause the loss of biological function of the molecule in question. The pathological effects of these modifications may be more relevant on proteins that have a complex tertiary and quaternary structure. In addition, such protein modifications can cause protein denaturation and unfolding which facilitates their aggregation into highly cytotoxic, amorphous and insoluble aggregates known as lipofuscin<sup>175</sup> that accumulate in aging especially in non-dividing cells such as cardiomyocytes<sup>176</sup>.

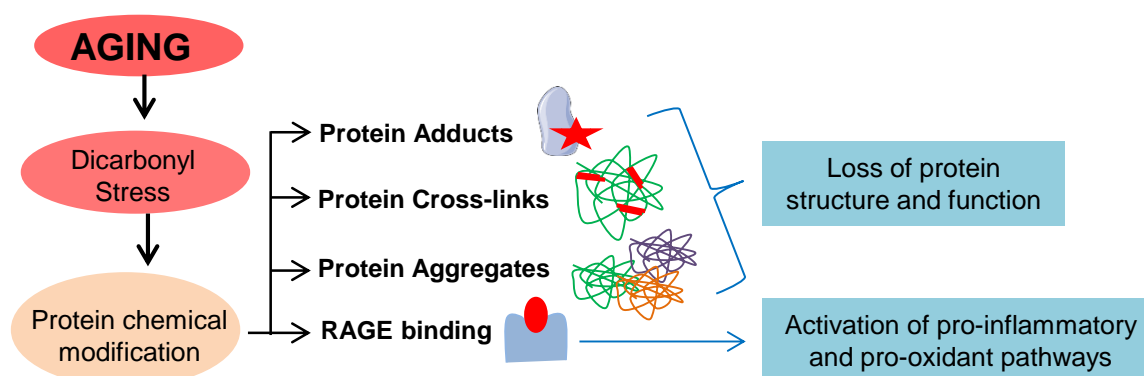


**Figure 18:** Scheme depicting the pathogenic mechanisms of non-enzymatic reactions in aging.

Adding to that, dicarbonyl compounds are membrane-permeable and can cross the plasma membrane to reach the extracellular space and even the plasma. Extra-cellularly formed dicarbonyl

adducts can react with a specific membrane receptor, the “receptor for advanced glycation end products” RAGE of the immunoglobulin superfamily, and activate a deleterious intracellular signalling cascade<sup>162</sup> which leads to a pro-inflammatory and pro-oxidant state<sup>160,177</sup>.

Finally, two more factors may contribute to the toxicity of these post-translational modifications. First, their irreversible nature and the absence of endogenous removal pathways favour their accumulation throughout time. Unfortunately, none of the drugs developed so far to reduce precursor availability (MGO quenching) or break down already formed dicarbonyl-induced modifications have proved sufficiently effective or safe. Among those drugs are aminoguanidine<sup>178</sup>, metformin<sup>159</sup>, carnosine<sup>179</sup>, pyridoxamine (PM)<sup>180</sup>, Rifampicin<sup>181</sup>, and Algebrum<sup>182,183</sup>. Second, the vast diversity and heterogeneity of these glycation products (Table 1) probably exerts an additive effect on their toxicity where our body is exposed to terminally damaged proteins of varying chemical properties and reactivities<sup>159,162,171,184</sup>.

**Table 1:** summarizes the most known and characterized dicarbonyl-derived AGEs.

MG-derived AGEs	G-derived AGEs	3-DG-derived AGEs
MG-H1	G-H1	3-DG-H1
MG-H2	G-H2	3-DG-H2
MG-H3	G-H3	3-DG-H3
Pentosidine	Pentosidine	Pentosidine
Carboxyethyllysine (CEL)	Carboxymethyllysine (CML)	Carboxymethyllysine (CML)
Carboxyethylarginine (CEA)	Carboxymethylarginine (CMA)	Pyrraline
Tetrahydropyrimidine (THP)	Carboxymethylcyteine (CMC)	Formyllysine
ArgPyrimidine	Carboxymethylorthinine (CMO)	DOGPIC
MODIC	GODIC	DOGDIC
MOLD	GOLD	DOLD
	GOLA	Lysyl-pyrrolypyridine

Over the last few decades, many studies have identified increased dicarbonyl stress-induced modifications in various tissues as a major causative mechanism for the development of many age-related diseases<sup>160,185</sup>. Neurological pathologies such as Alzheimer’s<sup>186</sup>, Parkinson’s and Huntington’s diseases<sup>187</sup>, and CVDs including atherosclerosis<sup>162</sup>, diabetic cardiomyopathy, myocardial dysfunction and HF<sup>20</sup>, in addition to other age-associated pathologies such as glaucoma<sup>188</sup> and kidney disease<sup>189</sup> have all been linked to the increased accumulation of those chemically modified proteins in the tissue.

### 1.5.2.3. The glyoxalase pathway

The glyoxalase-I (GLO-I) enzyme is a ubiquitously expressed and evolutionarily conserved cytosolic enzyme that exerts an essential role in the organism by detoxifying these highly reactive dicarbonyls. It is responsible for the elimination of more than 99% of MGO and can also detoxify GO. The extreme efficiency of the GLO system makes the function of other dicarbonyl detoxification pathways including the NADPH-dependent aldo-keto reductases (AKR)<sup>160,162</sup> and aldehyde dehydrogenases (ALDH)<sup>159</sup> negligible. Importantly, and to our knowledge, there is no viable model of GLO-I knockout because an organism that completely lacks GLO-1 is incompatible with life. In fact studies in *C. elegans*<sup>190,191</sup> have linked GLO-I to longevity, where genetic knockdown of the gene shortened lifespan while its induction prolonged it. Unfortunately, deficiency of GLO-1 system has been demonstrated in aging<sup>20,192</sup>, and has been related to the development of many age-related diseases. Our group has recently demonstrated that although GLO-1 expression remained preserved in the aged heart of humans and mice, its activity declines significantly in advanced age<sup>20</sup>. The deficiency in the GLO-1 system was identified as the cause behind the increased accumulation of terminally modified proteins in the aged myocardium of both humans and mice.

The GLO system comprises two enzymes: the rate-limiting GLO-I and GLO-II with glutathione (GSH) as a cofactor<sup>159</sup>. In the first step of this reaction, GSH reacts with MGO to produce a hemithioacetal which is then converted into S-D-lactoylglutathione by GLO-I (Fig. 19). This intermediate is consequently converted into the non-toxic metabolite D-lactate by GLO-II in a second reaction<sup>161</sup>. Although S-D-lactoylglutathione is a non-toxic metabolite, its conversion into D-lactate is essential for recycling the cofactor and anti-oxidant GSH whose bioavailability may otherwise be compromised<sup>161</sup>. The GLO system is the major detoxification pathway for GO as well, and converts it into glycolate.

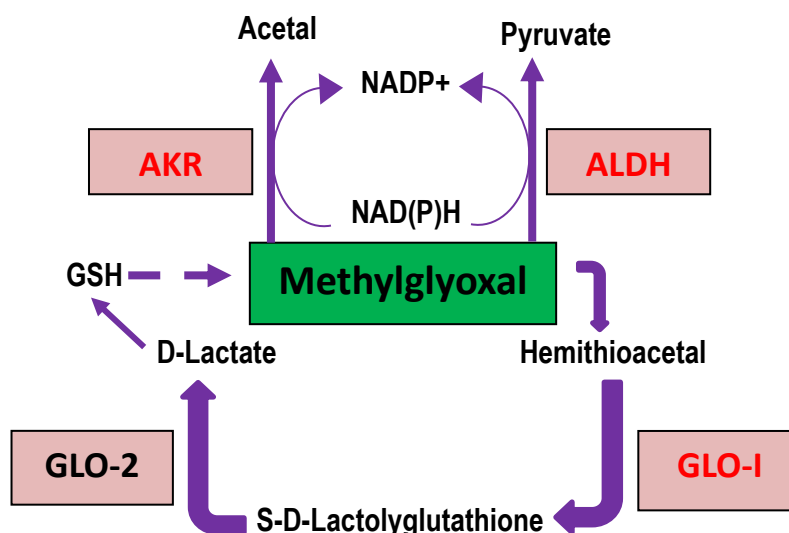


**Figure 19:** Schematic representation of the GLO-I, AKR, and ALDH pathways for the elimination of MGO.

### 1.5.3. Aging transforms mitochondria into a hub of molecular damage

Although there is a global increase in molecular damage during aging, mitochondria confer an environment which facilitates their targeting by pernicious molecules such as dicarbonyl compounds and thereby transform into hubs of molecular damage in advanced age. In the first place, mitochondria have an extremely high metabolic activity which can generate reactive intermediates such as ROS. On the one hand, ROS can be directly implicated in mitochondrial dysfunction secondary to direct molecular oxidative damage, however, ROS can also be involved in the increased chemical transformation of proteins mediated by dicarbonyl compounds, especially that several of these final modified products require an oxidation step during their formation<sup>193</sup>. Importantly, the increased lipid peroxidation of mitochondrial membranes by ROS in aging may be an important source for the generation of mitochondrial MGO and GO<sup>194</sup> which consequently react with and modify proteins. In fact, whether produced inside the mitochondria or diffused from the cytosol, mitochondria are able to accumulate both MGO and GO<sup>195</sup> and have been previously described to be important targets of dicarbonyl-induced chemical modifications<sup>196,197</sup>. The decreased GLO-I efficiency in the aged heart<sup>20</sup> may be another mechanism that favours the diffusion of the accumulated non-detoxified dicarbonyl compounds into the mitochondria as well. In fact, dicarbonyl targeting of non-mitochondrial proteins may also end up altering mitochondrial function. Our group has demonstrated that in the aged heart, increased dicarbonyl stress that arises partly as a consequence of a deficient GLO-I deficiency can lead to the modification of the RyR receptor. The latter becomes leaky, thereby exposing mitochondria chronically to an increased Ca<sup>2+</sup> load. This defect in the RyR gating properties leads to the accumulation of intra-mitochondrial Ca<sup>2+</sup> that can ultimately affect its energetic function and favour the development of HF<sup>20</sup>. Last but not least, mitochondria lack an intra-mitochondrial GLO system that can detoxify the toxic dicarbonyl intermediates which facilitates their accumulation and makes their reaction with mitochondrial proteins more probable. The increased oxidative stress in aging<sup>19</sup> and the parallel decrease in antioxidant mechanisms<sup>20</sup> in addition to the increased dicarbonyl stress and the consequent accumulation of dicarbonyl-modified proteins produce a harmful positive feedback loop that favours the accumulation of molecular damage in mitochondrial proteins in particular<sup>193,198,199</sup>.

Importantly, recently, several studies have described a mechanism in which defective cytosolic proteins become transported into the mitochondria for their proteolysis, a process denominated as mitochondria-associated proteostasis<sup>200,201</sup>. Taking into consideration the overall decrease in proteostasis in aging<sup>55</sup>, this mechanism may increase the accumulation of dysfunctional proteins intra-mitochondrially and exacerbate organelle damage.

## Introduction

Taking all the above into consideration, it would not come as a surprise if some mitochondrial proteins with a vital role could be a target of these molecular damages in aging. Importantly, the  $F_0F_1$ -ATP synthase contains many positively charged amino acids that can be targeted by reactive dicarbonyls, and has an essential function that is intimately related to its tertiary and quaternary structure (dimers and oligomers). Since the bioenergetic efficiency of mitochondria decreases with aging, and since  $F_0F_1$ -ATP synthase is found at a location which favours molecular damage at the IMM, we wonder whether it could be an important target of dicarbonyl damage in aging.

## 2. Hypothesis

---









The heart develops an energy supply/demand mismatch during aging that underlies its reduced tolerance to exercise and stress, the severity of which determines the onset of HF and may be involved in the increased death of aged cardiomyocytes after I/R injury. The mitochondrial  $F_0F_1$ -ATP synthase plays a fundamental role in energy production in the heart (>90% of ATP) through OXPHOS and mitochondrial cristae morphogenesis, and recent evidences suggest that it may be the true molecular entity of mPTP, precipitating energy collapse and cell death under certain pathological conditions. Dicarbonyl compounds accumulate in the aged cardiomyocytes, are particularly reactive in mitochondria, and tend to interact with proteins that are rich in positively charged amino acids, inducing deleterious structural and functional consequences.

**Hypothesis:**

Because cardiac  $F_0F_1$ -ATP synthase is an abundant protein with multiple positively charged amino acids and a very complex structure, the present thesis hypothesized that it could be a molecular target of dicarbonyl compounds during aging. The chemical modification of  $F_0F_1$ -ATP synthase as a consequence of the dicarbonyl attack would have deleterious consequences on the ultra-structure and the bio-energetic function of mitochondria that would ultimately reduce its energetic efficiency and increase the susceptibility of the cells to mPTP in response to stress.



### 3. Objectives

---









**Objectives:**

The main objective of the present thesis is to evaluate whether the  $F_0F_1$ -ATP synthase is a target of dicarbonyl damage in cardiomyocytes during aging and the consequences this may have on the structure and the bioenergetic function of the mitochondria.

Our secondary objectives are:

1. Evaluate the accumulation, distribution, types and targets of dicarbonyl-induced protein modifications in myocardial proteins during aging using proteomic analysis.
2. Explore whether the mitochondrial  $F_0F_1$ -ATP synthase constitutes a target of dicarbonyl damage in aging by applying immunological techniques and proteomics analysis.
3. Investigate whether a dicarbonyl attack on  $F_0F_1$ -ATP synthase may have functional consequences on mitochondrial bioenergetics (respiration, ATPase activity, mPTP susceptibility) and/or on mitochondrial ultrastructure (TEM).
4. Establish a model that can prove the cause-effect relationship between increased dicarbonyl modification of  $F_0F_1$ -ATP synthase, if present, and the observed functional decline observed in aging.







## *4. Materials and Methods*

---



## **4.1. Biological Models**

The results of this thesis were obtained from myocardial tissue, isolated adult cardiomyocytes and isolated mitochondria from mouse hearts and from rat myocyte cell line H9c2. All procedures on animals were approved by the Ethical Committee of the Vall d'Hebron Research Institute (reference number CEEA 53/20) and were conducted in accordance with the EU directive 2010/63EU and Spanish transposition RD 53/2013 on protection of animals for scientific purposes.

### **MOUSE MYOCARDIUM**

The mice were euthanized with an intra-peritoneal injection of 0.3-0.4mL sodium pentobarbital (150 mg/Kg). Myocardium, cardiomyocytes and mitochondria were obtained from young (5-6 months) and old ( $\geq 20$  months) C57BL/6J mice.

#### Myocardial homogenates

Myocardial homogenates were used for the mass spectrometry study. Protein extracts were obtained by heart tissue homogenization with ceramic beads (MagNa Lyser Green Beads apparatus, Roche, Germany) in extraction buffer (50mmol/L Tris-HCl, 1mmol/L EDTA, 1.5% SDS, pH 8.5) (see below).

#### Isolation of adult mouse cardiomyocytes

Calcium tolerant rod-shaped cardiomyocytes from young and old mice were isolated by retrograde perfusion of the heart in a Langendorff system. The heart was rapidly excised and transferred into cold physiological serum to remove excess blood, cannulated through the aorta in the Langendorff system and washed with a calcium-free modified Krebs buffer containing (in mmol/L): NaCl 100, HEPES sodium salt 10, MgSO<sub>4</sub> 1.2, KH<sub>2</sub>PO<sub>4</sub> 1.3, KCl 2.6, glucose 11, and 2,3-butanedione monoxime 10 (BDM) to prevent contraction, pH 7.3, at 37°C. The aorta was cannulated just below the aortic arch where the subclavian, carotid and brachiocephalic ramifications are present, but not too deep, to avoid penetrating the ventricle with the cannula. The filling of coronary vessels with the Krebs solution induces the swelling of the myocardium and is indicative of proper aortic cannulation. A concentration of 0.03% of type II collagenase (Worthington, LS004176) with 15  $\mu$ mol/L of calcium were added to 80mL of Krebs buffer, and the heart was perfused during 15 min at an approximate rate of 1 drop/s to allow the digestion of the extracellular matrix and the disruption of cell-to-cell connections. After 15 min, the heart, which should have a lighter color and a very soft texture due to tissue digestion, was withdrawn from the cannula, the atria removed and the ventricles cut into small pieces and then minced as finely as possible with a scalpel. The digested tissue was placed in a



## Materials and Methods

plastic container and incubated with Krebs buffer containing collagenase for an additional 10 min at 37°C. During this time, the solution was pipetted up and down to help disaggregate the tissue.

The digested tissue was then filtered through a nylon mesh with 180µm pore, and centrifuged at 25xg for 3 min at room temperature. The supernatant containing endothelial cells and fibroblasts was discarded, and the pellet (rich in cardiomyocytes) was subjected to a gradual normalization of calcium concentration up to 1 mmol/L to specifically select calcium-tolerant cardiomyocytes. For this purpose, the pellet was resuspended in Krebs buffer with 125 µmol/L of calcium and centrifuged again 3 times (25xg, 2 min). After each centrifugation, the supernatant was discarded and an increasing concentration of calcium (125 µmol/L, 200 µmol/L and 1 mmol/L) was added to the pellet. During the isolation protocol, the calcium is added gradually to avoid calcium-induced hypercontracture, a pathological response that is triggered in cardiomyocytes previously depleted of calcium (“the calcium paradox”). The final pellet rich in rod-shaped calcium-tolerant cardiomyocytes was resuspended in M199 medium supplemented with 4% fetal bovine serum (FBS) and seeded in wells pre-coated with 5% laminin. About 30min after plating, round non-attached cells were discarded by changing the medium. Only when the initial yield of rod-shaped cardiomyocytes was ≥50%, preparations were considered suitable for experiments. Experiments were performed within the next few hours after cell isolation.

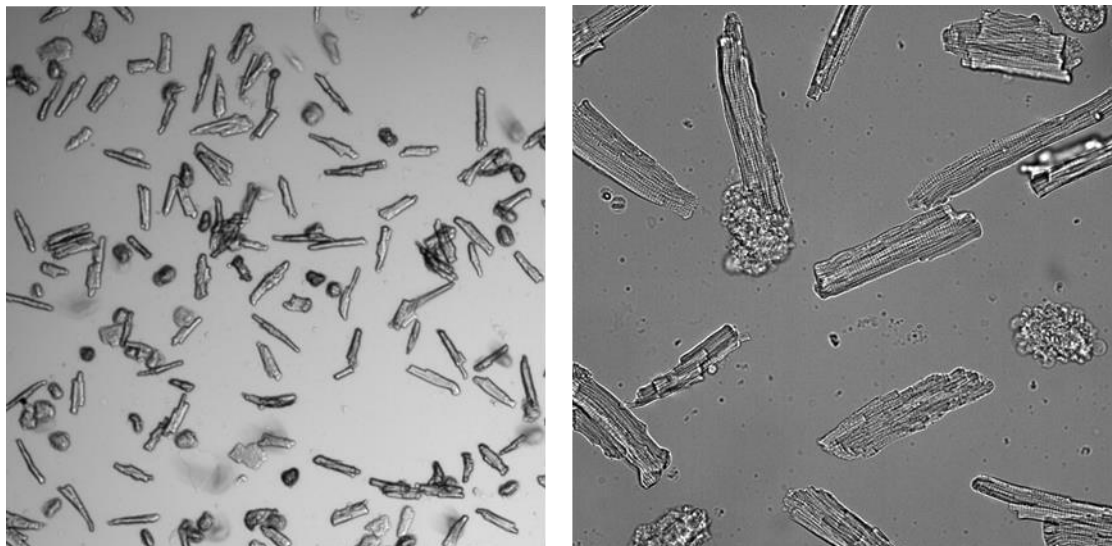


**Figure 20:** Representative images of isolated cardiomyocytes. Elongated cells are the rod-shaped  $\text{Ca}^{2+}$ -tolerant viable cardiomyocytes, while the round cells are the dead calcium intolerant cells. Left image was acquired with 5X magnification and right image was acquired with 40X magnification.

### Isolation of cardiac mitochondria

Mitochondria from mouse myocardium were obtained using differential centrifugation according to the method initially described by Palmer et al.<sup>202</sup>.

In mice, both subsarcolemmal mitochondria (SSM, located beneath the sarcolemma) and interfibrillar mitochondrial (IFM, located in direct contact with the myofibrils) subpopulations were obtained. Briefly, after excision of the heart, the atria were removed and the ventricular tissue was homogenized in cold sucrose isolation buffer (in mmol/L: sucrose 290, MOPS 10, EGTA 1, pH 7.4) with a Potter-Elvehjem tissue homogenizer. The homogenates were centrifuged at 800xg for 5 min at 4°C and the resulting supernatant was centrifuged at 5000xg for 5 min at 4°C to obtain the SSM population. The pellet obtained after the initial centrifugation at 800xg was resuspended in cold potassium isolation buffer (in mmol/L: KCl 100, MOPS 50, EGTA 1, pH 7.4), treated with proteinase K ( $\geq 30$  units/mg, Sigma P2308) and homogenized again in the tissue homogenizer. Importantly, after homogenization, 1 mmol/L of phenylmethanesulfonyl fluoride (PMSF), a proteinase K inhibitor, was added to prevent continued enzymatic digestion of the sample. This homogenate was centrifuged at 800xg for 5 min at 4°C and the resulting supernatant was subsequently centrifuged at 5000xg for 5 min to obtain the IFM pellets. When needed, an additional step of Percoll gradient (Sigma, P1644) at 17% was performed (12500xg, 8min, 4°C) to obtain a purer mitochondrial preparation. Isolated mitochondria were stored on ice until use.

### **H9c2 MYOBLASTS**

#### Culture and maintenance of H9c2 cell line

H9c2 myoblastic cell line from *Rattus norvegicus* heart tissue was commercially obtained (Sigma, 88092904) and maintained in high glucose Dulbecco's Modified Eagle Medium supplemented with 10% FBS and 1% penicillin/streptomycin in a saturated humidity incubator with 5% CO<sub>2</sub>, at 37°C. The culture medium was replaced every 2-3 days and the cells were split at sub-confluence (70-80%) with 0,05% trypsin-EDTA. Briefly, the cells were washed with phosphate buffered saline (PBS) and incubated with trypsin for 3 min at 37°C. Trypsin was then inactivated with FBS-supplemented DMEM, and the cells were collected and centrifuged at 250xg during 5 min, after which the pellet was resuspended in fresh culture medium and seeded. The cells were used between passages 10-20. For storage, the cells were frozen in freezing medium containing 95% DMEM culture medium supplemented with 5% DMSO. The cells were initially stored at 4°C for 2h, then transferred to -80°C for 24h after which they were placed in liquid nitrogen for long term storage. This process allows for gradual freezing and ensures minimal cell death. For thawing, the cells were defrosted at 37°C,

## Materials and Methods

transferred to fresh culture medium and centrifuged at 250xg during 5 min to remove DMSO. The pellet was finally resuspended in fresh culture medium and seeded.

The bioenergetic profile of H9c2 cells is highly dependent on oxidative phosphorylation, by contrast to other cell lines that are much more glycolytic, and also they have an active mitochondrial network with significant respiratory activity. These features resemble those present in adult cardiomyocytes, making these cells a reliable model to study mitochondrial function<sup>203</sup>.

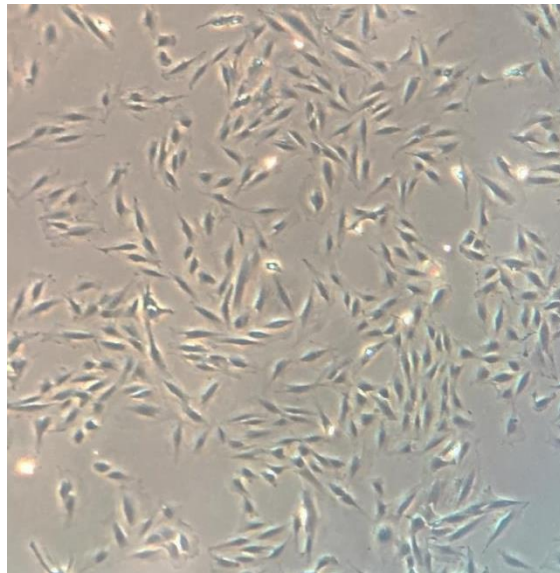


**Figure 21:** H9c2 cell culture at 70-80% confluence

### Induction of dicarbonyl stress in H9c2 cells

We established a dicarbonyl stress model in H9c2 cells to simulate the conditions present in aging and evaluate the cause-effect relationship between the increased dicarbonyl stress and the consequences it may have on mitochondrial energy production and sensitivity to damage (mPTP opening) seen in aging. For this purpose, two experimental groups were established: 1) the control group; and 2) the dicarbonyl stress group that simulates pro-glycative conditions. For the dicarbonyl stress group, H9c2 cells were treated for 3 consecutive days with 5 $\mu$ mol/L of the glyoxalase inhibitor S-p-bromobenzylglutathione cyclopentyl diester (SML, Sigma SML 1306) with an exogenous addition of 200 $\mu$ mol/L of MG (Sigma, M0252) to overload the detoxification system and favor accumulation of dicarbonyl modified proteins. The medium was replaced daily with fresh treatment throughout the 3 days of treatment after which the assays were performed. In the control group, the medium was replaced daily with fresh DMEM during 3 consecutive days.

### Isolation of mitochondria from H9c2 cells

Isolated mitochondria from H9c2 cells were used to determine the ATP hydrolase activity (see protocol below) and were obtained using differential centrifugations following a method similar to

that used for the isolation of cardiac mitochondria. Briefly, the adherent cells were washed with PBS, trypsinized and pelleted with a centrifugation at 250xg for 5 min at room temperature, after which cold sucrose isolation buffer supplemented with 100 units/mL DNase (ROCHE, 04536282001,) and 10-15 units proteinase K were added. The samples were homogenized with Potter-Elvehjem tissue homogenizer and proteinase K was inhibited with 1 mmol/L PMSF. The homogenate was centrifuged at 800xg for 5 min at 4°C. The supernatant was finally centrifuged at 5000xg for 5 min at 4°C to obtain the final H9c2 mitochondrial pellet which was stored on ice until use.

## 4.2. Biochemical Determinations

### MOUSE MYOCARDIUM

#### Western blot of dicarbonyl modifications, and of F<sub>0</sub>F<sub>1</sub>-ATP synthase subunits, IF1 and OPA1

Western blot analysis was employed to determine the impact of increased dicarbonyl stress present in aged mice, on the abundance of MGO-modified proteins, and to evaluate the relationship between increased dicarbonyl stress and the expression levels of several mitochondrial proteins including different subunits of F<sub>0</sub>F<sub>1</sub>-ATP synthase, IF1 and OPA1.

In mice, freshly isolated SSM and IFM from young and old mouse hearts were purified with a Percoll gradient, and solubilized with 1% n-dodecyl β-D-maltoside (DDM) when needed. Top speed centrifugations of lysed samples followed by protein concentration quantification of obtained supernatants were performed.

SSM and IFM samples were mixed with Laemmli sample buffer at 1X final concentration and heated at 95°C for 5 min. 20-50µg of protein was loaded into a polyacrylamide gel (at adequate acrylamide concentration) and the electrophoresis was performed under denaturing conditions in TRIS/Glycine/SDS buffer at constant 80-120mV. Proteins were transferred in TRIS/Glycine buffer, pH 8.5 with 10% methanol/membrane during the time optimized for each protein at constant 100mV. Nitrocellulose membranes of 0.45µm pore or polyvinylidene difluoride membranes (PVDF) of 0.22µm pore were used depending on the molecular weight of the protein of interest. All membranes were blocked with non-protein blocking agent Roti-block at 1X for 1h at room temperature.

Membranes were blotted against CML, MGO-modified proteins, F<sub>0</sub>F<sub>1</sub>-ATP synthase subunits α, β, δ and OSCP (ATP5A, ATPB, ATP5H, and ATP5O, respectively), in addition to IF1 and OPA1 at the conditions detailed in the following table. Anti-SDHA (succinate dehydrogenase) was used as a loading control for CML and MGO blotted membranes. Anti-VDAC (voltage-dependent anion

## Materials and Methods

channel) was used as a loading control for the rest of the primary antibodies. All primary antibodies (Ab) were incubated overnight at 4°C, and all secondary Abs (anti-mouse, Sigma A4416, 1:10000 and anti-rabbit, Pierce 31460, 1:10000) were incubated for 1h at room temperature. The signal was detected by chemi-luminescence in Odyssey imaging system from LI-COR, and the density of the bands was quantified as mean gray value in inverted images using ImageJ software.

Table 2: Summary of antibody dilutions and µg of proteins used for the Western Blots

<b>1° Ab</b>	<b>Reference</b>	<b>1° Ab Dilution</b>	<b>µg SSM or IFM</b>	<b>µg H9c2 extracts</b>
MGO	Cell Biolabs STA-011	1:1000	50	50
CML	Abcam ab27684	1:1000	50	50
ATP5A	Abcam ab176569	1:10000	35	50
ATPB	Novus Biologicals NBP2-67171	1:10000	35	50
ATP5H	Abcam ab173006	1:2000	20	50
ATP5O	SantaCruz sc-365162	1:2000	20	50
IF1	Abcam ab110277	1:1000	35	50
OPA1	Novus Biologicals NBP1-71656	1:1000	35	50
GLO-1	SantaCruz sc133214	1:500		50
SDHA	Abcam ab14715	1: 20000		
VDAC	Abcam ab14734	1:5000		
β-Actin	Sigma A5441	1:5000		

## Proteomics

Mass spectrometry analysis, and modified peptide and protein identification and quantification  
Protein extracts were obtained by heart tissue homogenization with ceramic beads (MagNa Lyser Green Beads apparatus, Roche, Germany) in extraction buffer (50mmol/L Tris-HCl, 1mmol/L EDTA, 1.5% SDS, pH 8.5). Proteins were digested on-filter by the Fasilox approach using 50 mmol/L iodoacetamide to block free (reduced) thiol groups and 40 mmol/L DTT followed by 50 mmol/L N-ethyl-maleimide to reduce-alkylate disulfide bonds<sup>204</sup>. The resulting peptides were labeled with TMT 10-plex following manufacturer instructions. The TMT10-plex experiment was composed from 4 biological replicates coming from young, 4 from old, and two channels reserved for internal standard (I.S.) samples. The I.S. was created by pooling all the samples and was used as reference to express

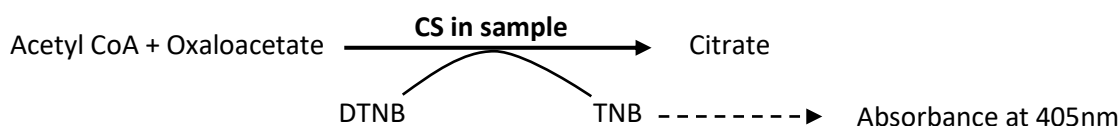
relative quantification values. The labelled peptides were separated by high pH reversed-phase (Thermo Scientific) into 5 fractions and analyzed by nano-liquid chromatography-tandem mass spectrometry (nanoLC-MS/MS) using a FUSION mass spectrometer (Thermo Scientific). Peptide and protein identification were performed using the SEQUEST HT algorithm integrated in Proteome Discoverer 2.1 (Thermo Scientific). MS/MS scans were searched against a mouse target database (UniProtKB/Swiss-Prot, July 2016, 16958 protein sequences) including as variable modifications the following AGEs in 5 different search batches: 2-ammonio-6-[4-(hydroxymethyl)-3-oxidopyridinium-1-yl]-hexanoate (HMOP, 108.021129 Da) in Lys, hydroxyphenylglyoxal (1HPG, 132.021129 Da) in Arg, bis-hydroxyphenylglyoxal (BHPG, 282.052824 Da) in Arg, methylglyoxal-derived hydroimidazolone (MG-H1, 54.010565 Da) in Arg, dihydroxyimidazolidine in Arg (DHI, 72.021129 Da), glyoxal-derived hydroimidazolone (G-H1, 39.994915 Da) in Arg, malondialdehyde (MDA, 54.010565 Da) adduct in Lys and carboxymethyl (CM, 58.005479 Da) in Lys and Trp residues. Other variable modifications included Met oxidation (15.994915 Da), Cys carbamydomethylation (57.021464 Da) and methylthiolation (45.987721 Da), and TMT10-plex (229.162932 Da) on Lys and peptide N-terminus. Precursor mass tolerance was set to 800 ppm and fragment mass tolerance at 0.03 Da; precursor charge range was set to 2-4; and 3 was the maximum fragment charge. 2 miss-cleavages were allowed and only y- and b-ions were used for scoring. The same MS/MS spectra were also searched against an inverted database constructed from the same target database. False discovery rate (FDR) of peptide identifications was calculated by the refined method with an additional filter for precursor mass tolerance of 15 ppm<sup>205,206</sup>. Quantitative information was extracted from MS/MS spectra of TMT-labeled peptides using Proteome Discoverer 2.1 (Thermo Scientific). Modified peptides and protein quantification was performed using the Generic Integration Algorithm<sup>207,208</sup> on the basis of the WSPP model<sup>209</sup> with some modifications<sup>210</sup>. Peptide and protein abundance changes are expressed in standardized units corrected by the corresponding protein abundance (zpq) or the experiment mean (zq). Significant peptide or protein abundance changes across the different samples were detected by applying Student's t test to zpq or zq data, respectively, and differences were considered statistically significant at  $p < 0.05$ . Differences between normal distributions in terms of zpq or zq were analyzed by two-tailed Kolmogorov-Smirnov test.

#### Determination of mitochondrial content

To quantify mitochondrial content, citrate synthase (CS) activity was quantified. CS is a mitochondrial matrix enzyme that catalyzes the first step of the Krebs cycle. Therefore, the quantification of CS activity can be used as an indicator of the amount of mitochondria present in the sample (mitochondrial pool). To liberate the CS from mouse mitochondria, the samples were first lysed with 0.1% Triton-X and then mixed with 0.3mmol/L Acetyl-CoA and 0.1mmol/L 5,5'-

## Materials and Methods

dithiobis-(2-nitrobenzoic acid) (DTNB, Ellman's reagent) in TRIS-HCl pH=8 buffer. The reaction was initiated with 0.1mmol/L oxaloacetate (OAA). The CS allows the reaction between Acetyl-CoA and OAA to produce citrate from the conversion of DTNB into 2-nitro-5-thiobenzoate (TNB), whose absorbance can be monitored spectrophotometrically at 405nm. Therefore, a kinetics reaction was performed during 5 min, and the Beer-Lambert equation was used to obtain units of CS per min (USC/min) which was finally normalized by mg of protein.



### Protein quantification

Protein concentration in mouse samples was determined by Bradford assay method and expressed as mg/mL. The sample was solubilized in 0.15% sodium deoxycholate (SOD) and then diluted in water. An albumin standard curve ranging from 0-200ug/mL was used, and after the addition of the reagents, the absorbance of both standards and samples was determined spectrophotometrically at 595nm, and the concentration was calculated from the absorbance-concentration curve of the standards ( $y = ax + b$ ).

### **H9c2 MYOBLASTS**

#### Western blot of dicarbonyl modifications, and of F<sub>0</sub>F<sub>1</sub>-ATP synthase subunits, IF1 and OPA1

In the H9ce model, Western blot analysis was performed to determine the effect of increased dicarbonyl stress on the abundance of MGO-modified proteins, and on several mitochondrial proteins including different subunits of F<sub>0</sub>F<sub>1</sub>-ATP synthase, IF1 and OPA1, in addition to the expression of the cytosolic GLO-1 protein.

In H9c2 cells exposed to dicarbonyl stress for 3 days (and the corresponding control), whole cell homogenates were obtained by lysing and scraping the cells with lysis buffer (in mmol/L: 50 TRIS HCl, 10 EDTA, 150 NaCl, 1% Triton X-100, 1 reducing agent dithiothreitol (DDT) supplemented with phosphatase inhibitors sodium fluoride (NaF, 10mmol/L), sodium orthovanadate (Na<sub>3</sub>VO<sub>4</sub>, 2mmol/L) and protease inhibitors (PI, 1%), and after a top speed centrifugation, protein was quantified by the Lowry method.

For all western blots with H9c2 cell extracts, 50 µg of protein was used. The electrophoresis, transfer, blocking and primary and secondary antibody incubations were performed in conditions similar to those applied for SSM and IFM mouse samples. Anti-GLO1 was used at 1:500. Anti-β-actin was used as a loading control for all H9c2 samples.

#### MTT protocol for H9c2 viability

To determine the effect of the chronic dicarbonyl stress (SML-MG) on cell viability throughout time, MTT assay was performed. The MTT (thiazolyl blue tetrazolium bromide) assay measures viable cells by evaluating mitochondrial dehydrogenase activity, which cleaves the tetrazolium ring of the MTT, yielding purple formazan crystals that are insoluble in aqueous solution. The crystals are then dissolved resulting in a purple solution that is colorimetrically quantified at 620 nm, such that higher absorbance values suggest a higher number of viable cells and vice versa. The cells were treated with either SML (5 $\mu$ mol/L), MG (200 $\mu$ mol/L) or SML-MG (5 and 200 $\mu$ mol/L, respectively) during 3 consecutive days, and the MTT was added directly to the culture medium of control and treated H9c2 cells at 0.5mg/mL final concentration. After 3h of incubation at 37°C with 5% CO<sub>2</sub>, the medium was gently aspirated and the formazan crystals were solubilized with DMSO for 30 min at 37°C, after which the absorbance was read at 620nm. The assay was performed at days 0, 1, 2 and 3 and values were expressed as changes in cell viability with respect to day 0 of each treatment group (considered as the initial cell number).

#### Determination of mitochondrial content

To quantify total mitochondrial content, citrate synthase activity was quantified in isolated mitochondria of H9c2 cells. Mitochondria were first lysed with 0.1% Triton-X and then the reaction was initiated similarly to mouse mitochondrial samples by the addition of 0.3mmol/L acetyl-CoA and 0.1mmol/L DTNB and 0.1mmol/L OAA in TRIS-HCl pH=8 buffer.

#### Protein quantification

Protein concentration was determined by either Bradford or Lowry assay methods and expressed as mg/mL. The choice to use one or another assay was based on the sample buffer composition that may contain agents that react non-specifically with the assay reagents. Bradford assay was performed similarly to mouse samples quantifications. For the Lowry assay, an albumin standard curve ranging from 0-800 $\mu$ g/mL was used. After the addition of the reagents and incubating them 30min at 37°C, the absorbance of both standards and samples was determined spectrophotometrically at 562nm, and the concentration was calculated from the absorbance-concentration curve of the standards ( $y = ax + b$ ).



### 4.3. Microscopy studies

#### MOUSE MYOCARDIUM

##### Immunofluorescence for intracellular MGO-derived modification

To determine intracellular MGO-modified proteins, isolated cardiomyocytes were washed with PBS, and fixed with 4% formaldehyde during 10min at room temperature. The fixed cells were permeabilized with 0.1% Triton X-100 for 20min at room temperature and blocked with Roti-block at 1X in PBS-Tween 0.05% during 1h. The primary Ab anti-MGO (Cell Biolabs STA-011, 1:50) was added and incubated overnight at 4°C, after which the cells were washed with PBS-Tween 0.05%, and the secondary Abs conjugated to an Alexa fluorescent probe were added. ALEXA anti-mouse 546 IgG (Invitrogen, A11003) 1:1000 was added for 1h at room temperature. After another washing step, the nuclei were stained with Hoescht-33342 at 5µg/mL. Mounting medium and cover slips were added to the slides, and Z-plane images were acquired with the spectral FluoView-1000 Olympus confocal microscope. The quantification of the intracellular AGEs fluorescence was determined as mean gray value in 16-bit images (Image J).

##### Co-localization of F<sub>0</sub>F<sub>1</sub>-ATP synthase and MGO-derived modifications

Isolated mouse cardiomyocytes were fixed and permeabilized as described in the previous method. The cells were incubated simultaneously with anti-F<sub>0</sub>F<sub>1</sub>-ATP synthase (subunit  $\alpha$ , Abcam ab176569, 1:199) and anti-MGO (Cell Biolabs, STA-00, 1:50) at 4°C overnight, and incubated with secondary antibodies ALEXA anti-rabbit 488 IgG (Invitrogen, A11008) and ALEXA anti-mouse 546 IgG (Invitrogen, A11003) both at 1:1000, for 1h at room temperature. Central Z-planes were captured with a confocal microscope (FluoView-1000 Olympus) and the degree of colocalization was determined by the Mander's correlation coefficient using the Image Correlator Plus plugin of ImageJ in 8-bit images. An increased colocalization between F<sub>0</sub>F<sub>1</sub>-ATP synthase and MGO was considered indicative of increased MGO-induced ATP synthase modification. These images were also used to quantify the abundance of both F<sub>0</sub>F<sub>1</sub>-ATP synthase and MGO-derived modifications. Equal expression levels of F<sub>0</sub>F<sub>1</sub>-ATP synthase in young and old cardiomyocytes with a specific increase in MGO-derived modifications only in cardiomyocytes from old mouse hearts indicate that the increased MGO-derived modification levels are the determining factor for the increased colocalization observed.

Proximity ligation assay (PLA) for  $F_0F_1$ -ATP synthase modification by MGO

A proximity ligation assay (PLA) is a highly specific and sensitive assay that combines immunological (Ab binding) and molecular (DNA amplification) techniques to detect protein-protein interactions or protein post-translational modifications in cell or tissue samples. Only when the target proteins are encountered at close proximity (10-40nm) is a positive fluorescent spot, indicative of protein interactions or of a post-translational modification, produced. These fluorescent spots are acquired by a confocal fluorescent microscope and the number of spots per cell area ( $\text{spots}/\mu\text{m}^2$ ) analysed.

Briefly, after the cells are fixed and permeabilized, two different primary Abs are used to bind the proteins of interest. Following primary Ab incubation, secondary Abs are added. In this technique the secondary Abs called PLA probes (PLUS and MINUS) are conjugated to a sequence of oligonucleotides known as a ligation arm. When the distance between them is inferior to 10-40nm, connecting oligonucleotides can hybridize to the ligation arms in the presence of a DNA ligase, producing a closed circular DNA which functions as a primer for rolling circle amplification (RCA). Accordingly, the addition of a DNA polymerase will allow for concatemeric sequence amplification meanwhile incorporating fluorescently-labeled nucleotides into the amplified sequence. This allows the signal to be amplified up to a 1000 times, and produces an individual fluorescent spot at the site of protein interaction/modification.

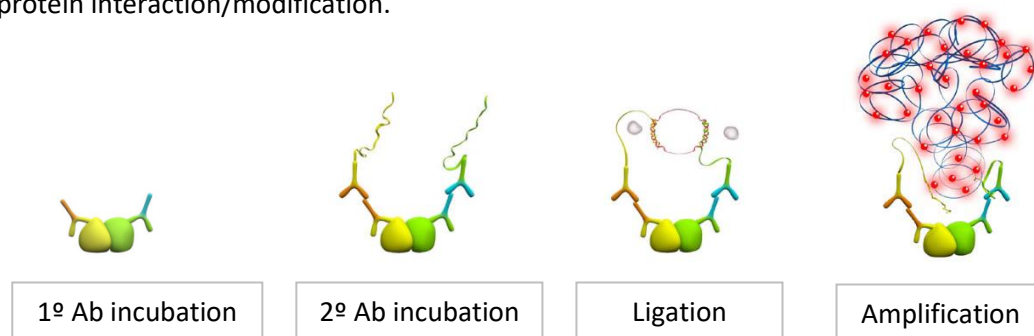


**Figure 22:** Illustrations of the different steps of a PLA.

For the PLA addressed to evaluate the MGO-induced modification of  $F_0F_1$ -ATP synthase, isolated mouse cardiomyocytes were washed with PBS, fixed with 4% formaldehyde for 10 min, and permeabilized with 0.1% Triton X-100 for 20 min. Non-specific Ab binding was prevented by blocking with polymer-based blocking reagent Roti-Block at 1x for 1h at room temperature, and then the primary antibodies were added. The cardiomyocytes were labeled simultaneously with primary Ab: rabbit monoclonal anti-ATP5a ( $\alpha$  subunit of mitochondrial  $F_0F_1$ -ATP synthase, Abcam ab176569) at 1:100, and mouse monoclonal anti-MGO (Cell Biolabs, STA-011) and incubated overnight at 4°C. Next, the PLA probes anti-mouse MINUS (Sigma, DUO92004) and anti-rabbit PLUS (Sigma, 92002) were added for 1h at 37°C. Then, ligase and a ligation buffer containing connecting oligonucleotides

## Materials and Methods

were added for 30 min at 37°C. Finally, polymerase and an amplification buffer containing fluorescent oligonucleotides were added for 1h and 30 min at 37°C. The nuclei of the cells were stained with Hoescht 33342 at 5µg/ml for 10 min, and ultimately, mounting medium and cover slips were added to the slides.

The prepared samples were left at room temperature protected from light for at least 30 min before fluorescent images were acquired by a confocal microscope (FluoView-1000, Olympus). The number of positive fluorescent spots was quantified using the “analyze particles” tool of the FIJI software. In cardiomyocytes, 3 central Z-planes were analyzed excluding the nuclear area. The number of spots was normalized by the area of the cells and expressed as spots per area (µm<sup>2</sup>).

### PLA to evaluate dimerization of mitochondrial F<sub>0</sub>F<sub>1</sub>-ATP synthase

This type of PLA aims to evaluate the degree of dimerization of the mitochondrial F<sub>0</sub>F<sub>1</sub>-ATP synthase by assessing the proximity between two F<sub>0</sub>F<sub>1</sub>-ATP synthase monomers. Normally, two different primary Abs raised in two different species are used in PLAs. In this case however, our target protein, the mitochondrial F<sub>0</sub>F<sub>1</sub>-ATP synthase, is made up of several protein subunits, some of which are present in more than one copy. Therefore, using two different primary Abs may lead to binding to two different subunits of the same monomer, consequently invalidating the results. Accordingly, a single primary Ab should be used, and this Ab should be directed against a subunit present in a single copy per monomer. The detection of interaction shall be achieved by using equal amounts of PLUS and MINUS secondary Ab probes raised against the same species.

For this PLA, the fixation, permeabilization and blocking of the isolated cardiomyocytes were performed similarly to the previous PLA. Here however, one primary antibody only was used: mouse monoclonal anti-ATP5h (d subunit of mitochondrial F<sub>0</sub>F<sub>1</sub>-ATP synthase, Abcam ab110275) at 1:100. Secondary PLA probes directed against the same species were then added: anti-mouse MINUS and anti-mouse PLUS (Sigma, DUO92001). While the fluorescent interaction between two primary antibodies is indicative of dimerization between two independent monomers, a decrease in the number of positive fluorescent spots can be indicative of an increased intermolecular distance between two monomers and therefore decreased dimerization of F<sub>0</sub>F<sub>1</sub>-ATP synthase.

### Transmission Electron microscopy and quantification of mitochondrial cristae tip curvature

To determine age-dependent differences in mitochondrial ultrastructure in mouse hearts, TEM images were acquired from myocardium of young and old mice. The hearts were cannulated through the aorta on Langendorff aperture. First, the hearts were perfused by Ca Tyrode solution for 5 min (in mmol/l: 135 NaCl, 5.4 KCl, 5 MgCl<sub>2</sub>, 1 CaCl<sub>2</sub>, 0.33 NaH<sub>2</sub>PO<sub>4</sub>, 10 HEPES, pH 7.3), followed by

perfusion with calcium free Tyrode solution (in mmol/l: 135 NaCl, 5.4 KCl, 5 MgCl<sub>2</sub>, 0.02 CaCl<sub>2</sub>, 0.33 NaH<sub>2</sub>PO<sub>4</sub>, 10 HEPES, pH 7.3), and finally by perfusion fixation with 2.5% glutaraldehyde) in 0.15 mol/L sodium cacodylate buffer (pH 7.4). Small pieces from left ventricle and papillary muscle were cut (~1 mm<sup>3</sup>), post-fixed overnight in 4°C in 2% osmium tetroxide partially reduced by 0.8% K<sub>4</sub>Fe(CN)<sub>6</sub> in 0.15 mol/L Na-cacodylate buffer. Samples were contrasted en bloc with 1% uranylacetate in diH<sub>2</sub>O, dehydrated in graded series of acetone, embedded in Spurr's resin. Longitudinal, ultrathin sections (65–80 nm) were cut from the resin-embedded blocks with a diamond knife (Diatome-US, USA) using a Leica UCT ultramicrotome and caught on a copper grid covered with formvar film. Images of longitudinal oriented cardiomyocytes were obtained via an FEI Tecnai 12 TEM fitted with an AMT XR-111 10.5 Mpx CCD camera at 3,200 – 15,000× magnification (80 kV).

Low magnification images were used to compare differences in mitochondrial shape, size, and distribution in young and old mouse myocardium, while high magnification images were used to compare other mitochondrial ultrastructural aspects including cristae shape and pattern, and cristae tip curvature. Morphometric analysis of mitochondrial cristae tip curvature was performed using Kappa, ImageJ, NIH (Mary H, Brouhard GJ. Kappa ( $\kappa$ ): Analysis of Curvature in Biological Image Data using B-splines).

## **H9c2 MYOBLASTS**

### Immunofluorescence for intracellular MGO-modified protein accumulation

To determine intracellular MGO-modified proteins, similarly to isolated cardiomyocytes, control and SML-MG treated H9c2 cells were washed, fixed, permeabilized and blocked and posteriorly incubated overnight with anti-MGO (Hycult biotec HM5014, 1:50). Secondary Ab ALEXA anti-mouse 546 IgG, Invitrogen, A11003) at 1:1000 was added for 1h at room temperature. A single central Z-plane image was acquired with the spectral FluoView-1000 Olympus confocal microscope and the quantification of the intracellular MAGEs fluorescence was determined as mean gray value in 16-bit images (Image J).

### PLA for F<sub>0</sub>F<sub>1</sub>-ATP synthase glycation and dimerization in H9c2

The same protocol applied for determining F<sub>0</sub>F<sub>1</sub>-ATP synthase glycation and dimerization in isolated cardiomyocytes was employed for H9c2 cells on day 3 of dicarbonyl stress induction and the respective controls. In this model however, only one single central Z-plane image was acquired and the total number of positive fluorescent spots obtained per field were normalized against the number of nuclei and therefore expressed as spots/cell.

## 4.4. Functional Assays

### 4.4.1. Functional assays to evaluate the activity of F<sub>0</sub>F<sub>1</sub>-ATP synthase

#### MOUSE MYOCARDIUM

##### Mitochondrial respiration by Oximetry

Age-associated changes in mitochondrial respiration were measured using a Clark-type electrode (Hansatech) in isolated SSM and IFM from young and old mouse hearts. The electrode contains a platinum cathode and a silver anode that can detect soluble oxygen in a liquid phase across an oxygen-permeable polytetrafluoroethylene (PTFE) membrane with saturated KCL as an electrolyte. When oxygen comes in contact with the polarized platinum (700mV), it becomes reduced and therefore generates a detectable current that is stoichiometrically related to the oxygen concentration. Therefore, O<sub>2</sub> consumption by the mitochondria is detected by a decrease in the amount of oxygen reduced at the level of the electrode, in other words, by a lower current.

After instrument equilibration with assay buffer (in mmol/L: 100 KCL, 50 MOPS, 1 EGTA, 5 KH<sub>2</sub>PO<sub>4</sub>, 1 MgCl<sub>2</sub>, pH 7.4), the zero oxygen value was established by the addition of sodium dithionite. The chamber was thoroughly washed after dithionite addition, and when a stable signal was reestablished, the experiment was initiated. Isolated mitochondria were added to the chamber containing assay buffer with complex 1 substrates malate (2mmol/L) and glutamate (5mmol/L) or complex 2 substrate succinate (6mmol/L) in addition to rotenone (0.6μmol/L) to inhibit complex 1. O<sub>2</sub> consumption was registered for 30-40 sec to obtain the E2 respiration state corresponding to the basal respiration. Then 0.5mmol/L of ADP was added to activate oxidative phosphorylation and ATP synthesis that corresponds to state 3 (E3) respiration. Finally, 1μmol/L of oligomycin was added to inhibit the F<sub>0</sub>F<sub>1</sub>-ATP synthase and to obtain state 4 (E4) respiration that corresponds to respiration uncoupled from ATP synthesis. The rates obtained for each of states E2, E3 and E4 were normalized against units of citrate synthase per mg of protein (USC/mg) and expressed as nmol O<sub>2</sub>/min\*USC.

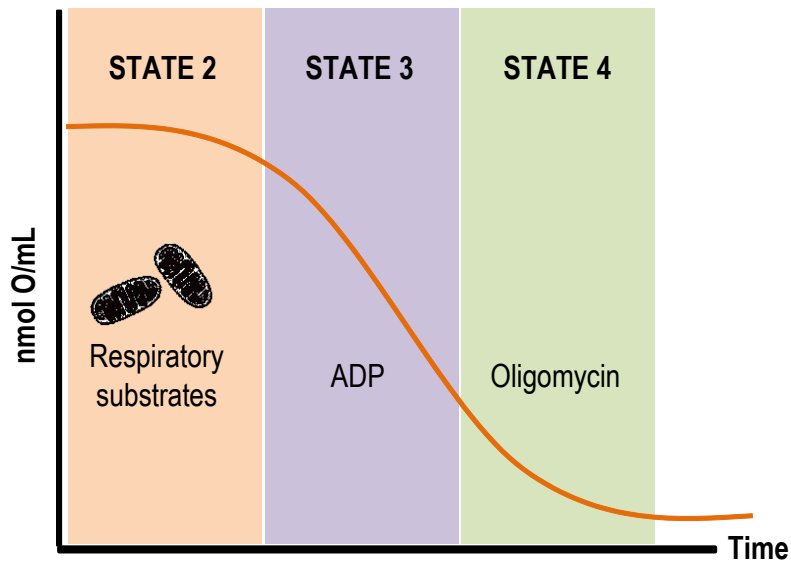


**Figure 23:** Representative figure of the curves obtained in the different mitochondrial respiratory states.

#### ATPase activity in isolated mitochondria

To investigate the potential impact of aging on  $F_0F_1$ -ATP synthase activity, the hydrolytic function of the enzyme was quantified in isolated mouse mitochondria. Reversal of mitochondrial  $F_0F_1$ -ATP synthase activity from ATP synthesis to hydrolysis occurs when mitochondrial membrane potential is lost; this makes possible the measurement of ATPase activity *in vitro* in isolated and solubilized mitochondria, in which the mitochondrial membrane potential is non-existent. Isolated SSM and IFM from young and old mouse hearts were solubilized with non-ionic detergent DDM at 1% final concentration. The mitochondria were incubated with DDM on ice for 30, and then centrifuged at top speed (21,000xg, 20 min, 4°C). Solubilized mitochondrial protein concentration was quantified by Bradford method.

Next, oligomycin-sensitive ATPase activity was determined in two independent steps. In the first step, 100ug of solubilized mitochondria were added with or without 10 $\mu$ mol/L of oligomycin (Agilent, 103015). Reaction was initiated by adding KCl-MOPS buffer (in mmol/L: 100 KCL, 50 MOPS, pH 7.4), with 2mmol/L ATP in addition to 10 $\mu$ mol/L diadenosine pentaphosphate pentasodium salt (Ap5a) to inhibit adenylate cyclase, one of the major ATP-consuming mitochondrial enzyme. The reaction was allowed to proceed for 15 min before it was stopped with oligomycin in those did not contain oligomycin from t=0min.

In the second step, the remaining ATP, which has not been hydrolyzed in step one, was quantified. For this purpose, 50uL of sample was added to KCl-MOPS buffer containing 2.5mmol/L glucose, 2 units/mL of hexokinase/glucose-6-phosphate dehydrogenase (G6PD) and 2mmol/L NADP sodium salt. The conversion of glucose to glucose-6-phosphate by hexokinase consumes the remaining ATP

## Materials and Methods

present in the samples, while the conversion of glucose-6-phosphate to 6-phospho-gluconate by G6PD consumes NADP yielding NADPH, which changes the absorbance at 340nm, therefore allowing colorimetric analysis. Absorbance at 340nm was measured after 15 min of reaction and the mmol/L of remaining ATP was calculated using an ATP standard curve coupled to NADPH production as with the solubilized mitochondrial samples.

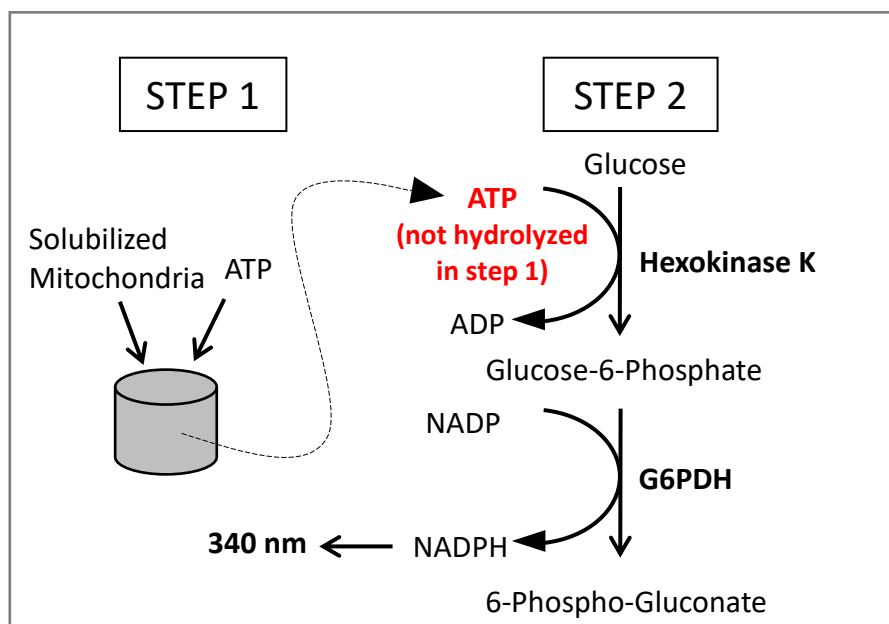


**Figure 24:** Scheme of the protocol used to assess ATPase function *in vitro*.

Finally, the percentage of hydrolysed ATP was calculated by considering 2mmol/L ATP from standard curve as 100% ATP, and applying the following formula:

$$\% \text{ hydrolysed ATP} = \frac{2\text{mmol/L ATP Standard} - \text{mmol/L ATP in Sample}}{2\text{mmol/L ATP Standard}} \times 100$$

The data obtained from samples incubated with oligomycin at t=0 min were used to calculate the percentage of oligomycin inhibition by applying the following formula:

$$\% \text{ oligomycin inhibition} = \frac{2\text{mmol/L ATP Standard} - (\text{mmol/L ATP in Sample} + \text{Oligomycin})}{2\text{mmol/L ATP Standard}} \times 100$$

### Blue Native In-Gel Activity of Mitochondrial ATPase Activity

Unlike the *in vitro* ATPase activity determination that only demonstrates the total ATPase activity (sum of all forms; monomers, dimers, oligomers), blue native (BN) in-gel activity ATPase allows to quantify the effect of aging on the hydrolytic activity of F<sub>0</sub>F<sub>1</sub>-ATP synthase in each of its different

monomeric, dimeric and oligomeric forms, as well as their relative abundance. Blue native in-gel activity was performed in isolate SSM and IFM of murine heart. BN-polyacrylamide gel electrophoresis (BN-PAGE) employs non-denaturing conditions to resolve proteins solubilized in non-ionic detergents, therefore ensuring optimal maintenance of native protein structure and function. In this method, the denaturing SDS used in the conventional electrophoresis to confer the proteins the negative charge essential for their migration, is replaced by Coomassie G-250, which gives a negative charge without interfering with the native protein structure.

For the BN electrophoresis, highly purified SSM and IFM from young and old mice were obtained according to the normal mitochondrial isolation protocol followed by Percoll purification. The obtained pellets were posteriorly reconstituted in extraction buffer (in mmol/L: 30 HEPES, 150 potassium acetate, 2 6-aminocaproic acid, 20% glycerol, pH 7.4), the protein concentration quantified, and the samples finally solubilized with digitonin at a proportion of 0.5mg of digitonin/mg of mitochondrial protein. The solubilization was performed on ice during 1h, after which a centrifugation at 21000xg for (20min, 4°C) was carried out. The supernatant was collected and the protein concentration was determined again. Subsequently, 20ug of each of the SSM and IFM preparations were mixed with the G-250 sample additive at a final concentration equivalent to 1/4<sup>th</sup> of the detergent and were loaded into a Native-PAGE Bis Tris 3-12% gradient gel. The electrophoresis was performed in an anode and a cathode running buffer, where the cathode buffer contained 0.002% of G-250 cathode buffer additive, and the samples were resolved at a constant 10-12mA during 4h.

For the ATPase in-gel activity, after electrophoresis the gel was carefully transferred to a recipient containing assay buffer (in mmol/L: 35 TRIS HCl, 270 glycine, 14 MgSO<sub>4</sub>, 1 ATP and 0.2% of lead nitrate (Pb(NO<sub>3</sub>)<sub>2</sub>, pH 7.8), while reserving some lanes of the gel to place in another recipient containing the assay buffer with 10μmol/L of oligomycin (to serve as a control for the specificity of the probe). The gels were left to incubate overnight at room temperature. When ATPase activity is present, the ATP is converted into ADP and phosphate. The released phosphate will therefore bind to the Pb present in the buffer, causing the precipitation of lead phosphate at the sites of enzymatic activity. Those precipitations develop silver-white colored bands, by contrast to lanes in which oligomycin is present and no precipitation develops. The gels were transferred into a clear plastic bag, and an image was acquired with the GelXs Doc, Quantity One from Bio-Rad. The mean grey value of each monomeric and oligomeric form of the F<sub>0</sub>F<sub>1</sub>-ATP synthase was quantified using FIJI software and expressed as a percentage of the total ATPase (whole lane precipitation bands).



**H9c2 MYOBLASTS**Mitochondrial ATP Production in by Seahorse Analyzer

To assess the impact of dicarbonyl stress on the activity of  $F_0F_1$ -ATP synthase, ATP production rate was monitored by real-time ATP rate assay using respiratory modulators oligomycin and rotenone/antimycin (Rot/AA) in a Seahorse XF analyzer (Agilent Technologies, Seahorse Bioscience, Santa Clara, USA). This test allows the quantification of the relative contribution of OXPHOS with respect to glycolytic pathways for ATP generation. Control and SML-MG treated cells were trypsinized on day 3 of glycative treatment and seeded at 15000 cells/well in culture media (0.2%FBS  $\pm$  5 $\mu$ mol/L SML-200 $\mu$ mol/L MG where it corresponds) in Seahorse XF HS Mini 8-well plates precoated with 0.1% gelatin, at 37°C. On the day prior to the experiment, the sensor cartridge was hydrated with XF calibrant and stored overnight in a non-CO<sub>2</sub> incubator.

After 24h of cell passaging, culture medium was replaced by DMEM medium pH 7.4 (bicarbonate free) supplemented with 25mmol/L glucose, 1mmol/L pyruvate and 2mmol/L L-glutamine and incubated at 37°C (1h, non-CO<sub>2</sub> incubator). After loading the respiratory modulators oligomycin and Rot/AA into the ports of the sensor cartridge, the cartridge and the XFp Miniplate were loaded into the Seahorse analyzer. Following an equilibration period, 3 running cycles were performed. Real-Time ATP rate assay was performed using 1.5  $\mu$ mol/L oligomycin, and 0.5  $\mu$ mol/L of each Rot/AA. In each cycle, 3 different recordings were determined with a 5min interval between each.

At the end of the experiment, cells were lysed (0.1% Triton X-100) and protein was determined by Bradford. The ATP production rate was calculated from the rate of O<sub>2</sub> consumption coupled to ATP production (OCR data) during OXPHOS (mitoATP) and from lactate production during glycolysis (ECAR data), which was converted to glycolytic ATP production rate (glycoATP). MitoATP and GlycoATP rates (pmols/min) were normalized by  $\mu$ g of protein. Changes in the bioenergetics profile as a consequence of in vitro dicarbonyl stress were described as the relative difference between mitoATP and glycoATP production rates compared to the total ATP rate.

Agilent Seahorse XF Real-Time ATP Rate Assay

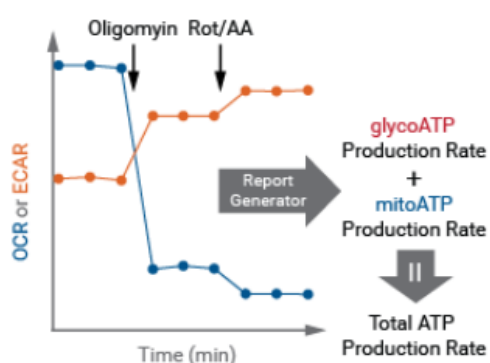


**Figure 25:** Scheme of the experimental protocol (Agilent, Seahorse) used to analyse the bioenergetics profile of H9c2 cells.

#### ATPase activity in isolated mitochondria

Isolated H9c2 mitochondria were used to determine the effect of induced dicarbonyl stress on *in vitro* ATPase activity. The same protocol applied for isolated mouse mitochondria was used here. Briefly, mitochondria from control and SML-MG treated H9c2 cells were solubilized with 1% DDM, for 5 min on ice, and then centrifuged at top speed (21,000xg, 20 min, 4°C) and protein concentration determined. In the first step of the reaction, 20ug of H9c2 solubilized mitochondria were added with or without 1umol/L of oligomycin. Reaction was initiated by adding KCl-MOPS buffer (in mmol/L: 100 KCL, 50 MOPS, pH 7.4), with 1mmol/L ATP for H9c2 mitochondria in addition to 10umol/L Ap5a. The reaction was allowed to proceed for 15 min before it was stopped with oligomycin except in those wells that already contained oligomycin from t=0min. The second step was performed in the same conditions applied for isolated mouse mitochondria.

#### **4.4.2. Functional assays to evaluate the susceptibility to mPTP**

##### **MOUSE MYOCARDIUM**

#### ROS-induced mPTP in isolated mouse cardiomyocytes

ROS are, along with calcium, one of the most prominent triggers of mitochondrial permeability transition pore (mPTP). Therefore, experimental induction of oxidative damage through intermittent laser illumination is a standardized method used to evaluate the susceptibility of the mitochondria to suffer mPTP<sup>211</sup>. For this purpose, cells are loaded with a photon-sensitive fluorescent mitochondrial marker, like tetramethylrhodamine ethyl ester (TMRE), which generates a significant amount of ROS when irradiated with laser. This marker is taken up by the mitochondria in a manner dependent on the membrane potential, and upon irradiation, the susceptibility to mPTP is quantified as the time at which irreversible mitochondrial depolarization and energy collapse is produced. In cardiomyocytes, this phenomenon is detected as cell shortening secondary to energy exhaustion (rigor contracture). Therefore, isolated cardiomyocytes from young and old mouse hearts were loaded with 100nmol/L of TMRE during 15 minutes in control HEPES buffer (in mmol/L: 140 NaCl, 20 HEPES acid, 1 CaCl<sub>2</sub>, 3.6 KCl, 1.2 MgSO<sub>4</sub>, 5 glucose, pH 7,4) and were consequently exposed to intermittent laser irradiation in a confocal microscope (Ex/Em 561/590nm, Zeiss LSM980). The excitation was performed at 5% laser intensity with 2 seconds intervals, and the changes were recorded until the cells underwent rigor or hypercontracture shortening. In a subset of cells, the control HEPES buffer was supplemented with the mPTP inhibitor cyclosporine A (CsA 1μmol/L) or substituted by HEPES buffer at pH 6,4 to inhibit mPTP opening. The images were analyzed in ZenBlue software and the time to the onset of cell shortening, in addition to the percentage of decrease in cell length were compared between young and old mouse cardiomyocytes.

### **H9c2 MYOBLASTS**

#### ROS-induced mPTP in H9c2 cells

The same method used in isolated cardiomyocytes was applied in H9c2 cells to determine the effect of dicarbonyl stress on mPTP susceptibility. Briefly, control and SML-MG treated cells were loaded with 100nmol/L of TMRE during 15 minutes and consequently exposed to intermittent laser irradiation in a confocal microscope (Ex/Em 561/590nm, Zeiss LSM980) at 0.5% laser intensity with 2 seconds intervals, and the changes in fluorescence were recorded during 15min. In a subset of cells, CsA or pH 6,4 were added as well. Images were analyzed in ZenBlue software and the time at 30% loss of TMRE fluorescence was compared between control and SML-MG groups. Unlike, cardiomyocytes, these cells do not undergo cell shortening upon energy collapse, so another parameter (time at 30% depolarization) was used to compare the susceptibility to mPTP between groups.

#### Spontaneous time-dependent mPTP

The impact of dicarbonyl stress on spontaneous time-dependent mPTP was determined in control and SML-MG treated H9c2 cells by evaluating the overlap coefficient between mitochondrial calcein and mitotracker red (MTR) throughout time. Calcein uptake by the mitochondria depends of mitochondrial membrane potential, and the fluorochrome is lost upon mPTP and mitochondrial membrane depolarization, whereas MTR covalently binds to mitochondrial proteins and its fluorescence remains stable. Therefore, hypothetically, if mitochondrial abundance is not altered upon dicarbonyl stress induction, the MTR signal should remain constant throughout time, and the changes of calcein to MTR overlap can be indicative of calcein release, or in other words, mPTP. For this purpose, control and SML-MG treated H9c2 were simultaneously loaded with calcein (1 $\mu$ mol/L, 15min, 37 $^{\circ}$ C) and mitotracker red (MTR, 200nmol/L, 30min, 37 $^{\circ}$ C) on days 0, 1, 2 and 3. To remove the contribution of the cytosolic calcein signal, the cells were post-incubated with 1mmol/L cobalt chloride (CoCl<sub>2</sub>)<sup>212</sup> for 15min at 37 $^{\circ}$ C. In some replicates, 0.2 $\mu$ mol/L CsA was presented during dicarbonyl stress induction to inhibit mPTP-dependent calcein release. Occurrence of mPTP was determined on days 0, 1, 2 and 3 as CsA-sensitive decay in the coefficient overlap between calcein and MTR fluorescence (Zeiss LS980) using 8-bit images (Image J) such that a decrease in the value of the overlap is indicative of a decreased calcein signal and therefore more mPTP.

#### **4.5. Statistical Analysis**

Data are expressed as mean  $\pm$  standard error of the mean (SEM). When data followed a normal distribution, a two-tailed t-test for independent or paired samples was applied. For data not following a normal distribution, the non-parametric Mann-Whitney test for medians was applied. ANOVA analysis was used for comparisons between more than two groups. Differences of  $p \leq 0.05$  were considered as statistically significant. Statistical analyses were performed with SPSS v.20 software (New York, NY, USA).

## Materials and Methods

### Reagent

2,3-butanedione monoxime 10 (BDM)  
5,5'-dithiobis-(2-nitrobenzoic acid) (DTNB)  
Acetyl-CoA  
Adenine triphosphate (ATP)  
Adenosine diphosphate (ADP)  
Calcein-AM  
Cobalt chloride  
Cyclosporine A (CsA)  
Diadenosine pentaphosphate pentasodium salt (Ap5a)  
Dimethyl sulfoxide (DMSO )  
Dithiothreitol (DDT)  
DNase  
Dulbecco's Modified Eagle Medium (DMEM)  
Electrophoresis buffer (TRIS/Glycine/SDS buffer)  
enhanced chemiluminescence substrates (ECL)  
Fetal bovine serum (FBS)  
Formaldehyde  
G-250 cathode buffer additive  
Gelatin  
Glucose  
Glutamate  
Hexokinase/Glucose-6-phosphate dehydrogenase  
Hoescht 33342  
Laemmli sample buffer  
Laminin  
Lead nitrate ( $Pb(NO_3)_2$ )  
L-glutamine  
M199 medium  
Malate  
Methylglyoxal (MG)  
Mitotracker red (MTR)  
Mounting medium  
NADP sodium salt  
Native-PAGE Bis Tris 3-12% gradient gel  
Native-PAGE G-250 sample additive  
NativePAGE running buffer  
n-dodecyl  $\beta$ -D-maltoside (DDM)  
Nitrocellulose membranes (NC)  
Non-protein blocking agent Roti-block  
Oligomycin  
Oxaloacetate (OAA)  
Penicillin/Streptomycin (P/S)  
Percoll  
Phenylmethanesulfonyl fluoride (PMSF)  
Phosphate buffered saline (PBS)

### Reference

Sigma, B0753  
Sigma, D8310  
Sigma, A2181  
Sigma, A9187  
Sigma, A5285  
Molecular Probes, C3100MP  
Sigma, C3169  
Sandimmun  
Sigma, D4022  
Panreac, A3672  
Thermo Scientific, 20291  
ROCHE, 04536282001  
ATCC, 30-2002  
BioRad, 1610772  
GE Lifesciences, RPN2236  
Gibco, 10270  
PanReac, 252931  
Invitrogen, BN2002  
Gibco, 214340  
Agilent Technologies, 103577-100  
Sigma, G1501  
G6PD, Sigma H8629  
Sigma, B2261  
Sigma, S3401  
Sigma, L2020  
Sigma, 203580  
Agilent Technologies, 103579-100  
Gibco™, 22340020  
Sigma, M6413  
Sigma, M0252  
Invitrogen, M22425  
Sigma, M1289  
Roche, 10128040001  
Invitrogen, BN1001  
Invitrogen, BN2004  
Invitrogen BN2001  
Sigma, D4641  
GE Lifesciences, 10600008  
Roth, A151.1  
Millipore, 495455  
Sigma, O4126  
Panreac, A8943  
Sigma, P1644  
Sigma P7626  
Medicago, 09-8912-100

PLA ligase and a ligation buffers	Sigma, DUO92008
PLA polymerase and amplification buffers	Sigma, DUO92008
Polyvinylidene difluoride membranes (PVDF)	BioRad, 1620174
Protease inhibitors (PI)	Sigma, P8340
Proteinase K	Sigma P2308
Pyruvate	Agilent Technologies, 103578-100
Rotenone	Sigma, R8875
Seahorse DMEM medium pH 7.4	Agilent Technologies, 103575-100
Seahorse real-time ATP rate assay	Agilent Technologies, 103591-100
Seahorse XF calibrant	Agilent Technologies, 103059-000
Seahorse XF HS Mini 8-well plates	Agilent Technologies, 103022-100
Sodium deoxycholate (SOD)	Sigma, D6750
Sodium dithionite	Sigma, 71699
Sodium Fluoride (NaF)	Sigma, S7920
Sodium orthovanadate ( $\text{Na}_3\text{VO}_4$ )	Sigma, S6508
S-p-bromobenzylglutathione cyclopentyl diester (SML)	Sigma, SML 1306
Succinate	Sigma, S3674
Tetramethylrhodamine ethyl ester (TMRE)	Thermofischer, T669
Thiazolyl blue tetrazolium bromide (MTT)	Sigma, M2128
Triton X-100	Sigma, T8787
Trypsin-EDTA	Gibco, 25300-062
Type II collagenase	Worthington, LS004176









## 5. Results

---



## 5.1. Aging increases the accumulation of dicarbonyl-derived protein modifications in the aged mouse myocardium and F<sub>0</sub>F<sub>1</sub>-ATP synthase is a prominent modification target

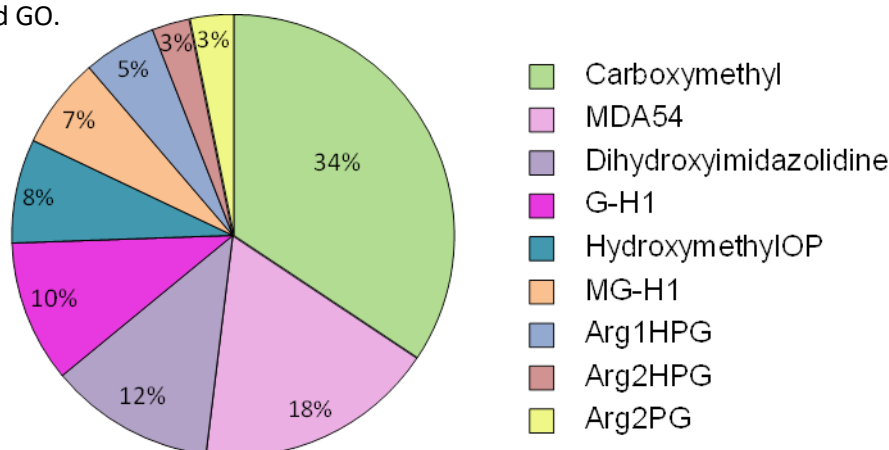
Many aged tissues and many age-related diseases have been characterized by the increased accumulation of dicarbonyl-modified proteins collectively known as AGEs<sup>20,162</sup>. AGEs are terminally modified compounds formed by non-enzymatic reactions between dicarbonyl intermediate products and proteins that ultimately impair protein structure, conformation and activity.

A previous study disclosed that due to an age-dependent deficiency in the GLO-I activity, the main detoxification enzymatic system of the most reactive precursors MGO and GO, the aged myocardial tissue accumulates significantly higher levels of dicarbonyl-modified peptides in comparison with the young one<sup>20</sup>. However, the types and distribution of modifications and whether these affected only extra-cellular or intra-cellular proteins were not evaluated.

### 5.1.1. The myocardium predominantly accumulates dicarbonyl-induced modifications

A descriptive analysis of the types of dicarbonyl-induced modifications detected in the myocardium by a post-translational modifications (PTMs) massive proteomics study detected 9 different types of adducts and demonstrated that CML (34%) was the most abundant type of dicarbonyl adduct in the heart, followed by MDA54 (18%) and dihydroxyimidazolidine (12%) (Fig. 1).

Interestingly, 5 out of the 9 detected modifications, adding up to 81% of the total, derived almost exclusively from the dicarbonyl products MGO and GO, whose contribution to the overall amount of modifications is directly affected by the deficiency in the GLO-I system previously described. Dihydroxyimidazolidine, MDA54, and MG-H1 derive exclusively from MGO, and G-H1 exclusively from GO. CML on the other hand can be produced from GO or glucose. Finally, all of Arg1HPG, Arg2HPG, Arg2PG and hydroxymethylOP derive from phenylglyoxal, an aldehyde related to both MGO and GO.



## Results

**Figure 1: The types of dicarbonyl-induced modifications in murine myocardium.** Pie chart represents the different types of dicarbonyl modifications present in the mouse myocardium and the abundance of each type expressed as percentage of the total. CML (34%), MDA54 (18%), dihydroxyimidazolodine (12%), G-H1 (10%), hydroxymethylOP (8%), MG-H1 (7%), Arg1HPG (5%), Arg2HPG (3%), and Arg2PG (3%) were identified in the indicated proportions.

### 5.1.2. Myocardial dicarbonyl adducts almost exclusively affect lysine and arginine

Next, a qualitative analysis of the types of amino acids affected by the different dicarbonyl reactions demonstrated that lysines and arginines are the amino acids that form the predominant targets of dicarbonyl modifications in the heart (Table 1). Interestingly, these two amino acids have a very high probability of falling in functional areas of the proteins such as protein-protein interaction sites producing total loss of function of the target protein<sup>171</sup>.

		Lysine	Arginine	Tryptophan
1	<b>Carboxymethyl</b>	82%		18%
2	<b>MDA54</b>	55%	45%	
3	<b>HydroxymethylOP</b>	100%		
4	<b>Dihydroxyimidazolodine</b>		100%	
5	<b>G-H1</b>		100%	
6	<b>MG-H1</b>		100%	
7	<b>Arg1HPG</b>		100%	
8	<b>Arg2HPG</b>		100%	
9	<b>Arg2PG</b>		100%	

**Table 1: The amino acid targets of the different types of dicarbonyl reactions in murine myocardium.** The table represents the kinds of amino acid that constitute targets of dicarbonyl reactions detected by the proteomics analysis. Lysine and arginine are the most affected amino acids followed by tryptophan. The numbers indicate the percentage of the given type of modification that affects each kind of amino acid.

### 5.1.3. Dicarbonyl-induced modifications majorly accumulate on mitochondrial proteins

Next, we evaluated the distribution of dicarbonyl-induced modifications. While it is clear that the aged murine heart accumulates significantly higher levels of these modifications than the young one<sup>20</sup>, it was not known whether they affect predominantly intra- or extracellular proteins and whether a specific organelle is more abused in this context. The analysis clearly demonstrated

that the absolute majority of the detected dicarbonyl adducts affect intracellular proteins (since they affect proteins that are found in subcellular compartments like the cytosol and other organelles) while a small minority (less than 7%) affect extracellular ones (in the Others category) (Fig. 2). This analysis also disclosed that mitochondria harbour the highest percentage of dicarbonyl-modified proteins (Fig. 2). Significant amounts of modified peptides were also found affecting myofibril, cytoskeleton and cytosolic proteins (Fig. 2).

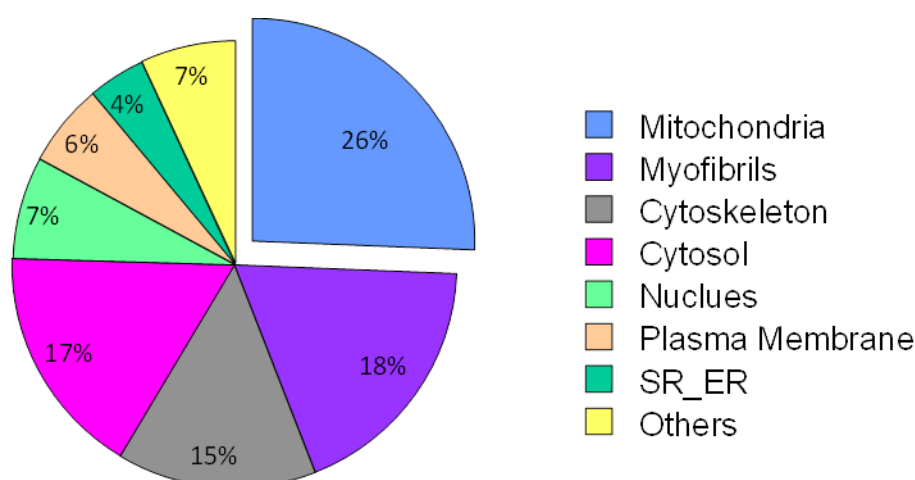


**Figure 2: The distribution of dicarbonyl-modified proteins in subcellular compartments of the myocardial tissue.** Pie chart represents the distribution of dicarbonyl-modified proteins in the different compartments of the cell, where the mitochondria harbours the highest number (26%), followed by the myofibrils (18%), cytockeleton (15%), cytosol (17%), nucleus (7%), plasma membrane (6%), SR\_ER (4%) and the final 7% in other compartments including the golgi apparatus, the endosome, the lysosome, the peroxisome and the extracellular space.

The age-dependent increase in mitochondrial dicarbonyl-modified peptides was corroborated by Western Blot analysis in purified SSM and IFM from young and old mouse hearts that were immunoblotted against MGO-derived modifications (MAGEs) and CML. Immuno-labeling against MAGEs disclosed a significant increase in aging specifically affecting the IFM subpopulation (Fig. 3), while immunoblotting against CML demonstrated a significant age-dependent increase in both SSM and IFM from old mouse hearts (Fig. 4). These findings led us to wonder whether the  $F_0F_1$ -ATP synthase could be a target of dicarbonyl modification in advanced age in mouse hearts.

## Results

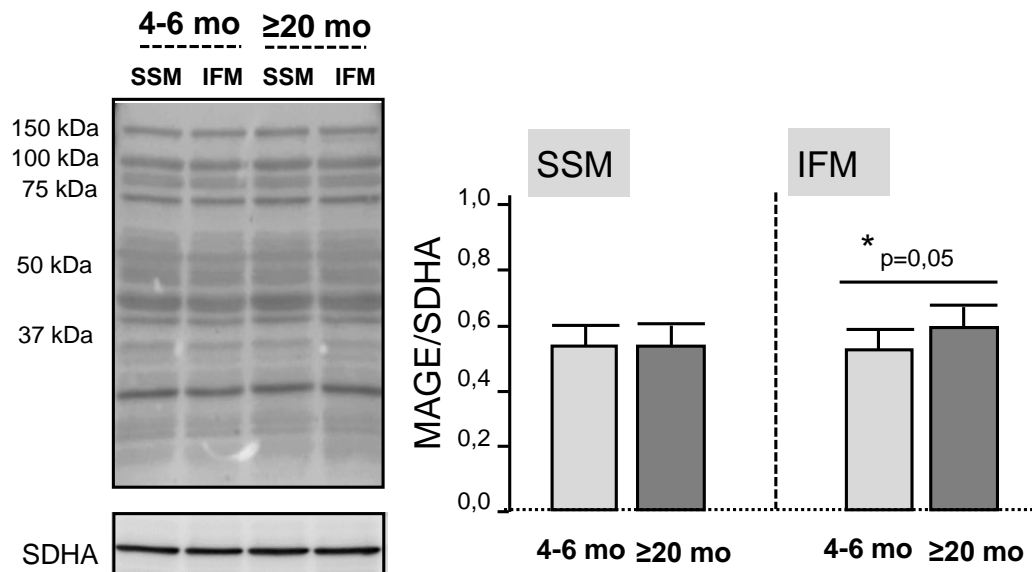


**Figure 3: Aging increases MAGEs in IFM of old mouse hearts.** Methylglyoxal-derived modifications (MAGEs) levels in SSM and IFM from young and old mouse hearts detected by WB; SDHA (succinate dehydrogenase complex) was used as loading control. Bar graphs represent the ratios between the optical density of the overall MAGEs in each mitochondrial population/group of age and SDHA and disclose a significantly higher MAGE accumulation specifically affecting the IFM subpopulation from old mouse hearts. Data are expressed as mean±SEM (n=5 mice per group, \*p=0.05).

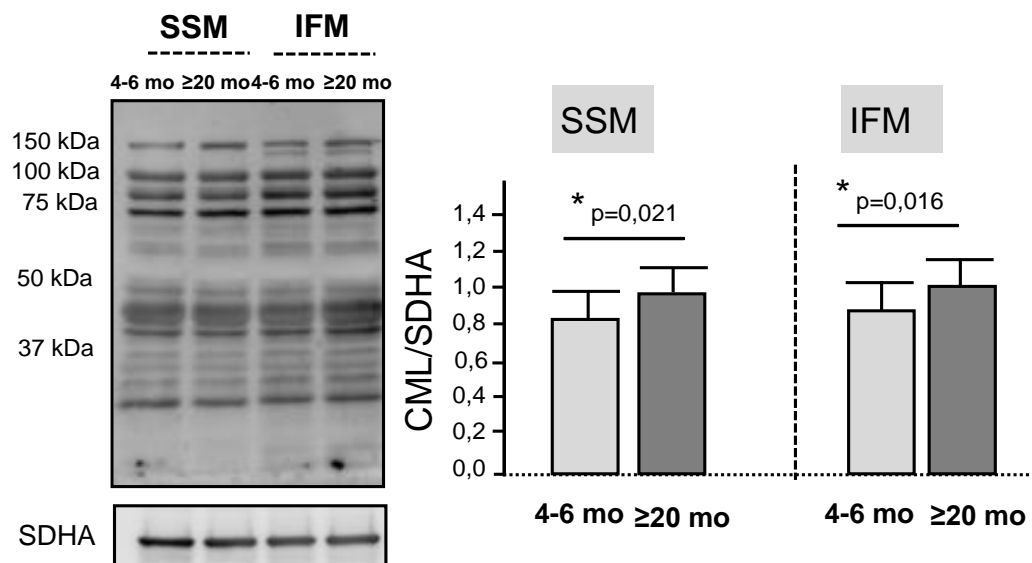


**Figure 4: Aging increases CML in SSM and IFM of old mouse hearts.** CML levels in SSM and IFM from young and old mouse hearts detected by WB; SDHA (succinate dehydrogenase complex) was used as loading control. Bar graphs represent the ratios between the optical density of the overall CML proteins in each mitochondrial population/group of age and SDHA and disclose a significantly higher CML accumulation affecting both the SSM (\*p=0.021) and IFM (\*p= 0.016) subpopulations of old mouse hearts. Data are expressed as mean±SEM (n=5 mice per group).

#### 5.1.4. The F<sub>0</sub>F<sub>1</sub>-ATP synthase is a prominent target of dicarbonyl-modification in aged myocardium

Since F<sub>0</sub>F<sub>1</sub>-ATP synthase is a molecule rich in positively charged amino acids at the level of several essential subunits, therefore making it a potential target of dicarbonyl attack, and since it is an essential molecule for providing the energy the heart needs on beat-to-beat basis, we quantified the degree of F<sub>0</sub>F<sub>1</sub>-ATP synthase dicarbonyl-modification in the myocardium of young and old mice.

A high throughput differential proteomics analysis in whole myocardial homogenates from young and old mice revealed a significantly higher degree of dicarbonyl-induced modification in subunits  $\alpha$ , d, OSCP, e and g but not in subunit  $\beta$  of the mitochondrial F<sub>0</sub>F<sub>1</sub>-ATP synthase in the myocardium of the old mice. Importantly, both subunits e and g have been described to be essential for F<sub>0</sub>F<sub>1</sub>-ATP synthase dimerization<sup>113</sup>, a process that increases the bio-energetic efficiency of mitochondria and plays a role in cristae morphogenesis. The sigmoidal curve presented below demonstrates a shift to a higher abundance of the mentioned dicarbonyl-modified F<sub>0</sub>F<sub>1</sub>-ATP synthase subunits in myocardium of the old heart with respect to the global F<sub>0</sub>F<sub>1</sub>-ATP synthase peptides (Fig. 5).



Gene	Protein	Peptides	Zq	
			Young	Old
alpha	Atp5a1	GV <sup>R<sub>MDA</sub></sup> LTELLK		
d	Atp5h	YTALVDQEEK <sup>K<sub>CM</sub></sup> EDVK		
alpha	Atp5a1	ELIIGDR <sup>R<sub>DHI</sub></sup> QTGK		
alpha	Atp5a1	GQ <sup>R<sub>DHI</sub></sup> ELIIGDR		
alpha	Atp5a1	TSIAIDTIINQ <sup>K<sub>CM</sub></sup> R		
alpha	Atp5a1	GQ <sup>R<sub>MDA</sub></sup> ELIIGDR		
alpha	Atp5a1	<sup>R<sub>DHI</sub></sup> TGAIVDVPPVGEELLGR		
OSCP	Atp5o	VGQLL <sup>K<sub>CM</sub></sup> DPK		
alpha	Atp5a1	VVDALGNAIDG <sup>K<sub>MDA</sub></sup> GPIGSKTR		
d	Atp5h	IQEYE <sup>K<sub>CM</sub></sup> QLEK		
alpha	Atp5a1	QQQYSPMAIEEQVAVIYAGV <sup>R<sub>GH1</sub></sup> GYLDK		
g	Atp5l	LATF <sup>W<sub>CM</sub></sup> HYAK		
g	Atp5l	VELVPPTPAEIPTAIQSV <sup>K<sub>CM</sub></sup> K		
alpha	Atp5a1	GMSLNLEPDNVGVVVFVFGND <sup>K<sub>CM</sub></sup> LIK		
alpha	Atp5a1	QTG <sup>K<sub>CM</sub></sup> TSIAIDTIINQK		
alpha	Atp5a1	VVDALGNAIDG <sup>K<sub>CM</sub></sup> GPIGSK		
F6	Atp5j	<sup>R<sub>DHI</sub></sup> QASGGPVDIGPEYQQDLDR		
alpha	Atp5a1	<sup>R<sub>MDA</sub></sup> TGAIVDVPPVGEELLGR		
alpha	Atp5a1	GYLD <sup>K<sub>CM</sub></sup> LEPSK		
alpha	Atp5a1	AM <sup>K<sub>CM</sub></sup> QVAGTMK		
alpha	Atp5a1	HALIYDDL <sup>K<sub>CM</sub></sup> QAVAYR		
alpha	Atp5a1	EPMQTGI <sup>K<sub>CM</sub></sup> AVDSLVPPIGR		
alpha	Atp5a1	ISEQSDA <sup>K<sub>CM</sub></sup> LK		
alpha	Atp5a1	QVAGTM <sup>Ox<sub>K<sub>CM</sub></sub></sup> LELAQYR		
e	Atp5i	IER <sup>R<sub>MDA</sub></sup> ELAEAQDDSIK		
OSCP	Atp5o	LDQVE <sup>K<sub>CM</sub></sup> ELLR		
d	Atp5h	EDV <sup>K<sub>CM</sub></sup> <sup>SC<sub>RED</sub></sup> AEFVSGSGLR		
d	Atp5h	IPVPED <sup>K<sub>CM</sub></sup> YTALVDQEEK		
alpha	Atp5a1	VGL <sup>K<sub>CM</sub></sup> APGIIPR		
alpha	Atp5a1	SDG <sup>K<sub>CM</sub></sup> ISEQSDAK		
alpha	Atp5a1	DNG <sup>K<sub>CM</sub></sup> HALIYDDLK		

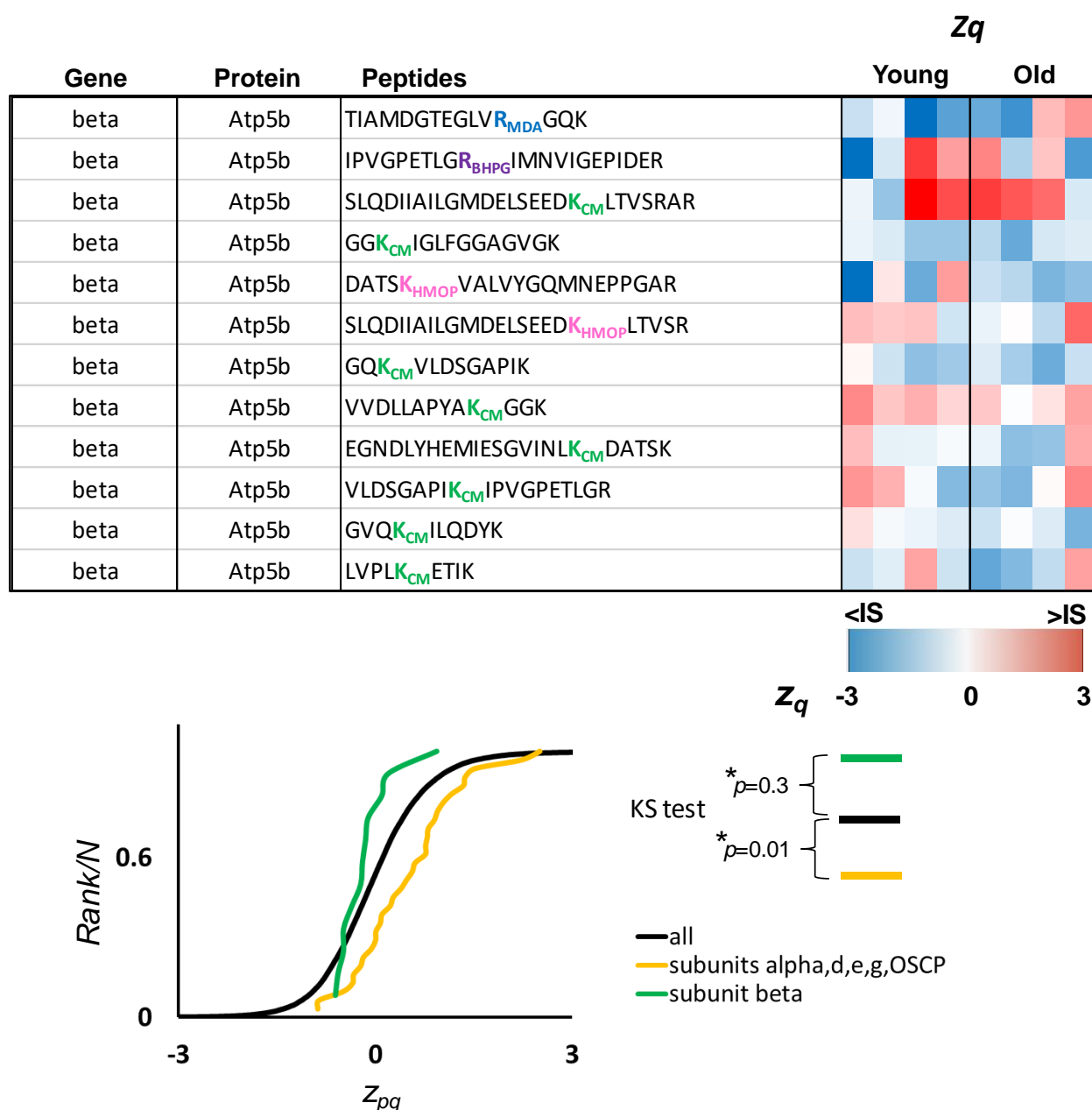


**Figure 5: Quantitative proteomics analysis of dicarbonyl-modified peptides from cardiac  $F_0F_1$ -ATP synthase during aging.** The heat-maps show ATP synthase dicarbonyl-modified peptides, protein-corrected standardized peptide  $z_{pq}$  values, whose magnitude is shaded according to the color scale at the bottom. DHI: Dihydroxy methylglyoxal adduct; CM: Carboxymethylation; MDA: MDA adduct +54; BHPG: bis(hydroxyphenylglyoxal); HMOP: 2-ammonio-6-[4-(hydroxymethyl)-3-oxidopyridinium-1-yl]- hexanoate. The cumulative distributions of the  $z_{pq}$  (old versus young) values from all nonmodified peptides from all proteins (All), as well as from dicarbonyl-modified peptides from the ATP synthase subunit(s) are shown. Differences were analyzed by two-tailed Kolmogorov-Smirnov test.

## Results

To corroborate the increased dicarbonyl-induced modification of  $F_0F_1$ -ATP synthase, both immunofluorescence colocalization and PLA were performed in isolated cardiomyocytes from young and old mouse hearts. In the immunofluorescence assay, isolated cardiomyocytes were simultaneously labelled against the subunit  $\alpha$  of  $F_0F_1$ -ATP synthase and MAGEs. The quantification of the degree of colocalization between  $F_0F_1$ -ATP synthase and the intracellular MAGEs using Mander's coefficient disclosed a significantly higher value in cardiomyocytes from old mouse hearts. These results indicate an increased  $F_0F_1$ -ATP synthase dicarbonyl modification associated with aging (Fig. 6). Immunofluorescence quantification was also performed for each of subunit  $\alpha$  and MAGEs and indicated significantly increased level of intracellular MAGE levels and preserved  $F_0F_1$ -ATP synthase expression in aging (Fig. 6-inset).

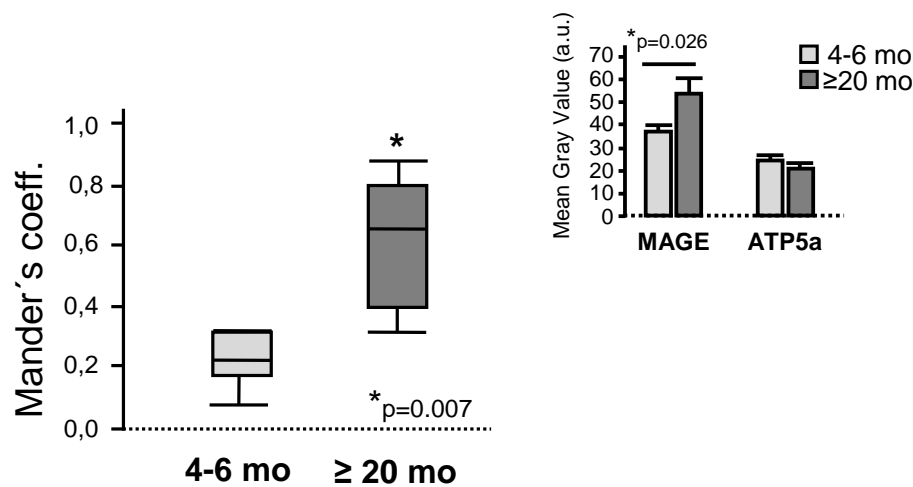


**Figure 6: Increased  $F_0F_1$ -ATP synthase dicarbonyl modification in aging.** B) Box plots represent the colocalization between  $F_0F_1$ -ATP synthase and MAGEs, as quantified by Mander's coefficient in central confocal Z-planes images of isolated immunolabeled cardiomyocytes and disclosed is significantly higher colocalization in cardiomyocytes from old mouse hearts (\* $p=0.007$ ). C) Inset represents the gray value of the respective anti-MAGE and anti-ATP5A fluorescent signals in those cardiomyocyte, and demonstrates significantly higher MAGE levels in cardiomyocytes from old mouse heart (\* $p=0.026$ ) with a conserved expression of  $F_0F_1$ -ATP synthase. Data correspond to mean $\pm$ SEM (n=16-24 cardiomyocytes, n=5 mice per group).

Finally, a PLA addressed to detect an inter-molecular interaction <40nm distance between  $F_0F_1$ -ATP synthase and MAGEs revealed an increased positive cross-reactivity in the cardiomyocytes from old mouse hearts, confirming an increased  $F_0F_1$ -ATP synthase dicarbonyl-induced modification in aged cardiomyocytes (Fig. 7).

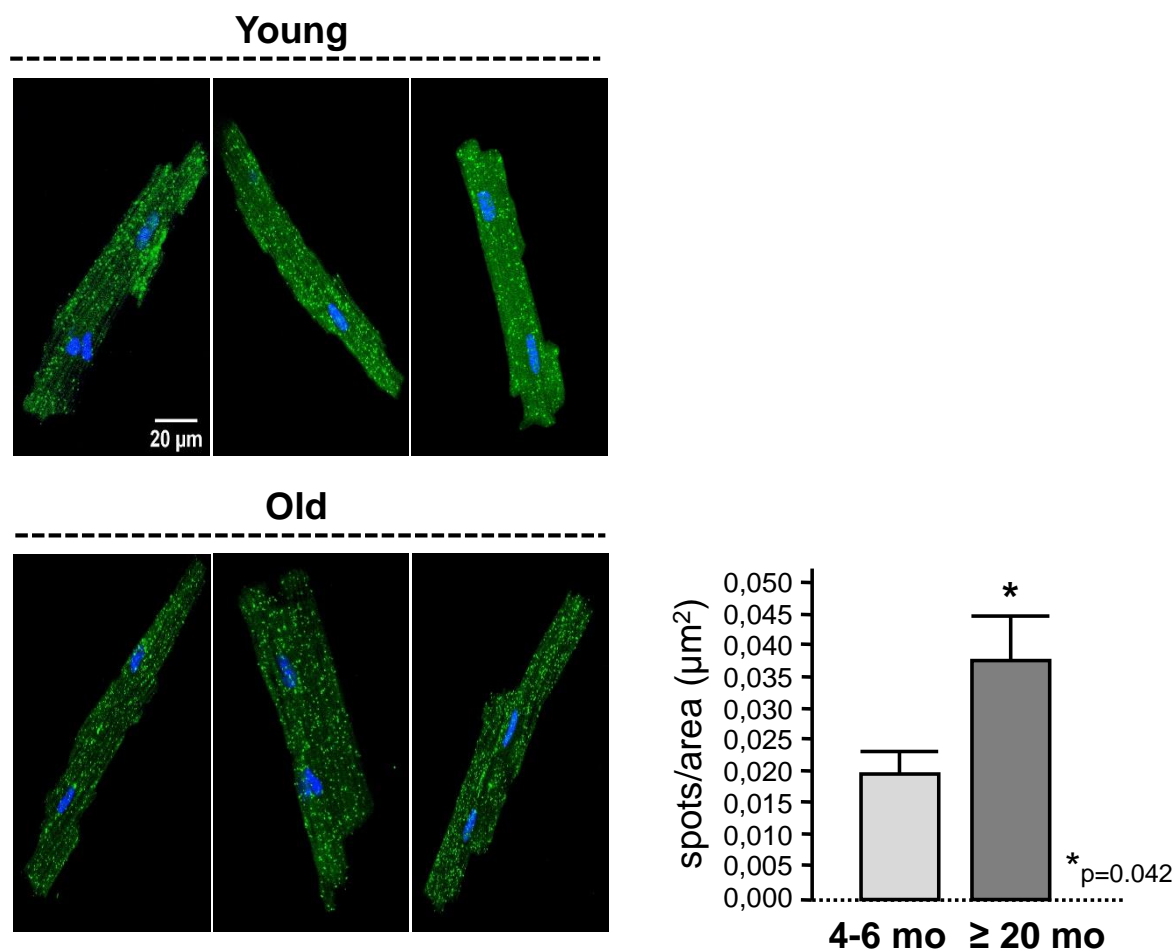


**Figure 7: Increased  $F_0F_1$ -ATP synthase dicarbonyl modification in aging.** Fluorescent confocal images of the interaction between  $F_0F_1$ -ATP synthase and MAGE in 6 representative cardiomyocytes (3 per group of age) detected by PLA. Positive cross-reactivity spots indicating  $F_0F_1$ -ATP synthase dicarbonyl-induced modification are shown in green, nuclei are shown in blue (Hoescht). Bar graphs correspond to the number of amplification spots resulting from  $F_0F_1$ -ATP synthase and MAGE interaction and indicate significantly higher  $F_0F_1$ -ATP synthase modification in cardiomyocytes from old mouse hearts. Data are expressed as mean $\pm$ SEM (n=12-13 cardiomyocytes, n=4 mice per group, \*p=0.042).

## **5.2. F<sub>0</sub>F<sub>1</sub>-ATP synthase dimerization is impaired in hearts from aged mice**

The F<sub>0</sub>F<sub>1</sub>-ATP synthase has long been recognized as an essential protein involved in mitochondrial cristae folding. Monomers of F<sub>0</sub>F<sub>1</sub>-ATP synthase self-associate into long rows of dimers that drag and fold the IMM into elongated tubular cristae<sup>114,115</sup>, a mitochondrial architectural signature which increases the cells' respiratory efficiency<sup>91</sup> by forming H<sup>+</sup> traps and increasing the surface area onto which bioenergetics molecules are incorporated. For this purpose, we explored whether the increased dicarbonyl-modification of F<sub>0</sub>F<sub>1</sub>-ATP synthase in the aged heart could affect its dimerization.

The quantification of the F<sub>0</sub>F<sub>1</sub>-ATP synthase dimerization was performed by two independent techniques: 1) blue native polyacrylamide gel electrophoresis (BN-PAGE) of purified heart mitochondria, and 2) competitive immuno-staining and PLA in intact cardiomyocytes.

### **5.2.1. Aging decreases the proportion of oligomerized mitochondrial F<sub>0</sub>F<sub>1</sub>-ATP synthase and increases its monomeric form**

Digitonin-solubilized SSM and IFM from hearts of young and old mice were resolved in native conditions and the gels were posteriorly incubated in an ATP-containing solution to determine the ATPase activity of F<sub>0</sub>F<sub>1</sub>-ATP synthase in-gel. Upon ATP hydrolysis into ADP by F<sub>0</sub>F<sub>1</sub>-ATP synthase, the liberated phosphate reacts with the lead in the assay solution and precipitates as lead phosphate at the site of the enzymatic activity. This reaction allows the visualization of the ATPase activity by the monomeric (Vm), dimeric (Vd) and oligomeric (Vo) forms of the F<sub>0</sub>F<sub>1</sub>-ATP synthase (Fig. 8A).

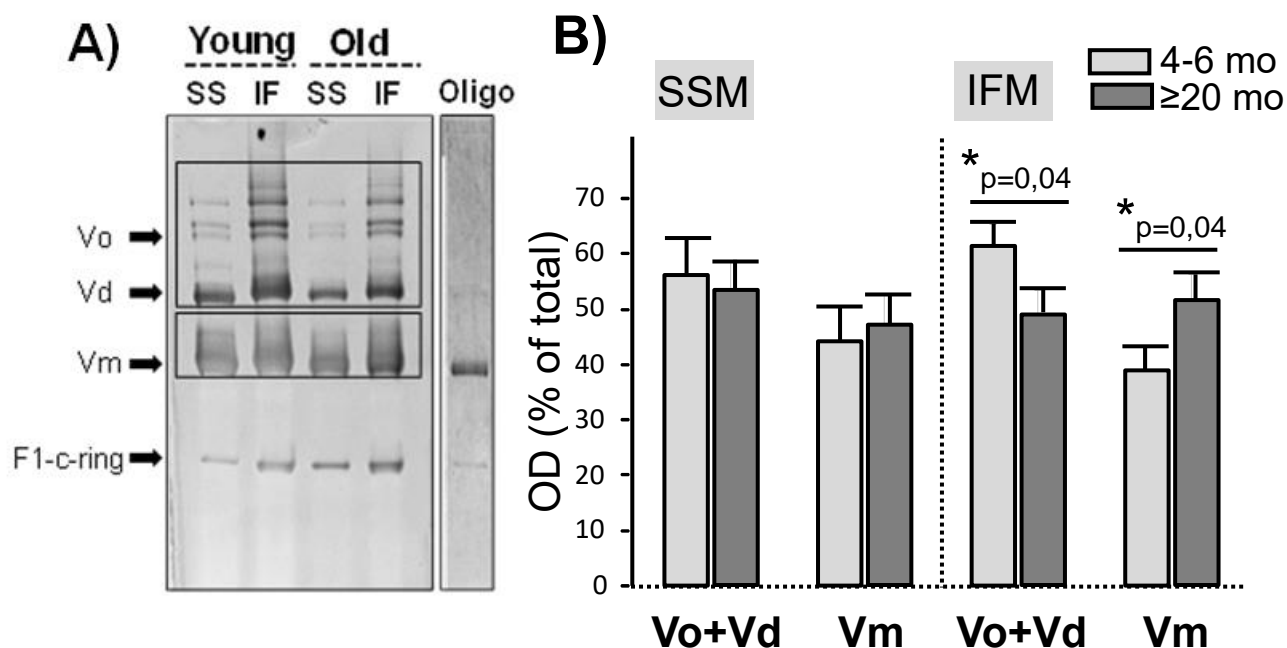


**Figure 8: Effect of aging on  $F_0F_1$ -ATP synthase dimerization in solubilized SSM and IFM.** A) Blue native gel with precipitated lead phosphate bands corresponding to ATPase activity of the monomeric (Vm), dimeric (Vd) and oligomeric (Vo) forms of  $F_0F_1$ -ATP synthase (complex V) and in the presence of  $F_0F_1$ -ATP synthase inhibitor oligomycin (oligo) in digitonin-solubilized SSM and IFM from young and old mouse hearts. B) Bar graph corresponds to the quantification of the optical density (OD) expressed as percentage of ATPase activity in the Vm and the Vo+Vd forms with respect to the total and disclose a significantly reduced proportion of the oligomerized forms of  $F_0F_1$ -ATP synthase in IFM of old mouse hearts. Data corresponds to mean $\pm$ SEM from n=6 young and n=5 old mice (\*p=0.04).

The optical density of the bands corresponding to the ATPase activity of each of the monomeric, and oligomeric (Vd + Vo) forms in addition to the total ATPase activity (sum of all forms) was quantified. The activity of each of these forms was expressed as a percentage of the total and the results indicated that the total ATPase activity did not change in the SSM or IFM with age. However, there was a significant reduction in the proportion of oligomerized  $F_0F_1$ -ATP synthase with a simultaneous significant increase in the monomeric form in the aged mouse heart specifically affecting the IFM subpopulation. This data may be indicating an age-dependent reduction in  $F_0F_1$ -ATP synthase oligomerization probably as a consequence of its increased glycation in advanced age.

### 5.2.2. Aging decreases $F_0F_1$ -ATP synthase dimerization in mouse cardiomyocytes

To confirm the decreased  $F_0F_1$ -ATP synthase found with in-gel ATPase activity in aging, we performed a PLA in isolated cardiomyocytes from young and old mouse hearts. PLA using competitive immunolabeling against subunit "d" of  $F_0F_1$ -ATP synthase (present in a single copy per  $F_0F_1$ -ATP synthase monomer)<sup>139</sup> disclosed a significantly reduced number of positive fluorescent spots (Fig. 9B) in old mouse cardiomyocytes. This result may indicate an increased distance between  $F_0F_1$ -ATP synthase monomers and therefore a decrease in  $F_0F_1$ -ATP synthase dimerization in aging.

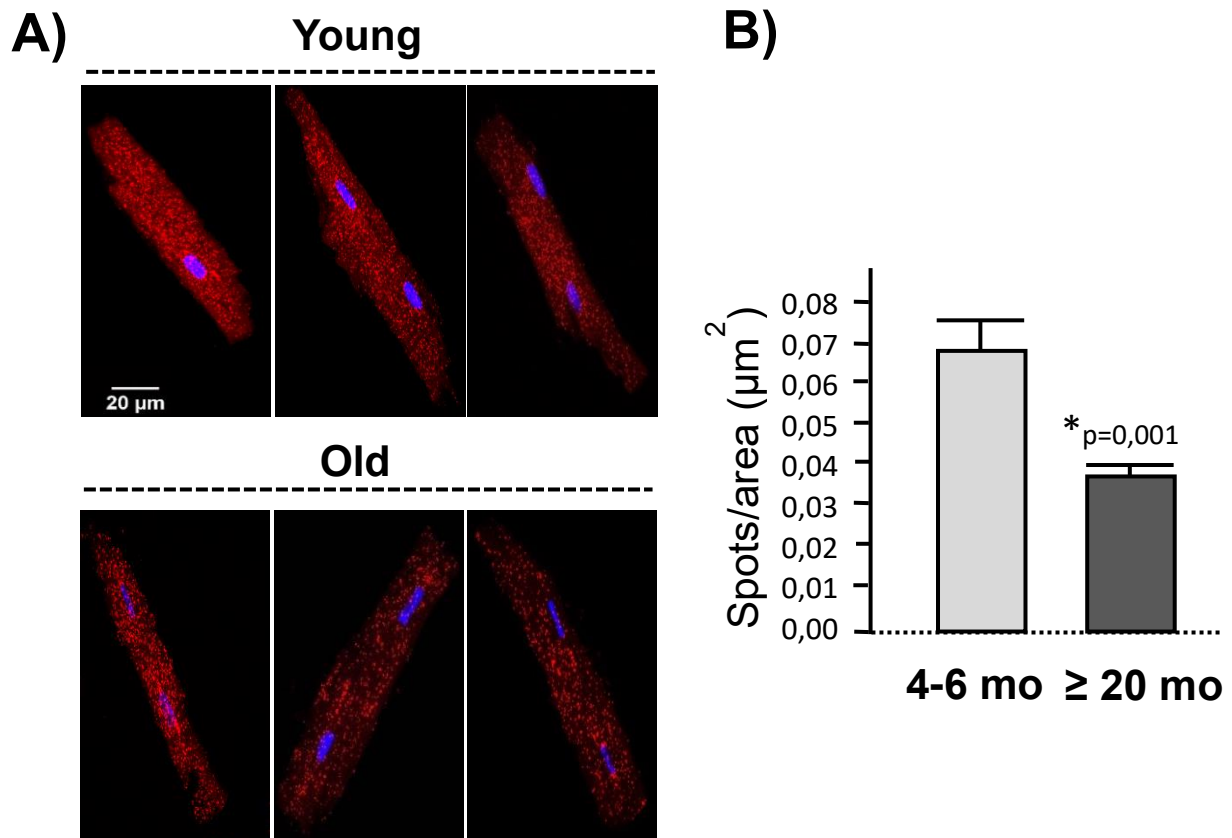


**Figure 9: Effect of aging on  $F_0F_1$ -ATP synthase dimerization in isolated cardiomyocytes.** A) Fluorescent confocal images of the monomer-monomer interaction within  $F_0F_1$ -ATP synthase in 6 representative cardiomyocytes (3 per group of age), detected by competitive immunolabeling against “d” subunits and PLA. Positive cross-reactivity spots (in red) indicate enzyme dimerization, nuclei are shown in blue (Hoescht). B) Bar graphs correspond to the quantification of the number of amplification spots resulting from  $F_0F_1$ -ATP synthase dimerization and demonstrate a significantly reduced number of spots that point to a lower degree of  $F_0F_1$ -ATP synthase dimerization in aged cardiomyocytes. Data correspond to mean $\pm$ SEM from n=15-23 cardiomyocytes, n=6 mice per group (\* $p=0.001$ ).

### 5.3. F<sub>0</sub>F<sub>1</sub>-ATP synthase expression is preserved in the aged heart

Because changes in the abundance of F<sub>0</sub>F<sub>1</sub>-ATP synthase could be the underlying cause for the reduced *in situ* dimerization of the enzyme, we evaluated the effect of aging on the expression levels of different subunits of the F<sub>0</sub>F<sub>1</sub>-ATP synthase by a proteomic analysis, WB analysis and an immunofluorescence assay.

#### 5.3.1. The expression of F<sub>0</sub>F<sub>1</sub>-ATP synthase is not modified in aging

High throughout differential proteomics using myocardium of young and old mice revealed no age-dependent differences in the relative abundance of the different subunits of F<sub>0</sub>F<sub>1</sub>-ATP synthase. The proteomics analysis detected peptides corresponding to 15 out of the 17 subunits that form the F<sub>0</sub>F<sub>1</sub>-ATP synthase but none of those peptides showed a significant change in old mice with respect to the young ones (Fig. 10). The similar distribution of the colour codes for each of the detected subunits disclosed similar expression levels in both young and old mouse hearts.

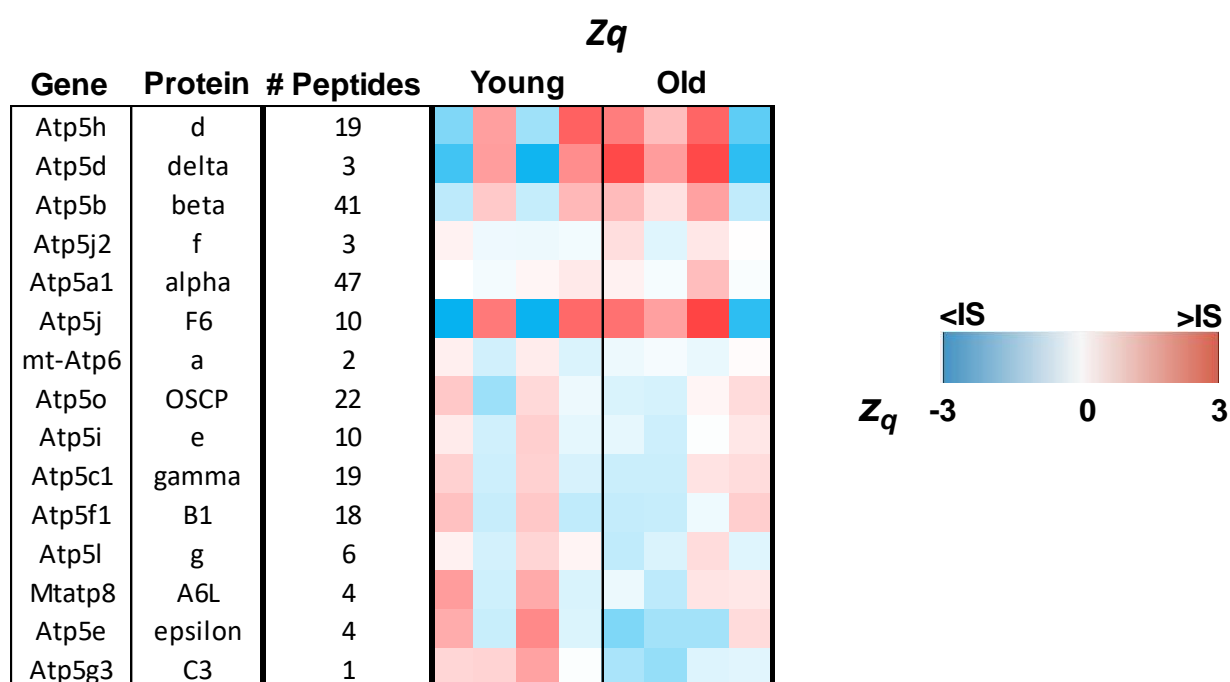


**Figure 10: Quantitation of ATP synthase subunits by MS proteomics.** Data were obtained from the analysis of heart samples from young (n = 4) and old mice (n = 4). The color for each protein corresponds to its standardized protein value (zq) and is shaded according to the color scale at the bottom. IS: internal standard. Data disclosed no age-associated changes in the expression levels of the detected peptides corresponding to 15 F<sub>0</sub>F<sub>1</sub>-ATP synthase subunits.



## Results

To corroborate a preserved expression level of  $F_0F_1$ -ATP synthase, WB analysis of the expression levels of subunits  $\alpha$  (ATP5A),  $\beta$  (ATPB),  $d$  (ATP5H) and OSCP (ATP5O) in isolated SSM and IFM of young and old mouse hearts was performed. The results did not disclose any age-related changes in protein levels (Fig. 11 A, B, C, D) thereby confirming the finding obtained with proteomics.

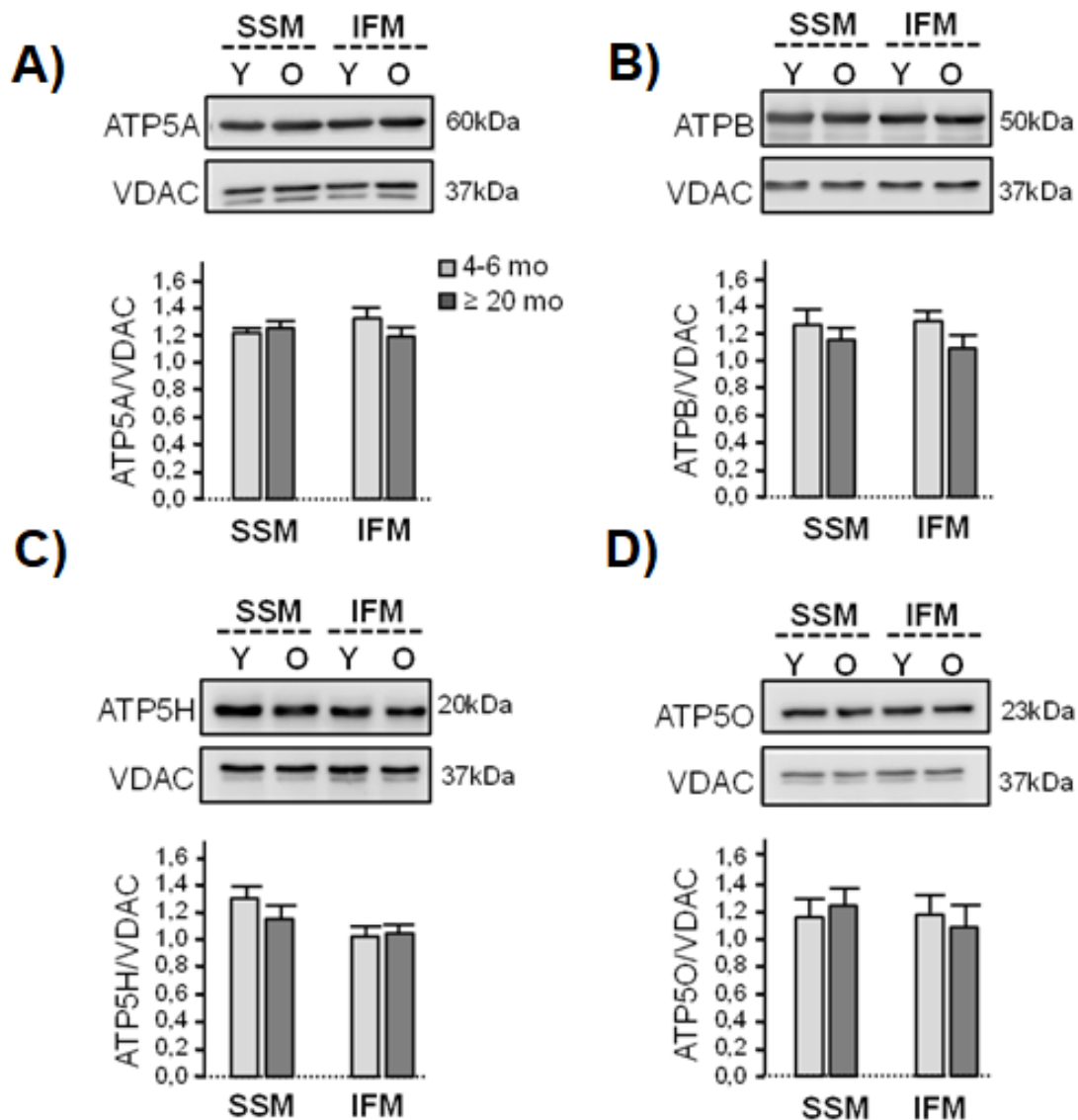


**Figure 11: Effect of aging on  $F_0F_1$ -ATP synthase expression.** Expression levels of  $F_0F_1$ -ATP synthase subunits  $\alpha$  (ATP5A),  $\beta$  (ATPB),  $d$  (ATP5H) and OSCP (ATP5O) subunits in purified heart SSM and IFM of young and old mice, detected by WB did not detect any age-dependent alteration in protein expression levels; VDAC (voltage-dependent anion channel) was used as loading control. Bar graphs represent the ratios between the optical density of each of these proteins and VDAC. Data are expressed as mean $\pm$ SEM (n=4-6 mice per group, p=ns). Aging does not affect the expression levels of  $F_0F_1$ -ATP synthase subunits  $\alpha$ ,  $\beta$ ,  $d$  or OSCP.

Finally, to evaluate the intracellular distribution and abundance of  $F_0F_1$ -ATP synthase, an immunofluorescence assay addressed to label subunit  $\alpha$  of the enzyme in isolated cardiomyocytes was performed and images were acquired with a fluorescent confocal microscope. This subunit is well represented in the enzyme because it is part of the catalytic head of the  $F_0F_1$ -ATP synthase. The quantification of the fluorescence pattern did not detect any age-dependent alteration (Fig. 12). Therefore, the results obtained using 3 independent methods indicate that the expression of the  $F_0F_1$ -ATP synthase is preserved in the aged heart.

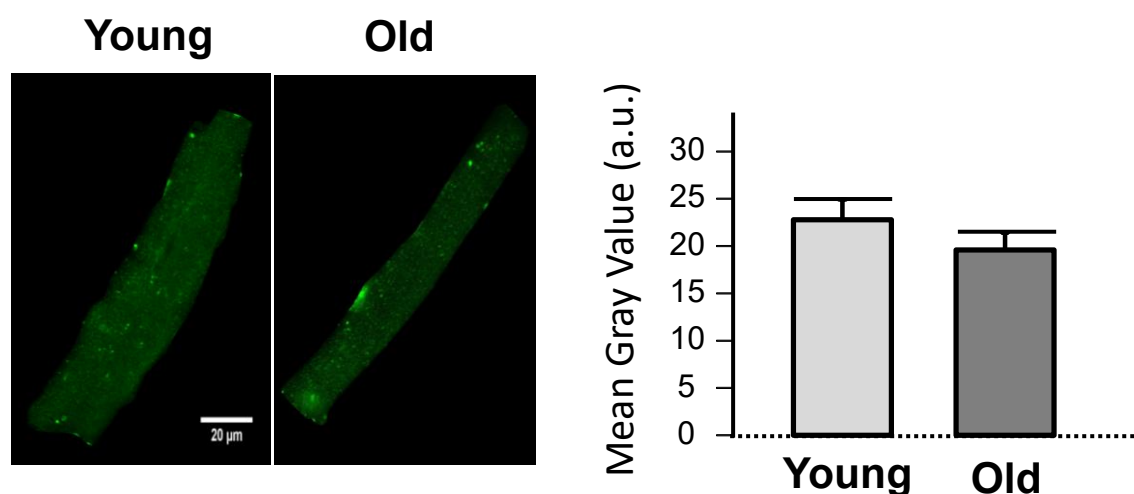


**Figure 12: Effect of aging on the expression of subunit  $\alpha$  of  $F_0F_1$ -ATP synthase.** Immunofluorescence images of isolated cardiomyocytes from young and old mouse hearts immunolabelled against subunit  $\alpha$  of  $F_0F_1$ -ATP synthase (green). Bar graphs represent the quantification of the mean gray values of the fluorescence intensity in  $n=2-3$  mice per group. The results indicate no changes in expression levels associated with aging. Data are expressed as mean $\pm$ SEM ( $p=ns$ ).

### 5.3.2. Aging does not alter the expression of other cristae-shaping proteins

Since other mitochondrial proteins have been proposed to participate in shaping the mitochondrial cristae like IF-1 (suggested to stabilize  $F_0F_1$ -ATP synthase dimers<sup>213</sup>) and OPA-1 (previously described to have an involvement in cristae remodelling<sup>214</sup>) we evaluated whether the expression levels of these proteins might be altered by age. WB quantification of IF1 and OPA1 expression in purified SSM and IFM from young and old mouse hearts did not show any modification with age (Fig. 13).

## Results

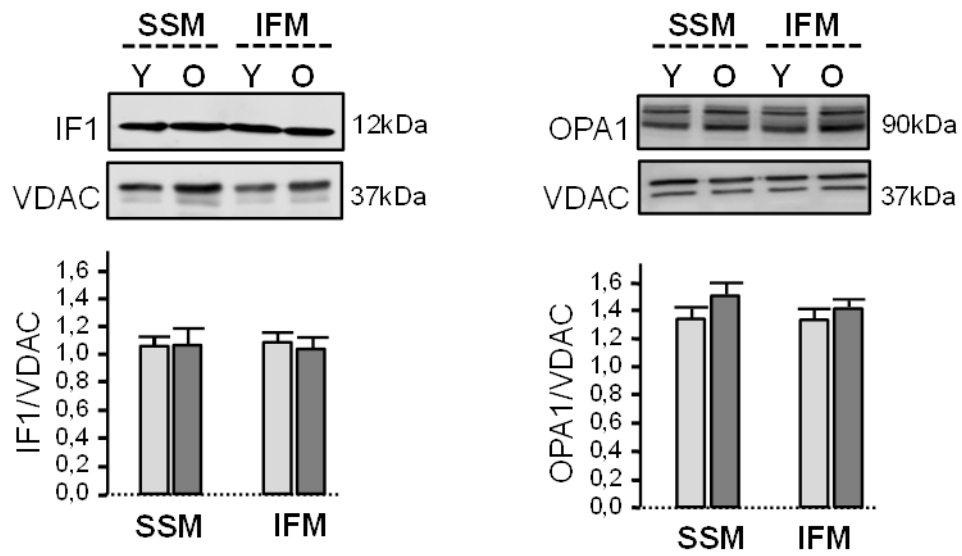


**Figure 13: Effect of aging on the expression of other cristae-shaping proteins.** Expression levels of IF1 and OPA1 in purified heart SSM and IFM of young (Y) and old (O) mice, detected by WB, did not disclose any age-dependent alteration in protein levels; VDAC (voltage-dependent anion channel) was used as a loading control. Bar graphs represent the ratios between the optical density of each of these proteins and VDAC. Data are expressed as mean±SEM (n=4-5 mice per group, p=ns).

## 5.4. Impact of Aging on F<sub>0</sub>F<sub>1</sub>-ATP Synthase activity

Since dicarbonyl-induced post-translational modifications can affect both the structure and the function of target proteins, we evaluated the effect of F<sub>0</sub>F<sub>1</sub>-ATP synthase modification and its decreased dimerization in aging on its activity in both the forward mode (ATP synthesis) and the reverse mode (ATP hydrolysis).

### 5.4.1. Dicarbonyl modification of F<sub>0</sub>F<sub>1</sub>-ATP synthase is associated with decreased mitochondrial state 3 respiration

Given that ATP synthesis requires the presence of a membrane potential that is generated by the ETC, the function of F<sub>0</sub>F<sub>1</sub>-ATP synthase in ATP synthesis cannot be dissected from the ETC and therefore can only be studied in the context of mitochondrial respiration by oximetry. Therefore, to evaluate the effect of F<sub>0</sub>F<sub>1</sub>-ATP synthase dicarbonyl-induced modification present in aging on the activity of F<sub>0</sub>F<sub>1</sub>-ATP synthase, crude SSM and IFM were obtained from young and old mouse hearts and oxygen consumption was evaluated in the presence of substrates that feed complex I (malate + glutamate) or complex II (succinic acid).

Oxygen consumption was evaluated at basal conditions and in the presence of ADP and oligomycin. The addition of ADP provides the substrate necessary to activate ATP synthesis at the level of F<sub>0</sub>F<sub>1</sub>-ATP synthase and therefore triggers mitochondrial respiration (state 3 respiration) directly coupled to ATP production, thereby providing an indirect measure of complex V function. Oligomycin modulates respiration by binding to F<sub>0</sub> domain of F<sub>0</sub>F<sub>1</sub>-ATP synthase and blocking its bidirectional function, consequently halting the entire respiratory machinery and providing information about oxygen consumption sensitive to the F<sub>0</sub>F<sub>1</sub>-ATP synthase inhibition (state 4 respiration).

Aging did not modify oxygen consumption in SSM and IFM at basal conditions (state 2) (Fig. 14. A-B). However, addition of ADP to stimulate F<sub>0</sub>F<sub>1</sub>-ATP synthase disclosed a significant reduction of the oxygen consumption (state 3) in the IFM of the aging group. This reduction was independent of the substrates used to feed the respiratory complexes (either complex 1 or complex 2). Importantly, no age-dependent differences were observed in the oxygen consumption in the SSM subpopulation (Fig. 14. A-B). Finally, aging did not modify the oxygen consumption sensitive to the F<sub>0</sub>F<sub>1</sub>-ATP synthase inhibitor oligomycin (state 4) in any of mitochondrial populations. Altogether, and since the only age-dependent alteration was observed with state 3 ADP-dependent respiration, these results indicate that the glycation of F<sub>0</sub>F<sub>1</sub>-ATP synthase during aging reduces OXPHOS efficiency in IFM secondary to a deleterious structural effect of glycation on F<sub>0</sub>F<sub>1</sub>-ATP synthase.

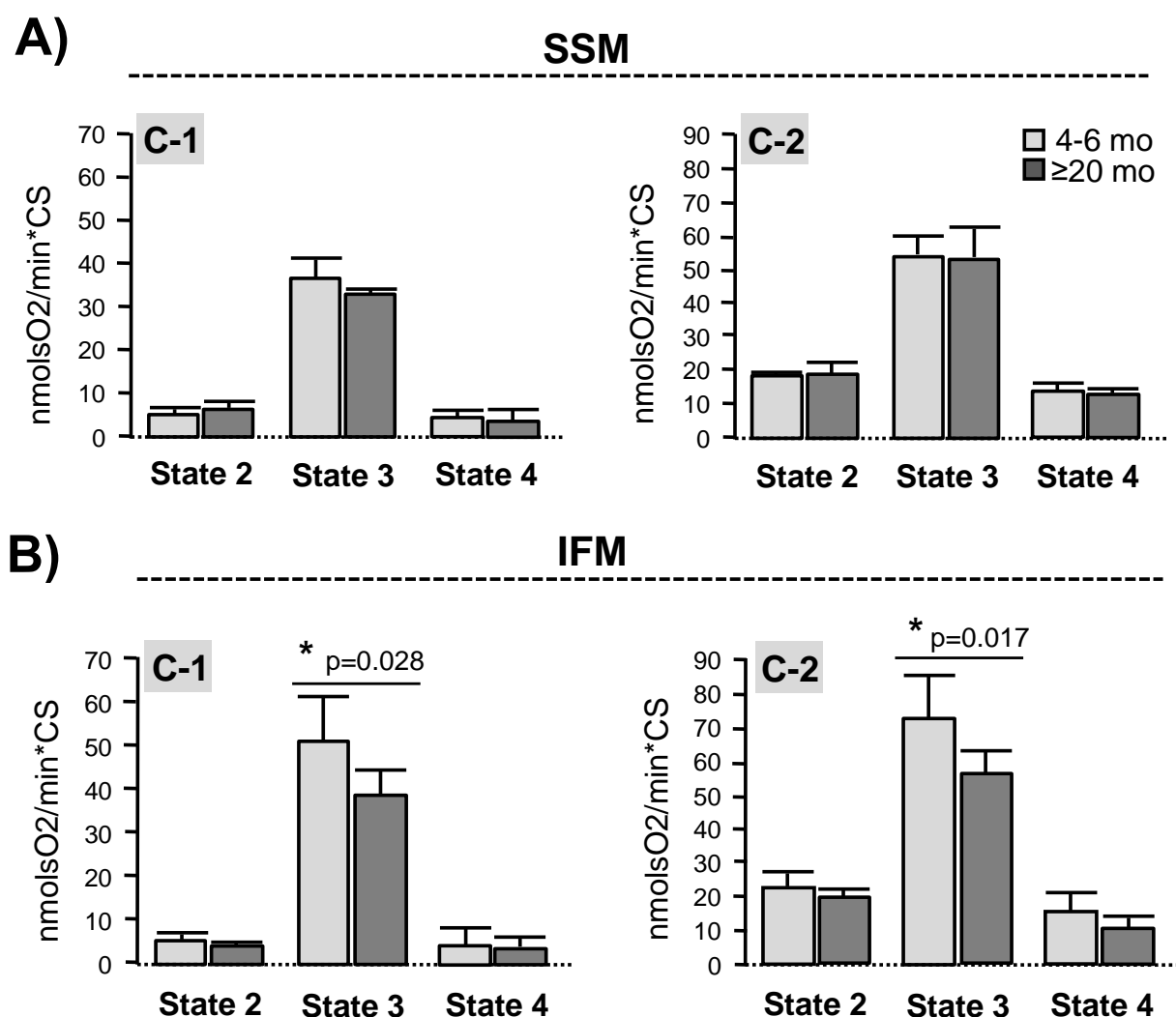


**Figure 14: Altered ADP-dependent mitochondrial oxygen consumption in aging.** Baseline oxygen consumption (state 2), ADP-stimulated oxygen consumption (state 3) and oligomycin-sensitive oxygen consumption (state 4) in isolated SSM and IFM from young and old mice hearts, in the presence of respiratory substrates for complex 1 (C-1) or complex 2 (C-2), as quantified by oxymetry. Results indicate a significant decrease in ADP-dependent respiration (state 3) specifically affecting IFM of old mouse hearts (\* $p=0.028$  with C-1 and \* $p=0.017$  with C-2 substrates). Data are expressed as mean $\pm$ SEM and correspond to nmolO<sub>2</sub>/min\*citrate synthase (CS) (n=6 mice per age group).

#### 5.4.2. Aging does not modify F<sub>0</sub>F<sub>1</sub>-ATP synthase hydrolytic activity

Next, we investigated the impact of aging on the *in vitro* activity of F<sub>0</sub>F<sub>1</sub>-ATP synthase in solubilized mitochondria. In this model, the contribution of mitochondrial architecture and H<sup>+</sup> gradient are absent and thereby only the ATP hydrolyase activity (i.e., ATP hydrolysis) can be evaluated.

The rate of ATP hydrolysis in solubilized SSM and IFM from young and old mice was evaluated *in vitro* in a 2-step reaction where in the first step ATP is added to solubilized mitochondria to allow ATP hydrolysis during 15 minutes, while in the second step, the unhydrolyzed

ATP is coupled to a reaction that produces NADPH. Spectrophotometrical analysis of absorbance changes due to NADPH production are proportional to the amount of ATP remaining in the sample, thereby allowing the calculation of the percentage of hydrolysed ATP.  $F_0F_1$ -ATP hydrolase activity was equal in mitochondria from young and old mice. (Fig. 15.A). Also, the efficiency of oligomycin inhibition on  $F_0F_1$ -ATP hydrolytic activity showed no age-dependent alterations (Fig. 15.B).

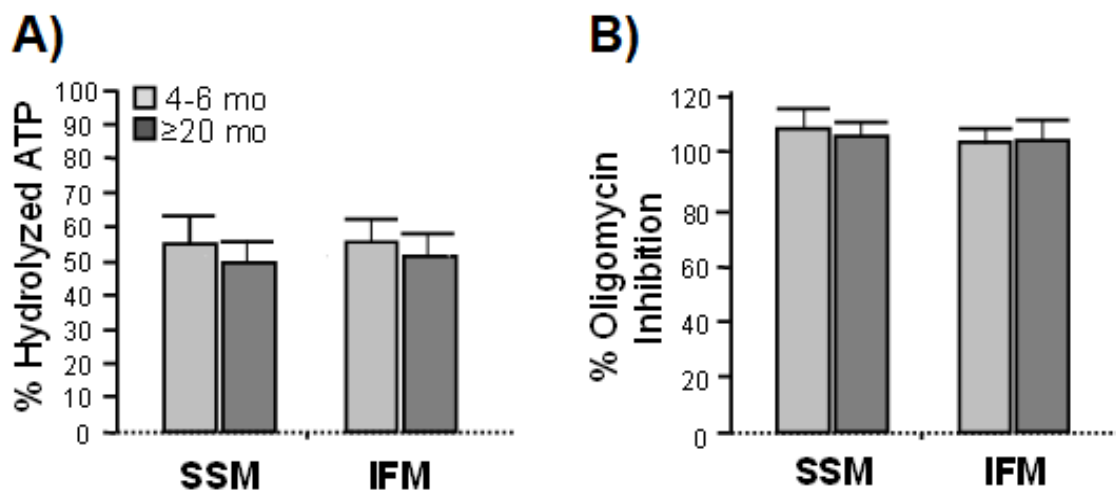


**Figure 15: *In vitro*  $F_0F_1$ -ATP hydrolase activity is not altered in aging.** A) ATPase activity *in vitro* in solubilised SSM and IFM quantified from changes in NADPH absorbance and expressed as percentage of hydrolysed ATP with respect to the total ATP. B) Percentage of inhibition of ATPase activity achieved after the addition of 10  $\mu\text{mol/L}$  oligomycin. Data are expressed as mean $\pm$ SEM ( $n=7$  mice per group,  $p=ns$ ) and indicate no age-dependent alterations in *in vitro*  $F_0F_1$ -ATP hydrolase activity nor in oligomycin sensitivity in neither of the mitochondrial subpopulations.

These data, together with the quantification of the total in-gel ATP hydrolase activity using BN-PAGE (see above), indicate that the dicarbonyl-induced modification of  $F_0F_1$ -ATP synthase during aging does not have a direct functional impact on the enzyme *in vitro*. However, the modification reduces the efficiency of  $F_0F_1$ -ATP synthase to generate ATP *in situ*, in which adequate mitochondrial cytoarchitecture and inner membrane folding plays a critical role for the efficiency of ATP generation.

## 5.5. Mitochondrial Ultra-Structural Alterations in Aging

### 5.5.1. Aging disturbs mitochondrial organization and ultrastructure in mouse hearts

To determine whether aging has a direct impact on the ultrastructure of the mitochondria in the heart, transmission electron microscope (TEM) images were obtained from the myocardium of young and old mice and analysed. The images displayed SSM, IFM and PNM organized beneath the sarcolemma, between the myofibrils and around the nucleus, respectively. However, the observation of low magnification images (1100X) disclosed a significantly disorganized mitochondrial arrangement specifically in the IFM subpopulation of the aged myocardium, and a greater heterogeneity of mitochondrial size and shape in the global mitochondrial population of the old mouse hearts in comparison with the young one (Fig. 16).

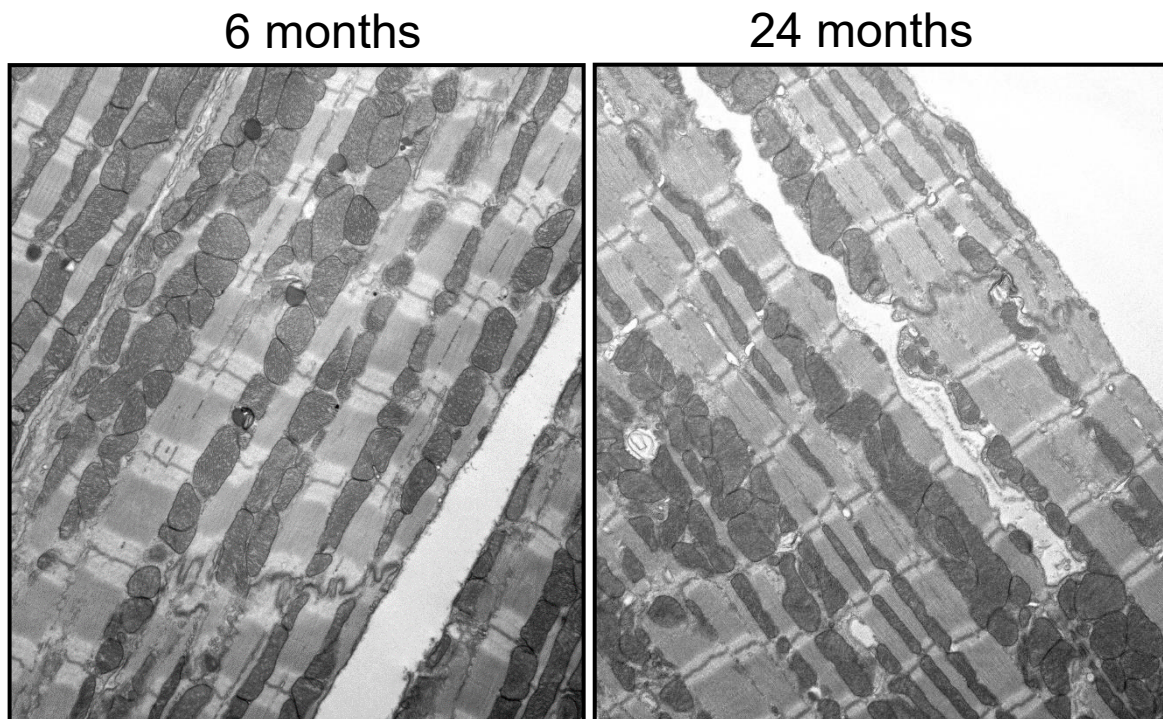


**Figure 16:** Ultrastructural images of murine myocardium. Representative low-magnification (1100X) images obtained with TEM from hearts of 1 young (left) and 1 old (right) mouse showing a more heterogeneous morphology, size and distribution of the mitochondria in the myocardium of old mice.

High magnification images (15000X) disclosed some morphological features affecting mitochondrial structure that were only present in the myocardium of old mice. Among them was the appearance of onion-like mitochondria in which the highly folded and parallel organization of the cristae was lost, and was instead replaced, in some mitochondria, with cristae organized in concentric circles known as “onion-like” cristae (Fig. 17) typically observed in pathological

conditions. Different degrees of cristae alterations were observed starting from a partially semi-circle to a completely concentric structure.

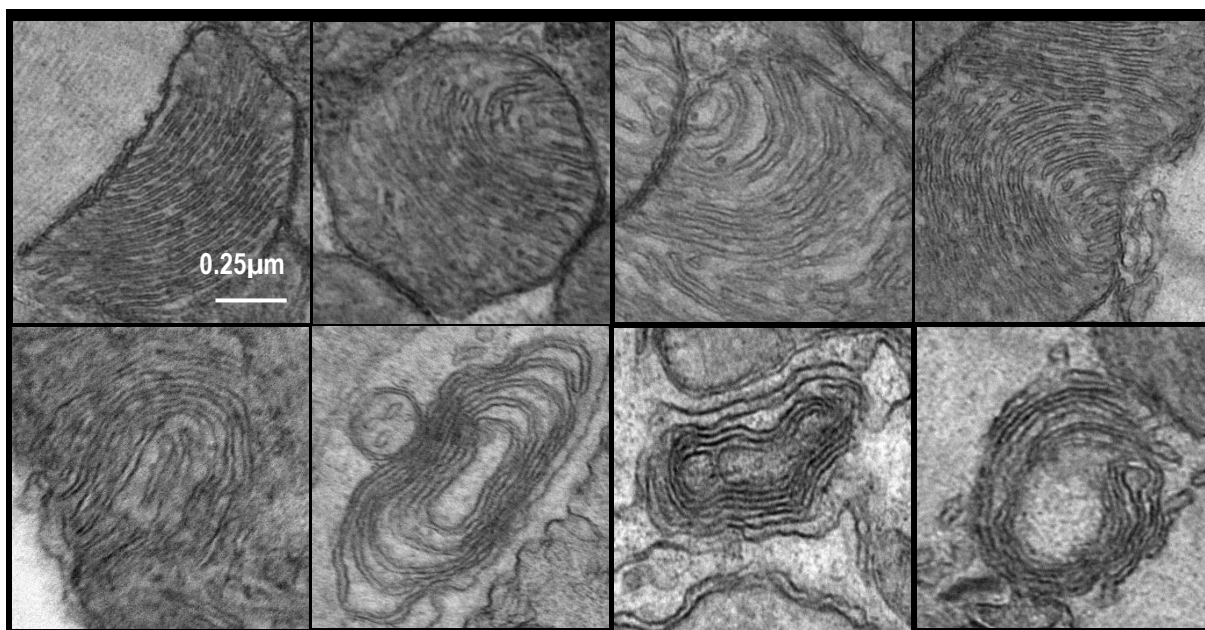


**Figure 17:** Onion-like mitochondria. Representative high-magnification (1500X) images obtained with TEM depicting different degrees of abnormal cristae morphology observed in mitochondria of aged heart. Images demonstrate mitochondrial inner membrane invaginations with partly semi-circular morphology to a fully concentric onion-like morphology.

Finally, the cristae tips, in which the  $F_0F_1$ -ATP synthase plays an essential role in their morphogenesis, presented an aberrant morphology where they appeared more squared and blunted in comparison to the young cristae tips, or the tip presented a double fold separated by a flat plateau (Fig. 18).

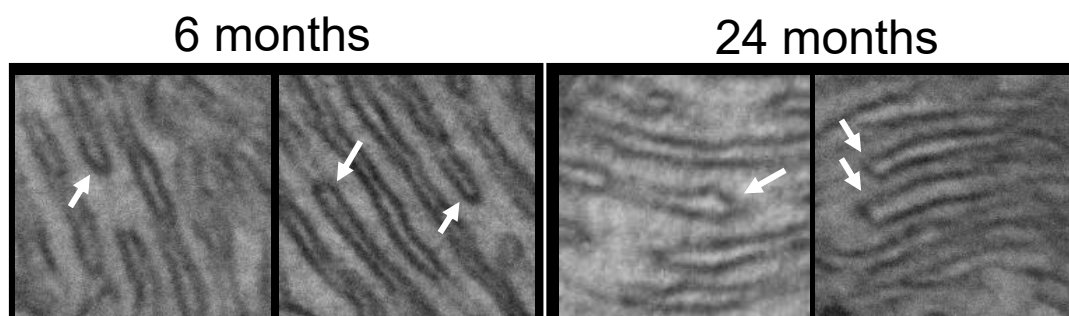


**Figure 18:** Ultrastructure of mitochondrial cristae tips observed with transmission electron microscope. Representative high-magnification (1500X) images from hearts of 2 young and 3 old mice showing normal cristae tips from young mouse hearts (left) vs abnormal wider cristae tips from old mouse hearts (right). The white arrows point to the examples of cristae tips.



## Results

The quantification of the curvature of the cristae tips using the b-spline coefficient ( $\mu\text{m}^{-1}$ , Fiji, Kappa-Curvature Analysis plugin) revealed a significantly lower curvature value in the mitochondria from old mouse myocardium when compared to the young ones (Fig. 19), indicating a higher prevalence of cristae tips with a wider angulation, which probably reflects a more loosely folded IMM.

Given that mitochondrial oxidative phosphorylation efficiency is directly affected by the structure of the cristae foldings, these pathological findings may be the underlying cause for the energetic deficiency observed in aging.

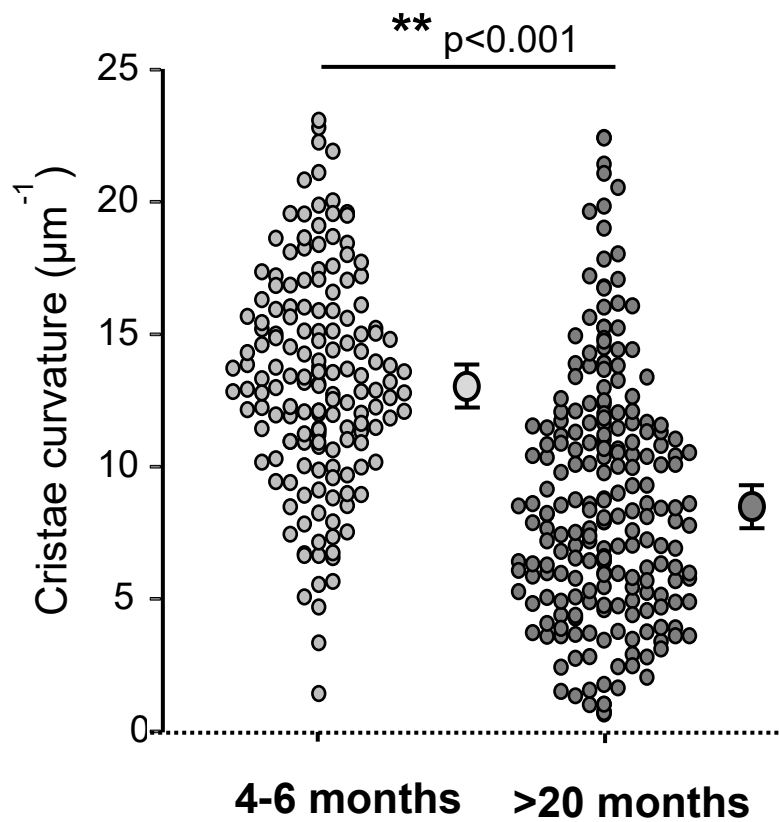


**Figure 19: Mitochondrial cristae tip curvature.** Quantification of the cristae tip curvature using the b-spline coefficient ( $\mu\text{m}^{-1}$ ) in 150 and 200 cristae tips from 2 young and 3 old mice, respectively. Data are expressed as mean $\pm$ SEM (\* $p < 0.001$ ) and disclose a significantly reduced cristae curvature in mitochondria of old mouse hearts.

## 5.6. $F_0F_1$ -ATP Synthase dicarbonyl-induced modification favours mitochondrial energy collapse

Recent studies suggested that the  $F_0F_1$ -ATP synthase may be the molecular entity of mPTP, an IMM pore that, if persists open results in energy collapse and cell death. Either a change in the dimerization state of  $F_0F_1$ -ATP synthase<sup>135</sup> or an alteration of the c-ring<sup>141</sup> were thought to cause pore opening. Therefore, we investigated whether the dicarbonyl-induced modification of  $F_0F_1$ -ATP synthase and the consequent reduction in its dimerization could have an effect on the susceptibility of mitochondria to undergo mPTP and energy collapse.

### 5.6.1. $F_0F_1$ -ATP synthase dicarbonyl modification increases the susceptibility to mPTP

To evaluate the effect of  $F_0F_1$ -ATP synthase dicarbonyl-induced modification on cardiomyocyte susceptibility to undergo mPTP, a standardized ROS-induced model of mPTP was used. For this purpose, isolated cardiomyocytes from young and old mouse hearts were loaded with TMRE and exposed to intermittent laser illumination under controlled conditions. TMRE is a fluorochrome that accumulates in mitochondria and releases ROS when illuminated with laser, thereby triggering mPTP in a calcium-independent manner<sup>211</sup> (Fig. 20A). Laser illumination induced flickering of mitochondrial fluorescence, reflecting transient depolarizations that culminated in permanent depolarization and mPTP. The occurrence of mPTP was identified as pH-sensitive drop in TMRE fluorescence coincident with rigor-shortening development in cardiomyocytes secondary to energetic collapse. The time necessary to induce mPTP (min at which cell shortening occurred), was considered an indicator of the mitochondrial susceptibility to undergo mPTP.

The necessary time to induce mPTP was significantly shorter in cardiomyocytes from old mouse hearts under control conditions, indicating a greater susceptibility of aging cells to undergo mitochondrial energy collapse (Fig. 20B). In our model, the mPTP inhibitor CsA failed to delay mPTP independently of age (Fig. 20B). Given that the mechanism of action of CsA depends on its calcium desensitization effect (it increases the threshold of calcium required to trigger mPTP<sup>215</sup>), our results indicate that in our model of mPTP occurs exclusively as a consequence of ROS, without the contribution of calcium. By contrast, acidic pH (6.4) was able to significantly delay the occurrence of mPTP in both young and old cardiomyocytes; however, the protective effect of pH was less pronounced in cardiomyocytes from old mouse hearts (Fig. 20B). Importantly, since  $H^+$  exerts its mPTP-inhibitory effect by binding to the OSCP subunit of  $F_0F_1$ -ATP synthase<sup>150</sup>, the increased glycation of OSCP in the aged mouse heart (Fig. 5) may explain the reduced inhibitory effect of the acidic pH on mPTP.

## Results

Finally, the degree of cell shortening, calculated as the percentage of cell shortening with respect to the initial length, was significantly more pronounced in cardiomyocytes from old mouse hearts. This result indicates the occurrence of a more severe pathological response in aged cardiomyocytes in contrast with young cardiomyocytes (rigor) (Fig. 20C).

All these results suggest that the dicarbonyl modification of  $F_0F_1$ -ATP synthase and the concomitant reduction in its dimerization state observed in aging may underlie the increased susceptibility of cardiomyocytes to undergo mPTP and energy collapse.

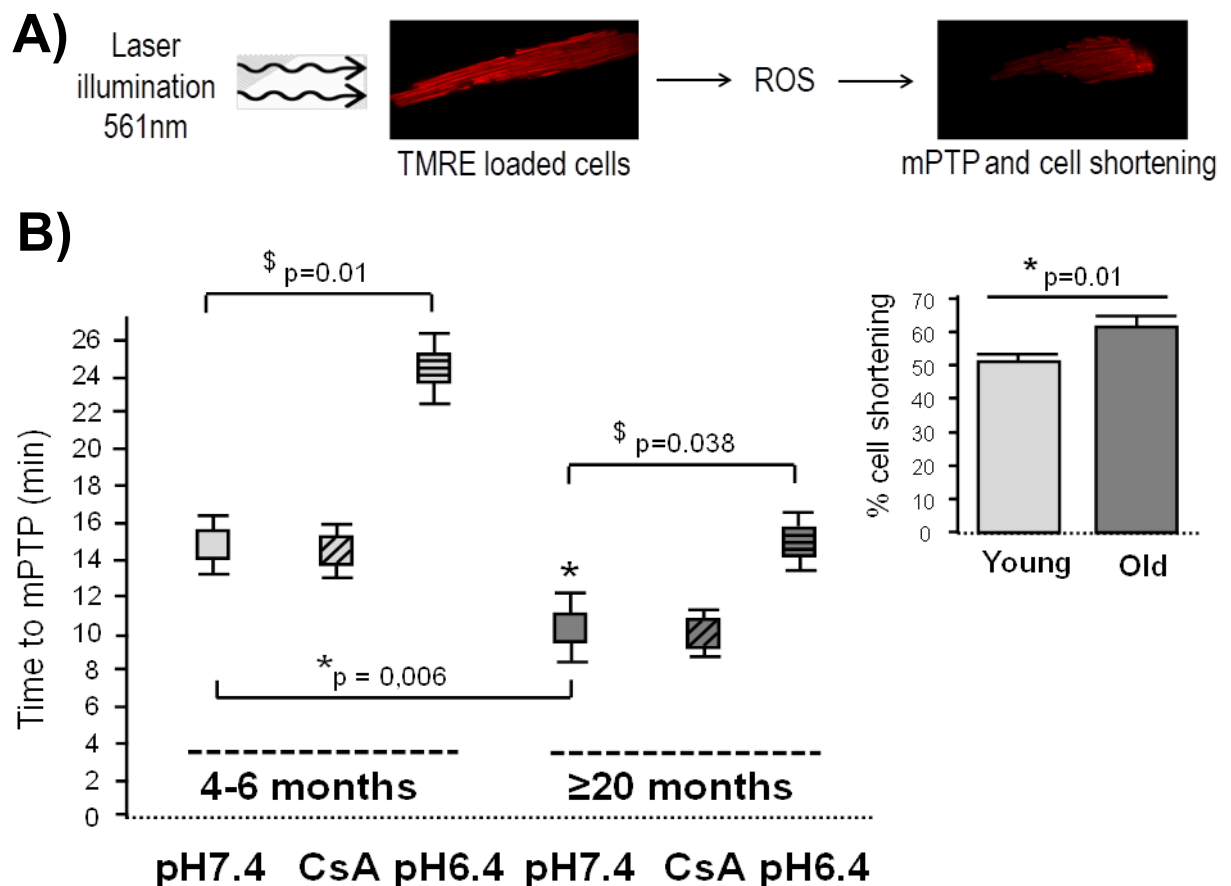


**Figure 20:  $F_0F_1$ -ATP synthase dicarbonyl-induced modification increases the susceptibility of cardiomyocytes to mPTP.** A) Scheme of protocol used to trigger mPTP in cardiomyocytes. Cells were loaded with TMRE and exposed to intermittent laser illumination (561nm) to induce ROS production that triggers mPTP, energy collapse and cell shortening. B) Susceptibility to undergo ROS-induced mPTP in cardiomyocytes from young and old mice, calculated as the time (in min) necessary to induce cell shortening using this protocol under control conditions (pH7.4), and in the presence of CsA (1 $\mu$ M) or acidic buffer (pH 6.4) to inhibit mPTP. The result indicates significantly higher susceptibility to undergo mPTP in aged cardiomyocytes under control conditions (\* $p=0.006$ ), no protection against mPTP by CsA independently of age, and a significant delay of mPTP with acidic buffer. The protective effect of pH was partially lost in the old cardiomyocytes (\* $p=0.01$ ) (\* $p=0.038$ ). The inset represents the degree of cell shortening secondary to mPTP in each group of age and disclose significantly greater cell shortening in cardiomyocytes of old mouse hearts (\* $p=0.01$ ). Data are expressed as mean $\pm$ SEM (n=18-23 cardiomyocytes, n=6 mice per group).

## 5.7. Induction of dicarbonyl modification of F<sub>0</sub>F<sub>1</sub>-ATP synthase in H9c2 cells recapitulates the age-dependent alteration in OXPHOS deficiency and increases mPTP susceptibility

In order to establish a cause-effect relationship between the dicarbonyl-induced modification of F<sub>0</sub>F<sub>1</sub>-ATP synthase and the OXPHOS deficiency and mPTP susceptibility observed in the aged cardiomyocytes, we exposed H9c2 cells to the chronic dicarbonyl stress present in aging. These cells share many functional characteristics with adult cardiomyocytes including a high dependency on mitochondrial metabolism and active oxidative phosphorylation<sup>203</sup>. Since in the aged mouse heart the dicarbonyl stress was present secondary to a deficiency in the GLO-I system, we simulated this stress by pharmacologically targeting GLO-I and inhibiting its activity with 5µmol/L of SML in the presence of an excess of MG (200µmol/L) during 3 consecutive days.

### 5.7.1. Dicarbonyl stress does not alter GLO-I expression but induces MAGE accumulation

We first investigated whether the treatment to induce dicarbonyl stress affected the expression levels of GLO-I in whole cell homogenates derived from both control and SML-MG treated cells by WB. The result indicated no changes in GLO-I expression upon dicarbonyl stress induction (Fig. 21), similarly to what has been previously described for aged cardiomyocytes<sup>20</sup>.

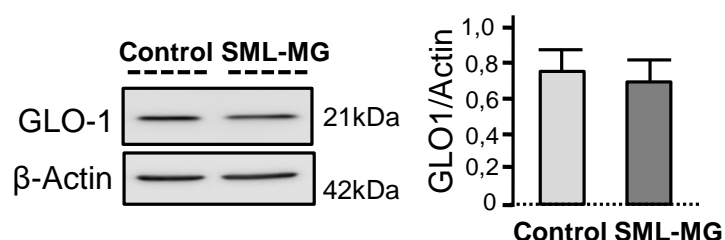


**Figure 21: Dicarbonyl stress does not modify GLO-1 expression.** Expression levels of GLO-1 in control and SML-MG treated H9c2 cells by WB.  $\beta$ -Actin was used as a loading control. Bar graphs represent the ratios between the optical density of GLO-1 and Actin. Data are expressed as mean $\pm$ SEM (n=3 independent experiments, p=ns) and indicate no significant alterations in GLO-1 expression under dicarbonyl stress.

Next, we evaluated whether this cell model was able to reproduce the increased in MGO-modified protein (MAGE) accumulation observed in aged cardiomyocytes<sup>20</sup>. For this purpose, both control and SML-MG treated H9c2 cells were immuno-labelled with anti-MAGEs that specifically target MGO-derived AGEs, during 3 consecutive days. The quantification of the mean gray value after immuno-fluorescent labelling disclosed a significant increase in intracellular MAGEs on the third day of the dicarbonyl stress induction with respect to the control group (Fig. 22). The increase in fluorescence was not statistically significant on days 1 and 2 (data not shown). For this purpose

## Results

most of the upcoming experiments in H9c2 were only performed on day 3 of the dicarbonyl stress induction in which MAGE accumulation becomes significant.

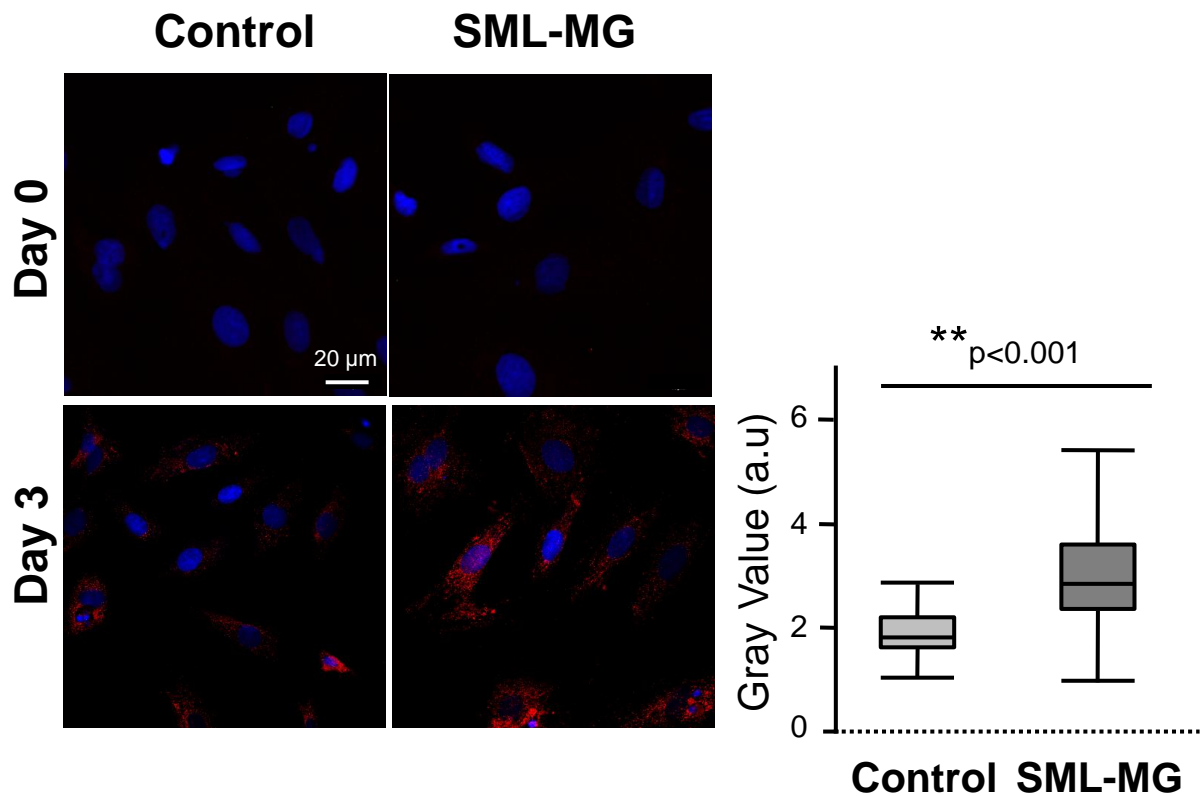


**Figure 22: Dicarbonyl stress induces intracellular MAGEs accumulation.** Immunofluorescence images of intracellular MAGEs (red) in H9c2 cells on baseline (day 0) and on day 3 of dicarbonyl stress, and the corresponding controls; nuclei are shown in blue (Hoescht). Box plots represent the quantification of MAGE immunolabelling in each group (n=80-86 cells per group, 3 independent experiments) and disclose a significantly higher MAGE accumulation in H9c2 cells treated with SML-MG (\*p<0.001).

The effect of dicarbonyl stress on MAGE accumulation was corroborated by WB analysis. The results demonstrated significantly higher MAGE levels in the SML-MG treated H9c2 cells in comparison with almost undetectable MAGE levels in the corresponding control group on the third day of the dicarbonyl stress induction (Fig. 23).

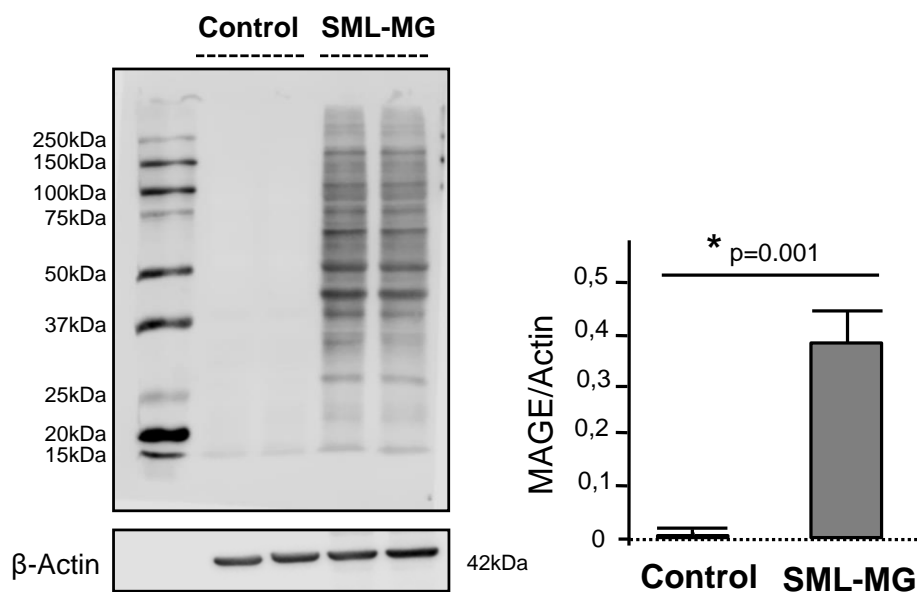
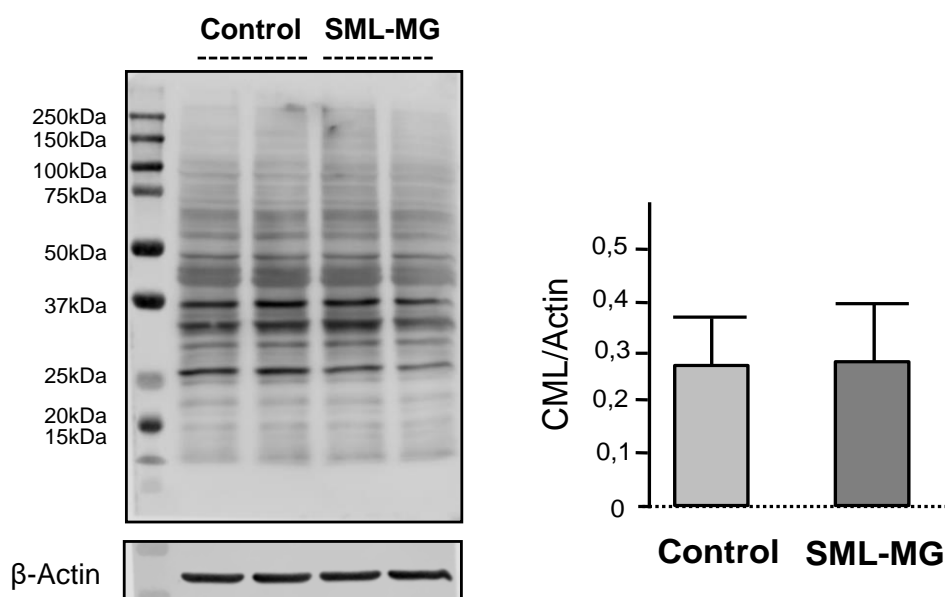


**Figure 23: Dicarbonyl stress induces intracellular MAGE accumulation.** MAGE levels in lysates from H9c2 cells on day 3 of dicarbonyl stress and the corresponding controls, detected by WB;  $\beta$ -actin was used as loading control. Bar graphs represent the ratio between the optical density of the overall MAGE-modified proteins in each group of cells and  $\beta$ -actin. Data are expressed as mean $\pm$ SEM (n=3 independent experiments) and indicated significantly higher levels of MAGEs in extracts of SML-MG treated H9c2 cells (\*p=0.001).

Given that GLO-I also detoxifies GO, we evaluated whether the SML-MG treatment caused an increase in CML-modified protein levels that principally derive from GO. No differences in CML levels were detected between the control and the SML-MG treated groups on the third day of the glycative treatment (Fig. 24). Because CML forms at a much slower rate (weeks) than MAGEs (days), this finding indicates that 3 days of dicarbonyl stress specifically affects MAGEs accumulation.



## Results

**Figure 24: Dicarbonyl stress does not induce intracellular CML accumulation after 3 days.** CML levels in lysates from H9c2 cells on day 3 of dicarbonyl stress and the corresponding controls, detected by WB;  $\beta$ -actin was used as loading control. Bar graphs represent the ratio between the optical density of the overall CML-modified proteins in each group of cells and  $\beta$ -actin. Data are expressed as mean $\pm$ SEM (n=3 independent experiments) and do not demonstrate increased CML accumulation after 3 days of dicarbonyl stress induction.

### 5.7.2. Dicarbonyl stress induces $F_0F_1$ -ATP synthase modification

We investigated whether our model of induced dicarbonyl stress was able to reproduce the increased dicarbonyl-induced modification of  $F_0F_1$ -ATP synthase present in aging. For this purpose, a PLA was performed on control and SML-MG treated H9c2 cells on day 3 of the dicarbonyl stress induction. The cells were simultaneously labelled against subunit  $\alpha$  of  $F_0F_1$ -ATP synthase and MAGEs and the molecular interaction between them was quantified as the number of fluorescent spots. The quantification disclosed significantly increased cross-reactivity between MAGE and the subunit  $\alpha$  of ATP synthase in the SML-MG cells. These results indicate increased dicarbonyl modification of  $F_0F_1$ -ATP synthase in the SML-MG cells with respect to the control group (Fig. 25).

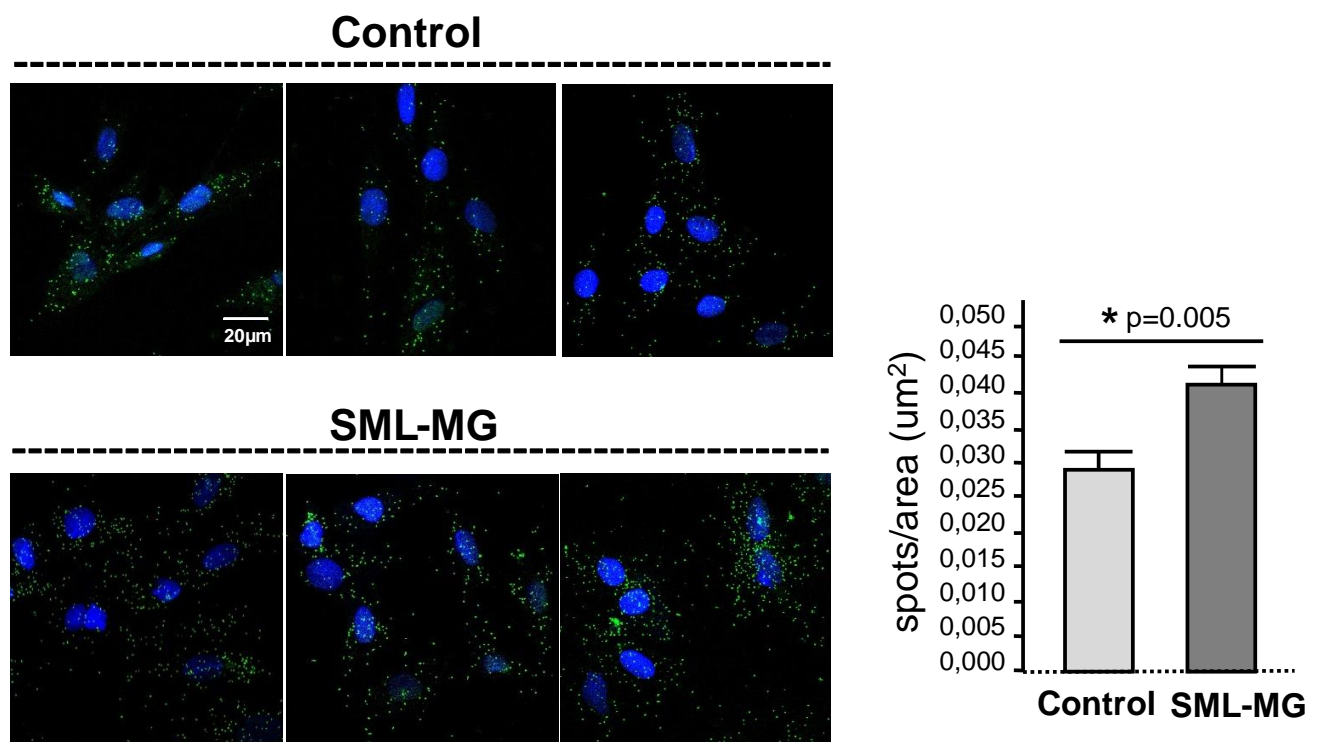


**Figure 25: Dicarbonyl increases  $F_0F_1$ -ATP synthase chemical modification.** Fluorescent confocal images of central Z-planes of H9c2 cells on day 3 of dicarbonyl stress and the corresponding controls depicting the interaction between  $F_0F_1$ -ATP synthase and MAGEs as detected by PLA. Positive cross-reactivity spots indicating  $F_0F_1$ -ATP synthase glycation are shown in green, nuclei are shown in blue (Hoescht). Bar graphs correspond to the quantification of the number of amplification spots resulting from  $F_0F_1$ -ATP synthase and MAGE interaction and demonstrate significantly higher  $F_0F_1$ -ATP synthase dicarbonyl-induced modification in the SML-MG treated cells (\*p=0.005). Data correspond to mean $\pm$ SEM (n=80-120 cells per group, 3 independent experiments).

### 5.7.3. Dicarbonyl stress reduces F<sub>0</sub>F<sub>1</sub>-ATP synthase dimerization

Finally, to investigate whether the dicarbonyl-induced modification of F<sub>0</sub>F<sub>1</sub>-ATP synthase is the causative mechanism involved in the reduced enzyme dimerization observed in the aged mouse hearts, we evaluated the degree of F<sub>0</sub>F<sub>1</sub>-ATP synthase dimerization in our model of induced dicarbonyl stress. PLA against subunit d of F<sub>0</sub>F<sub>1</sub>-ATP synthase was performed in control and SML-MG cells on day 3 of the glycative treatment. The quantification of the positive cross-reactivity spots demonstrated a significantly reduced number of spots in the SML-MG group, indicating an increased molecular distance between 2 monomers of the F<sub>0</sub>F<sub>1</sub>-ATP synthase and therefore a reduced F<sub>0</sub>F<sub>1</sub>-ATP synthase dimerization secondary to its dicarbonyl modification (Fig. 26).

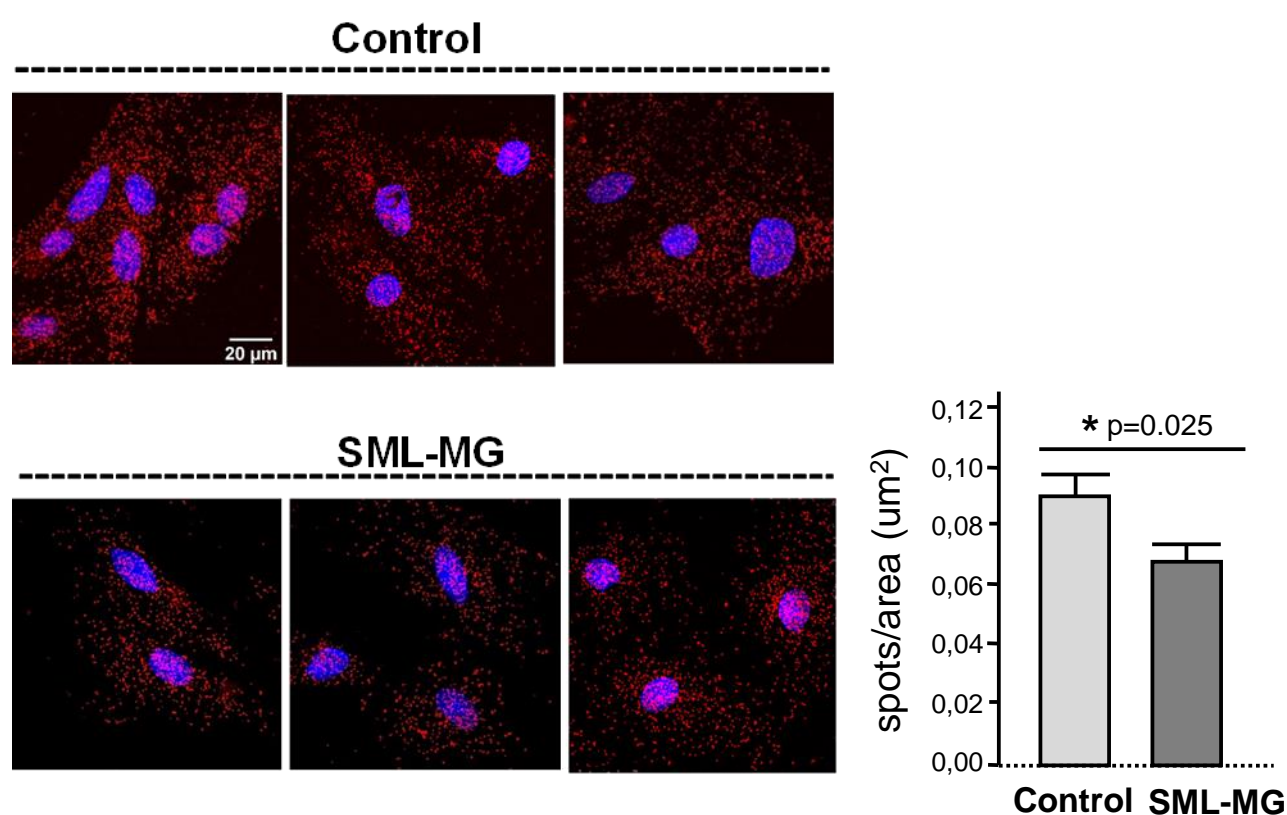


**Figure 26: Dicarbonyl stress decreases F<sub>0</sub>F<sub>1</sub>-ATP synthase dimerization.** Fluorescent confocal images of the monomer-monomer interaction within F<sub>0</sub>F<sub>1</sub>-ATP synthase in H9c2 cells on day 3 of dicarbonyl stress, and the corresponding controls, detected by competitive immunolabeling against “d” subunit and PLA. Positive cross-reactivity spots (in red) indicate enzyme dimerization, nuclei are shown in blue (Hoescht). Bar graphs correspond to the quantification of the number of amplification spots resulting from F<sub>0</sub>F<sub>1</sub>-ATP synthase dimerization and depict significantly reduced F<sub>0</sub>F<sub>1</sub>-ATP synthase dimerization in the SML-MG group (\*p=0.025). Data correspond to mean±SEM (n=60-70 cell per group, 3 independent experiments).



#### 5.7.4. Increased MAGE accumulation does not affect F<sub>0</sub>F<sub>1</sub>-ATP synthase expression levels

To evaluate whether decreased F<sub>0</sub>F<sub>1</sub>-ATP synthase could be due a decreased abundance of the protein, WB analysis was performed against several subunits of the enzyme. Similar to what was observed in the aged heart, neither subunits  $\alpha$ ,  $\beta$ ,  $d$  nor OSCP presented significant changes in expression levels in the SML-MG group in comparison with the control group in cell extracts obtained on day3 of the dicarbonyl stress induction (Fig. 27).

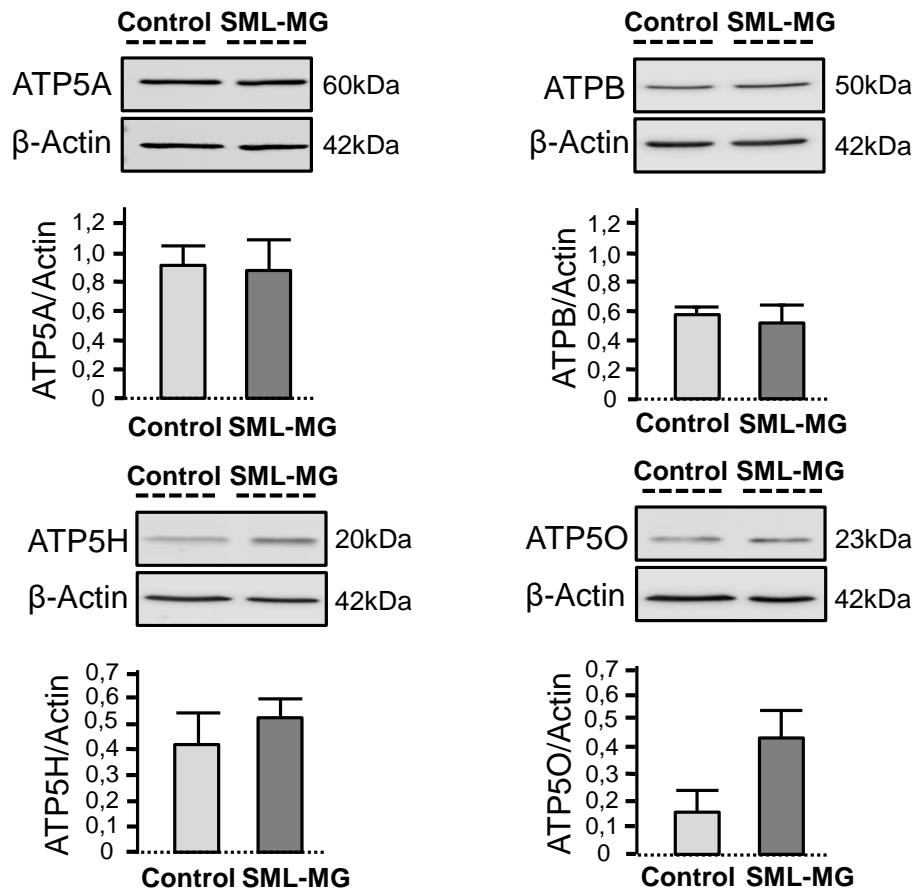


**Figure 27: Effect of dicarbonyl stress on F<sub>0</sub>F<sub>1</sub>-ATP synthase expression.** Expression levels of F<sub>0</sub>F<sub>1</sub>-ATP synthase subunits  $\alpha$  (ATP5A),  $\beta$  (ATPB),  $d$  (ATP5H) and OSCP (ATP5O) in H9c2 cell extracts on day 3 of dicarbonyl stress, and the corresponding controls, detected by WB;  $\beta$ -actin was used as loading control. Bar graphs represent the ratios of the optical density of each of these proteins and  $\beta$ -actin and did not detect any alteration in protein expression levels associated with increased dicarbonyl stress. All data are expressed as mean  $\pm$  SEM (n=3 independent experiments, p=ns).

In this model of dicarbonyl stress, we also investigated whether there were changes in expression levels of IF1 and OPA1 that are thought to stabilize F<sub>0</sub>F<sub>1</sub>-ATP synthase dimers and play a role in cristae morphogenesis. As observed in aging mouse mitochondria, the levels of IF1 and OPA1 remained preserved in the cell extracts of both control and SML-MG cells (Fig. 28).

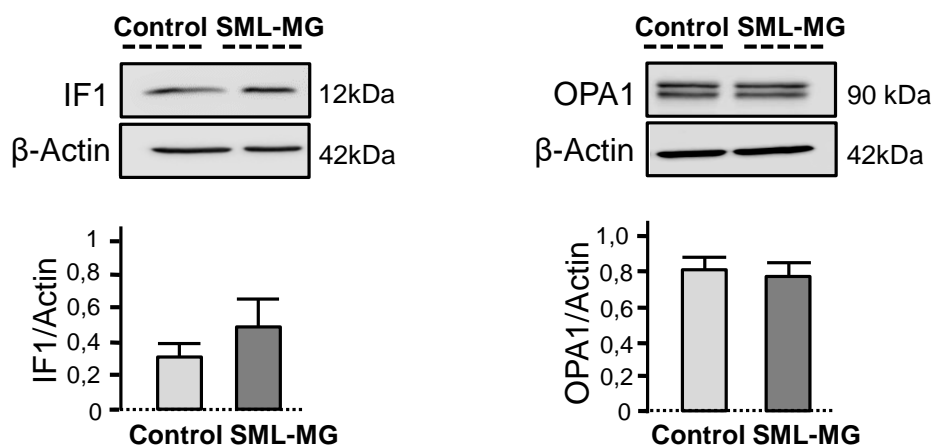
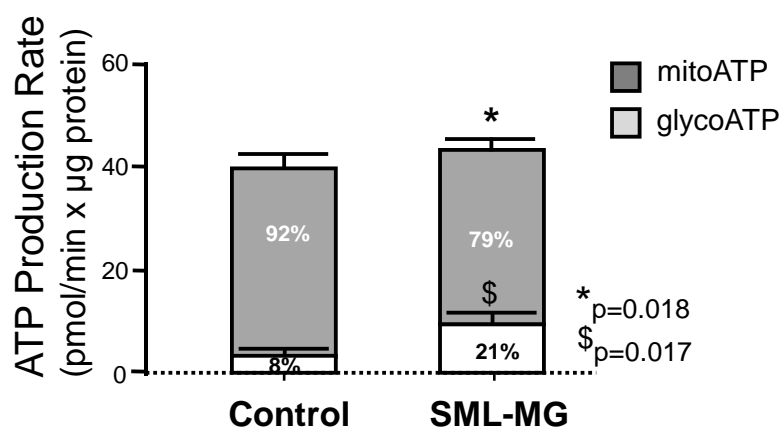


**Figure 28: IF1 and OPA1 remain preserved following 3 days of dicarbonyl stress.** Expression levels of IF1 and OPA1 in H9c2 cell extracts on day 3 of dicarbonyl stress, and the corresponding controls, detected by WB;  $\beta$ -actin was used as loading control. Bar graphs represent the ratios of the optical density of each of these proteins and  $\beta$ -actin and did not detect any alteration in protein expression levels associated with increased dicarbonyl stress. All data are expressed as mean $\pm$ SEM (n=3 independent experiments, p=ns).

### 5.7.5. Reduced $F_0F_1$ -ATP synthase dimerization decreases the mitochondrial OXPHOS capacity

To evaluate the effect of  $F_0F_1$ -ATP synthase chemical modification and its decreased dimerization on the OXPHOS capacity, we performed a Seahorse ATP production rate assay. This assay allows the quantification of the relative contribution of the glycolytic pathway (cytosolic) and the oxidative phosphorylation pathway (mitochondrial) to total cellular ATP production. The cells from the SML-MG group exhibited a significant reduction in the amount of ATP produced through OXPHOS and a concomitant increase in the amount of ATP produced by the glycolytic pathway compared with the control cells (Fig. 29). This result demonstrates a clear reduction in the cells' OXPHOS efficiency and an increase in the ATP flux from the glycolytic pathway probably as a compensatory mechanism. The decreased contribution of the OXPHOS pathway for ATP production may be secondary to the decreased  $F_0F_1$ -ATP synthase dimerization that drives cristae folding and is essential for optimizing the mitochondria's OXPHOS capacity.



## Results

**Figure 29: F<sub>0</sub>F<sub>1</sub>-ATP synthase decreases OXPHOS capacity.** ATP production rates determined by Seahorse Analyzer in H9c2 cells on day 3 of dicarbonyl stress and the corresponding controls. Bar graphs represent the relative contribution of OXPHOS and glycolytic pathways, respectively, to the total rates of ATP production (pmolATP/min x  $\mu$ g protein) in each group; data correspond to mean $\pm$ SEM (n=3 independent experiments (\*p=0.018 refers to the difference in OXPHOS contribution between control and SML-MG group, \$p=0.017 refers to the difference in glycolysis contribution between control and SML-MG group). The result indicated a significant reduction in OXPHOS contribution to cellular ATP production paralleled by a significant increase in glycolytic ATP production.

### 5.7.6. F<sub>0</sub>F<sub>1</sub>-ATP synthase dicarbonyl-induced modification does not alter its *in vitro* activity

To investigate whether the dicarbonyl-induced modification of F<sub>0</sub>F<sub>1</sub>-ATP synthase has an effect on its ATPase activity, we evaluated *in vitro* ATP hydrolysis in mitochondria isolated from control and SML-MG treated H9c2 cells as changes in NADPH absorbance. Similarly to what was observed in aged mouse heart, the changes in NADPH absorbance and the consequent quantification of the percentage of ATP hydrolysed did not reveal any changes in F<sub>0</sub>F<sub>1</sub>-ATP synthase hydrolytic activity as a consequence of its chemical modification (Fig. 30A). In addition, oligomycin was able to inhibit ATP hydrolysis to a similar extent in mitochondria of both control and SML-MG groups (Fig. 30B).

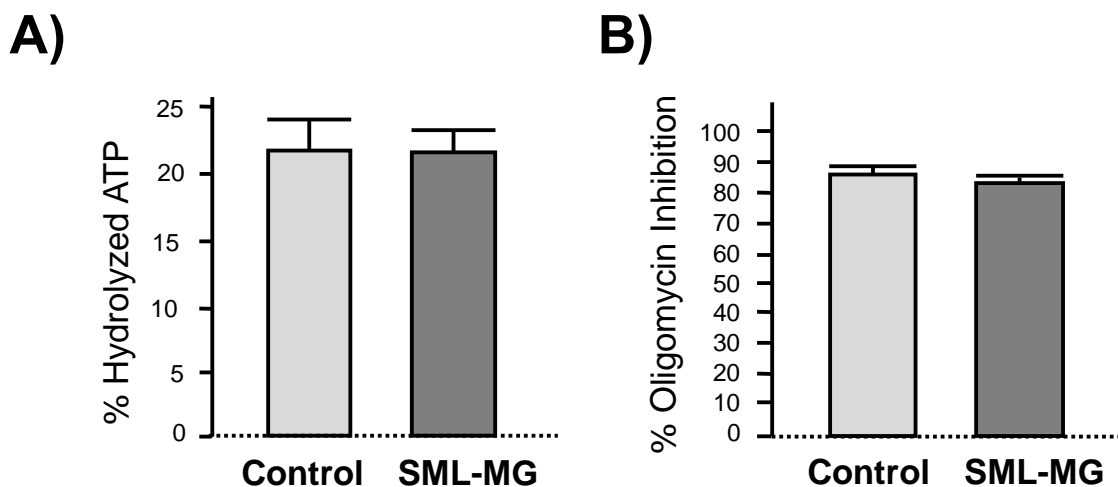
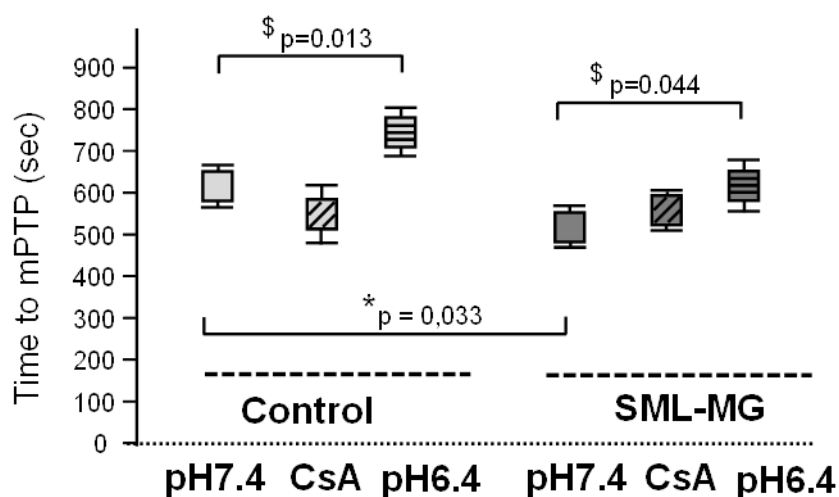


**Figure 30: Reduced F<sub>0</sub>F<sub>1</sub>-ATP synthase dimerization does not alter the enzyme hydrolase activity *in vitro*.** A) Bar graph represents *in vitro* ATPase activity in solubilised mitochondria from H9c2 cells on day 3 of dicarbonyl stress and the corresponding controls, quantified from changes in NADPH absorbance and expressed as percentage of hydrolyzed ATP with respect to the total ATP. The result does not show any modifications in F<sub>0</sub>F<sub>1</sub>-ATP synthase activity *in vitro* secondary to its glycation. B) Bar graph shows the percentage of inhibition of ATPase activity achieved after the addition of 1 $\mu$ mol/L oligomycin and does not demonstrate any changes associated with dicarbonyl stress. Data are expressed as mean $\pm$ SEM (n=3 independent experiments, p=ns).

### 5.7.7. Altered F<sub>0</sub>F<sub>1</sub>-ATP synthase dimerization increases the susceptibility to mPTP

To evaluate the cause-effect relationship between increased F<sub>0</sub>F<sub>1</sub>-ATP synthase dicarbonyl-induced modification and the susceptibility to undergo mPTP, H9c2 were exposed to intermittent laser illumination, as described for aged cardiomyocytes. Briefly, control and SML-MG treated cells were loaded with TMRE and exposed to laser irradiation to induce ROS production and mPTP opening, and the susceptibility to mPTP was determined as the time to achieve a 30% reduction in initial fluorescence indicative of TMRE loss secondary to mitochondrial depolarization and permeabilization. Unlike mPTP in cardiomyocytes that can be visualized in rigor shortening indicative of severe energetic collapse, H9c2 cells do not undergo this phenomenon and therefore another parameter had to be employed to measure the susceptibility to mPTP. In this case, irreversible mitochondrial depolarization and mPTP were considered to occur at an arbitrary value that corresponded to 30% loss of the initial fluorescence value.

In the SML-MG group, the time to mPTP was significantly shorter when compared with the control group indicating a higher susceptibility to undergo mitochondrial permeabilization in the dicarbonyl stress conditions (Fig. 31). CsA did not delay the occurrence of mPTP (pH7.4) in any group of cells, similar to what was observed in isolated cardiomyocytes (Fig. 31), indicating that in this model, Ca<sup>2+</sup> overload does not play any role in mPTP. By contrast, the acidic pH (pH6.4) was very protective and significantly delayed the time to mPTP, although its protective effect was less pronounced in cells exposed to dicarbonyl stress conditions (SML-MG group) (Fig. 31).



## Results

**Figure 33: Altered  $F_0F_1$ -ATP synthase dimerization increases the susceptibility to mPTP.** Fluorescence confocal images of TMRE-loaded H9c2 cells (red) at different time points of laser irradiation (564nm). Graph demonstrates the susceptibility to undergo ROS-induced mPTP in H9c2 cells on day 3 of dicarbonyl stress and the corresponding controls, calculated as the time (in sec) necessary to achieve 30% of mitochondrial membrane depolarization in TMRE-loaded cells exposed to 561nm laser illumination under control conditions (pH7.4), and in the presence of CsA (1 $\mu$ M) or acidic buffer (pH 6.4). Data correspond to mean $\pm$ SEM from 3 independent experiments. The results indicate that dicarbonyl-induced modification of  $F_0F_1$ -ATP synthase and its altered dimerization increases the susceptibility of the cells to undergo mPTP (\*p=0.033). The acidic pH (6.4) significantly delayed mPTP in both control (\*p=0.013) and SML-MG (\*p=0.044) groups, however, the protective effect of acidosis was partially lost in the cells exposed to glycative conditions.

### 5.7.8. Altered $F_0F_1$ -ATP synthase dimerization reduces cell survival

#### 5.7.8.1. Altered $F_0F_1$ -ATP synthase dimerization increases spontaneous mPTP

To investigate whether  $F_0F_1$ -ATP synthase dicarbonyl-induced modification favours long-term spontaneous mPTP, we quantified calcein leak from mitochondria throughout 3 consecutive days in control and SML-MG cells. These cells were simultaneously loaded with calcein (whose uptake depends on the  $\Delta\psi_m$  and is released upon mitochondrial permeabilization), and MTR (that covalently binds to mitochondrial membranes independently from  $\Delta\psi_m$  or mPTP). To quench cytosolic calcein fluorescence that can interfere with the interpretation of the data, posterior incubation with  $CoCl_2$  was performed. Occurrence of spontaneous mPTP would be detected as a reduction in the overlap coefficient between calcein and MTR. In these experiments, CsA was added to the culture medium throughout the 3 days of experiments to inhibit mPTP. Since the cells cannot be maintained at an acidic pH during a prolonged period of time, a group at pH 6.4 was not included to inhibit mPTP in this experiment, and only CsA was used.

The obtained results indicated a significantly higher mitochondrial calcein release on days 2 and 3 of glycative treatment in the SML-MG group with respect to its corresponding control, as detected by a significantly lower red-green co-localization coefficient (Fig. 34). In this experiment, CsA was capable of attenuating mPTP. Unlike the ROS-induced mPTP experiment, CsA had a protective effect here probably through other mechanisms that involve increased calcium accumulation in the mitochondria secondary to the dicarbonyl modification of the ryanodine receptor<sup>20</sup>.

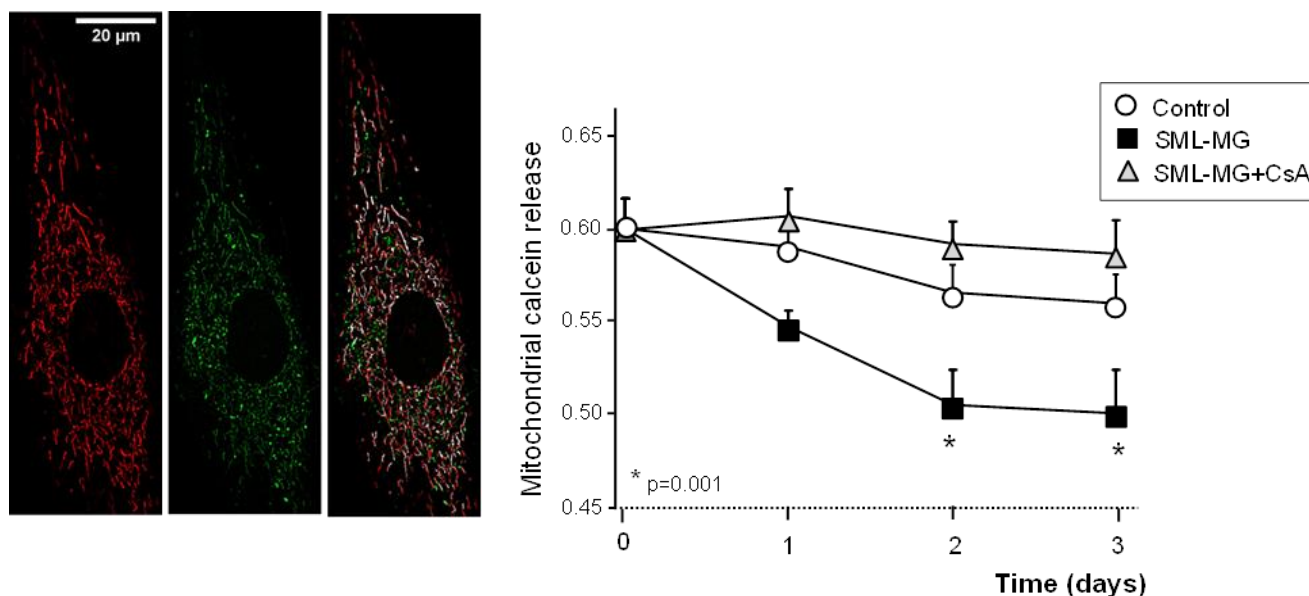


**Figure 34: Altered  $F_0F_1$ -ATP synthase dimerization increases spontaneous mPTP-dependent cell death.** Spontaneous mPTP throughout 3 days in H9c2 cells exposed to dicarbonyl stress and the corresponding controls, simultaneously loaded with calcein/CoCl<sub>2</sub> and mitotracker red (MTR). Representative images of MTR (red), calcein (green) and the colocalized image in 16-bit background subtracted images. Occurrence of mPTP is detected as a reduction in the overlap between mitochondrial calcein and MTR and indicated as “mitochondrial calcein release”. Data are represented as mean±SEM (n=3 independent experiments) and disclose a significantly increased calcein release depicted by a reduced colocalization coefficient in the SML-MG group with respect to the control (\*p=0.001).

#### 5.7.8.2. Reduced $F_0F_1$ -ATP synthase dimerization decreases cell viability

Finally, to evaluate the contribution of increased spontaneous mPTP secondary to  $F_0F_1$ -ATP synthase chemical modification on cell viability, we performed the MTT assay. Cell viability in control, SML, MG and SML-MG treated cells was evaluated throughout the 3 days of dicarbonyl stress induction. These 4 groups were used as to evaluate whether the produced changes in cell viability are due to an early acute cytotoxic effect of one of the used compounds, or whether increased cell mortality is a consequence of a prolonged chronic exposure to the drugs, and whether there is an additive effect for the use of SML and MG in conjunction.

There were no significant differences in cell viability between the groups on day 0 and 1. Of note, more viable cells were detected on day 1 probably because the cells retain their capacity to multiply for a few hours after switching to the serum-starved culture medium. Significant reduction in cell viability was obtained on days 2 and 3 in all of the SML, MG and SML-MG groups with respect to the control, and the combined SML-MG treatment had an additive effect on the decreased viability (Fig. 35). This result indicates that the increase in spontaneous mPTP throughout time associated with  $F_0F_1$ -ATP synthase dicarbonyl-induced modification is paralleled by a decrease in cell

## Results

viability and these changes become significant on day 3 of the dicarbonyl stress induction in which MAGEs accumulation becomes more pronounced.

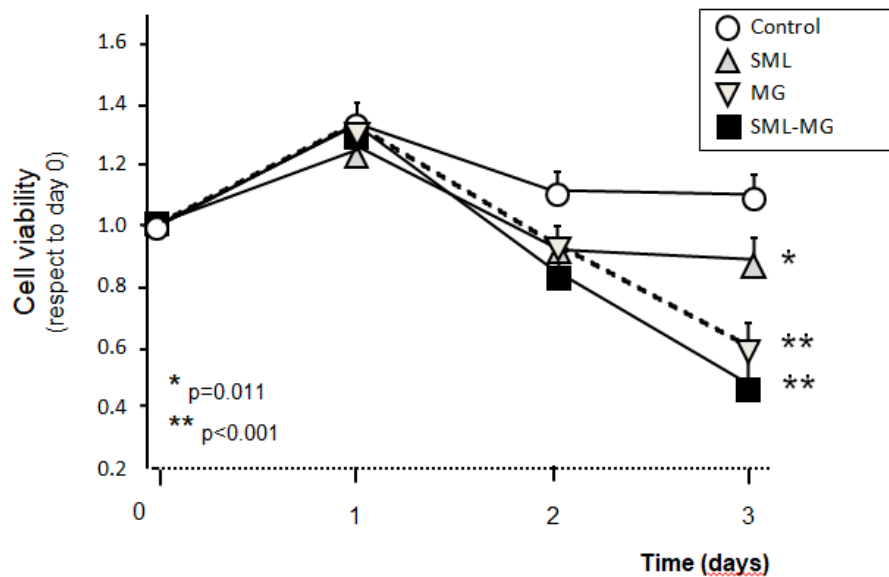


**Figure 35: Altered  $F_0F_1$ -ATP synthase dimerization decreases cell survival.** Spontaneous cell death throughout 3 days in H9c2 cells exposed to dicarbonyl stress and the corresponding controls, quantified by MTT assay and expressed with respect to baseline (day0). Data correspond to mean $\pm$ SEM (\* $p=0.011$  and \*\* $p<0.001$  with respect to controls,  $n=3$  independent experiments) and depict a significantly increased cell death in the SML, MG and SML-MG groups on day 3 of the dicarbonyl stress induction with respect to the control.

Overall, the data obtained in H9c2 cells demonstrate that the experimental induction of  $F_0F_1$ -ATP synthase dicarbonyl-induced modification recapitulates the reduction in enzyme dimerization and OXPHOS efficiency of the aged cardiomyocytes and increases the susceptibility of the cells to develop mitochondrial failure and death in response to stress.

## Summary of results:

1. The aged murine heart accumulates non-enzymatic glycation modifications derived from the chemical attack of dicarbonyl compounds to different peptides. The resulting chemical adducts distribute mainly on intracellular proteins and principally affect mitochondrial proteins at the Arg, Lys and Trp residues, as determined by mass spectrometry and Western Blot analysis
2. The mitochondrial  $F_0F_1$ -ATP synthase is a prominent target of dicarbonyl stress in the aged heart as identified by proteomics, immuno-fluorescent co-localization and PLA. The most prevalent types of chemical adducts within  $F_0F_1$ -ATP synthase are CML, dihydroxyimidazolidine, G-H1 and MDA54 and affect subunits  $\alpha$ ,  $d$ , OSCP,  $g$  and  $e$  (both subunits  $g$  and  $e$  play an essential role for  $F_0F_1$ -ATP synthase dimerization), but not subunit  $\beta$  (involved in ATP production) as detected by proteomics.
3. The degree of spontaneous dimerization/oligomerization of the  $F_0F_1$ -ATP synthase was found to be significantly decreased in mitochondria from aged mouse hearts and this decline specifically affected the IFM subpopulation, as determined by BN-electrophoresis followed by in-gel ATPase activity of cardiac mitochondria (SSM and IFM) and by PLA in intact cardiomyocytes.
4. The expression levels of the different subunits of  $F_0F_1$ -ATP synthase was found to be preserved in the aged heart as demonstrated by proteomics (whole heart homogenates), immuno-fluorescence (intact cardiomyocytes) and Western Blot (SSM and IFM). The expression of other mitochondrial proteins implicated in cristae morphogenesis, OPA1 and IF1, was not modified in aging as determined by Western Blot.
5. ADP-dependent  $O_2$  consumption (state 3 respiration) was found to be significantly reduced in intact IFM from aged mouse heart with respect to young ones. State 3 respiration was not affected by aging in SSM.
6. The ATPase activity was preserved in aging, as deduced from the *in vitro* quantification of ATP hydrolysis and in in-gel enzyme assay solubilized SSM and IFM from mouse hearts and.
7. TEM ultra-structural images of intact mouse myocardium displayed pathological features in some IFM of aged mice, such a concentric cristae organization ("onion-like" mitochondria) that were not present in IFM of young mice. The cristae tips which the  $F_0F_1$ -ATP synthase fold were found to be altered in aged cardiomyocytes as disclosed from decreased curvature of the cristae tips (less acute curves, more widened tips) assessed from TEM images.
8. The susceptibility of cardiomyocytes to undergo pathological mPTP and rigor contracture was significantly increased in aged cardiomyocytes exposed to ROS-overload with respect to young ones.



9. Induction of chronic dicarbonyl stress in H9c2 cells to simulate the intracellular conditions present in aging increased F<sub>0</sub>F<sub>1</sub>-ATP synthase glycation and this effect was associated with less enzyme dimerization, decreased ATP production through OXPHOS, preserved ATPase activity, and an increased susceptibility to mPTP secondary to ROS-overload. Importantly, defective ATP synthase dimerization was associated with an increased spontaneous mPTP throughout time and less cell survival.

## *6. DISCUSSION*

---







The aging heart is characterized by a low tolerance to exercise and stress, a factor whose severity determines the onset of HF. Moreover, it becomes more vulnerable to I/R injury and other forms of damage, exhibiting larger myocardial infarctions and more cardiomyocyte death, as demonstrated in different experimental models. The heart is the organ that demands and consumes the highest amount of energy of the entire organism (equivalent to 6kg of ATP/day), which is obtained primarily from OXPHOS at the IMM. The mitochondrial  $F_0F_1$ -ATP synthase, one of the most abundant proteins in the myocardium, is the molecule responsible for the last step of OXPHOS and produces >90% of the ATP in the heart. For all that, cardiomyocytes are highly dependent on mitochondrial respiration and cardiac mitochondria occupy up to 40% of cellular volume. In addition, heart mitochondria are very densely packed with highly invaginated cristae unlike other less energy-demanding organs where cristae are much sparser. Recent studies demonstrated that one of the main mechanisms responsible for the folding of the IMM is the spontaneous self-assembly of  $F_0F_1$ -ATP synthase monomers into long rows of dimers (and oligomers) that bend the membrane into cristae invaginations<sup>105,216,217</sup>, thereby increasing the surface area of the IMM and augmenting the respiratory efficiency of the mitochondria.

The present study demonstrates for the first time, that the aged heart develops an impaired *in situ* dimerization of the  $F_0F_1$ -ATP synthase at IMM, as detected by BN-electrophoresis in solubilized mitochondria and PLA in isolated cardiomyocytes. This altered dimerization was associated with an abnormal cristae tip curvature and pathological cristae organization (less densely packed and onion-like cristae) in heart mitochondria of aged mice, as detected by ultra-structural images (TEM) of intact myocardium.

Changes in expression levels of  $F_0F_1$ -ATP synthase were not identified as the cause behind this decreased dimerization, as each of proteomics, Western Blot analysis and immuno-fluorescence disclosed preserved levels of several subunits of  $F_0F_1$ -ATP synthase in aging. Rather, the age-dependent glycation of several subunits of  $F_0F_1$ -ATP synthase, including subunit g involved in the dimerization of the molecule, detected by high throughput proteomics and two independent immunofluorescence techniques (immuno-fluorescent co-localization and PLA) was identified as the mechanism responsible for the observed impaired dimerization.

Importantly, altered dimerization did not modify the activity of  $F_0F_1$ -ATP synthase detected by ATPase in-gel activity or *in vitro*, but reduced its efficiency to generate  $H^+$  gradient-driven ATP synthesis in intact mitochondria as disclosed by a significantly decreased ADP-dependent mitochondrial respiration in which  $F_0F_1$ -ATP synthase plays an important role. The defective  $F_0F_1$ -ATP synthase dimerization was also associated with an increased sensitivity of cells to undergo

energy collapse through mPTP opening as seen in isolated cardiomyocytes where energy collapse was driven by a ROS overload.

All these results were corroborated in a proof-of-concept model of H9c2 cells, where the induction of dicarbonyl stress produced an MGO-derived modification of F<sub>0</sub>F<sub>1</sub>-ATP synthase glycation and recapitulated the age-related defective F<sub>0</sub>F<sub>1</sub>-ATP synthase dimer assembly. The defective F<sub>0</sub>F<sub>1</sub>-ATP synthase dimerization was associated with a decreased ATP production by the OXPHOS pathway and a compensatory increase in ATP production via glycolysis, and also with an increased sensitivity of the cells to ROS-induced and spontaneous mPTP.

Because F<sub>0</sub>F<sub>1</sub>-ATP synthase is a fundamental energy-converting molecular machine in the heart and has been recently proposed to be the physical entity for the mPTP channel, our results identify a previously unrecognized pathophysiological mechanism involved in mitochondrial energy efficiency and cardiomyocyte death during aging.

### **6.1. Dicarbonyl stress and protein damage in the aged myocardium**

Dicarbonyl stress refers to the increase in the levels of highly toxic and reactive dicarbonyl compounds (mainly MGO, GO and 3-DG) as a consequence of either an increased generation or decreased detoxification mechanisms. Dicarbonyl stress has been linked to several age-related diseases<sup>16,166,167</sup>, while efficient dicarbonyl removal was associated with healthy aging<sup>168</sup>. Increased dicarbonyl stress in aging may be a direct consequence of a deficiency in the GLO-I system<sup>20</sup> responsible for the detoxification of the most reactive and cytotoxic dicarbonyls MGO and GO. If not properly eliminated, these compounds can interact with proteins forming irreversible chemical adducts (collectively named as AGEs)<sup>167,218</sup>. The increased oxidative stress present in aging<sup>19</sup> and the decrease in antioxidant mechanisms<sup>19,25</sup> contribute to the chemical reactivity of dicarbonyl compounds.

The formation of dicarbonyl-induced PTMs on proteins can have deleterious consequences as a result of the alteration they produce in the tertiary and quaternary structure and in the function of the target protein<sup>218-220</sup>. Several studies have evidenced increased accumulation of dicarbonyl modifications in different aged tissues and have linked this to the onset and progression of several age-related diseases including CVDs<sup>162,221,222</sup> and neurodegenerative diseases<sup>186,187</sup>; however, those proteins that are the most susceptible to this kind of modifications by dicarbonyl compounds are still not known, nor are the functional consequences that those modifications may produce on each of the molecular targets. Importantly, our group has recently described a deficiency of the GLO-I system in the hearts of aged humans and mice<sup>20</sup> as a mechanism of dicarbonyl stress, which was correlated with an increased accumulation of dicarbonyl-induced modifications on intracellular

proteins and had important functional consequences on SR-mitochondria communication and calcium handling<sup>20</sup>. However, while there is no doubt that the aged myocardium accumulates significantly higher amounts of dicarbonyl-modified peptides than the young one, neither the most prevalent type of chemical modification nor their intracellular location and target proteins have been systematically evaluated. In the present thesis, we performed a massive spectrometry analysis of PTMs using myocardial homogenates of young and old mice to investigate the most prevalent types of dicarbonyl chemical adducts present in aging and the potential protein targets. This approach allowed the identification of nine different types of chemical adducts (from most to least abundant: CML, MDA54, dihydroxyimidazolidine, G-H1, hydroxymethyl-OP, MG-H1, Arg1HPG, Arg2HPG, Arg2PG). Other types of glycation products including pentosidine, GOLD, MOLD and others have not been detected probably due to their cross-linking nature makes them resistant to the proteolytic treatment required prior to the proteomics study and therefore go undetected.

Importantly, the absolute majority of the dicarbonyl-induced modifications detected by our proteomics study targeted the positively charged arginine and lysine residues. According to a study<sup>170</sup> those two amino acids are the ones with the highest probability of falling in protein active sites, therefore, it can be expected that many of these PTMs can cause consequences on protein function and/or structure especially in proteins with very complex tertiary and quaternary structures. More than 90% of the detected dicarbonyl-induced modifications were found on intracellular proteins. Importantly, the highest load of PTMs was detected on mitochondrial proteins followed by cytosolic proteins and principally affected OXPHOS and contractile proteins, respectively. The highly oxidative environment of the mitochondria<sup>19</sup> in addition to the absence of an intra-mitochondrial detoxification system for MGO, and the fact that MGO is membrane permeable and can cross into the mitochondria<sup>161</sup> may be factors that explain this significant accumulation of modified products on mitochondrial proteins. The age-dependent increase in these modifications in mitochondria was confirmed by Western blot analysis in isolated SSM and IFM from myocardium of young and old mice which demonstrated an increase in MGO-derived adducts specifically on IFM, while CMLs increased significantly in both SSM and IFM of aged myocardium. Although the myocardium accommodates different kinds of cells including cardiomyocytes, fibroblasts, endothelial cells, vascular smooth muscle cells, nerve cells, and immune cells; it is safe to say that the cardiomyocyte contribution to mitochondria and mitochondrial protein is the highest as these cells are the richest in mitochondria<sup>223</sup>.



## 6.2. Aging increases dicarbonyl modification of mitochondrial $F_0F_1$ -ATP synthase in the heart

The  $F_0F_1$ -ATP synthase is one of the most conserved, widespread, and abundant proteins on earth. It uses the electrical power of IMM to convert ADP into ATP, the most abundant energy-containing chemical compound in all biological systems<sup>224</sup>. Of the proteins that make up the proteome of the heart, the  $F_0F_1$ -ATP synthase may be the most vital as it is required to produce massive amounts of energy, in quantities superior to any other organ, on a beat-to-beat basis. Only in the heart, the  $F_0F_1$ -ATP synthase generates 6 Kg of ATP per day<sup>225</sup>. Given that (1) the  $F_0F_1$ -ATP synthase is a protein whose function depends on a very complex tertiary and quaternary structure (dimers and oligomers), (2) that it is one of the most abundant proteins of the IMM, (3) that it contains several positively charged amino acids that could be targeted by dicarbonyl reactions in different subunits within the molecule, and that (4) several previous studies indicate that old cardiomyocytes become less energy efficient, more intolerant to exercise and more susceptible to develop the “failing phenotype”, we investigated whether  $F_0F_1$ -ATP synthase could be a target of dicarbonyl modifications in aging. This hypothesis was tested using three independent techniques: mass spectrometry, immuno-fluorescent co-localization and PLA, and the results obtained were coincident in indicating an increased dicarbonyl-induced modification of the mitochondrial  $F_0F_1$ -ATP synthase associated with aging.

Mass spectrometry of whole heart homogenates of young and old mice specifically addressed to detect dicarbonyl-induced PTMs revealed that several subunits of the  $F_0F_1$ -ATP synthase become significantly more modified in aging, including the subunit g, involved in the dimerization of the  $F_0F_1$ -ATP synthase. Importantly, the subunit  $\beta$ , which forms the catalytic head of the enzyme (i.e., where the ATP synthesis occurs) was not identified as target of this damage. The most prevalent types of chemical adducts affecting the  $F_0F_1$ -ATP synthase were CML, dihydroxyimidazolidine, G-H1 and MDA54 at arginine, lysine and tryptophan amino acid residues. Our group has previously demonstrated increased Cys oxidation in both the  $F_0$  and the  $F_1$  domains of  $F_0F_1$ -ATP synthase of aged cardiomyocytes<sup>35</sup>. The finding that  $F_0F_1$ -ATP synthase is also a target of oxidation does not contradict with our results but rather supports the concept of a positive feedback loop between ROS and dicarbonyl-modified protein generation, as previously demonstrated<sup>35</sup>, in which a pro-oxidant environment has been shown to thermodynamically favour ROS-induced dicarbonyl reactions.

The dicarbonyl-induced modification of  $F_0F_1$ -ATP synthase was confirmed by immuno-labelling where the degree of co-localization between subunit  $\alpha$  of  $F_0F_1$ -ATP synthase and MGO-

derived chemical products was significantly higher in the aged mouse cardiomyocytes, and also by PLA which disclosed a significantly higher cross-reactivity between  $F_0F_1$ -ATP synthase and MGO-derived products in aged compared to young mouse cardiomyocytes. To our knowledge, this is the first evidence demonstrating that cardiac  $F_0F_1$ -ATP synthase is a target of glycative damage in aging.

Importantly, while other types of PTMs including phosphorylations, nitrosylations and acetylations are enzymatically controlled transient modifications that play a fundamental regulatory role over protein function, dicarbonyl compounds interact with proteins following a spontaneous and stochastic pattern and induce terminal chemical modifications that may lead to loss of protein structure and function. Once they are generated, no known endogenous mechanism controls their removal. Even oxidative PTMs which were originally thought to only have a damaging role were later described to play an essential physiological role at low levels and can have protective mitohormetic effects<sup>226,227</sup>. Dicarbonyl-induced modifications on the other hand have only been described in the context of pathologies, and to date no regulatory role for the “dicarbonyl proteome” has been described.

### **6.3. Modification of $F_0F_1$ -ATP synthase is associated with remodelled mitochondrial cristae secondary to its reduced dimerization**

Our results demonstrate that aging is associated with defective cristae morphology. TEM images of myocardial tissue disclosed that several IFM of old mouse myocardium presented defective cristae organization characterized by a concentric arrangement (onion-like mitochondria) and/or less densely packed cristae. Importantly, these pathological features were only identified in the aged myocardium and not in the young one. Apart from the alteration in the ultrastructure of the IMM, the quantification of cristae tip convexity using an automatized b-spline coefficient in high-magnification images of young and old mouse myocardium revealed that the curvature of the IMM was significantly reduced in the old animals, where the cristae tips tended to be more flattened rather than angular.

The invaginated architecture of the IMM is essential for increasing the energetic efficiency of the mitochondria as the tightly curved tips of the cristae create  $H^+$  traps that increase the local proton concentration thereby facilitating and increasing ATP production<sup>68,228</sup>. Also, the cristae foldings augment the surface area of the IMM onto which molecules with a bioenergetics role can be incorporated and seems to play a role in the assembly and the stabilization of the respiratory super-complexes that are essential for efficient energy production<sup>91</sup>. The importance of the cristae structure is demonstrated by how this architecture has been evolutionary conserved between species<sup>229</sup>, and the relationship between adequate cristae morphogenesis and its function is

## Discussion

reflected by the differences in cristae density between highly energetic demanding and low energy demanding organs. A clear example is the difference between mitochondria that derive from cardiomyocytes and mitochondria that derive from organs with less energy requirement. Whereas cardiomyocytes have mitochondria with tightly packed and invaginated cristae, cells with less energy demand, like hepatocytes have mitochondria with much lower cristae density<sup>230</sup>.

Experimental evidences indicate that the  $F_0F_1$ -ATP synthase is one of the most important players in cristae morphogenesis. Previous studies have demonstrated that the spontaneous self-assembly of  $F_0F_1$ -ATP synthase monomers into long rows of V-shaped dimers is the mechanism that drags and folds the flexible IMM into its highly curved cristae structure<sup>69,115,118,123</sup>. Therefore, rather than being the structure on which  $F_0F_1$ -ATP synthase dimers form, mitochondrial cristae *per se* are the morphological consequence of  $F_0F_1$ -ATP synthase dimerization. This concept is supported by cryo-electron images that demonstrate the specific location of  $F_0F_1$ -ATP synthase dimer ribbons at the tips of the mitochondrial cristae<sup>216,217</sup> and by studies in which interventions addressed to interfere with  $F_0F_1$ -ATP synthase dimerization resulted in altered cristae morphology. Impeding  $F_0F_1$ -ATP synthase dimerization by genetic deletion of the subunits involved in this process yielded defective cristae with randomly distributed  $F_0F_1$ -ATP synthase monomers in yeast<sup>118</sup>. In another study on yeast devoid of the dimerization subunits<sup>69</sup>, aberrant onion-like cristae organization appeared, demonstrating the critical role of  $F_0F_1$ -ATP synthase for adequate membrane folding, although the consequences of this altered mitochondrial ultrastructure on its function was not evaluated.

Importantly, our data suggest an altered  $F_0F_1$ -ATP synthase dimerization secondary to its dicarbonyl-induced modification as the underlying cause behind the defective cristae ultrastructure detected in the myocardium of aged mice. This result was obtained using different experimental approaches. First, BN-electrophoresis followed by in-gel ATPase activity of purified and solubilized SSM and IFM demonstrated a significantly decreased proportion of functional  $F_0F_1$ -ATP synthase dimers and oligomers and a concomitant increase in the proportion of monomers which specifically affected the aged IFM subpopulation. Importantly, these changes could not be attributed to decreased  $F_0F_1$ -ATP synthase expression with age, as different technical approaches including mass spectrometry, Western blot and immunofluorescence all disclosed that the expression levels of different subunits of  $F_0F_1$ -ATP synthase did not change in the mitochondria of aged individuals with respect to the young ones. Also, these changes in the dimerization state could not be ascribed to other mitochondrial proteins that have been described to interact and stabilize  $F_0F_1$ -ATP synthase dimers, like OPA-1 and IF1<sup>213,214</sup>, as detected by Western blot analysis of their expression levels.

Indeed, the impact of aging on these proteins remains controversial. While some studies suggested a decrease in OPA1 levels during aging<sup>231</sup>, other studies indicated an increase<sup>232</sup> or no change<sup>233</sup> in OPA1 with age.

The age-dependent decline in  $F_0F_1$ -ATP synthase dimers was corroborated in isolated cardiomyocytes where the degree of monomer-monomer interaction was addressed by competitive immunolabeling of one  $F_0F_1$ -ATP synthase subunit followed by a PLA. This approach disclosed less fluorescent positive spots in cardiomyocytes from aged mice, indicating less monomer-monomer interaction. Overall, the results obtained by BN and by PLA are coincident in demonstrating that during aging there is a reduction in the amount of functional dimers/oligomers of  $F_0F_1$ -ATP synthase in cardiomyocytes, and that this mechanism may be involved in the altered cristae tip curvature observed in the IMM of intact myocardium of old mice. The consequence of altered  $F_0F_1$ -ATP synthase dimerization on the development of pathological mitochondrial cristae features has also been observed in yeast and cell lines<sup>69,117</sup>. Also, in aged rat heart, evidence of altered cristae organization was presented<sup>85</sup>, however the mechanisms underlying this age-dependent alteration was not investigated. This is the first evidence that identifies an association between  $F_0F_1$ -ATP synthase modification by dicarbonyl stress and the presence of defective cristae ultra-structure in aging and proposes that the dicarbonyl-induced modification of several subunits of  $F_0F_1$ -ATP synthase, especially subunit g involved in enzyme dimerization, is proposed to be the mechanism involved in the defective enzyme dimerization during aging. The cause-effect relationship between both phenomena (i.e.,  $F_0F_1$ -ATP synthase glycation and less dimer formation) was explored in H9c2 cells (see below).

#### **6.4. Defective $F_0F_1$ -ATP synthase reduces mitochondrial energy efficiency**

To our knowledge, this is the first experimental evidence demonstrating a deficiency in  $F_0F_1$ -ATP synthase dimerization in a complex organ of mammals, i.e. the murine heart, during physiological aging (without any kind of genetic manipulation). To date, altered  $F_0F_1$ -ATP synthase dimerization has only been studied in simple organisms such as the fungus *P. anserina* where the functional consequences of altered dimerization on cristae morphology, energetic efficiency and mPTP were evaluated<sup>87,120,234</sup>. In those studies, the alteration of  $F_0F_1$ -ATP synthase dimerization was associated with pathological cristae remodelling, energy deficiency, excessive mPTP and increased cell death<sup>87,120,234</sup>. To investigate the functional consequences of altered  $F_0F_1$ -ATP synthase dimerization on OXPHOS and ATP hydrolysis in our model, we evaluated mitochondrial respiration and ATPase activity in mitochondria from young and old mouse hearts.

## Discussion

Mitochondrial ATP production is directly dependent on the trans-membrane  $H^+$  gradient produced by the ETC and hence requires the presence of an intact mitochondrial membrane, therefore, the function of  $F_0F_1$ -ATP synthase in ATP synthesis can only be evaluated in intact mitochondria where the cyto-structure of the IMM is preserved and where the contribution of other ETC enzymes is also present. The altered  $F_0F_1$ -ATP synthase dimerization in aging was associated with a preserved basal respiration (state 2) but with a significantly decreased state 3 respiration independently of the substrate being used to feed the ETC (substrates for complex I or II). State 3 is an ADP-dependent respiration which is directly coupled to ATP production at the level of  $F_0F_1$ -ATP synthase. Therefore, this decreased state 3 respiration may be providing an indirect evidence about a reduced  $F_0F_1$ -ATP synthase function in aging associated with its decreased dimerization. Importantly, this alteration specifically affected the IFM of old mouse hearts while SSM respiration remained preserved. The reverse activity of  $F_0F_1$ -ATP synthase on the other hand, does not require a trans-membrane  $H^+$  gradient and can be measured *in vitro* in solubilized mitochondria where mitochondrial cyto-architecture and other ETC components do not have any influence. In fact, the loss of the  $H^+$  gradient *per se* is a mechanism that activates ATPase activity<sup>108</sup>. Therefore, ATPase activity was evaluated in solubilized SSM and IFM of young and old mice by two independent methods. Both the *in-gel* ATP hydrolysis seen as the deposition of lead phosphate bands upon the liberation of a phosphate secondary to the transformation of ATP into an ADP, and the *in vitro* ATPase activity evaluated from changes in NADPH absorbance, indicated that aging did not modify the function of  $F_0F_1$ -ATP synthase in ATP hydrolysis. In addition, the sensitivity to oligomycin in both ATP synthesis and ATP hydrolysis was not affected in aging in neither SSM nor IFM, nor did it depend on the dicarbonyl-induced modification of  $F_0F_1$ -ATP synthase or on the relative abundance of the dimers and monomers. Since sensitivity to oligomycin seems to require an adequately assembled  $F_0F_1$ -ATP synthase holocomplex<sup>107</sup>, the result suggests that  $F_0F_1$ -ATP synthase glycation does not affect the assembly of the molecule but rather affects a process that occurs posterior to the monomer assembly, like for example, its dimerization.

Overall, these data suggest that the alteration in OXPHOS efficiency seen in state 3 respiration is not due to a functional consequence at the level of  $F_0F_1$ -ATP synthase monomers function, because these seem to be energetically self-sufficient as indicated from preserved ATPase function in aging. Rather, the effect of  $F_0F_1$ -ATP synthase glycation on energetic efficiency is an outcome of the failure to properly assemble into dimers which would consequently optimize energy production. Altogether, these data are consistent with the concept that impaired dimerization of  $F_0F_1$ -ATP synthase contributes to the reduced OXPHOS capacity of the aging heart due to the ultra-structural changes at the true bioenergetics site of cardiomyocytes, the IMM, seen as defective

cristae morphogenesis (wider cristae tips and pathological cristae organization, i.e, concentric cristae formations). It is important to take into consideration that the age-associated alterations of  $F_0F_1$ -ATP synthase may not be the only underlying cause for a reduced OXPHOS capacity. Other changes including a reduction in mitochondrial yield seen in elderly patients, or an intra-mitochondrial accumulation of calcium may also contribute to reducing the overall mitochondrial function with age<sup>20</sup>. However, alterations of  $F_0F_1$ -ATP synthase may still be on the top of the list considering that it is the true site where ATP synthesis occurs.

### 6.5. Glycation of $F_0F_1$ -ATP synthase increases mPTP susceptibility

The  $F_0F_1$ -ATP synthase is known for playing opposing roles on cellular bioenergetics. On the one hand, this molecule produces ATP which is essential to sustain life, while on the other hand  $F_0F_1$ -ATP synthase can switch into an ATP hydrolase, contributing to energy exhaustion in situations where the mitochondrial membrane potential is lost. This dual role  $F_0F_1$ -ATP synthase was first described by Jennings et al. who reported that in cardiomyocytes exposed to long periods of anoxia, it may reverse from ATP synthesis to hydrolysis, precipitating rigor shortening contraction and energy depletion<sup>235</sup>. While this switch into an energy dissipating machine might be crucial to rebuild the  $\Delta\psi_m$ , the exhaustion of ATP increases the probability of death in cells that are already jeopardized by oxygen deprivation<sup>236</sup>.

Our group has previously demonstrated that in aged cardiomyocytes, there is a significant delay in the reversion of  $F_0F_1$ -ATP synthase into its catalytic mode which accelerates mitochondrial membrane depolarization during ischemia and impairs energy recovery upon reperfusion<sup>35</sup>. This antagonistic role of  $F_0F_1$ -ATP synthase on cellular bioenergetics is not the only one, as more recently, this molecule has been implicated in a much more lethal mechanism, the mPTP<sup>135,141</sup>. Opening of mPTP produces an extreme case of energy uncoupling, and this pathological response has been shown to contribute to cell death during myocardial I/R injury, and other forms of damage<sup>50</sup>. Importantly, our group and others have described that the contribution of mPTP to mitochondrial failure during I/R injury is more relevant in cardiomyocytes of aged mice<sup>35,52</sup>. However, the mechanism that underlies this increased mPTP susceptibility in the aging heart is still controversial and the molecular identity of mPTP remains unknown.

Recent evidences from different groups suggest that the  $F_0F_1$ -ATP synthase could be the true molecular entity of the mPTP, although there is no consensus on the mechanisms leading to the energy-dissipating channel formation. Some authors propose a failure of  $F_0F_1$ -ATP synthase dimerization, a sequence of dimer dissociation followed by monomer re-arrangement, or a structural alteration in the c-ring as the mechanisms for pore opening. In Bernardí's model, the

## Discussion

presence of a Ca overload triggers dimer  $F_0F_1$ -ATP synthase dissociation and the pore forms at the interface between the pair of dissociated monomers<sup>135</sup>. In Bonora's model, they observed that following an mPTP trigger there is a significant reduction in  $F_0F_1$ -ATP synthase dimers which suggested that monomer re-arrangement is responsible for pore opening<sup>139</sup>. In the c-ring model, however, an mPTP trigger dislodges the  $F_1$  domain from the c-ring and the latter expands to form the pore<sup>141</sup>. While the exact location where the mPTP forms on the  $F_0F_1$ -ATP synthase is still not agreed upon (dimers, c-ring), there seems that there is very little doubt that this molecule is the true molecular entity of the mPTP as the majority of the triggers ( $Ca^{2+149}$ , Bz423<sup>151</sup>) and inhibitors ( $H^{+150}$ , ADP and AMP<sup>135</sup>) of this mechanisms bind/interact directly with the  $F_0F_1$ -ATP synthase to exert their effect.

To investigate whether the altered dimerization of  $F_0F_1$ -ATP synthase can increase the susceptibility of the cells to undergo mPTP, we evaluated the sensitivity of cardiomyocytes from young and old mouse hearts to develop ROS-induced mPTP. For this purpose, the cardiomyocytes were loaded with TMRE, a fluorochrome that accumulates in the mitochondria and produces massive amounts of ROS when excited by a laser source. Cells were then exposed to intermittent laser irradiation until an energy-collapse that precipitated in rigor-shortening was produced. The quantification of the time required to undergo rigor contraction indicated that cardiomyocytes of old mouse hearts had a significantly increased susceptibility to mPTP in comparison with the young mouse cardiomyocytes. In this assay, CsA failed to delay the time at which mPTP occurred in both age groups, while acidic pH significantly delayed rigor shortening, although this delay was milder in aged cardiomyocytes in comparison with young cardiomyocytes. The failure of CsA to exert any inhibitory effect over mPTP could be attributed to several mechanisms. First, and given that (1) the mechanism of action of CsA depends on its calcium desensitization effect (it increases the threshold of  $Ca^{2+}$  required to trigger mPTP<sup>215,237</sup>), (2) the induction of mPTP in our experiment was achieved by a ROS overload and not a  $Ca^{2+}$  overload, (3) no inhibitory effect of CsA on mPTP in the presence of a ROS trigger has been previously described, the absence of a  $Ca^{2+}$  overload in our model may explain why CsA failed to delay mPTP opening. In addition, although preclinical models demonstrated an inhibitory effect of CsA on pore opening<sup>131</sup>, the CIRCUS clinical trial in which CsA was tested in patients suffering a myocardial infarction, failed to demonstrate a clear reduction in infarct size<sup>132</sup> which may be indicating that CsA is not a gold standard drug for mPTP inhibition. With regards to the acidic pH, several studies have evidenced an inhibitory role of intra-cellular acidosis on pore opening<sup>134,238</sup>. Importantly, a recent study demonstrated that  $H^+$  needs to bind to a specific histidine of OSCP to mediate its effect over mPTP inhibition<sup>150</sup>. Our proteomics analysis demonstrated that the OSCP of the  $F_0F_1$ -ATP synthase is one of the subunits that are significantly

more glycated in aging, which might be the underlying cause for the decreased inhibitory effect of the acidic pH over mPTP in the aged cardiomyocytes.

#### **6.6. Induction of dicarbonyl stress in H9c2 cells simulates age-dependent changes in $F_0F_1$ -ATP synthase**

In aged mice, the increased dicarbonyl-induced modification of  $F_0F_1$ -ATP synthase was associated with a significant decrease in  $F_0F_1$ -ATP synthase dimerization and a reduction in energetic efficiency. Energy deficiency was not due to a direct functional alteration at the level of the  $F_0F_1$ -ATP synthase monomer, but was rather attributed to defective  $F_0F_1$ -ATP synthase dimerization that cannot optimize energy production. The results from mice, however, could not establish a cause-effect relationship between  $F_0F_1$ -ATP synthase modification and the observed functional consequences. Therefore, to establish whether the dicarbonyl-induced modification of  $F_0F_1$ -ATP synthase is the primary cause that interferes with the enzyme dimerization and therefore reduces the energetic capacity, we used an H9c2 cell line where we induced chronic dicarbonyl stress to simulate the conditions present in aging. These cells, unlike other models like HL-1, have many similarities with cardiomyocytes in relation to their high dependence on OXPHOS for ATP production<sup>203</sup>. H9c2 cells were exposed to dicarbonyl stress using a previously standardized pharmaceutical strategy that employs the use of the GLO-I inhibitor SML (5 $\mu$ mol/L) and MG (200 $\mu$ mol/L) during three consecutive days. The GLO-I inhibitor reduces the efficiency of the GLO system by competing with the cofactor GSH, while MG constitutes an external source of dicarbonyls which would further overwhelm the detoxification system. The intracellular accumulation of dicarbonyl modified proteins was evaluated during three consecutive days by immunofluorescence labelling of intracellular MGO-derived adducts, and disclosed a significantly increased accumulation of the terminally modified proteins only after the third day of the dicarbonyl stress induction and not acutely after the first day or two. The significant increase in dicarbonyl-modified compounds was confirmed by Western blot analysis of whole cell homogenates obtained on day three of dicarbonyl stress and demonstrated significantly higher levels of MGO-induced modifications in comparison with the control cells.

We then evaluated whether  $F_0F_1$ -ATP synthase is a biological target of dicarbonyl stress. To this end we performed a PLA that detects the interaction between subunit  $\alpha$  of  $F_0F_1$ -ATP synthase and MGO-induced modifications, which similarly to the aged mouse model, identified  $F_0F_1$ -ATP synthase as a prominent target of glycation. To investigate whether  $F_0F_1$ -ATP synthase modification affected its dimerization, we used a modification of the standard PLA, consisting in the employment of a primary antibody against a  $F_0F_1$ -ATP synthase subunit present in a single copy per monomer



## Discussion

(subunit d in this case) to assess the inter-molecular distance between two  $F_0F_1$ -ATP synthase monomers. This PLA disclosed an increased monomer-monomer distance in the cells exposed to dicarbonyl stress, which might be indicating an altered dimerization of  $F_0F_1$ -ATP synthase as a consequence of its increased dicarbonyl modification. In this model, and as observed in the aged mouse heart, changes in expression of  $F_0F_1$ -ATP synthase were not the underlying cause behind the decreased dimerization, as Western blot analysis disclosed a preserved expression level of several  $F_0F_1$ -ATP synthase subunits and also of OPA1 and IF1 which play a role in dimer stabilization.

Finally, and to establish whether this decreased  $F_0F_1$ -ATP synthase dimerization could cause a decline in ATP production through OXPHOS, we used a Seahorse real-time ATP rate assay. This assay evaluates the contribution of both OXPHOS and the glycolytic pathways to the overall ATP production. The results indicated that in H9c2 cells exposed to dicarbonyl stress, there is a significant decline in the relative amount of ATP produced through OXPHOS which was paralleled by a compensatory increase in ATP production through glycolysis. This data indicated that the decreased dimerization of  $F_0F_1$ -ATP synthase is associated with a significantly reduced OXPHOS capacity. Decreased  $F_0F_1$ -ATP synthase dimerization had no functional consequences on the ATPase activity. This conclusion is based on experiments in which the in vitro ATPase activity measured as changes in NADPH absorbance in solubilized mitochondria of H9c2 cells exposed to dicarbonyl remained unchanged with respect to their corresponding control.

Finally, to evaluate whether the altered dimerization state of the  $F_0F_1$ -ATP synthase could be the cause of the increased susceptibility to mPTP observed in aged cardiomyocytes, we evaluated the susceptibility to ROS-induced mPTP in H9c2 with increased dicarbonyl stress and their respective controls. Similarly to what was observed in old cardiomyocytes, the cells exposed to dicarbonyl stress developed faster mitochondrial depolarization indicative of pore opening in comparison with the control group. Again, CsA failed to delay mPTP, while  $H^+$  did have a protective effect. Interestingly, the delay in mPTP obtained with  $H^+$  was more pronounced in the control cells in comparison with the SML-MG treated ones. Importantly, MGO-induced modification of  $F_0F_1$ -ATP synthase was also associated with an increase in spontaneous mPTP throughout time in H9c2 cells, as detected from a reduced colocalization between calcein and MTR. Occurrence of mPTP was paralleled by an increase in cell death within the same time frame. This provides evidence showing that the glycation of  $F_0F_1$ -ATP synthase not only interferes with dimer formation but increases the susceptibility of the cells to undergo mPTP.

Overall, these experiments provide a proof-of-concept that demonstrates that the increased dicarbonyl stress present in aging and the consequent increase in dicarbonyl-induced modification of

$F_0F_1$ -ATP synthase may be the underlying cause for the reduced  $F_0F_1$ -ATP synthase dimerization and the consequent decrease in age-associated mitochondrial energetic efficiency, in addition to the increased susceptibility to mPTP and cell death. Although our data do not allow establishing the molecular entity of the mPTP channel, they do point to glycation-induced changes in  $F_0F_1$ -ATP synthase as the mechanism involved in the altered monomer-monomer interface and mPTP sensitization during aging.





## *7. Conclusion*

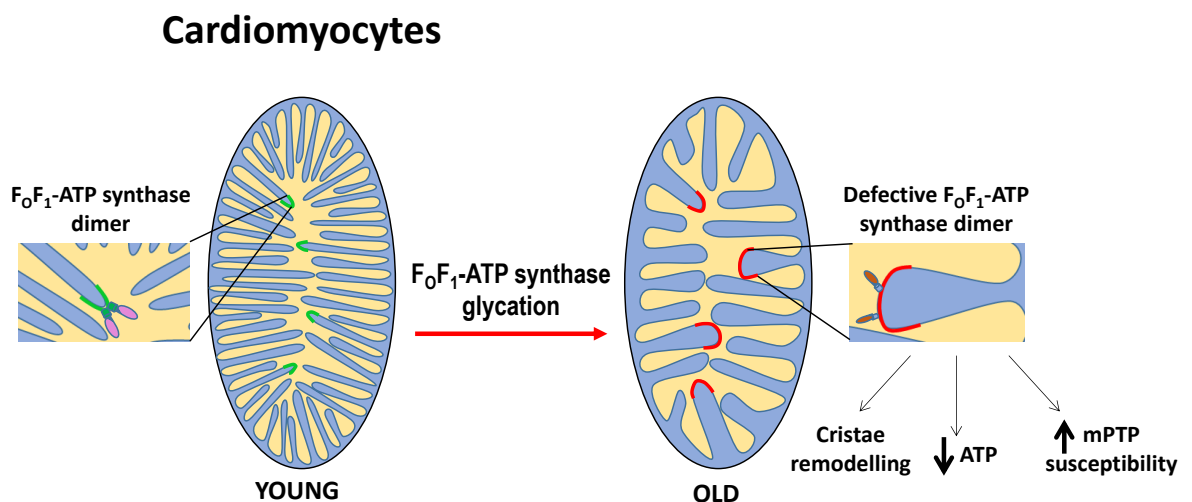
---





1. Advanced age is associated with an increased accumulation of dicarbonyl-modified protein on mitochondrial proteins of the heart.
2. The  $F_0F_1$ -ATP synthase constitutes a prominent target of this age-dependent modification which affects several of its subunits.
3. The dicarbonyl-induced modification of  $F_0F_1$ -ATP synthase alters its dimerization which underlies the pathological mitochondrial ultra-structural modifications and the decreased energetic efficiency present in aging.
4. Increased dicarbonyl modification of  $F_0F_1$ -ATP synthase also increases the susceptibility of aged cardiomyocytes to mPTP under stress.

These data identify a new pathophysiological mechanism responsible for the age-associated energetic decline and reduced tolerance to stress.







## *8. Future Studies*

---



- Establishing a threshold starting from which dicarbonyl-induced modifications start to have a toxic effect. There are several approaches to tackle this including the induction of the formation of one type of modification and evaluating the relationship between the amount of accumulated modifications and cell death. However, this approach also has its limitations as some pathways produce more than only one kind of modifications, and there is commercially no available antibody against each of the dicarbonyl-induced modifications known to date.
- Test several described drugs against the formation of dicarbonyl-induced modification in conjunction to test for a possible additive effect when targeting more than one generating pathway or mechanism. A possible drug combination may be one that quenches MGO, in conjunction with an antioxidant drug. This combination targets simultaneously one of the most toxic and reactive dicarbonyls (MGO), and by-products that can fuel dicarbonyl reactions.
- Test alternative pathways that can reduce dicarbonyl-modified protein accumulation. This may include the up-regulation of autophagy pathways which remove dysfunctional proteins including mitochondria and can therefore “empty” the cells from accumulated garbage, and improve the overall health of the proteome.







## *9. Bibliographic References*

---









1. Woolf SH, Masters RK, Aron LY. Effect of the covid-19 pandemic in 2020 on life expectancy across populations in the USA and other high income countries: simulations of provisional mortality data. *BMJ* [Internet]. 2021;n1343. Available from: <https://www.bmj.com/lookup/doi/10.1136/bmj.n1343>
2. Obas V, Vasan RS. The aging heart. *Clin Sci* [Internet]. 2018;132:1367–1382. Available from: <https://portlandpress.com/clinsci/article/132/13/1367/71946/The-aging-heart>
3. Long B, Brady WJ, Koefman A, Gottlieb M. Cardiovascular complications in COVID-19. *Am J Emerg Med* [Internet]. 2020;38:1504–1507. Available from: <http://www.ncbi.nlm.nih.gov/pubmed/32317203>
4. Tajbakhsh A, Gheibi Hayat SM, Taghizadeh H, Akbari A, Inabadi M, Savardashtaki A, Johnston TP, Sahebkar A. COVID-19 and cardiac injury: clinical manifestations, biomarkers, mechanisms, diagnosis, treatment, and follow up. *Expert Rev Anti Infect Ther* [Internet]. 2021;19:345–357. Available from: <http://www.ncbi.nlm.nih.gov/pubmed/32921216>
5. Paneni F, Diaz Cañestro C, Libby P, Lüscher TF, Camici GG. The Aging Cardiovascular System: Understanding It at the Cellular and Clinical Levels. *J Am Coll Cardiol* [Internet]. 2017;69:1952–1967. Available from: <http://www.ncbi.nlm.nih.gov/pubmed/28408026>
6. North BJ, Sinclair DA. The intersection between aging and cardiovascular disease. *Circ Res* [Internet]. 2012;110:1097–108. Available from: <http://www.ncbi.nlm.nih.gov/pubmed/22499900>
7. Stern S, Behar S, Gottlieb S. Aging and Diseases of the Heart. *Circulation* [Internet]. 2003;108. Available from: <https://www.ahajournals.org/doi/10.1161/01.CIR.0000086898.96021.B9>
8. Bernhard D, Laufer G. The Aging Cardiomyocyte: A Mini-Review. *Gerontology* [Internet]. 2008;54:24–31. Available from: <https://www.karger.com/Article/FullText/113503>
9. Anderson R, Richardson GD, Passos JF. Mechanisms driving the ageing heart. *Exp Gerontol* [Internet]. 2018;109:5–15. Available from: <http://www.ncbi.nlm.nih.gov/pubmed/29054534>
10. López-Otín C, Blasco MA, Partridge L, Serrano M, Kroemer G. The hallmarks of aging. *Cell* [Internet]. 2013;153:1194–217. Available from: <http://www.ncbi.nlm.nih.gov/pubmed/23746838>
11. Bergmann O, Bhardwaj RD, Bernard S, Zdunek S, Barnabé-Heider F, Walsh S, Zupicich J, Alkass K, Buchholz BA, Druid H, Jovinge S, Frisén J. Evidence for Cardiomyocyte Renewal in Humans. *Science (80- )* [Internet]. 2009;324:98–102. Available from: <https://www.sciencemag.org/lookup/doi/10.1126/science.1164680>
12. Henning RH, Brundel BJJM. Proteostasis in cardiac health and disease. *Nat Rev Cardiol* [Internet]. 2017;14:637–653. Available from: <http://www.ncbi.nlm.nih.gov/pubmed/28660894>
13. Hipp MS, Kasturi P, Hartl FU. The proteostasis network and its decline in ageing. *Nat Rev Mol Cell Biol* [Internet]. 2019;20:421–435. Available from: <http://www.ncbi.nlm.nih.gov/pubmed/30733602>
14. Koga H, Kaushik S, Cuervo AM. Protein homeostasis and aging: The importance of exquisite quality control. *Ageing Res Rev* [Internet]. 2011;10:205–15. Available from: <http://www.ncbi.nlm.nih.gov/pubmed/20152936>

15. Tomaru U, Takahashi S, Ishizu A, Miyatake Y, Gohda A, Suzuki S, Ono A, Ohara J, Baba T, Murata S, Tanaka K, Kasahara M. Decreased proteasomal activity causes age-related phenotypes and promotes the development of metabolic abnormalities. *Am J Pathol* [Internet]. 2012;180:963–972. Available from: <http://www.ncbi.nlm.nih.gov/pubmed/22210478>
16. Rabbani N, Xue M, Thornalley PJ. Methylglyoxal-induced dicarbonyl stress in aging and disease: first steps towards glyoxalase 1-based treatments. *Clin Sci* [Internet]. 2016;130:1677–1696. Available from: <https://portlandpress.com/clinsci/article/130/19/1677/71370/Methylglyoxalinduced-dicarbonyl-stress-in-aging>
17. Liguori I, Russo G, Curcio F, Bulli G, Aran L, Della-Morte D, Gargiulo G, Testa G, Cacciatore F, Bonaduce D, Abete P. Oxidative stress, aging, and diseases. *Clin Interv Aging* [Internet]. 2018;13:757–772. Available from: <http://www.ncbi.nlm.nih.gov/pubmed/29731617>
18. Uchiki T, Weikel KA, Jiao W, Shang F, Caceres A, Pawlak D, Handa JT, Brownlee M, Nagaraj R, Taylor A. Glycation-altered proteolysis as a pathobiologic mechanism that links dietary glycemic index, aging, and age-related disease (in nondiabetics). *Aging Cell* [Internet]. 2012;11:1–13. Available from: <http://www.ncbi.nlm.nih.gov/pubmed/21967227>
19. Bou-Teen D, Kaludercic N, Weissman D, Turan B, Maack C, Di Lisa F, Ruiz-Meana M. Mitochondrial ROS and mitochondria-targeted antioxidants in the aged heart. *Free Radic Biol Med* [Internet]. 2021;167:109–124. Available from: <http://www.ncbi.nlm.nih.gov/pubmed/33716106>
20. Ruiz-Meana M, Minguet M, Bou-Teen D, Miro-Casas E, Castans C, Castellano J, Bonzon-Kulichenko E, Igual A, Rodriguez-Lecoq R, Vázquez J, Garcia-Dorado D. Ryanodine Receptor Glycation Favors Mitochondrial Damage in the Senescent Heart. *Circulation* [Internet]. 2019;139:949–964. Available from: <http://www.ncbi.nlm.nih.gov/pubmed/30586718>
21. Brunk UT, Terman A. Lipofuscin: mechanisms of age-related accumulation and influence on cell function. *Free Radic Biol Med* [Internet]. 2002;33:611–9. Available from: <http://www.ncbi.nlm.nih.gov/pubmed/12208347>
22. Lesnefsky EJ, Hoppel CL. Oxidative phosphorylation and aging. *Ageing Res Rev* [Internet]. 2006;5:402–33. Available from: <http://www.ncbi.nlm.nih.gov/pubmed/16831573>
23. Sullivan PG, Balke CW, Esser KA. Mitochondrial buffering of calcium in the heart: potential mechanism for linking cyclic energetic cost with energy supply? *Circ Res* [Internet]. 2006;99:109–10. Available from: <http://www.ncbi.nlm.nih.gov/pubmed/16857968>
24. Shadel GS, Horvath TL. Mitochondrial ROS signaling in organismal homeostasis. *Cell* [Internet]. 2015;163:560–9. Available from: <http://www.ncbi.nlm.nih.gov/pubmed/26496603>
25. Fernandez-Sanz C, Ruiz-Meana M, Miro-Casas E, Nuñez E, Castellano J, Loureiro M, Barba I, Poncelas M, Rodriguez-Sinovas A, Vázquez J, Garcia-Dorado D. Defective sarcoplasmic reticulum-mitochondria calcium exchange in aged mouse myocardium. *Cell Death Dis* [Internet]. 2014;5:e1573. Available from: <http://www.ncbi.nlm.nih.gov/pubmed/25522267>
26. Chouchani ET, Kazak L, Spiegelman BM. New Advances in Adaptive Thermogenesis: UCP1 and Beyond. *Cell Metab* [Internet]. 2019;29:27–37. Available from: <http://www.ncbi.nlm.nih.gov/pubmed/30503034>
27. Abate M, Festa A, Falco M, Lombardi A, Luce A, Grimaldi A, Zappavigna S, Sperlongano P,

- Irace C, Caraglia M, Misso G. Mitochondria as playmakers of apoptosis, autophagy and senescence. *Semin Cell Dev Biol* [Internet]. 2020;98:139–153. Available from: <http://www.ncbi.nlm.nih.gov/pubmed/31154010>
28. Patel P, Karch J. Regulation of cell death in the cardiovascular system. *Int Rev Cell Mol Biol* [Internet]. 2020;353:153–209. Available from: <http://www.ncbi.nlm.nih.gov/pubmed/32381175>
  29. Halestrap AP, Pasdois P. The role of the mitochondrial permeability transition pore in heart disease. *Biochim Biophys Acta* [Internet]. 2009;1787:1402–15. Available from: <http://www.ncbi.nlm.nih.gov/pubmed/19168026>
  30. Gherardi G, Monticelli H, Rizzuto R, Mammucari C. The Mitochondrial Ca<sup>2+</sup> Uptake and the Fine-Tuning of Aerobic Metabolism. *Front Physiol* [Internet]. 2020;11. Available from: <https://www.frontiersin.org/article/10.3389/fphys.2020.554904/full>
  31. Maack C, O'Rourke B. Excitation-contraction coupling and mitochondrial energetics. *Basic Res Cardiol* [Internet]. 2007;102:369–92. Available from: <http://www.ncbi.nlm.nih.gov/pubmed/17657400>
  32. Hamilton S, Terentyev D. Altered Intracellular Calcium Homeostasis and Arrhythmogenesis in the Aged Heart. *Int J Mol Sci* [Internet]. 2019;20. Available from: <http://www.ncbi.nlm.nih.gov/pubmed/31091723>
  33. Herraiz-Martínez A, Álvarez-García J, Llach A, Molina CE, Fernandes J, Ferrero-Gregori A, Rodríguez C, Vallmitjana A, Benítez R, Padró JM, Martínez-González J, Cinca J, Hove-Madsen L. Ageing is associated with deterioration of calcium homeostasis in isolated human right atrial myocytes. *Cardiovasc Res* [Internet]. 2015;106:76–86. Available from: <http://www.ncbi.nlm.nih.gov/pubmed/25712961>
  34. Yaniv Y, Juhaszova M, Sollott SJ. Age-related changes of myocardial ATP supply and demand mechanisms. *Trends Endocrinol Metab* [Internet]. 2013;24:495–505. Available from: <http://www.ncbi.nlm.nih.gov/pubmed/23845538>
  35. Fernandez-Sanz C, Ruiz-Meana M, Castellano J, Miro-Casas E, Nuñez E, Inserte J, Vázquez J, Garcia-Dorado D. Altered FoF1 ATP synthase and susceptibility to mitochondrial permeability transition pore during ischaemia and reperfusion in aging cardiomyocytes. *Thromb Haemost* [Internet]. 2015;113:441–51. Available from: <http://www.ncbi.nlm.nih.gov/pubmed/25631625>
  36. Maejima Y, Adachi S, Ito H, Hirao K, Isobe M. Induction of premature senescence in cardiomyocytes by doxorubicin as a novel mechanism of myocardial damage. *Aging Cell* [Internet]. 2008;7:125–36. Available from: <http://www.ncbi.nlm.nih.gov/pubmed/18031568>
  37. Liang WJ, Gustafsson ÅB. The Aging Heart: Mitophagy at the Center of Rejuvenation. *Front Cardiovasc Med* [Internet]. 2020;7:18. Available from: <http://www.ncbi.nlm.nih.gov/pubmed/32140472>
  38. Quan Y, Xin Y, Tian G, Zhou J, Liu X. Mitochondrial ROS-Modulated mtDNA: A Potential Target for Cardiac Aging. *Oxid Med Cell Longev* [Internet]. 2020;2020:9423593. Available from: <http://www.ncbi.nlm.nih.gov/pubmed/32308810>
  39. Chistiakov DA, Shkurat TP, Melnichenko AA, Grechko A V, Orekhov AN. The role of mitochondrial dysfunction in cardiovascular disease: a brief review. *Ann Med* [Internet]. 2018;50:121–127. Available from: <http://www.ncbi.nlm.nih.gov/pubmed/29237304>

40. Inserte J, Garcia-Dorado D, Ruiz-Meana M, Padilla F, Barrabés JA, Pina P, Agulló L, Piper HM, Soler-Soler J. Effect of inhibition of Na<sup>(+)</sup>/Ca<sup>(2+)</sup> exchanger at the time of myocardial reperfusion on hypercontracture and cell death. *Cardiovasc Res* [Internet]. 2002;55:739–48. Available from: <http://www.ncbi.nlm.nih.gov/pubmed/12176123>
41. Garcia-Dorado D, Piper HM. Postconditioning: reperfusion of “reperfusion injury” after hibernation. *Cardiovasc Res* [Internet]. 2006;69:1–3. Available from: <http://www.ncbi.nlm.nih.gov/pubmed/16337162>
42. Classen JB, Mergner WJ, Costa M. ATP hydrolysis by ischemic mitochondria. *J Cell Physiol* [Internet]. 1989;141:53–9. Available from: <http://www.ncbi.nlm.nih.gov/pubmed/2777902>
43. Lopaschuk GD, Stanley WC. Glucose metabolism in the ischemic heart. *Circulation* [Internet]. 1997;95:313–5. Available from: <http://www.ncbi.nlm.nih.gov/pubmed/9008441>
44. Ruiz-Meana M, García-Dorado D. Fisiopatología del daño miocárdico por isquemia-reperusión: nuevas oportunidades terapéuticas en el infarto agudo de miocardio. *Rev Española Cardiol* [Internet]. 2009;62:199–209. Available from: <https://linkinghub.elsevier.com/retrieve/pii/S0300893209701629>
45. Schäfer C, Ladilov Y, Inserte J, Schäfer M, Haffner S, Garcia-Dorado D, Piper HM. Role of the reverse mode of the Na<sup>+</sup>/Ca<sup>2+</sup> exchanger in reoxygenation-induced cardiomyocyte injury. *Cardiovasc Res* [Internet]. 2001;51:241–50. Available from: <http://www.ncbi.nlm.nih.gov/pubmed/11470463>
46. Garcia-Dorado D, Ruiz-Meana M, Inserte J, Rodriguez-Sinovas A, Piper HM. Calcium-mediated cell death during myocardial reperfusion. *Cardiovasc Res* [Internet]. 2012;94:168–80. Available from: <http://www.ncbi.nlm.nih.gov/pubmed/22499772>
47. Piper HM, García-Dorado D, Ovize M. A fresh look at reperfusion injury. *Cardiovasc Res* [Internet]. 1998;38:291–300. Available from: [https://academic.oup.com/circovasces/article-lookup/doi/10.1016/S0008-6363\(98\)00033-9](https://academic.oup.com/circovasces/article-lookup/doi/10.1016/S0008-6363(98)00033-9)
48. Inserte J, Hernando V, Garcia-Dorado D. Contribution of calpains to myocardial ischaemia/reperfusion injury. *Cardiovasc Res* [Internet]. 2012;96:23–31. Available from: <http://www.ncbi.nlm.nih.gov/pubmed/22787134>
49. Valls-Lacalle L, Barba I, Miró-Casas E, Ruiz-Meana M, Rodríguez-Sinovas A, García-Dorado D. Selective Inhibition of Succinate Dehydrogenase in Reperfused Myocardium with Intracoronary Malonate Reduces Infarct Size. *Sci Rep* [Internet]. 2018;8:2442–2452. Available from: <http://www.ncbi.nlm.nih.gov/pubmed/29402957>
50. Baines CP. The mitochondrial permeability transition pore and ischemia-reperfusion injury. *Basic Res Cardiol* [Internet]. 2009;104:181–8. Available from: <http://www.ncbi.nlm.nih.gov/pubmed/19242640>
51. Zorov DB, Filburn CR, Klotz LO, Zweier JL, Sollott SJ. Reactive oxygen species (ROS)-induced ROS release: a new phenomenon accompanying induction of the mitochondrial permeability transition in cardiac myocytes. *J Exp Med* [Internet]. 2000;192:1001–14. Available from: <http://www.ncbi.nlm.nih.gov/pubmed/11015441>
52. Panel M, Ghaleh B, Morin D. Mitochondria and aging: A role for the mitochondrial transition pore? *Aging Cell* [Internet]. 2018;17:e12793. Available from: <http://www.ncbi.nlm.nih.gov/pubmed/29888494>

53. Rottenberg H, Hoek JB. The path from mitochondrial ROS to aging runs through the mitochondrial permeability transition pore. *Aging Cell* [Internet]. 2017;16:943–955. Available from: <https://onlinelibrary.wiley.com/doi/10.1111/ace.12650>
54. Willems L, Zatta A, Holmgren K, Ashton KJ, Headrick JP. Age-related changes in ischemic tolerance in male and female mouse hearts. *J Mol Cell Cardiol* [Internet]. 2005;38:245–56. Available from: <http://www.ncbi.nlm.nih.gov/pubmed/15698831>
55. Ruiz-Meana M, Bou-Teen D, Ferdinandy P, Gyongyosi M, Pesce M, Perrino C, Schulz R, Sluijter JPG, Tocchetti CG, Thum T, Madonna R. Cardiomyocyte ageing and cardioprotection: consensus document from the ESC working groups cell biology of the heart and myocardial function. *Cardiovasc Res* [Internet]. 2020;116:1835–1849. Available from: <http://www.ncbi.nlm.nih.gov/pubmed/32384145>
56. Lorgis L, Gudjoncik A, Richard C, Mock L, Buffet P, Brunel P, Janin-Manificat L, Beer J-C, Brunet D, Touzery C, Rochette L, Cottin Y, Zeller M. Pre-Infarction Angina and Outcomes in Non-ST-Segment Elevation Myocardial Infarction: Data from the RICO Survey. *PLoS One* [Internet]. 2012;7:e48513. Available from: <https://dx.plos.org/10.1371/journal.pone.0048513>
57. KLONER R, REZKALLA S. Preconditioning, postconditioning and their application to clinical cardiology. *Cardiovasc Res* [Internet]. 2006;70:297–307. Available from: <https://academic.oup.com/cardiovasces/article-lookup/doi/10.1016/j.cardiores.2006.01.012>
58. Paolisso P, Foà A, Bergamaschi L, Donati F, Fabrizio M, Chiti C, Angeli F, Toniolo S, Stefanizzi A, Armillotta M, Rucci P, Iannopollo G, Casella G, Marrozzini C, Galiè N, Pizzi C. Hyperglycemia, inflammatory response and infarct size in obstructive acute myocardial infarction and MINOCA. *Cardiovasc Diabetol* [Internet]. 2021;20:33. Available from: <https://cardiab.biomedcentral.com/articles/10.1186/s12933-021-01222-9>
59. Clavijo LC, Pinto TL, Kuchulakanti PK, Torguson R, Chu WW, Satler LF, Kent KM, Suddath WO, Pichard AD, Waksman R. Metabolic syndrome in patients with acute myocardial infarction is associated with increased infarct size and in-hospital complications. *Cardiovasc Revasc Med* [Internet]. 7:7–11. Available from: <http://www.ncbi.nlm.nih.gov/pubmed/16513517>
60. Rosca MG, Hoppel CL. New aspects of impaired mitochondrial function in heart failure. *J Bioenerg Biomembr* [Internet]. 2009;41:107–12. Available from: <http://www.ncbi.nlm.nih.gov/pubmed/19347572>
61. Lemieux H, Semsroth S, Antretter H, Höfer D, Gnaiger E. Mitochondrial respiratory control and early defects of oxidative phosphorylation in the failing human heart. *Int J Biochem Cell Biol* [Internet]. 2011;43:1729–38. Available from: <http://www.ncbi.nlm.nih.gov/pubmed/21871578>
62. Smith CS, Bottomley PA, Schulman SP, Gerstenblith G, Weiss RG. Altered creatine kinase adenosine triphosphate kinetics in failing hypertrophied human myocardium. *Circulation* [Internet]. 2006;114:1151–8. Available from: <http://www.ncbi.nlm.nih.gov/pubmed/16952984>
63. Brown DA, Perry JB, Allen ME, Sabbah HN, Stauffer BL, Shaikh SR, Cleland JGF, Colucci WS, Butler J, Voors AA, Anker SD, Pitt B, Pieske B, Filippatos G, Greene SJ, Gheorghiade M. Expert consensus document: Mitochondrial function as a therapeutic target in heart failure. *Nat Rev Cardiol* [Internet]. 2017;14:238–250. Available from: <http://www.ncbi.nlm.nih.gov/pubmed/28004807>



64. Garnier A, Fortin D, Deloménie C, Momken I, Veksler V, Ventura-Clapier R. Depressed mitochondrial transcription factors and oxidative capacity in rat failing cardiac and skeletal muscles. *J Physiol* [Internet]. 2003;551:491–501. Available from: <http://www.ncbi.nlm.nih.gov/pubmed/12824444>
65. Hyyti OM, Ledee D, Ning X-H, Ge M, Portman MA. Aging impairs myocardial fatty acid and ketone oxidation and modifies cardiac functional and metabolic responses to insulin in mice. *Am J Physiol Heart Circ Physiol* [Internet]. 2010;299:H868-75. Available from: <http://www.ncbi.nlm.nih.gov/pubmed/20601465>
66. Zhou B, Tian R. Mitochondrial dysfunction in pathophysiology of heart failure. *J Clin Invest* [Internet]. 2018;128:3716–3726. Available from: <http://www.ncbi.nlm.nih.gov/pubmed/30124471>
67. Gray MW, Burger G, Lang BF. Mitochondrial evolution. *Science* [Internet]. 1999;283:1476–81. Available from: <http://www.ncbi.nlm.nih.gov/pubmed/10066161>
68. Zick M, Rabl R, Reichert AS. Cristae formation-linking ultrastructure and function of mitochondria. *Biochim Biophys Acta* [Internet]. 2009;1793:5–19. Available from: <http://www.ncbi.nlm.nih.gov/pubmed/18620004>
69. Paumard P, Vaillier J, Couly B, Schaeffer J, Soubannier V, Mueller DM, Brèthes D, di Rago J-P, Velours J. The ATP synthase is involved in generating mitochondrial cristae morphology. *EMBO J* [Internet]. 2002;21:221–30. Available from: <http://www.ncbi.nlm.nih.gov/pubmed/11823415>
70. Cury DP, Dias FJ, Sosthenes MCK, Dos Santos Haemmerle CA, Ogawa K, Da Silva MCP, Mardegan Issa JP, Iyomasa MM, Watanabe I-S. Morphometric, quantitative, and three-dimensional analysis of the heart muscle fibers of old rats: transmission electron microscopy and high-resolution scanning electron microscopy methods. *Microsc Res Tech* [Internet]. 2013;76:184–95. Available from: <http://www.ncbi.nlm.nih.gov/pubmed/23180425>
71. Chen Y, Csordás G, Jowdy C, Schneider TG, Csordás N, Wang W, Liu Y, Kohlhaas M, Meiser M, Bergem S, Nerbonne JM, Dorn GW, Maack C. Mitofusin 2-containing mitochondrial-reticular microdomains direct rapid cardiomyocyte bioenergetic responses via interorganelle Ca<sup>2+</sup> crosstalk. *Circ Res* [Internet]. 2012;111:863–75. Available from: <http://www.ncbi.nlm.nih.gov/pubmed/22777004>
72. Kohlhaas M, Maack C. Adverse bioenergetic consequences of Na<sup>+</sup>-Ca<sup>2+</sup> exchanger-mediated Ca<sup>2+</sup> influx in cardiac myocytes. *Circulation* [Internet]. 2010;122:2273–80. Available from: <http://www.ncbi.nlm.nih.gov/pubmed/21098439>
73. Decuypere J-P, Monaco G, Missiaen L, De Smedt H, Parys JB, Bultynck G. IP 3 Receptors, Mitochondria, and Ca<sup>2+</sup> Signaling: Implications for Aging. *J Aging Res* [Internet]. 2011;2011:1–20. Available from: <http://www.hindawi.com/journals/jar/2011/920178/>
74. Fannin SW, Lesnefsky EJ, Slabe TJ, Hassan MO, Hoppel CL. Aging selectively decreases oxidative capacity in rat heart interfibrillar mitochondria. *Arch Biochem Biophys* [Internet]. 1999;372:399–407. Available from: <http://www.ncbi.nlm.nih.gov/pubmed/10600182>
75. Lemieux H, Vazquez EJ, Fujioka H, Hoppel CL. Decrease in mitochondrial function in rat cardiac permeabilized fibers correlates with the aging phenotype. *J Gerontol A Biol Sci Med Sci* [Internet]. 2010;65:1157–64. Available from: <http://www.ncbi.nlm.nih.gov/pubmed/20801909>

76. Santulli G, Xie W, Reiken SR, Marks AR. Mitochondrial calcium overload is a key determinant in heart failure. *Proc Natl Acad Sci U S A* [Internet]. 2015;112:11389–94. Available from: <http://www.ncbi.nlm.nih.gov/pubmed/26217001>
77. Lesnefsky EJ, Tandler B, Ye J, Slabe TJ, Turkaly J, Hoppel CL. Myocardial ischemia decreases oxidative phosphorylation through cytochrome oxidase in subsarcolemmal mitochondria. *Am J Physiol* [Internet]. 1997;273:H1544–54. Available from: <http://www.ncbi.nlm.nih.gov/pubmed/9321848>
78. Crochemore C, Mekki M, Corbière C, Karoui A, Noël R, Vendeville C, Vaugeois J-M, Monteil C. Subsarcolemmal and interfibrillar mitochondria display distinct superoxide production profiles. *Free Radic Res* [Internet]. 2015;49:331–7. Available from: <http://www.ncbi.nlm.nih.gov/pubmed/25689624>
79. Hoppel CL, Tandler B, Fujioka H, Riva A. Dynamic organization of mitochondria in human heart and in myocardial disease. *Int J Biochem Cell Biol* [Internet]. 2009;41:1949–56. Available from: <http://www.ncbi.nlm.nih.gov/pubmed/19446651>
80. Gomes LC, Di Benedetto G, Scorrano L. During autophagy mitochondria elongate, are spared from degradation and sustain cell viability. *Nat Cell Biol* [Internet]. 2011;13:589–98. Available from: <http://www.ncbi.nlm.nih.gov/pubmed/21478857>
81. Patten DA, Wong J, Khacho M, Soubannier V, Mailloux RJ, Pilon-Larose K, MacLaurin JG, Park DS, McBride HM, Trinkle-Mulcahy L, Harper M-E, Germain M, Slack RS. OPA1-dependent cristae modulation is essential for cellular adaptation to metabolic demand. *EMBO J* [Internet]. 2014;33:2676–91. Available from: <http://www.ncbi.nlm.nih.gov/pubmed/25298396>
82. Frezza C, Cipolat S, Martins de Brito O, Micaroni M, Beznoussenko G V, Rudka T, Bartoli D, Polishuck RS, Danial NN, De Strooper B, Scorrano L. OPA1 controls apoptotic cristae remodeling independently from mitochondrial fusion. *Cell* [Internet]. 2006;126:177–89. Available from: <http://www.ncbi.nlm.nih.gov/pubmed/16839885>
83. Hackenbrock CR. Ultrastructural bases for metabolically linked mechanical activity in mitochondria. I. Reversible ultrastructural changes with change in metabolic steady state in isolated liver mitochondria. *J Cell Biol* [Internet]. 1966;30:269–97. Available from: <http://www.ncbi.nlm.nih.gov/pubmed/5968972>
84. Chaanine AH. Morphological Stages of Mitochondrial Vacuolar Degeneration in Phenylephrine-Stressed Cardiac Myocytes and in Animal Models and Human Heart Failure. *Medicina (Kaunas)* [Internet]. 2019;55. Available from: <http://www.ncbi.nlm.nih.gov/pubmed/31163678>
85. El'darov CM, Vays VB, Vangeli IM, Kolosova NG, Bakeeva LE. Morphometric Examination of Mitochondrial Ultrastructure in Aging Cardiomyocytes. *Biochemistry (Mosc)* [Internet]. 2015;80:604–9. Available from: <http://www.ncbi.nlm.nih.gov/pubmed/26071780>
86. Perkins G, Bossy-Wetzel E, Ellisman MH. New insights into mitochondrial structure during cell death. *Exp Neurol* [Internet]. 2009;218:183–92. Available from: <http://www.ncbi.nlm.nih.gov/pubmed/19464290>
87. Daum B, Walter A, Horst A, Osiewacz HD, Kühlbrandt W. Age-dependent dissociation of ATP synthase dimers and loss of inner-membrane cristae in mitochondria. *Proc Natl Acad Sci U S A* [Internet]. 2013;110:15301–6. Available from:

- <http://www.ncbi.nlm.nih.gov/pubmed/24006361>
88. Siegmund SE, Grassucci R, Carter SD, Barca E, Farino ZJ, Juanola-Falgarona M, Zhang P, Tanji K, Hirano M, Schon EA, Frank J, Freyberg Z. Three-Dimensional Analysis of Mitochondrial Crista Ultrastructure in a Patient with Leigh Syndrome by In Situ Cryoelectron Tomography. *iScience* [Internet]. 2018;6:83–91. Available from: <http://www.ncbi.nlm.nih.gov/pubmed/30240627>
  89. Eramo MJ, Lisnyak V, Formosa LE, Ryan MT. The “mitochondrial contact site and cristae organising system” (MICOS) in health and human disease. *J Biochem* [Internet]. 2020;167:243–255. Available from: <http://www.ncbi.nlm.nih.gov/pubmed/31825482>
  90. Glytsou C, Calvo E, Cogliati S, Mehrotra A, Anastasia I, Rigoni G, Raimondi A, Shintani N, Loureiro M, Vazquez J, Pellegrini L, Enriquez JA, Scorrano L, Soriano ME. Optic Atrophy 1 Is Epistatic to the Core MICOS Component MIC60 in Mitochondrial Cristae Shape Control. *Cell Rep* [Internet]. 2016;17:3024–3034. Available from: <http://www.ncbi.nlm.nih.gov/pubmed/27974214>
  91. Cogliati S, Frezza C, Soriano ME, Varanita T, Quintana-Cabrera R, Corrado M, Cipolat S, Costa V, Casarin A, Gomes LC, Perales-Clemente E, Salviati L, Fernandez-Silva P, Enriquez JA, Scorrano L. Mitochondrial cristae shape determines respiratory chain supercomplexes assembly and respiratory efficiency. *Cell* [Internet]. 2013;155:160–71. Available from: <http://www.ncbi.nlm.nih.gov/pubmed/24055366>
  92. Quintana-Cabrera R, Quirin C, Glytsou C, Corrado M, Urbani A, Pellattiero A, Calvo E, Vázquez J, Enríquez JA, Gerle C, Soriano ME, Bernardi P, Scorrano L. The cristae modulator Optic atrophy 1 requires mitochondrial ATP synthase oligomers to safeguard mitochondrial function. *Nat Commun* [Internet]. 2018;9:3399. Available from: <http://www.ncbi.nlm.nih.gov/pubmed/30143614>
  93. Eydt K, Davies KM, Behrendt C, Wittig I, Reichert AS. Cristae architecture is determined by an interplay of the MICOS complex and the F1FO ATP synthase via Mic27 and Mic10. *Microb cell (Graz, Austria)* [Internet]. 2017;4:259–272. Available from: <http://www.ncbi.nlm.nih.gov/pubmed/28845423>
  94. Campanella M, Casswell E, Chong S, Farah Z, Wieckowski MR, Abramov AY, Tinker A, Duchon MR. Regulation of mitochondrial structure and function by the F1Fo-ATPase inhibitor protein, IF1. *Cell Metab* [Internet]. 2008;8:13–25. Available from: <http://www.ncbi.nlm.nih.gov/pubmed/18590689>
  95. Gu J, Zhang L, Zong S, Guo R, Liu T, Yi J, Wang P, Zhuo W, Yang M. Cryo-EM structure of the mammalian ATP synthase tetramer bound with inhibitory protein IF1. *Science* [Internet]. 2019;364:1068–1075. Available from: <http://www.ncbi.nlm.nih.gov/pubmed/31197009>
  96. Nuskova H, Mikesova J, Efimova I, Pecinova A, Pecina P, Drahota Z, Houstek J, Mracek T. Biochemical thresholds for pathological presentation of ATP synthase deficiencies. *Biochem Biophys Res Commun* [Internet]. 2020;521:1036–1041. Available from: <http://www.ncbi.nlm.nih.gov/pubmed/31732150>
  97. Jonckheere AI, Smeitink JAM, Rodenburg RJT. Mitochondrial ATP synthase: architecture, function and pathology. *J Inherit Metab Dis* [Internet]. 2012;35:211–25. Available from: <http://www.ncbi.nlm.nih.gov/pubmed/21874297>
  98. Pinke G, Zhou L, Sazanov LA. Cryo-EM structure of the entire mammalian F-type ATP

- synthase. *Nat Struct Mol Biol* [Internet]. 2020;27:1077–1085. Available from: <http://www.ncbi.nlm.nih.gov/pubmed/32929284>
99. Nesci S, Pagliarani A, Algieri C, Trombetti F. Mitochondrial F-type ATP synthase: multiple enzyme functions revealed by the membrane-embedded FO structure. *Crit Rev Biochem Mol Biol* [Internet]. 2020;55:309–321. Available from: <http://www.ncbi.nlm.nih.gov/pubmed/32580582>
  100. Arselin G, Vaillier J, Salin B, Schaeffer J, Giraud M-F, Dautant A, Brèthes D, Velours J. The modulation in subunits e and g amounts of yeast ATP synthase modifies mitochondrial cristae morphology. *J Biol Chem* [Internet]. 2004;279:40392–9. Available from: <http://www.ncbi.nlm.nih.gov/pubmed/15262977>
  101. Junge W, Lill H, Engelbrecht S. ATP synthase: an electrochemical transducer with rotatory mechanics. *Trends Biochem Sci* [Internet]. 1997;22:420–3. Available from: <http://www.ncbi.nlm.nih.gov/pubmed/9397682>
  102. Srivastava AP, Luo M, Zhou W, Symersky J, Bai D, Chambers MG, Faraldo-Gómez JD, Liao M, Mueller DM. High-resolution cryo-EM analysis of the yeast ATP synthase in a lipid membrane. *Science* [Internet]. 2018;360. Available from: <http://www.ncbi.nlm.nih.gov/pubmed/29650704>
  103. Guo H, Bueler SA, Rubinstein JL. Atomic model for the dimeric FO region of mitochondrial ATP synthase. *Science* [Internet]. 2017;358:936–940. Available from: <http://www.ncbi.nlm.nih.gov/pubmed/29074581>
  104. Spikes TE, Montgomery MG, Walker JE. Structure of the dimeric ATP synthase from bovine mitochondria. *Proc Natl Acad Sci U S A* [Internet]. 2020;117:23519–23526. Available from: <http://www.ncbi.nlm.nih.gov/pubmed/32900941>
  105. Hahn A, Parey K, Bublitz M, Mills DJ, Zickermann V, Vonck J, Kühlbrandt W, Meier T. Structure of a Complete ATP Synthase Dimer Reveals the Molecular Basis of Inner Mitochondrial Membrane Morphology. *Mol Cell* [Internet]. 2016;63:445–56. Available from: <http://www.ncbi.nlm.nih.gov/pubmed/27373333>
  106. Boyer PD. A model for conformational coupling of membrane potential and proton translocation to ATP synthesis and to active transport. *FEBS Lett* [Internet]. 1975;58:1–6. Available from: <http://www.ncbi.nlm.nih.gov/pubmed/1225567>
  107. Devenish RJ, Prescott M, Boyle GM, Nagley P. The oligomycin axis of mitochondrial ATP synthase: OSCP and the proton channel. *J Bioenerg Biomembr* [Internet]. 2000;32:507–15. Available from: <http://www.ncbi.nlm.nih.gov/pubmed/15254386>
  108. Nesci S, Trombetti F, Ventrella V, Pagliarani A. Opposite rotation directions in the synthesis and hydrolysis of ATP by the ATP synthase: hints from a subunit asymmetry. *J Membr Biol* [Internet]. 2015;248:163–9. Available from: <http://www.ncbi.nlm.nih.gov/pubmed/25655107>
  109. Yang K, Long Q, Saja K, Huang F, Pogwizd SM, Zhou L, Yoshida M, Yang Q. Knockout of the ATPase inhibitory factor 1 protects the heart from pressure overload-induced cardiac hypertrophy. *Sci Rep* [Internet]. 2017;7:10501. Available from: <http://www.nature.com/articles/s41598-017-11251-8>
  110. Zuurbier CJ, Bertrand L, Beauloye CR, Andreadou I, Ruiz-Meana M, Jespersen NR, Kula-Alwar D, Prag HA, Eric Botker H, Dambrova M, Montessuit C, Kaambre T, Liepinsh E, Brookes PS, Krieg T. Cardiac metabolism as a driver and therapeutic target of myocardial infarction. *J Cell*

- Mol Med* [Internet]. 2020;24:5937–5954. Available from: <http://www.ncbi.nlm.nih.gov/pubmed/32384583>
111. García-Bermúdez J, Cuezva JM. The ATPase Inhibitory Factor 1 (IF1): A master regulator of energy metabolism and of cell survival. *Biochim Biophys Acta - Bioenerg* [Internet]. 2016;1857:1167–1182. Available from: <https://linkinghub.elsevier.com/retrieve/pii/S0005272816300238>
  112. Arselin G, Giraud M-F, Dautant A, Vaillier J, Brèthes D, Couлары-Salin B, Schaeffer J, Velours J. The GxxxG motif of the transmembrane domain of subunit e is involved in the dimerization/oligomerization of the yeast ATP synthase complex in the mitochondrial membrane. *Eur J Biochem* [Internet]. 2003;270:1875–84. Available from: <http://www.ncbi.nlm.nih.gov/pubmed/12694201>
  113. Davies KM, Strauss M, Daum B, Kief JH, Osiewacz HD, Rycovska A, Zickermann V, Kühlbrandt W. Macromolecular organization of ATP synthase and complex I in whole mitochondria. *Proc Natl Acad Sci U S A* [Internet]. 2011;108:14121–6. Available from: <http://www.ncbi.nlm.nih.gov/pubmed/21836051>
  114. Anselmi C, Davies KM, Faraldo-Gómez JD. Mitochondrial ATP synthase dimers spontaneously associate due to a long-range membrane-induced force. *J Gen Physiol* [Internet]. 2018;150:763–770. Available from: <http://www.ncbi.nlm.nih.gov/pubmed/29643173>
  115. Blum TB, Hahn A, Meier T, Davies KM, Kühlbrandt W. Dimers of mitochondrial ATP synthase induce membrane curvature and self-assemble into rows. *Proc Natl Acad Sci U S A* [Internet]. 2019;116:4250–4255. Available from: <http://www.ncbi.nlm.nih.gov/pubmed/30760595>
  116. Allen RD. Membrane tubulation and proton pumps. *Protoplasma* [Internet]. 1995;189:1–8. Available from: <http://link.springer.com/10.1007/BF01280286>
  117. Habersetzer J, Larrieu I, Priault M, Salin B, Rossignol R, Brèthes D, Paumard P. Human F1Fo ATP synthase, mitochondrial ultrastructure and OXPHOS impairment: a (super-)complex matter? *PLoS One* [Internet]. 2013;8:e75429. Available from: <http://www.ncbi.nlm.nih.gov/pubmed/24098383>
  118. Davies KM, Anselmi C, Wittig I, Faraldo-Gómez JD, Kühlbrandt W. Structure of the yeast F1Fo-ATP synthase dimer and its role in shaping the mitochondrial cristae. *Proc Natl Acad Sci U S A* [Internet]. 2012;109:13602–7. Available from: <http://www.ncbi.nlm.nih.gov/pubmed/22864911>
  119. Rabl R, Soubannier V, Scholz R, Vogel F, Mendl N, Vasiljev-Neumeyer A, Körner C, Jagasia R, Keil T, Baumeister W, Cyrklaff M, Neupert W, Reichert AS. Formation of cristae and crista junctions in mitochondria depends on antagonism between Fcj1 and Su e/g. *J Cell Biol* [Internet]. 2009;185:1047–63. Available from: <http://www.ncbi.nlm.nih.gov/pubmed/19528297>
  120. Rampello NG, Stenger M, Westermann B, Osiewacz HD. Impact of F1Fo-ATP-synthase dimer assembly factors on mitochondrial function and organismic aging. *Microb cell (Graz, Austria)* [Internet]. 2018;5:198–207. Available from: <http://www.ncbi.nlm.nih.gov/pubmed/29610761>
  121. Carraro M, Checchetto V, Sartori G, Kucharczyk R, di Rago J-P, Minervini G, Franchin C, Arrigoni G, Giorgio V, Petronilli V, Tosatto SCE, Lippe G, Szabó I, Bernardi P. High-Conductance Channel Formation in Yeast Mitochondria is Mediated by F-ATP Synthase e and g Subunits. *Cell Physiol Biochem* [Internet]. 2018;50:1840–1855. Available from:

- <http://www.ncbi.nlm.nih.gov/pubmed/30423558>
122. Bornhövd C, Vogel F, Neupert W, Reichert AS. Mitochondrial membrane potential is dependent on the oligomeric state of F1F0-ATP synthase supracomplexes. *J Biol Chem* [Internet]. 2006;281:13990–8. Available from: <http://www.ncbi.nlm.nih.gov/pubmed/16551625>
  123. Strauss M, Hofhaus G, Schröder RR, Kühlbrandt W. Dimer ribbons of ATP synthase shape the inner mitochondrial membrane. *EMBO J* [Internet]. 2008;27:1154–60. Available from: <http://www.ncbi.nlm.nih.gov/pubmed/18323778>
  124. Hausenloy D, Wynne A, Duchon M, Yellon D. Transient mitochondrial permeability transition pore opening mediates preconditioning-induced protection. *Circulation* [Internet]. 2004;109:1714–7. Available from: <http://www.ncbi.nlm.nih.gov/pubmed/15066952>
  125. Ruiz-Meana M, Inserte J, Fernandez-Sanz C, Hernando V, Miro-Casas E, Barba I, Garcia-Dorado D. The role of mitochondrial permeability transition in reperfusion-induced cardiomyocyte death depends on the duration of ischemia. *Basic Res Cardiol* [Internet]. 2011;106:1259–68. Available from: <http://www.ncbi.nlm.nih.gov/pubmed/21959501>
  126. Garcia-Dorado D, Rodríguez-Sinovas A, Ruiz-Meana M, Inserte J. Protection Against Myocardial Ischemia-reperfusion Injury in Clinical Practice. *Rev Española Cardiol (English Ed)* [Internet]. 2014;67:394–404. Available from: <https://linkinghub.elsevier.com/retrieve/pii/S188558571400111X>
  127. Morciano G, Bonora M, Campo G, Aquila G, Rizzo P, Giorgi C, Wieckowski MR, Pinton P. Mechanistic Role of mPTP in Ischemia-Reperfusion Injury. *Adv Exp Med Biol* [Internet]. 2017;982:169–189. Available from: <http://www.ncbi.nlm.nih.gov/pubmed/28551787>
  128. GARCIA-DORADO D, RODRIGUEZ-SINOVAS A, RUIZ-MEANA M, INSERTE J, AGULLO L, CABESTRERO A. The end-effectors of preconditioning protection against myocardial cell death secondary to ischemia-reperfusion. *Cardiovasc Res* [Internet]. 2006;70:274–285. Available from: <https://academic.oup.com/cardiovasres/article-lookup/doi/10.1016/j.cardiores.2006.02.011>
  129. Argaud L, Gateau-Roesch O, Raisky O, Loufouat J, Robert D, Ovize M. Postconditioning Inhibits Mitochondrial Permeability Transition. *Circulation* [Internet]. 2005;111:194–197. Available from: <https://www.ahajournals.org/doi/10.1161/01.CIR.0000151290.04952.3B>
  130. Ong S-B, Dongworth RK, Cabrera-Fuentes HA, Hausenloy DJ. Role of the MPTP in conditioning the heart - translatability and mechanism. *Br J Pharmacol* [Internet]. 2015;172:2074–84. Available from: <http://www.ncbi.nlm.nih.gov/pubmed/25393318>
  131. Hausenloy DJ, Boston-Griffiths EA, Yellon DM. Cyclosporin A and cardioprotection: from investigative tool to therapeutic agent. *Br J Pharmacol* [Internet]. 2012;165:1235–45. Available from: <http://www.ncbi.nlm.nih.gov/pubmed/21955136>
  132. Monassier L, Ayme-Dietrich E, Aubertin-Kirch G, Pathak A. Targeting myocardial reperfusion injuries with cyclosporine in the CIRCUS Trial - pharmacological reasons for failure. *Fundam Clin Pharmacol* [Internet]. 2016;30:191–3. Available from: <http://www.ncbi.nlm.nih.gov/pubmed/26713664>
  133. Zhang C, Cheng Y, Liu D, Liu M, Cui H, Zhang B, Mei Q, Zhou S. Mitochondria-targeted cyclosporin A delivery system to treat myocardial ischemia reperfusion injury of rats. *J Nanobiotechnology* [Internet]. 2019;17:18. Available from:

<https://jnanobiotechnology.biomedcentral.com/articles/10.1186/s12951-019-0451-9>

134. Inserte J, Barba I, Hernando V, Abellán A, Ruiz-Meana M, Rodríguez-Sinovas A, Garcia-Dorado D. Effect of acidic reperfusion on prolongation of intracellular acidosis and myocardial salvage. *Cardiovasc Res* [Internet]. 2008;77:782–90. Available from: <http://www.ncbi.nlm.nih.gov/pubmed/18056767>
135. Giorgio V, von Stockum S, Antoniel M, Fabbro A, Fogolari F, Forte M, Glick GD, Petronilli V, Zoratti M, Szabó I, Lippe G, Bernardi P. Dimers of mitochondrial ATP synthase form the permeability transition pore. *Proc Natl Acad Sci U S A* [Internet]. 2013;110:5887–92. Available from: <http://www.ncbi.nlm.nih.gov/pubmed/23530243>
136. Urbani A, Giorgio V, Carrer A, Franchin C, Arrigoni G, Jiko C, Abe K, Maeda S, Shinzawa-Itoh K, Bogers JFM, McMillan DGG, Gerle C, Szabó I, Bernardi P. Purified F-ATP synthase forms a Ca<sup>2+</sup>-dependent high-conductance channel matching the mitochondrial permeability transition pore. *Nat Commun* [Internet]. 2019;10:4341. Available from: <http://www.ncbi.nlm.nih.gov/pubmed/31554800>
137. Giorgio V, Guo L, Bassot C, Petronilli V, Bernardi P. Calcium and regulation of the mitochondrial permeability transition. *Cell Calcium* [Internet]. 2018;70:56–63. Available from: <http://www.ncbi.nlm.nih.gov/pubmed/28522037>
138. Carraro M, Giorgio V, Šileikytė J, Sartori G, Forte M, Lippe G, Zoratti M, Szabó I, Bernardi P. Channel formation by yeast F-ATP synthase and the role of dimerization in the mitochondrial permeability transition. *J Biol Chem* [Internet]. 2014;289:15980–5. Available from: <http://www.ncbi.nlm.nih.gov/pubmed/24790105>
139. Bonora M, Morganti C, Morciano G, Pedriali G, Lebedzinska-Arciszewska M, Aquila G, Giorgi C, Rizzo P, Campo G, Ferrari R, Kroemer G, Wieckowski MR, Galluzzi L, Pinton P. Mitochondrial permeability transition involves dissociation of F<sub>1</sub>F<sub>0</sub> ATP synthase dimers and C-ring conformation. *EMBO Rep* [Internet]. 2017;18:1077–1089. Available from: <http://www.ncbi.nlm.nih.gov/pubmed/28566520>
140. Mnatsakanyan N, Llaguno MC, Yang Y, Yan Y, Weber J, Sigworth FJ, Jonas EA. A mitochondrial megachannel resides in monomeric F<sub>1</sub>F<sub>0</sub> ATP synthase. *Nat Commun* [Internet]. 2019;10:5823. Available from: <http://www.ncbi.nlm.nih.gov/pubmed/31862883>
141. Alavian KN, Beutner G, Lazrove E, Sacchetti S, Park H-A, Licznarski P, Li H, Nabili P, Hockensmith K, Graham M, Porter GA, Jonas EA. An uncoupling channel within the c-subunit ring of the F<sub>1</sub>F<sub>0</sub> ATP synthase is the mitochondrial permeability transition pore. *Proc Natl Acad Sci U S A* [Internet]. 2014;111:10580–5. Available from: <http://www.ncbi.nlm.nih.gov/pubmed/24979777>
142. Neginskaya MA, Solesio ME, Berezhnaya E V, Amodeo GF, Mnatsakanyan N, Jonas EA, Pavlov E V. ATP Synthase C-Subunit-Deficient Mitochondria Have a Small Cyclosporine A-Sensitive Channel, but Lack the Permeability Transition Pore. *Cell Rep* [Internet]. 2019;26:11-17.e2. Available from: <http://www.ncbi.nlm.nih.gov/pubmed/30605668>
143. Jonas EA, Porter GA, Beutner G, Mnatsakanyan N, Alavian KN. Cell death disguised: The mitochondrial permeability transition pore as the c-subunit of the F(1)F(O) ATP synthase. *Pharmacol Res* [Internet]. 2015;99:382–92. Available from: <http://www.ncbi.nlm.nih.gov/pubmed/25956324>
144. Bernardi P, Di Lisa F. The mitochondrial permeability transition pore: molecular nature and

- role as a target in cardioprotection. *J Mol Cell Cardiol* [Internet]. 2015;78:100–6. Available from: <http://www.ncbi.nlm.nih.gov/pubmed/25268651>
145. He J, Ford HC, Carroll J, Ding S, Fearnley IM, Walker JE. Persistence of the mitochondrial permeability transition in the absence of subunit c of human ATP synthase. *Proc Natl Acad Sci U S A* [Internet]. 2017;114:3409–3414. Available from: <http://www.ncbi.nlm.nih.gov/pubmed/28289229>
146. He J, Carroll J, Ding S, Fearnley IM, Walker JE. Permeability transition in human mitochondria persists in the absence of peripheral stalk subunits of ATP synthase. *Proc Natl Acad Sci U S A* [Internet]. 2017;114:9086–9091. Available from: <http://www.ncbi.nlm.nih.gov/pubmed/28784775>
147. Niedzwiecka K, Baranowska E, Panja C, Kucharczyk R. ATP Synthase Subunit a Supports Permeability Transition in Yeast Lacking Dimerization Subunits and Modulates  $\gamma$ PTP Conductance. *Cell Physiol Biochem* [Internet]. 2020;54:211–229. Available from: <http://www.ncbi.nlm.nih.gov/pubmed/32100973>
148. Carroll J, He J, Ding S, Fearnley IM, Walker JE. Persistence of the permeability transition pore in human mitochondria devoid of an assembled ATP synthase. *Proc Natl Acad Sci U S A* [Internet]. 2019;116:12816–12821. Available from: <http://www.ncbi.nlm.nih.gov/pubmed/31213546>
149. Giorgio V, Burchell V, Schiavone M, Bassot C, Minervini G, Petronilli V, Argenton F, Forte M, Tosatto S, Lippe G, Bernardi P.  $\text{Ca}^{2+}$  binding to F-ATP synthase  $\beta$  subunit triggers the mitochondrial permeability transition. *EMBO Rep* [Internet]. 2017;18:1065–1076. Available from: <http://www.ncbi.nlm.nih.gov/pubmed/28507163>
150. Antoniel M, Jones K, Antonucci S, Spolaore B, Fogolari F, Petronilli V, Giorgio V, Carraro M, Di Lisa F, Forte M, Szabó I, Lippe G, Bernardi P. The unique histidine in OSCP subunit of F-ATP synthase mediates inhibition of the permeability transition pore by acidic pH. *EMBO Rep* [Internet]. 2018;19:257–268. Available from: <http://www.ncbi.nlm.nih.gov/pubmed/29217657>
151. Johnson KM, Chen X, Boitano A, Swenson L, Oipari AW, Glick GD. Identification and validation of the mitochondrial F1F0-ATPase as the molecular target of the immunomodulatory benzodiazepine Bz-423. *Chem Biol* [Internet]. 2005;12:485–96. Available from: <http://www.ncbi.nlm.nih.gov/pubmed/15850986>
152. Leung AWC, Varanyuwatana P, Halestrap AP. The mitochondrial phosphate carrier interacts with cyclophilin D and may play a key role in the permeability transition. *J Biol Chem* [Internet]. 2008;283:26312–23. Available from: <http://www.ncbi.nlm.nih.gov/pubmed/18667415>
153. Gordan R, Fefelova N, Gwathmey JK, Xie L-H. Involvement of mitochondrial permeability transition pore (mPTP) in cardiac arrhythmias: Evidence from cyclophilin D knockout mice. *Cell Calcium* [Internet]. 2016;60:363–372. Available from: <http://www.ncbi.nlm.nih.gov/pubmed/27616659>
154. Kokoszka JE, Waymire KG, Levy SE, Sligh JE, Cai J, Jones DP, MacGregor GR, Wallace DC. The ADP/ATP translocator is not essential for the mitochondrial permeability transition pore. *Nature* [Internet]. 2004;427:461–5. Available from: <http://www.ncbi.nlm.nih.gov/pubmed/14749836>



155. Krauskopf A, Eriksson O, Craigen WJ, Forte MA, Bernardi P. Properties of the permeability transition in VDAC1(-/-) mitochondria. *Biochim Biophys Acta* [Internet]. 1757:590–5. Available from: <http://www.ncbi.nlm.nih.gov/pubmed/16626625>
156. Gutiérrez-Aguilar M, Douglas DL, Gibson AK, Domeier TL, Molkentin JD, Baines CP. Genetic manipulation of the cardiac mitochondrial phosphate carrier does not affect permeability transition. *J Mol Cell Cardiol* [Internet]. 2014;72:316–25. Available from: <http://www.ncbi.nlm.nih.gov/pubmed/24768964>
157. He L, Lemasters JJ. Regulated and unregulated mitochondrial permeability transition pores: a new paradigm of pore structure and function? *FEBS Lett* [Internet]. 2002;512:1–7. Available from: <http://www.ncbi.nlm.nih.gov/pubmed/11852041>
158. Radman M. Fidelity and infidelity. *Nature* [Internet]. 2001;413:115–115. Available from: <http://www.nature.com/articles/35093178>
159. Brings S, Fleming T, Freichel M, Muckenthaler MU, Herzig S, Nawroth PP. Dicarbonyls and Advanced Glycation End-Products in the Development of Diabetic Complications and Targets for Intervention. *Int J Mol Sci* [Internet]. 2017;18. Available from: <http://www.ncbi.nlm.nih.gov/pubmed/28475116>
160. Chaudhuri J, Bains Y, Guha S, Kahn A, Hall D, Bose N, Gugliucci A, Kapahi P. The Role of Advanced Glycation End Products in Aging and Metabolic Diseases: Bridging Association and Causality. *Cell Metab* [Internet]. 2018;28:337–352. Available from: <http://www.ncbi.nlm.nih.gov/pubmed/30184484>
161. Allaman I, Bélanger M, Magistretti PJ. Methylglyoxal, the dark side of glycolysis. *Front Neurosci* [Internet]. 2015;9:23. Available from: <http://www.ncbi.nlm.nih.gov/pubmed/25709564>
162. Vistoli G, De Maddis D, Cipak A, Zarkovic N, Carini M, Aldini G. Advanced glycoxidation and lipoxidation end products (AGEs and ALEs): an overview of their mechanisms of formation. *Free Radic Res* [Internet]. 2013;47 Suppl 1:3–27. Available from: <http://www.ncbi.nlm.nih.gov/pubmed/23767955>
163. Espinosa-Diez C, Miguel V, Mennerich D, Kietzmann T, Sánchez-Pérez P, Cadenas S, Lamas S. Antioxidant responses and cellular adjustments to oxidative stress. *Redox Biol* [Internet]. 2015;6:183–197. Available from: <https://linkinghub.elsevier.com/retrieve/pii/S2213231715000804>
164. Falfushynska HI, Sokolov E, Piontkivska H, Sokolova IM. The Role of Reversible Protein Phosphorylation in Regulation of the Mitochondrial Electron Transport System During Hypoxia and Reoxygenation Stress in Marine Bivalves. *Front Mar Sci* [Internet]. 2020;7. Available from: <https://www.frontiersin.org/article/10.3389/fmars.2020.00467/full>
165. Shin J, Zhang D, Chen D. Reversible Acetylation of Metabolic Enzymes Celebration: SIRT2 and p300 Join the Party. *Mol Cell* [Internet]. 2011;43:3–5. Available from: <https://linkinghub.elsevier.com/retrieve/pii/S1097276511004515>
166. Rabbani N, Xue M, Thornalley PJ. Dicarbonyl stress, protein glycation and the unfolded protein response. *Glycoconj J* [Internet]. 2021;38:331–340. Available from: <https://link.springer.com/10.1007/s10719-021-09980-0>
167. Rabbani N, Thornalley PJ. Dicarbonyl stress in cell and tissue dysfunction contributing to ageing and disease. *Biochem Biophys Res Commun* [Internet]. 2015;458:221–226. Available

- from: <https://linkinghub.elsevier.com/retrieve/pii/S0006291X15001874>
168. Nigro C, Leone A, Fiory F, Prevezano I, Nicolò A, Mirra P, Beguinot F, Miele C. Dicarbonyl Stress at the Crossroads of Healthy and Unhealthy Aging. *Cells* [Internet]. 2019;8. Available from: <http://www.ncbi.nlm.nih.gov/pubmed/31331077>
  169. Schwarzenbolz U, Mende S, Henle T. Model studies on protein glycation: influence of cysteine on the reactivity of arginine and lysine residues toward glyoxal. *Ann N Y Acad Sci* [Internet]. 2008;1126:248–52. Available from: <http://www.ncbi.nlm.nih.gov/pubmed/18448824>
  170. Gallet X, Charlotiaux B, Thomas A, Brasseur R. A fast method to predict protein interaction sites from sequences. *J Mol Biol* [Internet]. 2000;302:917–26. Available from: <http://www.ncbi.nlm.nih.gov/pubmed/10993732>
  171. Ahmed N, Thornalley PJ. Peptide mapping of human serum albumin modified minimally by methylglyoxal in vitro and in vivo. *Ann N Y Acad Sci* [Internet]. 2005;1043:260–6. Available from: <http://www.ncbi.nlm.nih.gov/pubmed/16037246>
  172. Thornalley PJ. Dicarbonyl intermediates in the maillard reaction. *Ann N Y Acad Sci* [Internet]. 2005;1043:111–7. Available from: <http://www.ncbi.nlm.nih.gov/pubmed/16037229>
  173. Desai KM, Chang T, Wang H, Banigesh A, Dhar A, Liu J, Untereiner A, Wu L. Oxidative stress and aging: is methylglyoxal the hidden enemy? *Can J Physiol Pharmacol* [Internet]. 2010;88:273–84. Available from: <http://www.ncbi.nlm.nih.gov/pubmed/20393592>
  174. Thornalley PJ. Protein and nucleotide damage by glyoxal and methylglyoxal in physiological systems--role in ageing and disease. *Drug Metabol Drug Interact* [Internet]. 2008;23:125–50. Available from: <http://www.ncbi.nlm.nih.gov/pubmed/18533367>
  175. Nowotny K, Jung T, Grune T, Höhn A. Accumulation of modified proteins and aggregate formation in aging. *Exp Gerontol* [Internet]. 2014;57:122–31. Available from: <http://www.ncbi.nlm.nih.gov/pubmed/24877899>
  176. Chaplygina A V, Vekshin NL. [Lipofuscin and mitolipofuscin in organs of young and adult rats.]. *Adv Gerontol = Uspekhi Gerontol* [Internet]. 31:197–202. Available from: <http://www.ncbi.nlm.nih.gov/pubmed/30080326>
  177. Perrone A, Giovino A, Benny J, Martinelli F. Advanced Glycation End Products (AGEs): Biochemistry, Signaling, Analytical Methods, and Epigenetic Effects. *Oxid Med Cell Longev* [Internet]. 2020;2020:3818196. Available from: <http://www.ncbi.nlm.nih.gov/pubmed/32256950>
  178. Freedman BI, Wuerth JP, Cartwright K, Bain RP, Dippe S, Hershon K, Mooradian AD, Spinowitz BS. Design and baseline characteristics for the aminoguanidine Clinical Trial in Overt Type 2 Diabetic Nephropathy (ACTION II). *Control Clin Trials* [Internet]. 1999;20:493–510. Available from: <http://www.ncbi.nlm.nih.gov/pubmed/10503809>
  179. Boldyrev AA, Aldini G, Derave W. Physiology and pathophysiology of carnosine. *Physiol Rev* [Internet]. 2013;93:1803–45. Available from: <http://www.ncbi.nlm.nih.gov/pubmed/24137022>
  180. Davies SS, Zhang LS. Reactive Carbonyl Species Scavengers- Novel Therapeutic Approaches for Chronic Diseases. *Curr Pharmacol reports* [Internet]. 2017;3:51–67. Available from: <http://www.ncbi.nlm.nih.gov/pubmed/28993795>

181. Golegaonkar S, Tabrez SS, Pandit A, Sethurathinam S, Jagadeeshaprasad MG, Bansode S, Sampathkumar S-G, Kulkarni MJ, Mukhopadhyay A. Rifampicin reduces advanced glycation end products and activates DAF-16 to increase lifespan in *Caenorhabditis elegans*. *Aging Cell* [Internet]. 2015;14:463–73. Available from: <http://www.ncbi.nlm.nih.gov/pubmed/25720500>
182. Yang S, Litchfield JE, Baynes JW. AGE-breakers cleave model compounds, but do not break Maillard crosslinks in skin and tail collagen from diabetic rats. *Arch Biochem Biophys* [Internet]. 2003;412:42–6. Available from: <http://www.ncbi.nlm.nih.gov/pubmed/12646266>
183. Willemsen S, Hartog JW, Hummel YM, Posma JL, van Wijk LM, van Veldhuisen DJ, Voors AA. Effects of alagebrium, an advanced glycation end-product breaker, in patients with chronic heart failure: study design and baseline characteristics of the BENEFICIAL trial. *Eur J Heart Fail* [Internet]. 2010;12:294–300. Available from: <http://www.ncbi.nlm.nih.gov/pubmed/20100811>
184. Ravichandran G, Lakshmanan DK, Raju K, Elangovan A, Nambirajan G, Devanesan AA, Thilagar S. Food advanced glycation end products as potential endocrine disruptors: An emerging threat to contemporary and future generation. *Environ Int* [Internet]. 2019;123:486–500. Available from: <http://www.ncbi.nlm.nih.gov/pubmed/30622074>
185. Semba RD, Nicklett EJ, Ferrucci L. Does Accumulation of Advanced Glycation End Products Contribute to the Aging Phenotype? *Journals Gerontol Ser A Biol Sci Med Sci* [Internet]. 2010;65A:963–975. Available from: <https://academic.oup.com/biomedgerontology/article-lookup/doi/10.1093/gerona/glq074>
186. Kong Y, Wang F, Wang J, Liu C, Zhou Y, Xu Z, Zhang C, Sun B, Guan Y. Pathological Mechanisms Linking Diabetes Mellitus and Alzheimer’s Disease: the Receptor for Advanced Glycation End Products (RAGE). *Front Aging Neurosci* [Internet]. 2020;12:217. Available from: <http://www.ncbi.nlm.nih.gov/pubmed/32774301>
187. Li J, Liu D, Sun L, Lu Y, Zhang Z. Advanced glycation end products and neurodegenerative diseases: mechanisms and perspective. *J Neurol Sci* [Internet]. 2012;317:1–5. Available from: <http://www.ncbi.nlm.nih.gov/pubmed/22410257>
188. Tezel G, Luo C, Yang X. Accelerated aging in glaucoma: immunohistochemical assessment of advanced glycation end products in the human retina and optic nerve head. *Invest Ophthalmol Vis Sci* [Internet]. 2007;48:1201–11. Available from: <http://www.ncbi.nlm.nih.gov/pubmed/17325164>
189. Bohlender JM, Franke S, Stein G, Wolf G. Advanced glycation end products and the kidney. *Am J Physiol Renal Physiol* [Internet]. 2005;289:F645-59. Available from: <http://www.ncbi.nlm.nih.gov/pubmed/16159899>
190. Morcos M, Du X, Pfisterer F, Hutter H, Sayed AAR, Thornalley P, Ahmed N, Baynes J, Thorpe S, Kukudov G, Schlotterer A, Bozorgmehr F, El Baki RA, Stern D, Moehrlen F, Ibrahim Y, Oikonomou D, Hamann A, Becker C, Zeier M, Schwenger V, Miftari N, Humpert P, Hammes H-P, Buechler M, Bierhaus A, Brownlee M, Nawroth PP. Glyoxalase-1 prevents mitochondrial protein modification and enhances lifespan in *Caenorhabditis elegans*. *Aging Cell* [Internet]. 2008;7:260–269. Available from: <https://onlinelibrary.wiley.com/doi/10.1111/j.1474-9726.2008.00371.x>
191. Schlotterer A, Pfisterer F, Kukudov G, Heckmann B, Henriquez D, Morath C, Krämer BK, Hammes H-P, Schwenger V, Morcos M. Neuronal damage and shortening of lifespan in *C. elegans* by peritoneal dialysis fluid: Protection by glyoxalase-1. *Biomed reports* [Internet].

- 2018;8:540–546. Available from: <http://www.ncbi.nlm.nih.gov/pubmed/29805788>
192. Aragonès G, Rowan S, Francisco SG, Whitcomb EA, Yang W, Perini-Villanueva G, Schalkwijk CG, Taylor A, Bejarano E. The Glyoxalase System in Age-Related Diseases: Nutritional Intervention as Anti-Ageing Strategy. *Cells* [Internet]. 2021;10:1852. Available from: <https://www.mdpi.com/2073-4409/10/8/1852>
  193. Nowotny K, Jung T, Höhn A, Weber D, Grune T. Advanced glycation end products and oxidative stress in type 2 diabetes mellitus. *Biomolecules* [Internet]. 2015;5:194–222. Available from: <http://www.ncbi.nlm.nih.gov/pubmed/25786107>
  194. Ademowo OS, Dias HKI, Burton DGA, Griffiths HR. Lipid (per) oxidation in mitochondria: an emerging target in the ageing process? *Biogerontology* [Internet]. 2017;18:859–879. Available from: <http://www.ncbi.nlm.nih.gov/pubmed/28540446>
  195. Pun PBL, Logan A, Darley-Usmar V, Chacko B, Johnson MS, Huang GW, Rogatti S, Prime TA, Methner C, Krieg T, Fearnley IM, Larsen L, Larsen DS, Menger KE, Collins Y, James AM, Kumar GDK, Hartley RC, Smith RAJ, Murphy MP. A mitochondria-targeted mass spectrometry probe to detect glyoxals: implications for diabetes. *Free Radic Biol Med* [Internet]. 2014;67:437–50. Available from: <http://www.ncbi.nlm.nih.gov/pubmed/24316194>
  196. Rabbani N, Thornalley PJ. Dicarbonyls linked to damage in the powerhouse: glycation of mitochondrial proteins and oxidative stress. *Biochem Soc Trans* [Internet]. 2008;36:1045–50. Available from: <http://www.ncbi.nlm.nih.gov/pubmed/18793186>
  197. Pun PBL, Murphy MP. Pathological significance of mitochondrial glycation. *Int J Cell Biol* [Internet]. 2012;2012:843505. Available from: <http://www.ncbi.nlm.nih.gov/pubmed/22778743>
  198. Yang Y-C, Tsai C-Y, Chen C-L, Kuo C-H, Hou C-W, Cheng S-Y, Aneja R, Huang C-Y, Kuo W-W. Pkc $\delta$  Activation is Involved in ROS-Mediated Mitochondrial Dysfunction and Apoptosis in Cardiomyocytes Exposed to Advanced Glycation End Products (Ages). *Ageing Dis* [Internet]. 2018;9:647–663. Available from: <http://www.ncbi.nlm.nih.gov/pubmed/30090653>
  199. Zhang M, Kho AL, Anilkumar N, Chibber R, Pagano PJ, Shah AM, Cave AC. Glycated proteins stimulate reactive oxygen species production in cardiac myocytes: involvement of Nox2 (gp91phox)-containing NADPH oxidase. *Circulation* [Internet]. 2006;113:1235–43. Available from: <http://www.ncbi.nlm.nih.gov/pubmed/16505175>
  200. Ruan L, Zhou C, Jin E, Kucharavy A, Zhang Y, Wen Z, Florens L, Li R. Cytosolic proteostasis through importing of misfolded proteins into mitochondria. *Nature* [Internet]. 2017;543:443–446. Available from: <http://www.ncbi.nlm.nih.gov/pubmed/28241148>
  201. Ruan L, Wang Y, Zhang X, Tomaszewski A, McNamara JT, Li R. Mitochondria-Associated Proteostasis. *Annu Rev Biophys* [Internet]. 2020;49:41–67. Available from: <http://www.ncbi.nlm.nih.gov/pubmed/31928428>
  202. Palmer JW, Tandler B, Hoppel CL. Biochemical properties of subsarcolemmal and interfibrillar mitochondria isolated from rat cardiac muscle. *J Biol Chem* [Internet]. 1977;252:8731–9. Available from: <http://www.ncbi.nlm.nih.gov/pubmed/925018>
  203. Kuznetsov A V, Javadov S, Sickinger S, Frotschnig S, Grimm M. H9c2 and HL-1 cells demonstrate distinct features of energy metabolism, mitochondrial function and sensitivity to hypoxia-reoxygenation. *Biochim Biophys Acta* [Internet]. 2015;1853:276–84. Available from: <http://www.ncbi.nlm.nih.gov/pubmed/25450968>

204. Bonzon-Kulichenko E, Camafeita E, López JA, Gómez-Serrano M, Jorge I, Calvo E, Núñez E, Trevisan-Herraz M, Bagwan N, Bárcena JA, Peral B, Vázquez J. Improved integrative analysis of the thiol redox proteome using filter-aided sample preparation. *J Proteomics* [Internet]. 2020;214:103624. Available from: <http://www.ncbi.nlm.nih.gov/pubmed/31874222>
205. Bonzon-Kulichenko E, Garcia-Marques F, Trevisan-Herraz M, Vázquez J. Revisiting peptide identification by high-accuracy mass spectrometry: problems associated with the use of narrow mass precursor windows. *J Proteome Res* [Internet]. 2015;14:700–10. Available from: <http://www.ncbi.nlm.nih.gov/pubmed/25494653>
206. Navarro P, Vázquez J. A refined method to calculate false discovery rates for peptide identification using decoy databases. *J Proteome Res* [Internet]. 2009;8:1792–6. Available from: <https://pubs.acs.org/doi/10.1021/pr800362h>
207. García-Marqués F, Trevisan-Herraz M, Martínez-Martínez S, Camafeita E, Jorge I, Lopez JA, Méndez-Barbero N, Méndez-Ferrer S, Del Pozo MA, Ibáñez B, Andrés V, Sánchez-Madrid F, Redondo JM, Bonzon-Kulichenko E, Vázquez J. A Novel Systems-Biology Algorithm for the Analysis of Coordinated Protein Responses Using Quantitative Proteomics. *Mol Cell Proteomics* [Internet]. 2016;15:1740–60. Available from: <https://linkinghub.elsevier.com/retrieve/pii/S1535947620336100>
208. Trevisan-Herraz M, Bagwan N, García-Marqués F, Rodríguez JM, Jorge I, Ezkurdia I, Bonzon-Kulichenko E, Vázquez J. SanXoT: a modular and versatile package for the quantitative analysis of high-throughput proteomics experiments. *Bioinformatics* [Internet]. 2019;35:1594–1596. Available from: <https://academic.oup.com/bioinformatics/article/35/9/1594/5106713>
209. Navarro P, Trevisan-Herraz M, Bonzon-Kulichenko E, Núñez E, Martínez-Acedo P, Pérez-Hernández D, Jorge I, Mesa R, Calvo E, Carrascal M, Hernáez ML, García F, Bárcena JA, Ashman K, Abian J, Gil C, Redondo JM, Vázquez J. General statistical framework for quantitative proteomics by stable isotope labeling. *J Proteome Res* [Internet]. 2014;13:1234–47. Available from: <http://www.ncbi.nlm.nih.gov/pubmed/24512137>
210. Bagwan N, Bonzon-Kulichenko E, Calvo E, Lechuga-Vieco AV, Michalakopoulos S, Trevisan-Herraz M, Ezkurdia I, Rodríguez JM, Magni R, Latorre-Pellicer A, Enríquez JA, Vázquez J. Comprehensive Quantification of the Modified Proteome Reveals Oxidative Heart Damage in Mitochondrial Heteroplasmy. *Cell Rep* [Internet]. 2018;23:3685–3697.e4. Available from: <https://linkinghub.elsevier.com/retrieve/pii/S2211124718308611>
211. Ruiz-Meana M, Abellán A, Miró-Casas E, Garcia-Dorado D. Opening of mitochondrial permeability transition pore induces hypercontracture in Ca<sup>2+</sup> overloaded cardiac myocytes. *Basic Res Cardiol* [Internet]. 2007;102:542–52. Available from: <http://www.ncbi.nlm.nih.gov/pubmed/17891523>
212. Petronilli V, Miotto G, Canton M, Brini M, Colonna R, Bernardi P, Di Lisa F. Transient and long-lasting openings of the mitochondrial permeability transition pore can be monitored directly in intact cells by changes in mitochondrial calcein fluorescence. *Biophys J* [Internet]. 1999;76:725–34. Available from: <http://www.ncbi.nlm.nih.gov/pubmed/9929477>
213. García JJ, Morales-Ríos E, Cortés-Hernandez P, Rodríguez-Zavala JS. The inhibitor protein (IF1) promotes dimerization of the mitochondrial F1F0-ATP synthase. *Biochemistry* [Internet]. 2006;45:12695–703. Available from: <http://www.ncbi.nlm.nih.gov/pubmed/17042487>
214. Varanita T, Soriano ME, Romanello V, Zaglia T, Quintana-Cabrera R, Semenzato M, Menabò R,

- Costa V, Civiletto G, Pesce P, Viscomi C, Zeviani M, Di Lisa F, Mongillo M, Sandri M, Scorrano L. The OPA1-dependent mitochondrial cristae remodeling pathway controls atrophic, apoptotic, and ischemic tissue damage. *Cell Metab* [Internet]. 2015;21:834–44. Available from: <http://www.ncbi.nlm.nih.gov/pubmed/26039448>
215. De Marchi E, Bonora M, Giorgi C, Pinton P. The mitochondrial permeability transition pore is a dispensable element for mitochondrial calcium efflux. *Cell Calcium* [Internet]. 2014;56:1–13. Available from: <http://www.ncbi.nlm.nih.gov/pubmed/24755650>
216. Davies KM, Daum B, Gold VAM, Mühleip AW, Brandt T, Blum TB, Mills DJ, Kühlbrandt W. Visualization of ATP synthase dimers in mitochondria by electron cryo-tomography. *J Vis Exp* [Internet]. 2014;51228. Available from: <http://www.ncbi.nlm.nih.gov/pubmed/25285856>
217. Dudkina N V, Oostergetel GT, Lewejohann D, Braun H-P, Boekema EJ. Row-like organization of ATP synthase in intact mitochondria determined by cryo-electron tomography. *Biochim Biophys Acta* [Internet]. 2010;1797:272–7. Available from: <http://www.ncbi.nlm.nih.gov/pubmed/19925775>
218. Brownlee M. Advanced protein glycosylation in diabetes and aging. *Annu Rev Med* [Internet]. 1995;46:223–34. Available from: <http://www.ncbi.nlm.nih.gov/pubmed/7598459>
219. Simm A. Protein glycation during aging and in cardiovascular disease. *J Proteomics* [Internet]. 2013;92:248–59. Available from: <http://www.ncbi.nlm.nih.gov/pubmed/23702329>
220. Rungratanawanich W, Qu Y, Wang X, Essa MM, Song B-J. Advanced glycation end products (AGEs) and other adducts in aging-related diseases and alcohol-mediated tissue injury. *Exp Mol Med* [Internet]. 2021;53:168–188. Available from: <http://www.ncbi.nlm.nih.gov/pubmed/33568752>
221. Semba RD, Bandinelli S, Sun K, Guralnik JM, Ferrucci L. Plasma carboxymethyl-lysine, an advanced glycation end product, and all-cause and cardiovascular disease mortality in older community-dwelling adults. *J Am Geriatr Soc* [Internet]. 2009;57:1874–80. Available from: <http://www.ncbi.nlm.nih.gov/pubmed/19682127>
222. Fishman SL, Sonmez H, Basman C, Singh V, Poretsky L. The role of advanced glycation end-products in the development of coronary artery disease in patients with and without diabetes mellitus: a review. *Mol Med* [Internet]. 2018;24:59. Available from: <http://www.ncbi.nlm.nih.gov/pubmed/30470170>
223. Lukyanenko V, Chikando A, Lederer WJ. Mitochondria in cardiomyocyte Ca<sup>2+</sup> signaling. *Int J Biochem Cell Biol* [Internet]. 2009;41:1957–71. Available from: <http://www.ncbi.nlm.nih.gov/pubmed/19703657>
224. Neupane P, Bhujju S, Thapa N, Bhattarai HK. ATP Synthase: Structure, Function and Inhibition. *Biomol Concepts* [Internet]. 2019;10:1–10. Available from: <http://www.ncbi.nlm.nih.gov/pubmed/30888962>
225. Kolwicz SC, Purohit S, Tian R. Cardiac metabolism and its interactions with contraction, growth, and survival of cardiomyocytes. *Circ Res* [Internet]. 2013;113:603–16. Available from: <http://www.ncbi.nlm.nih.gov/pubmed/23948585>
226. Bárcena C, Mayoral P, Quirós PM. Mitohormesis, an Antiaging Paradigm. *Int Rev Cell Mol Biol* [Internet]. 2018;340:35–77. Available from: <http://www.ncbi.nlm.nih.gov/pubmed/30072093>
227. Ristow M, Schmeisser K. Mitohormesis: Promoting Health and Lifespan by Increased Levels of

- Reactive Oxygen Species (ROS). *Dose Response* [Internet]. 2014;12:288–341. Available from: <http://www.ncbi.nlm.nih.gov/pubmed/24910588>
228. Lee JW. Protonic Capacitor: Elucidating the biological significance of mitochondrial cristae formation. *Sci Rep* [Internet]. 2020;10:10304. Available from: <http://www.ncbi.nlm.nih.gov/pubmed/32601276>
229. Pánek T, Eliáš M, Vancová M, Lukeš J, Hashimi H. Returning to the Fold for Lessons in Mitochondrial Crista Diversity and Evolution. *Curr Biol* [Internet]. 2020;30:R575–R588. Available from: <http://www.ncbi.nlm.nih.gov/pubmed/32428499>
230. Brandt T, Mourier A, Tain LS, Partridge L, Larsson N-G, Kühlbrandt W. Changes of mitochondrial ultrastructure and function during ageing in mice and *Drosophila*. *Elife* [Internet]. 2017;6. Available from: <http://www.ncbi.nlm.nih.gov/pubmed/28699890>
231. Wang G, Luo Y, Hu J, Wang J, Liu X, Li S. Effects of Aging on Expression of Mic60 and OPA1 and Mitochondrial Morphology in Myocardium of Tibetan Sheep. *Anim an open access J from MDPI* [Internet]. 2020;10. Available from: <http://www.ncbi.nlm.nih.gov/pubmed/33233488>
232. Ljubicic V, Menzies KJ, Hood DA. Mitochondrial dysfunction is associated with a pro-apoptotic cellular environment in senescent cardiac muscle. *Mech Ageing Dev* [Internet]. 2010;131:79–88. Available from: <http://www.ncbi.nlm.nih.gov/pubmed/20036683>
233. Marzetti E, Calvani R, Lorenzi M, Tanganelli F, Picca A, Bossola M, Menghi A, Bernabei R, Landi F. Association between myocyte quality control signaling and sarcopenia in old hip-fractured patients: Results from the Sarcopenia in Hip Fracture (SHIFT) exploratory study. *Exp Gerontol* [Internet]. 2016;80:1–5. Available from: <http://www.ncbi.nlm.nih.gov/pubmed/27064052>
234. Warnsmann V, Marschall L-M, Osiewacz HD. Impaired F1Fo-ATP-Synthase Dimerization Leads to the Induction of Cyclophilin D-Mediated Autophagy-Dependent Cell Death and Accelerated Aging. *Cells* [Internet]. 2021;10. Available from: <http://www.ncbi.nlm.nih.gov/pubmed/33808173>
235. Jennings RB, Reimer KA, Steenbergen C. Effect of inhibition of the mitochondrial ATPase on net myocardial ATP in total ischemia. *J Mol Cell Cardiol* [Internet]. 1991;23:1383–95. Available from: <http://www.ncbi.nlm.nih.gov/pubmed/1839801>
236. Lippe G, Coluccino G, Zancani M, Baratta W, Crusiz P. Mitochondrial F-ATP Synthase and Its Transition into an Energy-Dissipating Molecular Machine. *Oxid Med Cell Longev* [Internet]. 2019;2019:8743257. Available from: <http://www.ncbi.nlm.nih.gov/pubmed/31178976>
237. Briston T, Roberts M, Lewis S, Powney B, M Staddon J, Szabadkai G, Duchon MR. Mitochondrial permeability transition pore: sensitivity to opening and mechanistic dependence on substrate availability. *Sci Rep* [Internet]. 2017;7:10492. Available from: <http://www.ncbi.nlm.nih.gov/pubmed/28874733>
238. Inserte J, Ruiz-Meana M, Rodríguez-Sinovas A, Barba I, Garcia-Dorado D. Contribution of delayed intracellular pH recovery to ischemic postconditioning protection. *Antioxid Redox Signal* [Internet]. 2011;14:923–39. Available from: <http://www.ncbi.nlm.nih.gov/pubmed/20578958>